



The
University
Of
Sheffield.

Developing the synthesis of novel TiO_2 and Nb_2O_5 supports and their applications to the selective oxidation of alkanes

James Railton

A thesis submitted in partial fulfilment of the requirements for the degree of
Doctor of Philosophy

The University of Sheffield
Department of Chemistry

01/06/20

I, the author, confirm that the Thesis is my own work. I am aware of the University's Guidance on the Use of Unfair Means (www.sheffield.ac.uk/ssid/unfair-means). This work has not been previously been presented for an award at this, or any other, university.

Foreword

"You have rightly chosen," said God, "for in my garden of Paradise this little bird shall sing for evermore, and in my city of gold the Happy Prince shall praise me."

- Oscar Wilde (1854 – 1900), *The Happy Prince*, 1888

Acknowledgments

First and foremost, I would like to thank my supervisor, Dr. Marco Conte. I could not describe a more appropriate, professional and caring supervisor than what I have witnessed whilst studying with Marco. I cannot put into writing the appreciation of direction I have received in the past 4 years. Marco, I'd like to say thank you, thank you for your patience, your attention to detail and passion for the transfer of knowledge. I wish you the most successful of academic careers.

Next I would like to thank the members of Marco's group: Baozhai, Changyan, Prea and Dedi you have been fantastic to work with and your cooperation and friendliness has made the past 4 years a pleasure to be by your sides in our uphill battle with research. I would also like to mention the new arrivals of: Becks, Mohammed, Ghadeer and Meugyan, although I was not able to get to know you as much as I had wanted, the short time we spent together was indicative of the friendliness this group should pride itself on. I would also like to thank Hasina and all the masters students for their cooperation during all of our busy times. Good luck everyone!

I would also like to acknowledge the support of friends and co-workers during my time at Sheffield. I was incredibly fortunate enough to make lots of dear friends, to name them all would take up too much space! However, I would like to make a particular mention to the people I met in Sheffield: Alex, Jenny, Dave, Shannon and Joe and all those who went to tea on G floor! Along with my friends from Newcastle; Pasquale, Rob and Angelina.

The chemistry department stands on the shoulders of some incredible people, those directly involved with my research were Dr. Craig Robertson, Dr Sandra van Meurs, Simon Thorpe, Sharon Spey, Rob Hanson, Garry Turner, Heather Grievson and all the staff of the post graduate office, finance office and stores, you are all fantastic.

I thank my mam, dad and brother for all their support during this demanding and unfamiliar time during my PhD. I'd like to thank Laura's parents, Karen and Steven for all their support too. I thank my best friends April, Ryan and Oli for their effort on helping me whatever way they can. I love you all.

Lastly, and most importantly, I thank my exceptional girlfriend, Laura. On writing this acknowledgement we have been together almost 9 years. Throughout this entire time, you have been the most supportive person in my life and without you this journey would not have been the same.

Abstract

The theme of this project was based on selective alkane oxidation with oxygen as the sole oxidant in a solvent-free system by means of shape selective catalysis. This was to provide a competitor for the application of 'green' synthesis of linear primary alcohols, which are exceptionally relevant compounds for the fine chemicals industry from surfactants and coatings to cosmetics.

Groundwork for this project was based on the autoxidation of *n*-decane and subsequent analysis of complex reaction mixtures. Through standard solutions, calculators for conversion and selectivity were developed for ¹H-NMR and GC-MS analysis. The oxidation of *n*-decane is possible with no added initiator or catalyst when operating at temperatures >120 °C, with conversions up to 12% and the major products being (2- to 5-) decanol and decanone, this was ascribed to the presence of autoxidation phenomena. These bench mark studies were then extended to the oxidation of cyclooctane as a model system for cyclic hydrocarbons, and to investigate the effects of a lower bond dissociation energy to the activation of saturated alkanes and the effect that a different steric hindrance can have on the reactivity of micro and meso-porous materials.

Heterogeneous catalysts based on commercial bulk supports; like TiO₂ and Nb₂O₅; as well as porous supports like MCM-41 and ZSM-5 were developed, including particular emphasis for the development of micro- and meso- porous TiO₂ and Nb₂O₅. For these materials wetness impregnation was used to add a range of metal nanoparticles, especially focusing on Fe, Mn, and Pd, on supports which were characterized with a range of analytical techniques including: XRPD, ATR-FTIR, TGA, ICP-MS and XPS.

Catalytic tests with Fe/TiO₂ were used as a benchmark for our studies. It was found bulk Fe/TiO₂ could catalyse *n*-decane oxidation in conditions where no autoxidation had occurred. Using this catalyst optimised parameters for *n*-decane oxidation were determined (T = 115 °C, P_{O₂} = 1 bar M:S = 1:1000, t = 24 h, stirrer speed = 500-700 rpm). These parameters were then applied to the range of catalysts synthesised. It was found in most cases that iron was

the top performer on which ever support was used. Supported noble metals and manganese, despite their literature presence, were found to be poor catalysts at best. This is suspected to be due to the existence of inhibiting metal-support interactions. No clear selectivity for alcohols was observed from the range of catalysts tested. Cyclooctane oxidation was also possible with the catalysts developed. It was found that Fe/ZSM-5 and analogues are capable of very high conversion (>60%) and selectivity for cyclooctanone (>60%) potentially making them candidates to be used in the production of precursors for the fibres industry.

Microporous metal oxides with an additional metal within the framework were developed for their potential to create confined metal active sites. Additional dopant metals were chosen based on those found to be active in previous chapters/ those with significant literature presence. Synthesis was conducted via a template-assisted hydrothermal protocol with optimisation developed here. However, literature descriptions of template removal were unable to be replicated (most likely by incorrect synthesis parameters, like the pH, reported in the original references). Instead, several template removal techniques were trialled (calcination, acid washing, template oxidation) as well as an innovative synthesis via a peptization method. This also allowed development of a novel type of analysis where changes in pore structure and thermal stability of these materials were studied *in situ* using XRPD. We observed that template-free microporous titanium oxide was easily collapsing due to its delicate pore structure upon template removal. Undoped and metal doped template-including and pore-collapsed template-free material were unable to activate alkanes. However, microporous titanium oxide doped with iron nanoparticles was achieved through peptization of anatase followed by wetness impregnation. This material could activate cyclooctane with relatively low conversion (< 10%).

Novel microporous template-free iron-doped niobium oxide was synthesised successfully, with the porous framework intact. Again, literature descriptions of template removal were unable to be replicated for the same reasons of TiO₂. However, a novel and promising form of template removal with phthalic anhydride was developed. This material was then applied to alkane

oxidation, where it was unable to activate *n*-decane and gave low conversion (< 10%) for cyclooctane oxidation.

Thesis contents

Foreword.....	ii
Acknowledgments	iii
Abstract.....	iv
Thesis contents	1
Abbreviations	6
CHAPTER 1: Introduction.....	9
Abbreviations	10
1.1. Fundamental concepts of catalysis.....	11
1.2. Industrial manufacture of linear primary alcohols.....	16
1.2.1. Hydroformylation.....	16
1.2.2. Ziegler alcohol process	19
1.2.3. Shilov	20
1.3. Oxidation of alkanes using molecular oxygen.....	22
1.3.1. Autoxidation	27
1.3.2. Oxidation of alkanes via promoters or oxygen transfer reagents	29
1.3.3. Biocatalysts for alkane oxidation	31
1.4. Shape selective catalysis	34
1.4.1. Concept	34
1.4.2. Shape selective catalysts for the oxidation of alkanes.....	36
1.4.2.1. Molecular sieves and zeolites used in shape-selective catalysis.....	36
1.4.2.2. Metalloporphyrins	39
1.5. Microporous and mesoporous framework solids.....	41
1.5.1. Microporous and mesoporous metal oxides	42
1.5.2. Zeolites	47
1.5.3. Aluminophosphates.....	49
1.6. Supported metals for oxidation catalysis	51
1.6.1. Basic principles of supported nanoparticles, nanoclusters and isolated atoms	51
1.6.2. Nano-sized catalysts vs. bulk material.....	51
1.6.3. The effect of the support	53
1.6.4. Leaching	54
1.7. Project scope and thesis development	55
1.8. References.....	58
CHAPTER 2: Experimental methods and techniques.....	72
Abbreviations	74
2.1. Materials	76
2.1.1. For bulk catalyst synthesis	79

2.1.2.	For microporous synthesis	79
2.1.3.	For template removal	80
2.1.4.	For catalytic tests and calibration of equipment	80
2.2.	Synthesis	81
2.2.1.	Supported metals and metal oxides – working principles of deposition methods 81	
2.2.1.1.	Wetness impregnation	82
2.2.1.2.	Deposition-precipitation	83
2.2.1.3.	Coprecipitation.....	84
2.2.1.4.	Sol-immobilisation	85
2.2.2.	Supported metal oxides – actual preparation procedure(s)	86
2.2.2.1.	Wetness impregnation	86
2.2.2.2.	Hydrogenation	87
2.2.3.	Microporous materials	87
2.2.4.	Microporous titanium oxide	89
2.2.4.1.	Antonelli’s protocol.....	89
2.2.4.2.	Dai’s protocol.....	90
2.2.4.3.	Zhang’s protocol	90
2.2.4.4.	Peptization.....	91
2.2.5.	Microporous niobium oxide	92
2.2.5.1.	Ying’s protocol.....	92
2.2.5.2.	Antonelli’s protocol.....	93
2.3.	Template removal	94
2.3.1.	Microporous titanium oxide	94
2.3.1.1.	Calcination.....	94
2.3.1.2.	Solvent washes	94
2.3.1.3.	Acidic washes.....	94
2.3.1.3.1.	HNO ₃	94
2.3.1.3.2.	<i>p</i> -TSA.....	95
2.3.1.4.	Alternatives to acids.....	95
2.3.1.4.1.	H ₂ O ₂	95
2.3.1.4.2.	Phthalic anhydride.....	96
2.3.2.	Microporous niobium oxide (and microporous Fe/Nb ₂ O ₅)	96
2.3.2.1.	Acidic washes.....	96
2.3.2.2.	Phthalic anhydride	97
2.4.	Catalytic tests.....	98
2.4.1.	<i>n</i> -decane	98
2.4.1.1.	Atmospheric tests	98

2.4.1.2.	Pressurised tests	98
2.4.2.	Cyclooctane	99
2.4.3.	Dried metal salt tests.....	99
2.5.	Analytical methods	100
2.5.1.	Quantitative analysis of hydrocarbon reaction mixtures.....	100
2.5.2.	¹ H-NMR.....	101
2.5.2.1.	¹ H-NMR <i>n</i> -decane and <i>n</i> -octane.....	102
2.5.2.2.	¹ H-NMR Cyclooctane.....	103
2.5.3.	Gas chromatography – mass spectrometry (GC-MS).....	103
2.5.4.	Fourier transform infrared – attenuated total reflectance (FTIR-ATR).....	105
2.5.5.	Thermogravimetric analysis (TGA).....	106
2.5.6.	X-ray powder diffraction (XRPD)	107
2.5.6.1.	Determination of particle size.....	108
2.5.6.2.	Determination of pore size.....	108
2.5.7.	X-ray photoelectron spectroscopy (XPS).....	109
2.5.8.	Brunauer-Emmett-Teller (BET).....	110
2.5.9.	Inductively coupled plasma optical emission spectroscopy (ICP-OES).....	111
2.6.	References.....	114
CHAPTER 3: The autoxidation of alkanes and subsequent analysis of reaction mixtures		
121		
Abbreviations		122
3.1. Introduction		123
3.2. Results and discussion.....		126
3.2.1. Development of an ¹ H-NMR alkane oxidation quantification method		126
3.2.1.1. Application of ¹ H-NMR conversion calculator to the autoxidation of alkanes		
136		
3.2.2. Development of a GC-MS <i>n</i> -decane oxidation quantification calculator.....		140
3.3. The autoxidation of <i>n</i> -decane and determination of ideal oxidation conditions		147
3.4. Conclusion and future work		151
3.5. References.....		152
CHAPTER 4: Alkane oxidation with metal doped metal oxides and metal doped zeolites		
155		
Abbreviations		156
4.1. Introduction		157
4.2. Decane oxidation		158
4.2.1. Determination and optimization of oxidation conditions – avoiding autoxidation		
159		
4.2.1.1. Effect of changes of temperature		159

4.2.1.2.	Effect of changes of pressure	163
4.2.1.3.	Effects of changes of stirrer speed.....	167
4.2.1.4.	Changes of M:S (metal to substrate ratios) 1:2000 and 1:1000	170
4.2.1.5.	ICP-OES analysis for the determination of leaching.....	173
4.2.1.6.	Changes of metal loading wt%	174
4.2.2.	Catalytic activity amongst different supports.....	176
4.2.3.	Metal supported bulk TiO ₂	180
4.2.3.1.	Wet impregnation metal-doped bulk TiO ₂	180
4.2.3.2.	The effect of catalyst reduction on activity	185
4.2.4.	Alternative supports for <i>n</i> -decane oxidation.....	189
4.2.4.1.	Zeolite based catalysts	189
4.2.4.2.	Niobium oxide-based catalysts	198
4.3.	Cyclooctane oxidation	203
4.3.1.	Cyclooctane oxidation with iron-based materials	204
4.3.2.	Cyclooctane oxidation with noble metal-based materials.....	209
4.4.	Conclusion and future work.....	211
4.5.	References.....	214
CHAPTER 5: The synthesis of micro and mesoporous titanium oxide, varying template removal techniques and subsequent catalytic testing		221
Abbreviations		222
5.1.	Introduction	223
5.2.	Antonelli's protocol for the synthesis of microporous titanium oxide	225
5.2.1.	Change of ratio of titanium precursor to amine template	233
5.2.2.	Varying autoclave conditions.....	234
5.2.3.	Varying titanium alkoxide precursor.....	237
5.2.4.	Introduction of dopant metals during synthesis.....	239
5.2.5.	Thermal resistance and calcination for template removal	243
5.2.6.	Template removal: Acidification.....	246
5.2.6.1.	Acidification via HNO ₃	246
5.2.6.2.	Acidification with <i>p</i> -TSA.....	252
5.2.7.	Summary of template removal attempts – calcination and acidification	252
5.2.8.	Template removal: Alternatives to acid.....	253
5.2.8.1.	Hydrogen peroxide	253
5.2.8.2.	Phthalic anhydride	257
5.2.9.	Reaction resistance and catalytic tests.....	259
5.3.	Dai and Zhang synthesis of microporous titanium oxide	261
5.3.1.	Alternative synthesis of microporous titanium oxide with amine templates	262
5.3.2.	Template removal - Zhang	263

5.4. Non-template synthesis method: Peptization.....	265
5.4.1. Synthesis and subsequent metal loading	265
5.4.2. Catalytic testing.....	267
5.4.2.1. <i>n</i> -decane	267
5.4.2.2. Cyclooctane.....	268
5.5. Conclusions and future work	271
5.6. References.....	272
CHAPTER 6: The synthesis of microporous niobium oxide	275
Abbreviations	276
6.1. Introduction	277
6.2. The synthesis of microporous niobium oxide.....	278
6.2.1. Sun Tao's protocol for the synthesis of microporous niobium oxide	278
6.2.2. Antonelli's protocol for the synthesis of porous niobium oxide	283
6.3. Introduction of dopant metals during synthesis.....	285
6.4. Microporous Nb ₂ O ₅ thermal resistance and calcination for template removal	287
6.5. Template removal: Acidification.....	289
6.6. Template removal: Alternatives to acid.....	295
6.7. Catalyst testing and metal oxide framework reaction resistance.....	298
6.7.1. As synthesised materials.....	298
6.7.2. Template free materials.....	300
6.8. Conclusions and future work	305
6.9. References.....	306
CHAPTER 7: Conclusion and future work	309
References.....	316
Appendix	318
A.1 ¹ H NMR spectra of <i>n</i> -octane and corresponding oxidation products	319
A.2 ¹ H NMR spectra of <i>n</i> -decane and corresponding oxidation products	329

Abbreviations

AIPO – Aluminophosphate

ANA - Analcime

BDE – Bond Dissociation Energy

BET – Brunauer-Emmet-Teller

COSHH – Control Of Substances Hazardous To Health

CMB – Carbon Mass Balance

CP – Coprecipitation

CTAB – Cetyltrimethylammonium Bromide

DCM – Dichloromethane

DMF – Dimethylformamide

DP – Deposition Precipitation

EDTA – Ethylenediaminetetraacetic Acid

FID – Flame Ionisation Detection

FTIR-ATR – Fourier Transform Infra-Red – Attenuated Total Reflectance

GC-MS – Gas Chromatography – Mass Spectrometry

GIS – Gismondine

HPLC – High Performance Liquid Chromatography

ICP-OES – Inductively Coupled Plasma – Optical Emission Spectroscopy

IRE – Internal Reflection Element

IWI – Incipient Wetness Impregnation

KA Oil – Ketone-Alcohol oil

MCM-41 – Mobil Composition of Matter #41

MOF – Metal Organic Framework

M:S – Metal to substrate ratio

NIST – National Institute of Standards and Technology

NMR – Nuclear Magnetic Resonance

PO_2 – Pressure gauge O_2

POM – Polyoxometalate

p-TSA – *para* Toluene Sulphonic Acid

SBA-15 – Santa Barbara Amorphous Type Material #15

SHOP – Shell Higher Olefin Process

SI – Sol-immobilisation

TBHP – *tert* Butyl Hydroperoxide

TEM – Transmission Electron Microscopy

TEMPO – (2,2,6,6-Tetramethylpiperidin-1-yl)oxyl

TGA – Thermogravimetric Analysis

TMS-1 – Transition metal oxide molecular sieve #1

TS-1 – Titanium Silicate #1

UV – Ultra-Violet

WI – Wetness impregnation

XPS – X-ray Photoelectron Spectroscopy

XRPD – X-ray Powder Diffraction

ZSM-5 – Zeolite Socony Mobil #5

CHAPTER 1: Introduction

Contents

CHAPTER 1: Introduction.....	9
Abbreviations	10
1.1. Fundamental concepts of catalysis.....	11
1.2. Industrial manufacture of linear primary alcohols.....	16
1.2.1. Hydroformylation.....	16
1.2.2. Ziegler alcohol process	19
1.2.3. Shilov	20
1.3. Oxidation of alkanes using molecular oxygen.....	22
1.3.1. Autoxidation	27
1.3.2. Oxidation of alkanes via promoters or oxygen transfer reagents	29
1.3.3. Biocatalysts for alkane oxidation	31
1.4. Shape selective catalysis	34
1.4.1. Concept	34
1.4.2. Shape selective catalysts for the oxidation of alkanes.....	36
1.4.2.1. Molecular sieves and zeolites used in shape-selective catalysis.....	36
1.4.2.2. Metalloporphyrins	39
1.5. Microporous and mesoporous framework solids.....	41
1.5.1. Microporous and mesoporous metal oxides	42
1.5.2. Zeolites	47
1.5.3. Aluminophosphates.....	49
1.6. Supported metals for oxidation catalysis	51
1.6.1. Basic principles of supported nanoparticles, nanoclusters and isolated atoms	51
1.6.2. Nano-sized catalysts vs. bulk material.....	51
1.6.3. The effect of the support	53
1.6.4. Leaching	54
1.7. Project scope and thesis development	55
1.8. References.....	58

Abbreviations

AlPO – Aluminophosphate

ANA - Analcime

BDE – Bond Dissociation Energy

BET – Brunauer-Emmet-Teller

FTIR-ATR – Fourier Transform Infra-Red – Attenuated Total Reflectance

GC-MS – Gas Chromatography – Mass Spectrometry

GIS – Gismondine

MCM-41 – Mobil Composition of Matter #41

MOF – Metal Organic Framework

NMR – Nuclear Magnetic Resonance

POM – Polyoxometalate

SBA-15 – Santa Barbara Amorphous Type Material #15

SHOP – Shell Higher Olefin Process

TBHP – *tert* Butyl Hydroperoxide

TEM – Transmission Electron Microscopy

TS-1 – Titanium Silicate #1

UV – Ultra-Violet

XPS – X-ray Photoelectron Spectroscopy

XRPD – X-ray Powder Diffraction

ZSM-5 – Zeolite Socony Mobil #5

1.1. Fundamental concepts of catalysis

Linear, fatty (C_6 to C_{22}), primary (C_1 position) alcohols are important precursors for a range of chemicals in industry (Table 1.1.1).¹ The difference in polarity in these molecules, between the polar OH and non-polar alkyl chain, gives them desirable properties for creating pastes, lubricants and moisturisers.² They can be processed into other materials further down the production line ultimately being involved in sweeteners, perfumes and cosmetics. Currently there is a global demand for 2 million tons of fatty alcohols per year with an expected 4.3% annual growth rate.^{2,3} It is therefore a must that their production is efficient and cost effective.

Table 1.1.1: A selection of linear fatty primary alcohols with examples of their use in industry.

Alcohol	Example of use	References
1-octanol	Perfumes, flavourings, precursor to 1-octene (used in polymer industry)	[4-6]
1-decanol	Solvents, surfactants, lubricants and anti-foaming agents	[7]
1-dodecanol	Precursor to sodium dodecyl sulphate (used in fabric conditioners and degreasers)	[8,9]
1-hexadecanol	Flavours, intermediates for perfumes and bases of creams and ointments	[10]

The focus of this project is to catalyse the synthesis of linear fatty alcohols from the oxidation of alkanes (section 1.2-1.3). Specifically, 1-decanol was chosen as a target starting point due to its appropriate physical properties for our equipment (e.g. boiling point, viscosity, commercial availability) and from its relevance in industry as it is used to produce a range of products such as surfactants, lubricants and cosmetics.⁷ From what is found in C_{10} oxidation we can then apply and move onto varying chain length substrates.

A catalyst is something which speeds up a reaction, without being used up during the reaction. Its presence in a reaction provides an alternative and lower energy pathway for reagents and/or intermediates during a reaction (figure 1.1.1).¹¹ The rate constant, k_r (eq. 1.1.1), is increased either by reducing the activation energy E_a (here E_a is regarded in terms of Gibbs free energy) of the reaction, or by increasing the frequency factor A , or both of these factors. Activation entropy is also decreased when catalysis occurs via adsorbed species on a surface.¹² These factors keep the pre-exponential factor high.

$$k_r = A \cdot \exp\left(-\frac{E_a}{RT}\right) \quad \text{eq. 1.1.1}$$

Where A is the pre-exponential factor, E_a is the activation energy, R is the gas constant and T is temperature of the reaction.

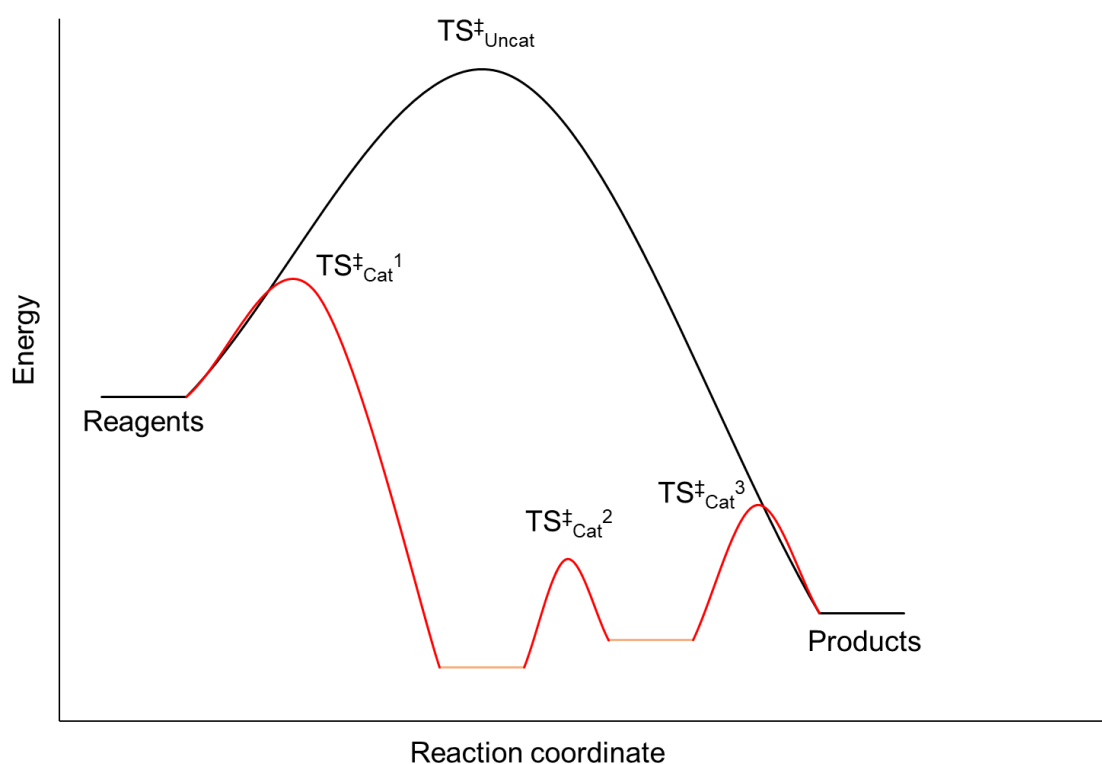


Figure 1.1.1: A schematic to show the concept of how a heterogeneous catalyst may affect the activation energy required for a reaction process to occur.^{11,13} Additional transition states may be present due to adsorption, desorption and intermediates not formed in the uncatalyzed reaction.

This allows a reaction to be faster than the uncatalysed reaction if the temperature is the same; or to have the same rate and to be conducted at lower temperatures and thus require a lower energy demand. However, this is not only the case, as (both desired and undesired) products whose production are typically higher in energy through unavailable pathways can also be reached. It is these properties that can be exploited and refined to lead a reaction to desired products.

Catalysis is a corner stone in industry. Approximately 90% of all chemicals produced have been made with at least one step involving a catalyst.¹⁴ Therefore the development of new, novel and more efficient catalysts is of high importance within chemistry, with intensive research of the field being conducted globally and within the UK.¹⁵ Catalysis is split into two main fields; heterogeneous catalysis, where the catalyst is in a different phase to its reactants (e.g. a solid catalyst with reactants in gaseous phase). Whereas in homogenous catalysis, the catalyst is in the same phase as its reactants (e.g. a catalyst soluble in aqueous phase with reactants in aqueous phase). Although the use of homogenous catalysts is present within industry (e.g. cobalt in hydroformylation, see section 1.2.1),¹⁶ typically heterogeneous catalysts are used and preferred due to their ease of separation from the reaction media (and in turn their recovery), or for the design of catalytic beds in flow reactors.¹⁷ Because of the advantages of heterogeneous catalysis, this will be the focus of this research project.

Selectivity is an important concept especially in industrial catalysis. It is essential that large scale reactions only produce desired products, as waste products can be costly to dispose of and ultimately lead to a less efficient, less economic and more wasteful process.^{18,19} Selectivity is often achieved through defined active sites, which is most common in homogenous catalysts (and predominantly in biocatalysts, section 1.3.3).²⁰ However, examples of selective heterogeneous catalysts exist. Selective oxidation of propylene to acrolein, which is needed for herbicides and acrylate polymers²¹ is achieved using a range of heterogeneous catalysts (e.g. silver on alumina catalysts and copper oxide catalysts

have been extensively studied).^{22,23} Modern catalysts have achieved selectivities of >95% at ~95% conversion, despite the large difference in enthalpy to the complete combustion products (-2060 kJ mol⁻¹ vs. -336 kJ mol⁻¹).¹⁴ This is crucial as a highly active oxidation catalyst is useless if the desired products are completely oxidised to CO₂ and H₂O. This is a relevant example where only a few products are possible, as molecules become larger and more complex, so does the challenge of selective catalysis.

The efficiency of a chemical reaction can be determined using *E* factor. *E* factor can be defined as the *mass ratio* of waste products and desired products, allowing a means to compare the efficiency between chemical processes.¹⁸ A list of *E* factor ranges for industrial sectors can be found in table 1.1.2.²⁴

Table 1.1.2: *E* factors for corresponding chemical industries.²⁴

Industry segment	<i>E</i> factor (kg waste product/ kg desired product)
Oil refining	< 0.1
Bulk chemicals	< 1 - 5
Fine chemicals	5 - >50
Pharmaceuticals	25 - >100

The oil refining industry is conducted on the largest scale of all chemical industries. However, it has impeccably efficient processes leading to its lower *E* factor. The fine chemicals and pharmaceutical industries therefore have scope for processes to be made more efficient. In our case we will focus on the fine chemicals sector, as this is where linear fatty alcohols are categorised.

Efficiency of a process can also be improved by choice of reagents. If possible, avoiding the use of stoichiometric reagents inherently reduces the cost of a process. For example, using molecular oxygen as the sole oxidant as opposed to those which need to be synthesised, such as H₂O₂ and aqueous metal complexes. Using H₂O₂ is preferred over

aqueous metal complexes due to water being the only by-product and is considered a 'green' oxidant.^{25,26} However, using molecular oxygen from the air would be ideal due to its much larger availability and not needing to synthesise H₂O₂. A range of reactions using molecular oxygen as the sole oxidant have been developed,²⁷ but the majority of oxidation reactions in industry do not exclusively use O₂ or are not sufficiently selective. The implications of using molecular oxygen are discussed in further detail in section 1.3.

Moreover, chemical reactions typically take place in a solvent.^{28,29} This is problematic for industrial processes as capital and energy are lost in either supplying fresh solvent or in processes which recycle it. Therefore, the use of 'neat' reagents is a desirable concept in industry.^{28,30} For example, the oxidation of hydrocarbons can be done without a solvent.³¹ Avoiding the use of solvents also makes separation of products easier. This is because the catalyst, unreacted reactants and products are only within the reaction mixture. Again, this saves time, energy and cost within an industrial process.

The effect of replacing stoichiometric oxygen-transfer reagents is twofold: additional materials are not required to be purchased for the input, and unwanted by-products from these are not made as an output.^{32,33} A significant example of this concept is the use of copper (supported onto a range of supports like zeolites and metal carbonates) for the oxidation of alcohols to aldehydes and ketones.³⁴ Traditionally, the conversion of alcohols to ketones is done with a stoichiometric oxidant, which is typically toxic (e.g. chromates, manganates).³⁵ However, a significant amount of literature was produced showcasing the oxidation of alcohols with copper complexes. Marko *et al.* showed that a copper phenanthroline complex deposited onto K₂CO₃ was capable of oxidising alcohol functional groups (on aryl/ olefin compounds).³⁶ This chemistry provides a means to oxidise alcohol groups to carbonyls with oxygen from air and water being the only by-product. Examples like this are showing progression towards the replacement of toxic oxygen-transfer stoichiometric reagents (e.g. high valent Mn and Cr salts)³⁷ for greener alternatives.

Within the context of this research project, we seek to oxidise alkanes without the addition of any stoichiometric oxygen-transfer oxidants (i.e. hydrogen peroxide and *tert* Butyl hydroperoxide) and develop a system which is solvent-free.

1.2. Industrial manufacture of linear primary alcohols

There are three main industrial processes to produce fatty alcohols which will be discussed here. It is important to highlight how primary fatty alcohols are currently synthesised and why there is a need for an alternative process for their production. In fact, our materials and the chemistry involved in the catalyst that we will develop are designed precisely to tackle the drawbacks of the current manufacturing routes.

Note, throughout the document 'primary' or 'terminal' will be used to refer to the C₁ position of an alkyl chain, whereas 'central' will be used for C_{n+1, n>0}.

1.2.1. Hydroformylation

Hydroformylation (also known as the oxo-process) is where a homogenous catalyst, typically cobalt based, is used to convert terminal olefins to their corresponding aldehydes.³⁸ This process is one of the largest commercial production scales which uses a homogenous catalyst. Because of its scale, the process has been optimised using multistep (and even some multiphase) reactors.³⁸⁻⁴¹ Hydroformylation was originally developed using a cobalt catalyst for the hydrocarbonylation of ethylene, but has been developed into other technologies, such as the production of alcohols described here. During the process of aldehyde production, the catalyst builds alkyl chains via alkene units and then terminates the process by adding a 'HC=O' moiety via hydrogen and carbon monoxide. The aldehyde is then reduced further down the production line to the corresponding alcohol, summarised in figure 1.2.1.1.⁴²

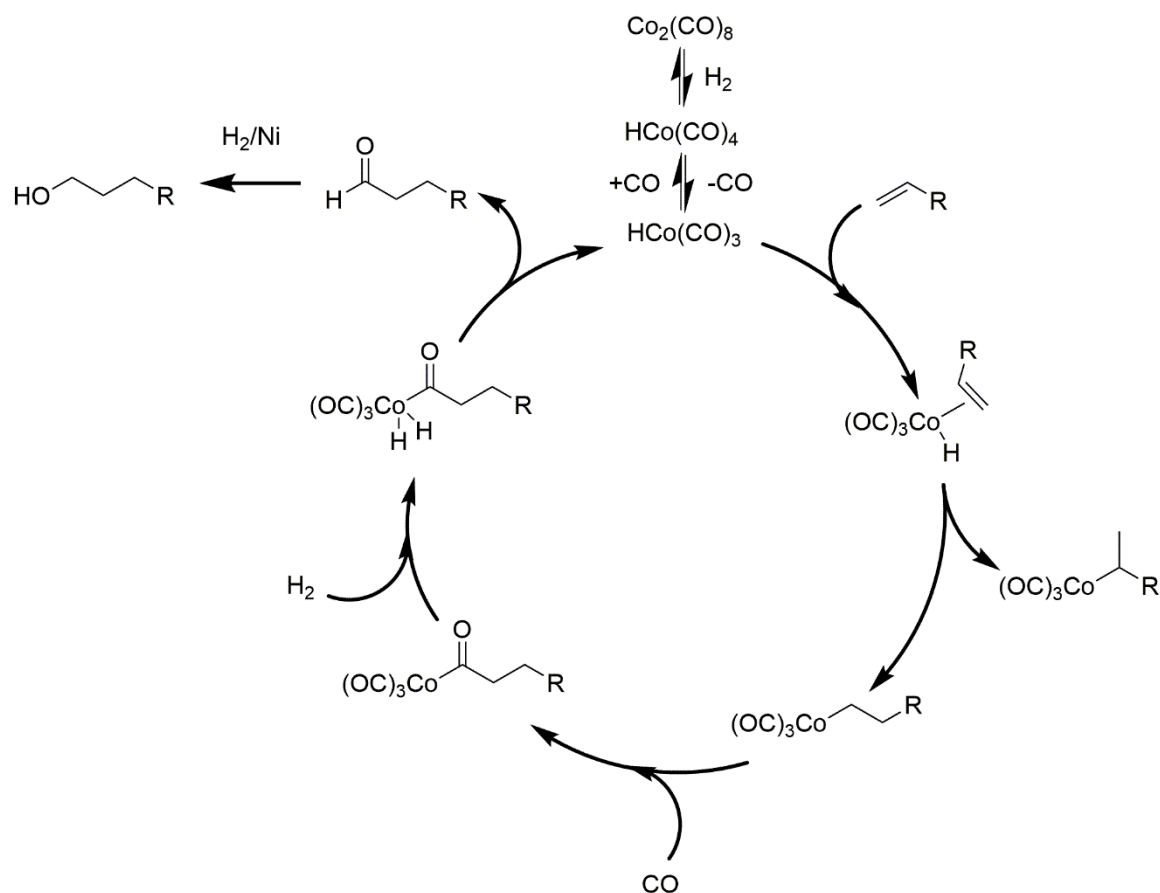


Figure 1.2.1.1: A catalytic cycle of the hydroformylation process using a cobalt catalyst.⁴²

The SHOP (Shell Higher Olefin Process) is a process which incorporates hydroformylation during the production of fatty alcohols. Ethene is oligomerized to C_{2x} olefins followed by distillation to separate products via chain length. The $\text{C}_{10} - \text{C}_{14}$ olefin fraction is then selected for carbonylation, where fractions of lower carbon length are recycled until the desired chain length is met.⁴³ However, there is a drawback with this process as chain lengths can only grow by C_2 . Therefore, once carbonylation occurs from the addition of 'HCO', aldehydes (and therefore alcohols) derived from this process will be limited to odd number carbon chain lengths.

Another problem with this process is the strong competition between production of long, linear olefins with branched central alkenes. This occurs due to the favourable

isomerisation of long chains, ultimately leading to a lower yield of aldehydes (figure 1.2.1.2).³⁸

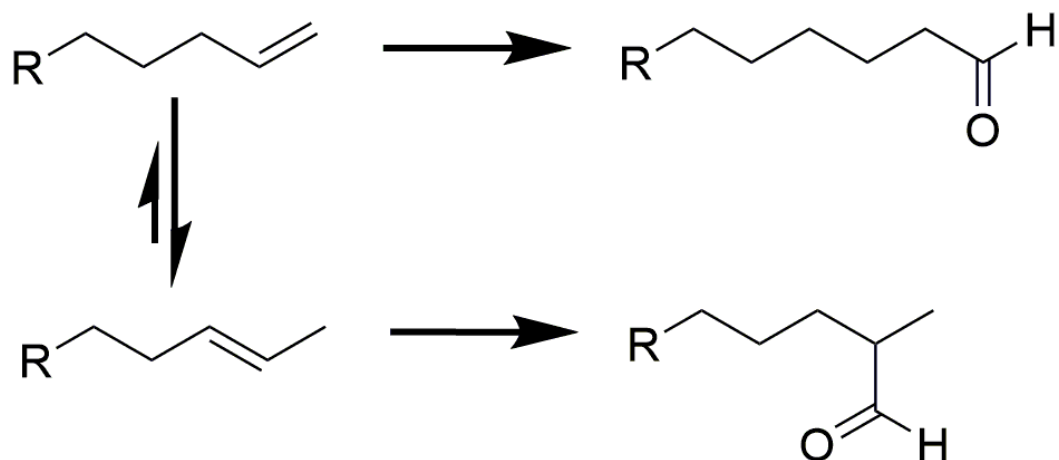


Figure 1.2.1.2: Competing favourable isomerisation reactions during hydroformylation leading to non-terminal carbonyl compounds.

Finally, none of the processes used industrially with this method are heterogeneous. Homogenous catalysts are problematic in industry due to their requirement for large scale separation from the products. Luft *et al.* studied the immobilisation of catalysts used for long chain alkene hydroformylation.⁴⁰ A rhodium catalyst was immobilised on activated carbon pellets used for the hydroformylation of 1-hexene. It was found that the initial reaction rate was 7 times lower than when using the heterogeneous catalyst in comparison to homogenous catalysts and also generated a reaction mixture with a lower *n/iso* ratio. Moreover, the study revealed that the overall leaching of the system after 100 days (more than 60 batches, which is low in comparison to conditions used in industry where 2 years is the average desired lifetime) was 6% of the original amount, a threshold beyond which the catalyst would need re-generation and in turn the process would not be fully economically viable. Although the heterogeneous catalysts performed worse than the homogenous, this study is crucial in taking steps toward making a heterogeneous hydroformylation process.

1.2.2. Ziegler alcohol process

The Ziegler process converts ethylene, hydrogen, oxygen and water to linear fatty alcohols via organoaluminium compounds (summarised in figure 1.2.2.1).²

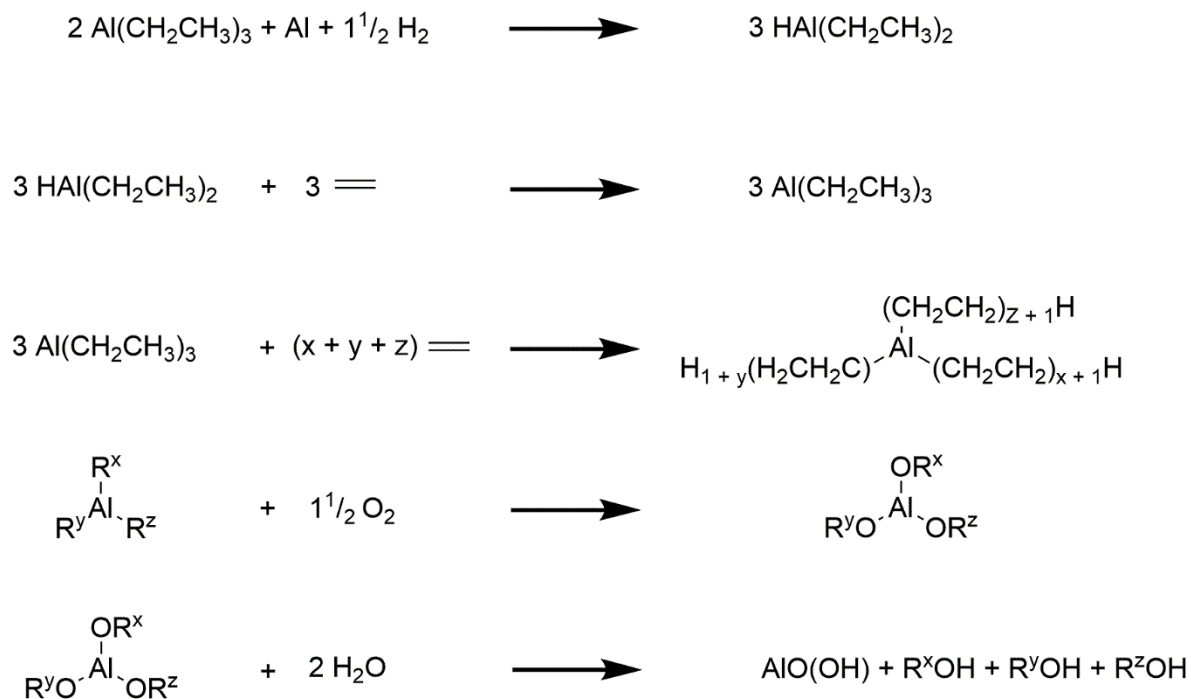


Figure 1.2.2.1: A scheme to show the steps during the Ziegler alcohol process.²

This is an elegant process by which only primary alcohols can be formed due to the hydrolysis step only being able to cleave one Al-C bond, which is always terminal. However, as the growth of the hydrocarbon chain practically follows a similar growth pattern to that of a polymer, it follows the resultant chain length of the resulting primary alcohol is not uniform in this process, and therefore a distribution amongst products occurs. Two industrial processes involved this synthesis: Alfol and Epal, the latter of which achieved a narrower distribution of products.^{2,44}

However, the Ziegler process is not strictly catalytic as a stoichiometric amount of aluminium reagents are required for this process. Therefore, during this synthesis a stoichiometric amount of undesired aluminium by-product is produced. Currently there are no systems which can *catalytically* produce long chain alcohols via the Ziegler alcohol process.

1.2.3. Shilov

The 'Shilov system' is a promising process where alkanes are activated via a homogenous platinum chloride catalyst in a biphasic system with one of the two phases being water.⁴⁵ Shilov *et al.* found that $[\text{Pt(IV)Cl}_6]^{2-}$ can be used as a primary oxidant generating a Pt(II) complex to convert alkanes to primary chloroalkanes (which can be converted into primary alcohols). It has a complex reaction mechanism, studied by Labinger and Bercaw, summarised in figure 1.2.3.1.⁴⁵⁻⁴⁷ The system gave excellent selectivity towards terminal functionalisation. The selectivity arises from steric factors as the bulky chloride ligands only allow for the terminal C-H bond to be activated.⁴⁸

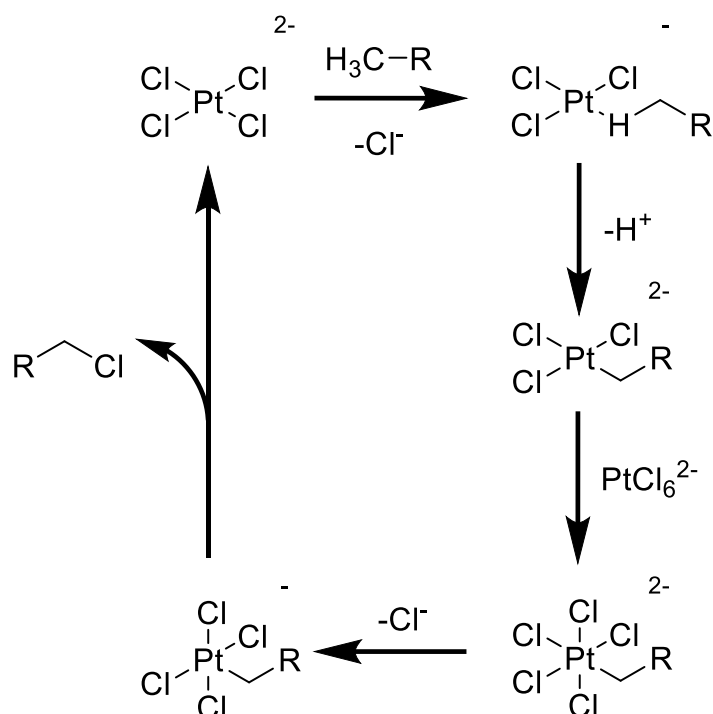


Figure 1.2.3.1: One of Labinger and Bercaw's proposed mechanisms for the Shilov system, the aqueous metal salt is in a separate phase to the organic hydrocarbon. Adapted from *R. H. Crabtree* with permission.⁴⁷

Nevertheless, there are draw backs of this process. In order for this reaction to continue a stoichiometric amount of platinum(IV) chloride salt needs to be fed to the system. The reaction is catalytic but provided stoichiometric amounts of platinum(IV) chloride are needed to regenerate the active species, the reaction is not feasible due to high cost and reservations are currently present due to low abundance of platinum. Furthermore, the system is biphasic from the nature of the reagents, thus alkane solubility - which is

inherently low in water - becomes a limiting factor in conversion. Finally, there is uncertainty how water affects the extent of the reaction as the reaction mechanism is still not entirely understood, with some studies suggesting the O incorporated in the final product is from water.⁴⁹

Sen *et al.* developed a catalytic Shilov system using oxygen as the oxidant, relinquishing the need for stoichiometric platinum(IV) chloride.⁵⁰ The system remained selective to the primary position of the alkyl chain utilising copper chloride to regenerate the active platinum species. However, the substrate used was ethanesulfonate and the study did not report any attempts with linear alkanes. To date no selective oxidation of alkanes via a Shilov system using molecular oxygen as the oxidant exists.

In summary the Shilov system shows fantastic promise with its selectivity but is far from being industrially applicable. Stoichiometric amounts of platinum chloride are not feasible for reaction scales required. The process is also limited to biphasic systems, where conversion is limited to the solubility of alkyl reagents. Finally, as mentioned in hydroformylation, the system would ideally be made heterogeneous and this may affect conversion and selectivity.

1.3. Oxidation of alkanes using molecular oxygen

The selective oxidation of linear fatty alkanes is a challenging reaction, regardless of the specific oxidizing agent used. This arises from very minor differences in bond dissociation energy of the C-H bonds amongst the alkyl chain, leading to no specific region significantly favouring oxidation and thus producing a range of potential products, e.g. *n*-octane oxidation (figure 1.3.1).^{51–53}

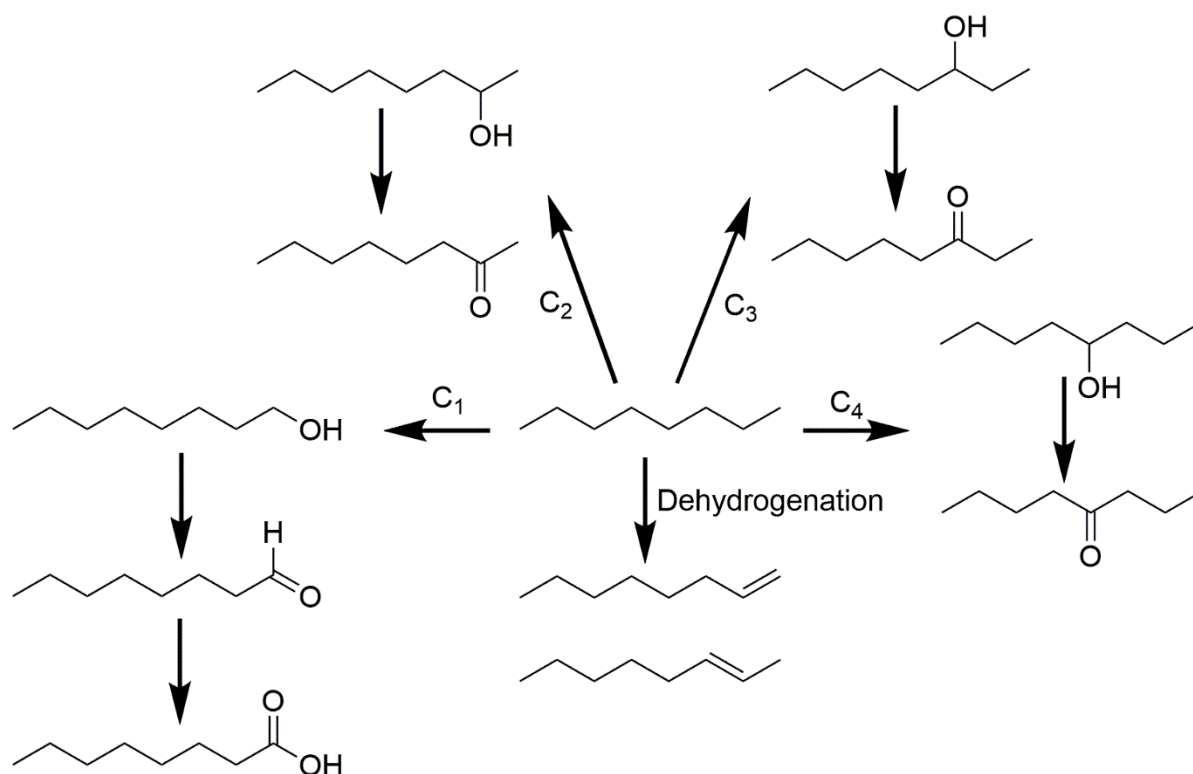


Figure 1.3.1: Examples of possible products during *n*-octane oxidation. Insertion of oxygen is possible to form alcohols and/or carbonyl compounds, at each position on the chain and dehydrogenation can lead to alkenes. Not shown here is the potential products from cracking (leading to shorter chain compounds) or condensation reactions between alcohols and acids.

In the example of *n*-octane from figure 1.3.1, there is a statistical probability of 33% (6H/18H) to oxidise the terminal C-H bond. This probability will decrease with substrates of longer chain lengths, due to more central CH₂ units capable of being oxidised (e.g. the terminal oxidation chance is 27% in *n*-decane, 23% in *n*-dodecane, and so on). However, the central CH₂ is energetically more favourable to oxidise over terminal CH₃.⁵⁴ For example, in butane the terminal C-H bonds have a bond dissociation energy (BDE) of ~101

kcal mol⁻¹ (423 kJ mol⁻¹), compared to the central C-H bonds with 98 kcal mol⁻¹ (410 kJ mol⁻¹).⁵⁵ Therefore, one can correctly assume that the product distribution will be proportionally low for terminal oxidation products of alkanes where no selectivity is induced. Furthermore, if alcohols are the desired product, oxidation to carbonyls must be prevented, despite alcohols having a tendency to be over oxidised.⁵⁶ This is due to the lower BDE of the C-H alpha to an OH group typically being ~30 kcal mol⁻¹ lower in energy compared to that of the saturated hydrocarbon.⁵⁷ Therefore, in order to selectively oxidise alkanes to linear primary alcohols, a catalyst needs to provide shape selectivity whilst avoiding over oxidation.

In this research work we are interested in the use of molecular oxygen as the sole oxidant. A common claim within literature is 'alkane oxidation via molecular oxygen', however, the term 'alkane' is broad within the field of alkane oxidation and type of alkane should always be clarified. For example, an article by Mizuno and Yamaguchi demonstrated how a ruthenium based polyoxometalate (POM) was capable of 'alkane' oxidation via autoxidation. A summary of their results is quoted in table 1.3.1.⁵⁸

Entries 1 – 4 show the proof of concept that ruthenium polyoxometalates can indeed oxidise alkanes, with the highest conversion and selectivity observed with adamantane. Adamantane is a useful model to show that a catalyst is capable of activating C-H bonds.

Table 1.3.1: From Mizuno and Yamaguchi, substrate (1 mmol), Ru POM (0.5 μ mol), isobutyl acetate (3 ml), O₂ atmosphere, ^a 373 K, ^b 383 K.⁵⁸ Reproduced from Ref.⁵⁸ with permission from the Centre National de la Recherche Scientifique (CNRS) and The Royal Society of Chemistry.

Entry	Substrate	Time (h)	Yield (%)
1 ^a	Adamantane	72	64
2 ^a	Cyclohexane	48	3
3 ^b	Cyclooctane	96	12
4 ^b	<i>n</i> -octane	96	3
5 ^a	2-adamantanol	96	99
6 ^a	Cyclohexanol	48	67
7 ^b	Cyclooctanol	96	98
8 ^b	1-octanol	48	14
9 ^b	2-octanol	120	90

Although the products of adamantane oxidation are still of commercial importance, the substrate is easy (in comparison to linear alkanes) to oxidise due to its several secondary C-H bonds. Moreover, selectivity is easier to achieve as owing to its symmetrical structure they are less possible by-products (figure 1.3.2)⁵⁹ compared to the linear alkanes quoted here. Furthermore, entries 5 – 8 show that the catalyst is capable of over oxidation from the high yields of alcohol oxidation, a problem common amongst catalysts in the literature.

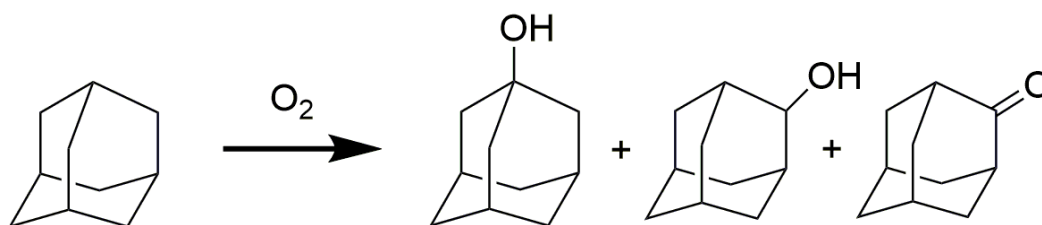


Figure 1.3.2: The oxidation products of adamantane. Although not a linear alkane, it is an important molecule to act as a model for C-H activation.

Mizuno *et al.* also showed that highly selective oxidation can be achieved when using bulky vanadium POM-based catalysts.⁵⁶ Using hydrogen peroxide and a homogenous catalyst, a range of alkane substrates were oxidised. Most interesting for this research was the oxidation of *n*-hexane. Although a lower yield of 56% was achieved (compared to 98% seen in adamantane), an exceptional 94% selectivity was observed for the corresponding alcohols. Results like this are both rare and highly significant due to the challenge of avoiding over-oxidation to ketones, acids and other oxidation products.

From all the literature considered in this research, only two research groups have shown the ability to oxidise long-chain linear alkanes, solvent-free, under mild conditions when using a catalyst. Richards *et al.* has numerous publications for the oxidation of *n*-hexadecane under mild oxidation conditions, these are summarised in table 1.3.2.^{29,30,60–62} These results are important in the field of alkane oxidation as conversions this high (even >5%) with no initiator and at 150 °C with no pressurized systems are not only rare, but also highly desired. Similarly, Bi *et al.* showed their 'SBA-15-apt-Ru-2' (a ruthenium-based POM on SBA-15, pore size = 4.5 – 5.2 nm) was capable of *n*-hexadecane conversions of up to 52% under identical conditions to that of Richards' group.⁶³ Out of all the literature on alkane oxidation, these are the only two groups that have succeeded in very high conversions, with very mild conditions.

Table 1.3.2: A compilation of results for the oxidation of *n*-hexadecane from Richards' research (highest conversions from each publication recorded here).^{29,30,60–62}

n-hexadecane (5 mL), T = 150 °C, air flow = 30 ml min⁻¹, t = 6 h

Catalyst	Conversion (%)	Pore size (nm)	Ref.
SBA-apts-Fe₄Se₂W₁₈ (Fe-POM immobilised on SBA-15)	18	5.8	[60]
Zr_{1-x}Fe_xO_y (Iron doped zirconia aerogels)	36.2	15.9 – 24.9	[30]
2-2-GMS (Gold nanoparticles dispersed in mesoporous silica)	52.3	5.6	[29]
SBA-15-apts-Cu₂₀ (Cu-POM immobilised on SBA-15)	29.4	5.4	[61]
PW₁₂-TiO₂-ACC (POM and TiO₂-NPs on mesoporous silica)	21	2.85	[62]

1.3.1. Autoxidation

The goal of this research is the selective oxidation of linear alkanes by means of molecular oxygen. Autoxidation phenomena, therefore, were processes which we wanted to avoid as much as possible. As it may be present during the oxidation of alkanes and its influence on reaction mixtures it will be discussed here.

Autoxidation is an ever-present phenomenon where the oxidation of a species can occur in an autocatalytic manner in the presence of an initiator or traces of a promoter (e.g. the walls of a reactor, residual alkyl hydroperoxide in solution, etc.),⁶⁴ a substrate and molecular oxygen. It is an important reaction which may occur wherever molecular oxygen is present, and drastically lowers selectivity of a reaction (if not controlled) due to its free-radical mechanism induced by the homolytic cleavage of the O-O bond in alkyl hydroperoxide intermediates, and is typically absent of a confined active site.⁶⁵ Autoxidation was first studied via the deterioration of rubber and naturally-occurring oils and has since been utilised within the petrochemical industry.⁶⁶ This would ideally be avoided completely due to its inherent low selectivity when oxidising linear alkanes.

The product distribution (often reported as a molar ratio between ketone and alcohol or vice-versa) from an oxidation reaction is a good initial indication of whether the reaction mechanism is occurring via autoxidation. In the oxidation of alkanes, the ratio of alcohols to ketones will be consistent for a given reaction when occurring via autoxidation only.⁶⁷ For example, autoxidation was observed in the oxidation of cyclohexane in the presence of ClO_2^- and a manganese porphyrin complex. During oxidation it was determined whether autoxidation was occurring by observing a 1:1 ratio of ketone and alcohol (indicative of autoxidation of cyclic alkanes),^{68,69} whereas the non-autoxidative pathway only produced the alcohol.⁶⁸ A rule of thumb can be applied to the expected selectivity from the autoxidation of linear fatty alkanes, where the ratio of carbonyls to alcohols is roughly 2:1 (to 3:2),⁷⁰ shown in figure 1.3.1.1 and figure 1.3.1.2.^{65,67,71,72} In the case of linear alkanes, oxidation can occur at any of the positions along the chain. When analysing reaction

mixtures this will give a quick indication on whether the mechanism has occurred via autoxidation.

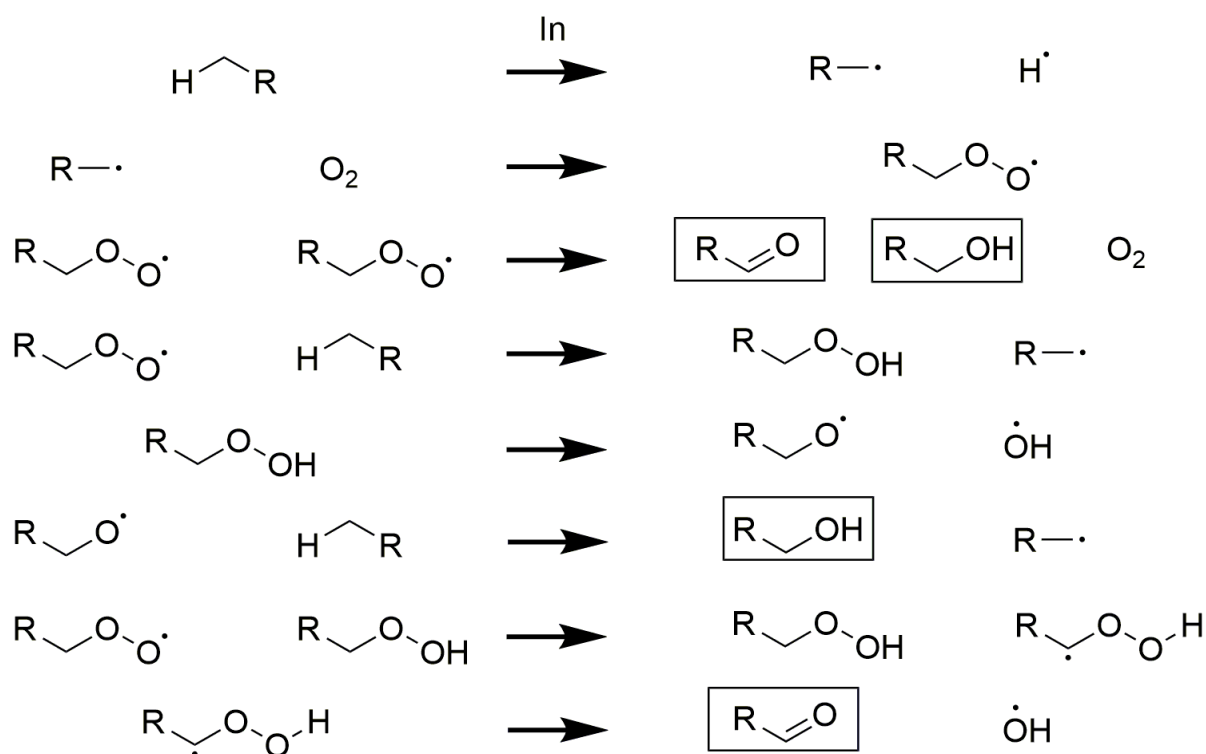


Figure 1.3.1.1: Possible mechanistic steps for the autoxidation of an alkane. 'In' represents an initiator (e.g. a metal centre, oxidising agent, intermediate). Alcohol and carbonyl products have been highlighted. Note: For sake of simplicity only the C₁ position has been shown here, oxidation is not limited to this position.

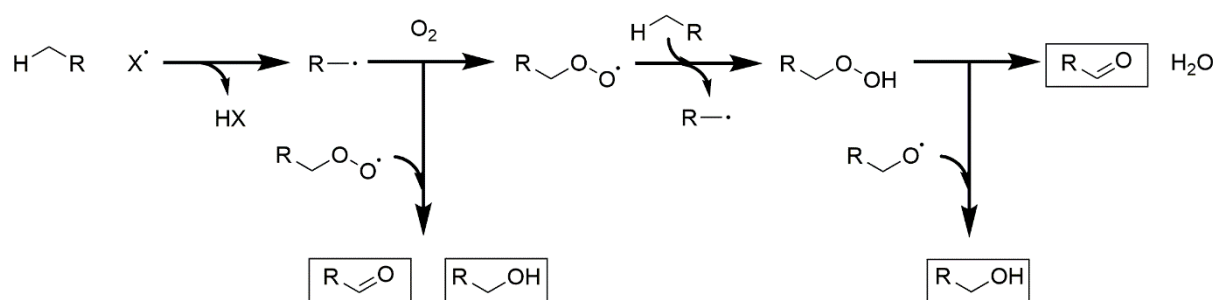


Figure 1.3.1.2: A step by step approach of potential routes for the autoxidation of an alkane.

For the context of this research, autoxidation would ideally be avoided. This is because, as shown by Iglesia *et al.*,⁷³ the generation of ROOH can be problematic for the selective oxidation of linear alkanes. Iglesia's research showed that their Mn exchanged ZSM-57 and ZSM-5 were capable of terminal *n*-hexane oxidation during the beginning of their reaction. However, terminal selectivity decreased with time as the non-catalytic autoxidation mechanism became the dominating reaction.

1.3.2. Oxidation of alkanes via promoters or oxygen transfer reagents

The replacement of stoichiometric reagents for catalytic systems is at the heart of making industrial processes more efficient.¹⁸ Therefore for our research we solely wanted to use oxygen from the air as the oxidant. Within the literature H₂O₂, TBHP (*tert* butyl hydroperoxide) and other oxidants are used extensively for the oxidation of alkanes, table 1.3.2.1.^{56,60,74–79} Although not the purpose of this research, promoters and oxygen transfer reagents will be briefly discussed due to their significant presence within the literature and to show how they may be used in the challenging nature of alkane oxidation.

Hydrogen peroxide is a candidate for 'green' oxidation as its only by-product is water. Que Jr. *et al.* demonstrated excellent selectivity of a homogenous system utilising a tris-pyridyl amine iron(II) complex.⁸⁰ Cyclohexane was oxidised to cyclohexanol, cyclohexanone and cyclohexene. Cyclohexanol was the major product in these reactions, showing how partial oxidation is capable in alkanes via hydrogen peroxide. Furthermore, hydrogen peroxide was utilised in the oxidation of linear alkanes.⁷⁴ TS-1 (titanium silicate-1) was used to catalyse linear alkane (C₃ – C₈) oxidation to alcohols and ketones. Interestingly, the major oxidation products for C₇ and C₈ alkanes were the C₂ alcohol and ketone, ascribed to the shape-selective nature of the catalyst (see section 1.4). While hydrogen peroxide is produced commercially, it still needs to be synthesised and is typically used stoichiometrically and therefore is still not completely 'green'.

Table 1.3.2.1: A summary of relevant and significant literature on alkane oxidation utilizing promoters and oxygen transfer reagents.

Oxidant	Catalyst	Substrate	Ref.
H ₂ O ₂	TS-1	Linear alkanes, branched alkanes and other alkanes	[74,81,82]
H ₂ O ₂	ZSM-5	Propane	[83]
H ₂ O ₂	Ti-Beta	Linear alkanes, alkenes and others	[84]
H ₂ O ₂	Fe/SBA-15	Cyclohexane, cyclic alkenes and others	[85]
H ₂ O ₂	Vanadium-POM/MCM-41	Cyclohexane, cyclic alkanes and others	[86]
TBHP	Au/SBA-15	<i>n</i> -hexane and alkyl substituted benzenes	[78]
TBHP	M/ZSM-5 (M = Co, Fe, Mn, Cu, Ni and Cr)	Cyclohexane	[87]
TBHP	Mn/Zeolite Y	Cyclohexane	[88]

TBHP has been applied to the oxidation of alkanes.^{78,79,87,89} For example, Zhou *et al.* showed that ethylbenzene can be converted almost entirely (>99% yield) to acetophenone. Furthermore, the study converted cyclohexane to cyclohexanone with 100% selectivity when using nickel doped carbon-MOF based materials.⁹⁰ Again, while these results are significant, TBHP is required and produces stoichiometric amounts of undesired *t*-butanol when used as a reagent in oxidation. Therefore, despite TBHP being used extensively within the literature, idealistically O₂ from air will be used to oxidise alkanes due to its prompt availability.

1.3.3. Biocatalysts for alkane oxidation

Although biocatalysts will not be experimentally used in the current research work, they will be briefly described here, as their impact and inspiration on chemical catalysts should be noted.^{91,92} Biocatalysts are catalysts based on enzymes.⁹³ They can be split into two fields: isolated and whole cell.⁹⁴ Isolated biocatalysts are those where the enzyme has been removed from the cell and catalyse a reaction, whereas whole cell involves the use of an enzyme still within a living cell. An enzyme's active site is an example of where shape selective catalysis can occur (see section 1.4).⁹⁵ They are capable of a multitude of chemically important reactions, from selective reactions to stereo chemical control in organic synthesis. For example, chiral resolution of racemic alcohols is achieved via the utilisation of the enzyme lipase.^{92,96}

Alkane hydroxylases have been studied extensively in the selective oxidation of alkanes, table 1.3.3.1.⁹⁷⁻⁹⁹ Cytochrome P450 is often used as inspiration for shape selective catalysts, its reaction mechanism for alkane hydroxylation is described in figure 1.3.3.1.⁹⁵ Another significant example is the use of *P.Putida Alk+* which has been used in the oxidation of *n*-octane,⁹⁶ where an industrial system has been developed by Mathys *et al.*¹⁰⁰ The system utilises a two-phase bioreactor and is capable of mass production of linear alcohols. Selective oxidation occurs as the enzymes are unable to further oxidise 1-octanol and only bind to terminal positions. However, to our knowledge, this system has not been conducted on a commercial scale.

Table 1.3.3.1: A summary of significant examples of alkane oxidation within the literature utilizing biocatalysts.

Catalyst	Substrate(s)	Ref.
P450	<i>n</i> -octane, <i>n</i> -hexane, cyclohexane, <i>n</i> -butane, propane	[101]
Terminal Alkane Hydroxylases AlkB and CYP153A6	<i>n</i> -octane, <i>n</i> -pentane, <i>n</i> -butane, propane, ethane	[98]
P450cam, P350-BM3	<i>n</i> -octane	[102]

Despite the potential for biocatalysts there are disadvantages to their use. When whole cells are used, typically a two-phase liquid system is required to avoid toxic products damaging the enzyme and when *in vitro* enzymes are used, additional cofactors are needed for functionality.¹⁰²

Finally, biotechnology may not be the ideal candidate to completely replace chemical processes in industry. Additional costs occur downstream due to low reactor productivities and essential separation of product from high volume reaction mixtures are required.¹⁰⁰ But as enzymes are adapted to a specific function, they act as a source of inspiration for the design of shape selective catalysts.

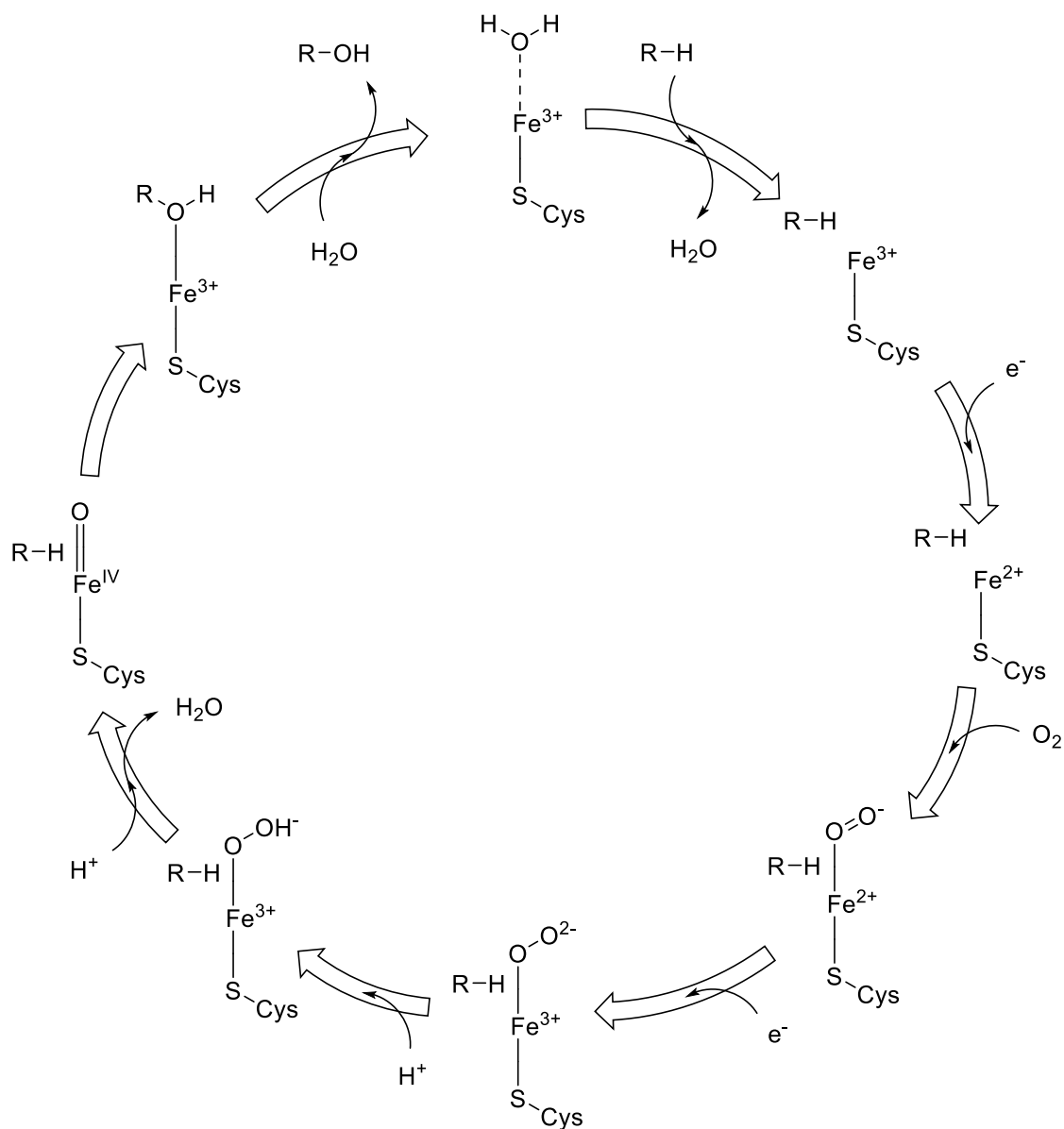


Figure 1.3.3.1: A generic mechanism of alkane oxidation with cytochrome P450. The iron centre is also complexed by a heme prosthetic group (not shown here). Diagram reproduced with permission from *Bordeaux et al.* copyright (2012).⁹⁵

1.4. Shape selective catalysis

1.4.1. Concept

As we will use elements of shape selective catalysis to develop and design some of the materials discussed in this thesis, the fundamental concepts of this approach will be described here. Shape selective catalysis occurs when the catalyst applies a steric factor to limit the potential products of a substrate.^{103–108} These processes take inspiration from enzymes where only a specific active site is capable of catalysis, leading to complementary substrates and products to be bound.¹⁰⁹ Typically, this is achieved in heterogeneous catalysts having a porous framework, or alternatively with homogenous catalysts with sufficiently bulky ligands shaping an active site.^{107,110,111}

Wright lists three important concepts that exemplify what porous solid shape selective catalysts are used for, summarised in figure 1.4.1.1.¹¹² *Reactant diffusion* selectivity is where the pore size is sufficiently small enough to restrict sterically bulky molecules, allowing smaller molecules to diffuse in, this means only a specific group of molecules in a mixture will react. *Product diffusion* selectivity is when different sized molecules are exposed to the catalyst. Smaller molecules will diffuse quickly and only react to a certain extent, whereas bulkier molecules will take more time to pass through the pores and react further. Finally, *transition state selectivity* occurs due to the physical constraints of the pore. Certain transition states will sterically not be adopted compared to when bulk surfaces are used and therefore drive selectivity to specific products.

Within the context of this research reactant selectivity will be developed. Instead of several molecules competing for an active site, several *parts* of a single molecule will compete for an active site. This is because we seek to selectively oxidise the terminal C-H bonds on an alkane over central positions by sterically deterring areas of the molecule from the active site.

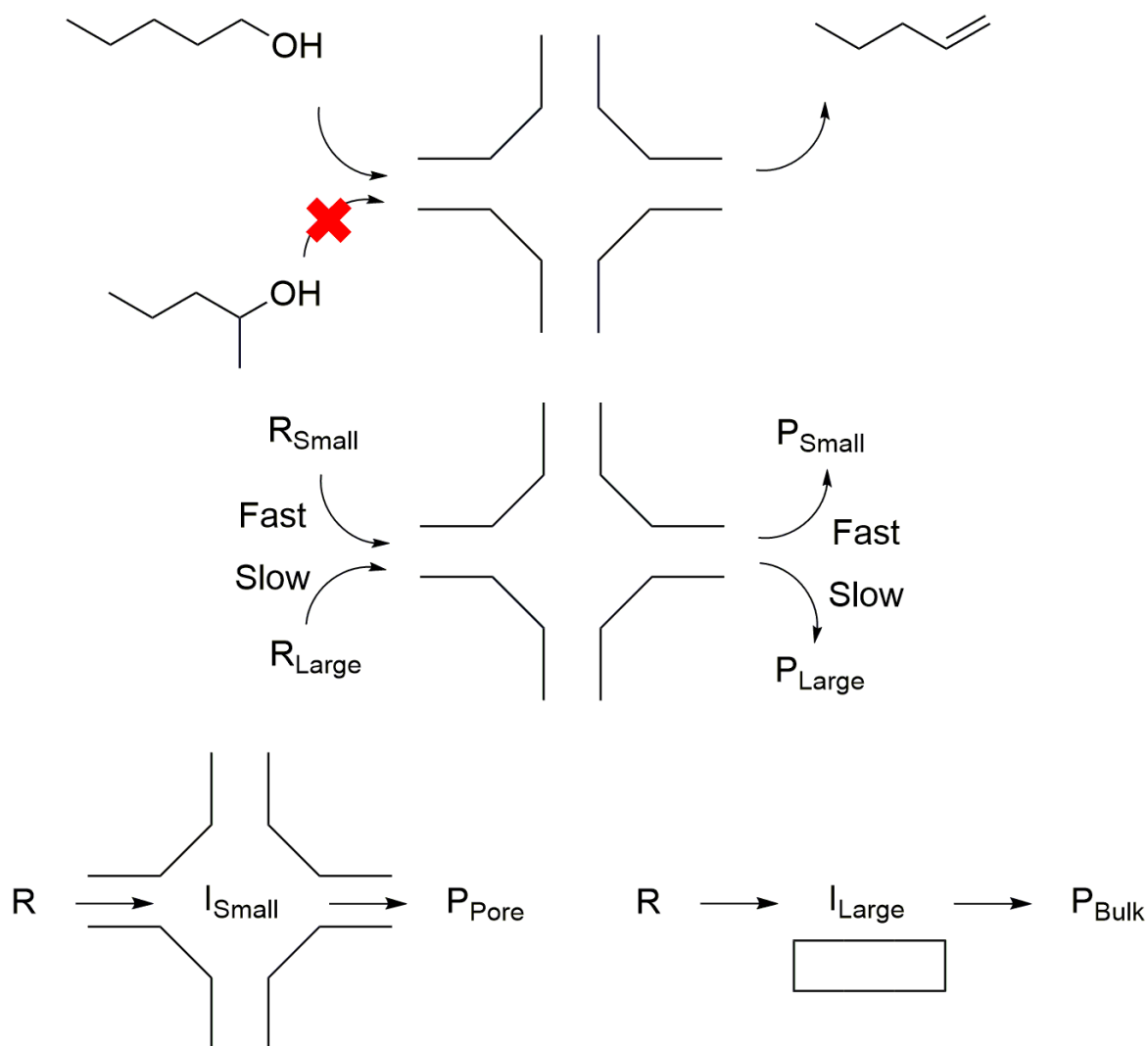


Figure 1.4.1.1: A concept diagram to exemplify the possibilities of shape selectivity. *Top:* Reactant selectivity, *Middle:* Product selectivity, *Bottom:* Transition state selectivity. Adapted from Wright.¹¹² Where 'R' is a reactant, 'I' is an intermediate/ transition state and 'P' is a product, with their relative sizes in subscript.

Not only does shape selectivity affect product distribution but can also change the robustness of a catalyst. Metal active sites on heterogeneous catalysts are susceptible to poisoning from a range of impurities, for example sulphur. Metal clusters incorporated into the framework of zeolites (see section 1.5.2) were found to have less activity reduction when exposed to a sulphur impurity, when compared to non-porous samples.¹¹³ The results summarised in table 1.4.1.1 demonstrate how the porous supported catalysts (with supports Gismondine and Analcime) prevented deactivation of metal active sites. This was

achieved through the steric hindrance of the sulphur impurity not being able to diffuse into the pores in contrast to the smaller reactant (as catalytic activity was still observed). However, the catalysts were deactivated to an extent, as this was due to the presence of exterior framework active sites which initially contributed to catalysis.

Table 1.4.1.1: Data demonstrating how microporous platinum catalysts (GIS – Gismondine, 0.45 nm x 0.31 nm; ANA – Analcime, 0.42 nm x 0.16 nm) suffer less in the presence of poisons compared to their bulk counterpart (SiO₂).¹¹³

Catalyst	Activity reduction factor (Impurity present)	Activity reduction (After impurity removal) (%)
Pt/SiO₂	530	100
Pt/GIS	13	15
Pt/ANA	7	30

1.4.2. Shape selective catalysts for the oxidation of alkanes

As mentioned previously, a significant desire for long chain linear alcohols is present within industry. These products must be made from the direct oxidation of only the primary position. Therefore, not only does the extent of alkane oxidation need to be controlled, but also the position of oxidation.

1.4.2.1. Molecular sieves and zeolites used in shape-selective catalysis

Zeolites are perhaps the most well-known solid materials to provide shape selectivity.¹¹⁴ They have been applied to reactions such as polymerisation, acid catalysis and a range of organic reactions.^{115–117} The most relevant reaction to this research is the oxidation of hydrocarbons. Herron *et al.* showed that Fe/Pd exchanged zeolite 5A was capable of shape selectivity during the oxidation of hydrocarbons.¹⁰⁹ A reaction mixture of *n*-octane and cyclohexane were reacted over zeolite 5A. The reaction mixture both inside and

outside the pores were compared. It was found that in the bulk reaction mixture cyclohexane and *n*-octane were activated almost equally. However, within the pores *n*-octane was selectively activated ~9 times as much compared to the cyclohexane which was speculated to have diffusion limitations. In addition, the reaction mixture within the pores showed a significant increase in selectively activating the C₁ position (and less with C₃ and C₄). It should be noted however this system was not practical. The reaction used a H₂/O₂ mixture and required dissolution of the zeolite in order to obtain the selectively oxidised materials. Tatsumi *et al.* showed similar results with TS-1.⁸² Dissolution of the catalyst was not required in their research. TS-1 showed higher turnover rates for *n*-hexane compared to cyclic/branched analogues. Furthermore, product selectivity was exclusively C₂ and C₃ oxidation, with no C₁ mentioned. It was found that these materials started to become less active as the reaction progressed. This was believed to be due to pore blockage from the products. Therefore, for the catalyst to be recycled the reaction must be stopped and the catalyst calcined. Perhaps it is these reasons why there is currently not an industrial process which uses zeolites for selective linear alkane oxidation.

There are several examples of alternatives to zeolites that can provide shape selectivity. For example shape-selective capabilities of AIPO (aluminophosphates) molecular sieves (section 1.5.3) have been shown by Raja and Thomas.^{103,108,118,119} Within their work of linear alkane oxidation, it was found that AIPOs are capable of significant shape selectivity compared to that of zeolite based catalysts.¹¹⁹ Some results are replicated in table 1.4.2.1.1. Specifically oxidising a C₁ position over others is not a simple task. The catalysts were able to completely avoid oxidising C₃ and C₄ positions. This demonstrates the potential of these catalysts reducing unwanted oxidation products.

Table 1.4.2.1.1: Selected results from Raja and Thomas *et al.* on the selective oxidation of linear alkanes.¹¹⁹

Substrate	Catalyst	Product distribution (mol %)				
		C ₁	C ₂	C ₃	C ₄	Other
<i>n</i> -hexane	CoAIPO-18	61.3	36.1	-	-	2.6
<i>n</i> -hexane	MnAIPO-18	65.5	31.7	-	-	2.8
<i>n</i> -octane	CoAIPO-18	60.3	30.7	6.4	-	2.5
<i>n</i> -octane	MnAIPO-18	62	36.3	-	-	1.7
<i>n</i> -octane	Fe/Pd Zeolite A	21	33	26	20	-
<i>n</i> -octane	ω -hydroxylase	90	10	-	-	-

MnAIPO has also been applied to *n*-dodecane oxidation on a 50 g scale.¹⁰⁸ MnAIPO-18 was shown to only produce C₁ and C₂ oxidised species, with no oxidation occurring on the C₃ – C₆ positions. The authors attributed the selectivity solely down to the confining nature of the pores. This is because several other catalysts were tested with varying pore sizes. Due to the dimensions of the pores in MnAIPO-18 only the C₁ and C₂ position could fit into a cavity where the active metal is present. It should be noted that the majority of the C₁ oxidised products were the carboxylic acid, with the alcohol not exceeding 10 mol% of the overall product distribution.

To our knowledge, AIPOs have never been used within industry for the oxidation of linear alkanes. However, from the extensive publication history, it is demonstrated how sought-after novel materials for the oxidation of linear alkanes are.

1.4.2.2. Metalloporphyrins

An important class of compounds which served as inspiration for selective oxidation was taken from nature and thus developed technologies in metalloporphyrin catalysis.¹²⁰ Metalloporphyrins are a class of metal complexes with a sterically defined pocket of reactivity imposed from the porphyrin ligand that surrounds the metal.¹⁰⁷ Although this research will focus on confined active sites within porous metal oxides, metalloporphyrins have extensive literature and success with alkane oxidation and thus will be discussed briefly here.

Enzymes use two possible mechanisms when conducting oxidation. These are categorised into monooxygenases and dioxygenases, which provide one of the oxygen atoms to the substrate or both of the oxygen atoms from molecular oxygen respectively, both are capable of selective activation of substrates.⁹¹ Many research groups have intended to mimic this design and implement it into their catalysts. For example, Mansuy found that metalloporphyrin catalysts are capable of mimicking both monooxygenase and dioxygenase pathways.¹²¹

Selective oxidation of alkanes has been achieved with the use of metalloporphyrin catalysts.^{106,107,121–123} Extensive research has been placed on these materials due to their biomimetic features. Suslick *et al.* demonstrated increased primary alcohol selectivity in linear C₅-C₁₄ alcohols and branched alkanes. Using iron and manganese-based catalysts, they demonstrated that manganese complexes had higher selectivity to alcohols than corresponding iron complexes. This is thought to be due to differences within their reaction mechanisms.

Heterogenous metalloporphyrin catalysts have also been developed. Halma *et al.* demonstrated that their iron-based metalloporphyrins were able to be immobilised on macroporous supports and then were used to oxidise *n*-heptane.¹⁰⁶ Remarkably, the supported materials showed an increase in alcohol yield compared to that of the

homogenous systems. The article stated that due to the added porosity of the support, the catalyst achieved micro-environments capable of mimicking those found in enzymes.

Despite their clear potential, metalloporphyrins are not currently used in industry as they have several drawbacks. For example, the active site is made up from an organic precursor, which must be synthesised (and therefore adds cost and time to catalyst development). Furthermore, as these catalysts are based on immobilised homogenous catalysts, their structural rigidity lies solely on their immobilisation. Therefore, leaching is a common issue amongst these catalysts.^{124,125} For example, iron porphyrins immobilised on MCM-41 were shown to suffer from leaching due to a decrease in activity after multiple runs of testing.¹²⁶

Metalloporphyrins are nevertheless crucial for research of shape selectivity and are certainly inspirational for catalyst design, however, their current drawbacks of robustness led us to focus on other catalysts.

1.5. Microporous and mesoporous framework solids

Porous materials fall into three categories: microporous ($d_{\text{pore}} < 2 \text{ nm}$), mesoporous ($2 < d_{\text{pore}} < 50 \text{ nm}$) and macroporous ($d_{\text{pore}} > 50 \text{ nm}$).¹²⁷ Significant research has gone into these materials due to their desirable characteristics applicable to catalysis. One of the most common examples of these materials are zeolites (porous silica/alumina based materials), and in a review from Corma, their unique properties were discussed:¹²⁸

- 1) High surface area and adsorption capacity
- 2) Control over adsorption (hydrophobicity and hydrophilicity can be controlled)
- 3) Generation of active sites
- 4) Control over pore size
- 5) Shape selectivity
- 6) Resistance to physical and chemical processes

The focus of this research is utilisation of shape selective catalysis, see section 1.4, from here the synthesis and development of porous frameworks will be discussed.

Control over pore-size is a significant theme in this research. As the formation of pores occurs via a supramolecular-templating approach, figure 1.5.1, the pore size can be altered by varying the length of the organic template.¹¹⁵ The organic material is then typically removed via calcination, or in some cases acid/ solvent washing, this is known as soft-template synthesis (see section 1.5.1).

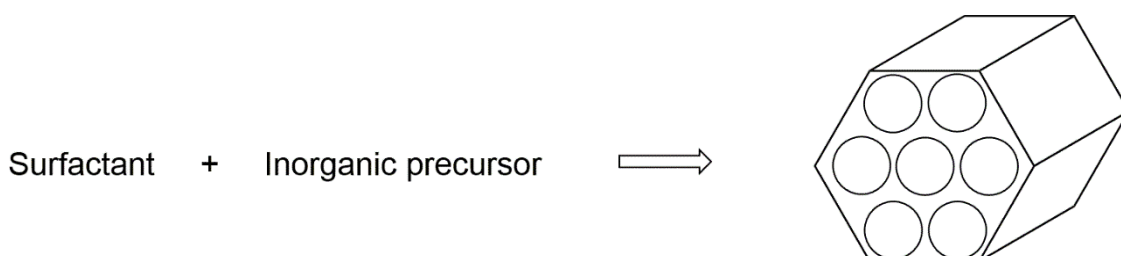


Figure 1.5.1: A simple schematic to show how porous materials are synthesised through a supramolecular templating approach.¹¹⁵

A range of analytical tools have been applied to microporous framework solids. Due to the complexity of their structure a combination of XRPD (x-ray powder diffraction), porosimetry/BET (Brunauer-Emmett-Teller) and TEM (transmission electron microscopy) are required for full characterization (amongst others).

Porosimetry/physisorption provides a means to determine pore volume, pore sizes (and its corresponding distribution) and even pore shape.^{129–131} Furthermore, hysteresis loops can be collected via these analytical methods.¹³² Hysteresis loops come in six different characteristic shapes, which can then be matched to physical properties of that material (e.g. amount of external surface versus internal).¹³³ TEM has been used to directly view the channels within a porous framework. For example, MCM-41 has repeating, regular hexagonal channels,¹³⁴ which were observed via TEM.¹³⁵ Knowing the magnification the pore diameter and length of channel can be determined.

1.5.1. Microporous and mesoporous metal oxides

Microporous and mesoporous metal oxides are pure metal oxides shaped into porous frameworks which are analogous to zeolites (section 1.5.2). A significant amount of work in this field was conducted by Ying.¹³⁶ The synthesis of microporous niobium oxide is a conceptual starting point for this research. The material was synthesised via a soft-templating approach utilising a niobium alkoxide precursor and amine template (figure 1.5.1.1). Soft templating specifically refers to the composition of the template. 'Soft-templates' are organic molecules, typically amines^{137,138} or other surfactants,¹³⁹ which form micelles. This is followed by their alignment to form tubes and ultimately a porous network, where then the template must be removed.¹³⁶ Template removal is crucial as diffusion of substrates in and out of the frameworks would be limited if blocked by alkyl chains. Alternatively, hard templating employs a pre-formed porous network (e.g. silica for mesoporous Fe₂O₃ synthesis),¹³⁸ where then the inorganic precursor binds and fills the pores. Once the inorganic precursor has covered the surface, the hard template is then

removed (typically with strong acid/base).^{140,141} Pores can also be made through etching techniques¹⁴² but this usually leads to a less uniform pore size distribution.

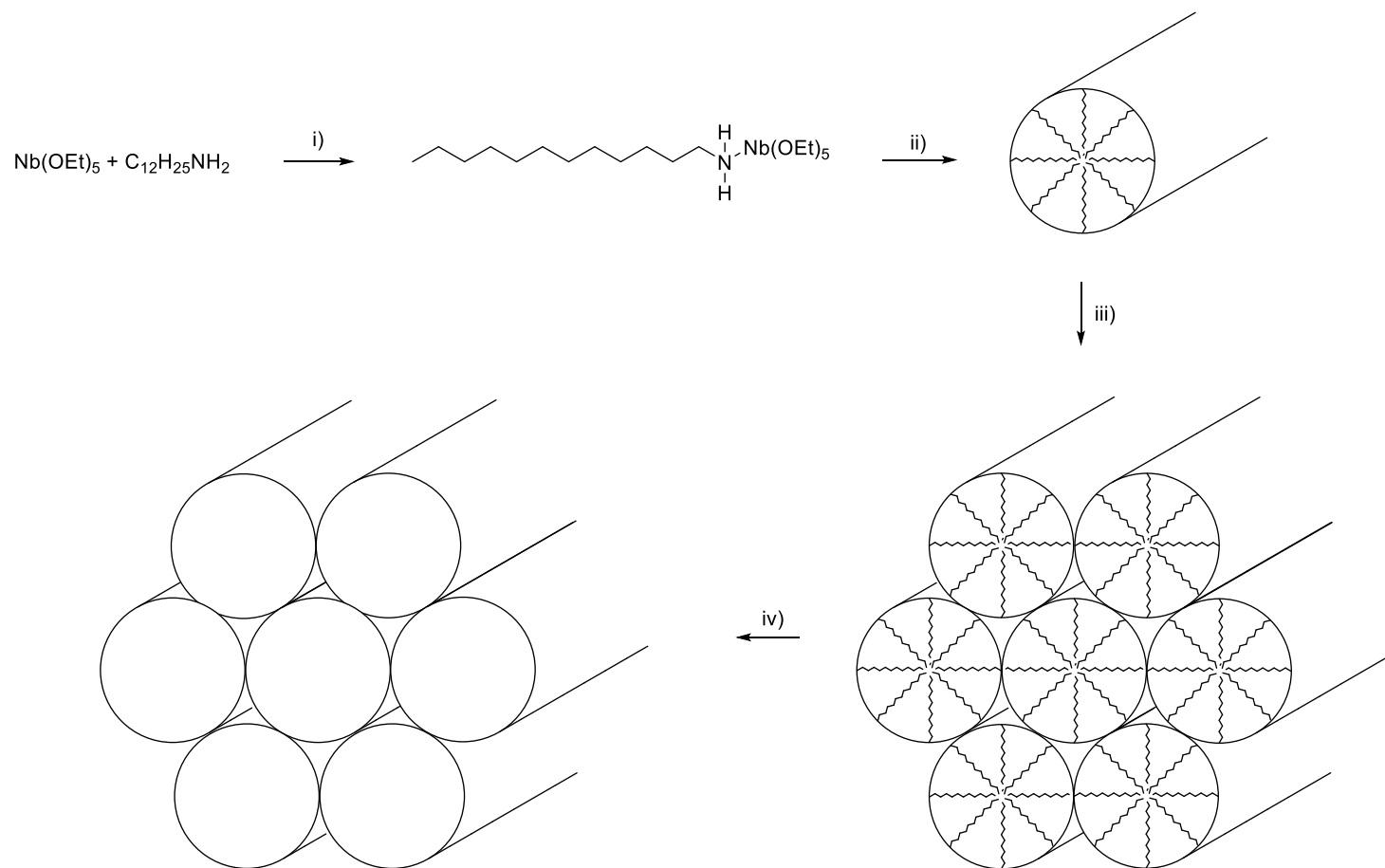


Figure 1.5.1.1: A simplified diagram of microporous niobium oxide synthesis via a templating mechanism, adapted with permission from *T. Sun et al.*¹³⁶. The synthesis is broken into steps; i) template (alkyl-amine) addition, ii) self-assembly, iii) condensation (under hydrothermal conditions), iv) template removal.

Synthesis of microporous niobium oxide achieved pore sizes of 17.7 Å – 25.1 Å.^{131,136} Like zeolites, it is possible to have control of pore size based on the organic template length.¹⁴³ The template, however, is removed through acidic washing as significant pore collapse and loss of surface area was found with calcination.¹³¹ Removal through acidic washing often leads to a decrease in the XRPD intensity of the reflections corresponding to the pores. But template-free porous metal oxides are obtained after the removal of the template, analogous to MCM-41. Table 1.5.1.1 shows a variety of authors who have reported synthesis of porous metal oxides and their corresponding physical pore sizes.

Porous metal oxides have been proposed to have a range of applications. Mesoporous zirconia was developed for its applications in oxygen sensing;¹³⁹ mesoporous tantalum oxide for ultra-stable ceramics;¹³¹ microporous titanium oxide for hydrogen storage;¹⁴⁴ and microporous niobium oxide for numerous applications.¹³⁶ Although these materials are often described for their 'applications in catalysis', to the best of our knowledge no template-assisted synthesised TiO₂ or Nb₂O₅ has thus far been used as a catalyst or a support for heterogeneous catalysts in linear alkane oxidation. This led us to the primary focus of this research; the synthesis of porous materials will be replicated to provide a shape selective site for alkane oxidation. In fact, these metal oxides are expected to be inert and allow different crystal structures, thus allowing to potentially obtain cages or channels containing a dopant metal as highly reactive regions to selectively oxidise substrates.

Table 1.5.1.1: A range of microporous and mesoporous metal oxides within the literature. Synthesis is typically conducted via hydrothermal conditions using an organic template.

Author	Material	Pore size	Ref
Antonelli	Titanium oxide	25 Å	[144]
Dai <i>et al.</i>	Titanium oxide	27 Å – 44 Å	[145]
Zhang	Titanium oxide	20 Å – 50 Å	[146]
Antonelli, Nakahira and Ying	Niobium oxide	22 Å – 39 Å	[147]
Tao and Ying	Niobium oxide	17.7 Å - 25.5 Å and 18.4 Å (with additional 9.95 Å and 6.04 Å)	[136,143]
Antonelli	Zirconium oxide	17 Å – 34 Å	[139]
Antonelli and Ying	Tantalum oxide	29 Å – 43 Å	[131]
Antonelli <i>et al.</i>	Iron oxide	18 Å – 28 Å	[148]

It should be noted a research group was able to synthesise porous titanium oxide without a template.¹⁴⁹ Treating bulk titanium oxide with a 'peptizing agent' (e.g. NaOH) under hydrothermal conditions leads to a change in crystal structure and ultimately a porous material. Varying the peptizing agent led to different morphologies such as rods, nanotubes and zeolitic-type frameworks. The mechanism of formation occurs by initial exfoliation of the bulk phase into sheets, where then the sheets 'scroll' and then form nanotubes (figure 1.5.1.2).¹⁵⁰

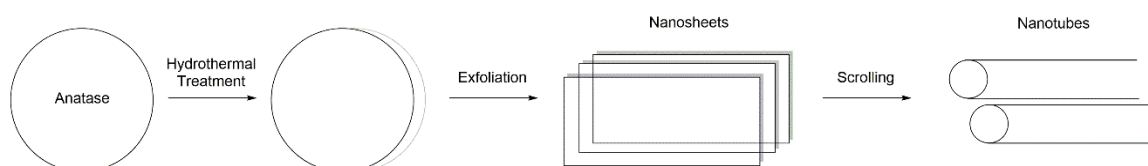


Figure 1.5.1.2: The mechanism of nanotube formation from the hydrothermal treatment of anatase with peptizing agents, reproduced with permission from A. Nakahira *et al.* Copyright (2010) American Chemical Society.¹⁵⁰

The synthesis provides a pathway to porous materials without having to remove the organic template, and thus will avoid any loss in crystallinity during the removal process.

1.5.2. Zeolites

A dominating presence within the field of porous framework solids lies with zeolites.^{72,151–155} Although within this research project porous metal oxides (i.e. silica and alumina-free) were the primary focus, zeolites were also studied due to their established utilisation in alkane oxidation (section 1.3). Zeolites can be synthesised in an analogous manner to porous metal oxides,^{156,157} and due to their regular shape their active sites are well understood.¹⁵⁸ For these reasons, zeolites will be discussed here and throughout the research project to provide crucial comparisons to the success of the application of porous metal oxides in alkane oxidation.

Zeolites are highly crystalline alumina-silica based materials. From their array of potential pore and channel shapes (figure 1.5.2.1) and tuneable chemical properties they have been applied extensively as shape selective catalysts.¹⁵³ Due to their framework, the Lewis acidity differs to that of amorphous $\text{SiO}_2/\text{Al}_2\text{O}_3$, and can be altered further through the addition of extra-framework ions (i.e. promoters).¹¹² This exemplifies how active sites within solid supports can be designed and give beneficial properties to that of the bulk material. Furthermore, pore size of these materials can be altered by changing their template length during their synthesis,¹⁵⁹ and even through surfactant-directed recrystallization of commercial zeolites.¹⁶⁰

Additional framework species can be added to zeolites to increase their catalytic abilities. For example iron has been incorporated into the structure of ZSM-5 and showed beneficial properties for the aromatization of hexane.¹⁶¹ The novelty of using zeolites is their well-defined channels, which provide well-defined active sites.¹⁵⁴ Significant interest has been placed in characterising these active sites, as this will allow an understanding of how the metal activates a substrate. For example, Fe/ZSM-5 was studied through UV/Raman techniques to determine the coordination centre around the active iron.¹⁶² This technique allowed observation of adsorption bands due to bridging oxygen between the dopant metal and the framework, proof that isolated iron sites were present on the support.

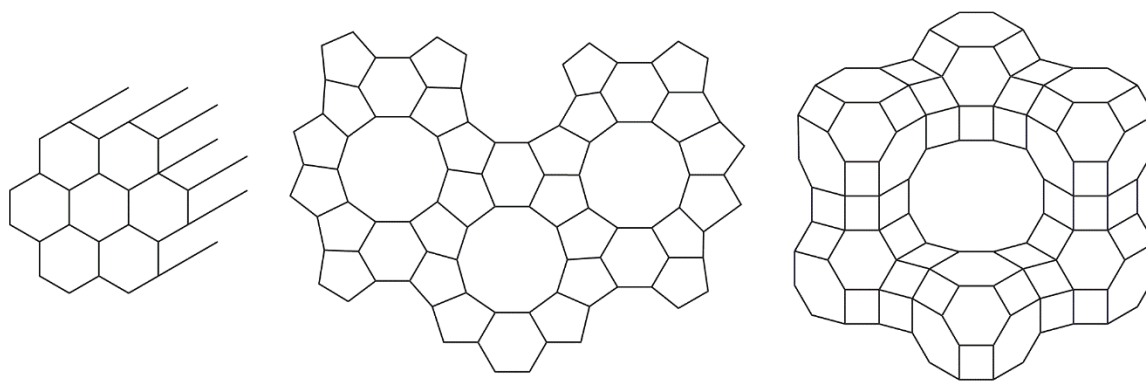


Figure 1.5.2.1: A diagram to show a sample of zeolite frameworks. Left: adjacent cylindrical channels in a honeycomb-like structure for MCM-41.¹⁶³ Middle: separated channels in H-ZSM-5.¹⁶⁴ Right: cage structure in Zeolite-Y.¹⁶⁵

A significant example where an ‘active site’ has been developed in a zeolite is from Thomas *et al.* based on MCM-41.¹⁶⁶ Titanium grafted onto MCM-41 was capable of oxidations of cyclohexene and pinene via TBHP. The study focused on the oxidant, TBHP, and its utilisation during the reaction. The results showed a 95% selectivity for TBHP towards the epoxidation of cyclohexene, and stated the reactivity was occurring within the pores of the support at these active sites.

Acid-site tuning was shown to have an influence on the hydroxylation of benzene.¹⁶⁷ Aluminium and iron were included into the structure of TS-1 and applied to the oxidation of benzene to selectively produce phenol. Al/TS-1 and Fe/TS-1 have a greater acidity than TS-1. Both doped zeolites showed a greater selectivity towards phenol than the by-product *p*-benzoquinone. This is an example of the fine tuning that can be applied to porous catalysts to influence the selectivity of products in a reaction mixture.

Despite their potential zeolites may have serious issues with deactivation.^{168–170} Due to their narrow shape and relatively hydrophobic channels (if compared to their external surface, due to a lower presence of exposed –OH groups) it is common for organic material to become trapped leading to deactivation of the catalyst, this is known as coking.¹⁶⁸ This means that the catalyst needs to be regenerated, typically through calcining the coked zeolite to remove any

organic material. In the example mentioned previously by Thomas *et al.*, their catalyst completely deactivated after 90 minutes when oxidising cyclohexene.¹⁶⁶ Although significant research has gone into preventing and limiting coke formation,¹⁶⁹ this requires specific parameters of the pore structure, acidity and even the reactor and operating conditions, which may not be suitable for all substrates.

1.5.3. Aluminophosphates

Aluminophosphates are analogous to zeolites, but their composition is primarily AlPO_4 , sometimes AlPO_{4-n} .¹⁷¹ Their advantage over the corresponding aluminosilicates is a higher degree of ionic character, making it more feasible to isomorphously substitute aluminium framework ions with dopant metals. The resulting doped materials are referred to as MeAPOs. Although not used within this research project, MeAPOs are promising candidates in selective alkane oxidation, their use in selective oxidation can be found in section 1.4.2.

The advantage of using MeAPOs over zeolites has been reported extensively within literature.^{72,79,172,173} For example, CoAPOs were used for the oxidation of cyclohexane, the results are summarized in table 1.5.3.1.¹⁷⁴ Ultimately, the CoAPO-5 was capable of higher conversion and did not deactivate. The catalysts were synthesised via a hydrothermal method where a fractional amount of aluminium precursor is replaced with cobalt salts. Examples like this are common in the literature and are discussed further in section 1.4.2.1.

Table 1.5.3.1: A summary of results from cyclohexane oxidation using various cobalt catalysts, showing the advantages of CoAPOs.¹⁷⁴

Catalyst	Conversion (%)	Comments
CoAPO-5	3	
Cobalt Naphthenate	0.5	Homogenous - Deactivated due to precipitation
Co/Y	0	Completely inactive due to cobalt cluster formation

Synthesis with varying metal dopants in APOs have been conducted. A vast array of transition metal doped AlPOs exist in the literature,¹⁷⁵ and there are even examples where multiple different metals have been doped into the same species (FeCoMnAPOs).¹⁷² This has generated a library of potential oxidising, porous and selective catalysts for alkane oxidation.

1.6. Supported metals for oxidation catalysis

1.6.1. Basic principles of supported nanoparticles, nanoclusters and isolated atoms

Metal nanoparticles, clusters and isolated atoms can be loaded within porous supports to create isolated active sites, which is a distinct feature of highly efficient catalysts like enzymes.^{113,116,129,142,154,176–178} This creates scope for the deposition onto porous metal oxides, mimicking examples in zeolites and AlPOs. For this reason, loading metal species onto a range of supports will be a significant part of this research and will be systematically discussed here.

Depositing a metal on a support provides an efficient way to maximise surface area for heterogeneous catalysts, but importantly, can provide a means to have nanoparticles with catalytic behaviour different to the bulk.¹⁷⁹ Nanoparticles are capable of chemistry different to that of isolated molecules and bulk material which is described by band theory.¹⁸⁰ Because of the presence of quantized energy levels, their chemical properties can differ to the bulk and molecular phases, even ranging from a non-active to an active catalyst. Furthermore, nanoparticles have a high proportion of 'bare' atoms at the surface which means an area of numerous unsaturated atoms are present to react.¹⁸⁰

1.6.2. Nano-sized catalysts vs. bulk material

To exemplify the potential of nanophase catalysts, key examples will be discussed here and compared to corresponding bulk material.

There are numerous examples of nanoparticles behaving significantly different to their bulk phase but perhaps the most iconic is gold.¹⁸¹ This is because gold had been regarded as characteristically inert in its bulk phase, however, Haurta *et al.* showed that gold supported on a range of transition metal oxides is an efficient catalyst for the oxidation of both CO and H₂.¹⁸² For example, Au/ α -Fe₂O₃ prepared via co-precipitation (see section 2.2 for preparation information), was found to have 100% efficiency when oxidising CO at 0 °C, in comparison to

that of fine gold powder which required a heat of 300 °C to reach a similar conversion value. It should be noted that the study tested activity from the support (i.e. with no active metal), these tests are crucial and discussed more in section 4.2.2 .

Gold has also been demonstrated to be an effective catalyst for the oxidation of *n*-alkanes.⁷⁸ Asefa and Biradar showed that gold nanoparticles deposited onto the mesoporous support SBA-15 is capable of 95% hexane conversion to the corresponding 2-hexanone (92%) and 2-hexanol (8%) at 70 °C, in the presence of TBHP. For seemingly inert materials such as alkanes to be activated to such a high conversion demonstrates the potential of using nanoparticles on supports as effective catalysts.

Iron nanoparticles have also shown differences to their bulk counterparts when comparing catalytic activity.^{178,183,184} Beller *et al.* have shown that nano- γ -Fe₂O₃ is capable of much higher conversions compared to its bulk phase. The iron nanoparticles were reported to have a much higher conversion of benzyl alcohol to benzaldehyde. Interestingly, the research studied two different particle sizes and showed that the selectivity for benzaldehyde is dramatically affected by particle size. The selectivity dropped from 97% to 35% when using particles of 20-50 nm and 3-5 nm respectively.

Particle size and its effect on cyclohexane oxidation was reported by Tyo *et al.*¹⁸⁵ Co₃O₄ supported on Al₂O₃ is capable of cyclohexane oxidation. The study showed how by halving the particle size of Co₃O₄ from 12 nm to 6 nm had a significant effect on the conversion and selectivity, summarised in table 1.6.2.1. Similar results with varying Pt particle diameter in Pt/Al₂O₃ were found with deep oxidation of dodecane.¹⁸⁶

Table 1.6.2.1: The effect of cobalt oxide particle size on turnover rates (TOR) for cyclohexane oxidative dehydrogenation utilising Co₃O₄ supported on Al₂O₃. Table adapted from Tyo *et al.*¹⁸⁵

per total cobalt TORs (mol atom ⁻¹ s ⁻¹)					
Particle	C ₆ H ₁₂	C ₆ H ₁₀	C ₆ H ₈	C ₆ H ₆	CO ₂
size	consumption	formation	formation	formation	formation
6 nm	3.68 x 10 ⁻³	1.72 x 10 ⁻³	0	1.45 x 10 ⁻⁴	3.71 x 10 ⁻³
12 nm	7.14 x 10 ⁻³	4.28 x 10 ⁻⁴	1.88 x 10 ⁻⁴	2.49 x 10 ⁻⁴	3.4 x 10 ⁻⁴

These results demonstrate the enhanced ability of nanoparticles when applied to catalysis and how selectivity of reaction products can be tuned via changing the size of the nanoparticles (which can be achieved with different loading techniques, see section 2.2.1).

1.6.3. The effect of the support

Choice of support for metal-loaded catalysts is as important as the choice of active metal.^{187–191} In the principle of metal-supported catalysis, ideally the support would be inert so that any activity is provided only by the active metal, with the support maintaining the metal dispersed and avoiding its sintering. However, this does not mean the support is useless for a chemical reaction, they may themselves provide a step in the mechanism,¹⁹² alter the steric area around the active metal¹⁹³ (thus providing shape selectivity,^{103,194} see section 1.4) or act as a promotor^{195–197} (or inhibitor).^{72,198} For example, Burch *et al.* showed how dramatic the effect of changing a support is when applied to the oxidation of methane.¹⁹⁹ Two supports, zirconia and alumina, doped with rhodium or palladium were studied for methane and propane oxidation. When rhodium is loaded onto alumina and subjected to oxidising conditions, a significant amount of deactivation is observed, whereas when zirconia is used deactivation does not occur. It was speculated in the study this is due to shifting interactions between the rhodium and alumina at higher temperatures causing deactivation.

1.6.4. Leaching

Leaching is a significant factor which must be considered when testing supported metals.²⁰⁰⁻
²⁰² If a metal leaches into a reaction mixture, it may lead to many implications such as; alternative homogenous mechanisms occurring, lower conversions after repeated use and even safety issues if toxic heavy metals/ metal complexes have leached into the products.

The use of supported metal oxides are wide spread and they are relatively simple to synthesise, however, there is the possibility of the active metal leaching into the reaction mixture and thus no longer being heterogeneous.²⁰⁰ For example, Sheldon *et al.* highlighted the importance of leaching studies. During their study on oxidation of α -pinene with a CrAPO-5 catalyst (a porous catalyst comprised of chromium doped aluminium phosphate) they saw that chromium was capable of oxidation with TBHP but not with bulkier oxidising agents.²⁰¹ Although they initially suspected that the reaction was occurring within the pores, they actually found that reaction with TBHP led to leaching, and ultimately homogenous reactions (not within the pores). This example shows it is essential for rigorous leaching tests to be conducted as it may completely change the understanding of a mechanism, further information can be found in section 2.5.9.

1.7. Project scope and thesis development

The 'holy grail' of selective alkane oxidation is the key aspect of this project. Considering the potential of zeolites, AIPOs and microporous materials, we were prompted to design novel materials for the oxidation of linear alkanes. Thus far there has been no catalyst capable of predominantly oxidising the primary position of linear alkanes, while selectively forming the alcohol. Zeolites are excellent candidates due to their robust hydrothermal stability, however, coking and over oxidation are significant drawbacks to their applications on industrial scales. AIPOs also showed great potential but over oxidation to carboxylic acids is prevalent in their use. Therefore, we propose microporous metal oxides with confined active sites (analogous to zeolites and AIPOs) may perhaps offer an alternative material to combat current drawbacks. These will be developed utilising a soft template approach, replicating those developed by Antonelli and Ying.^{136,144,147} However, the porous framework will also contain a small mol% (0.5 – 5 mol%) of dopant metal (e.g. Fe, Mn, Pd etc.). This will hopefully create sites confined within a porous framework analogous to the AIPOs described by Raja and Thomas,¹⁰⁸ but with different environments. These environments will ideally create differences in catalytic activity and thus preferentially produce alcohols.

Microporous metal oxides will be developed by following adapted literature procedures. The parameters for their synthesis will be adjusted in order to create a material which is robust, highly crystalline in the porous phase and template free. This will be characterised through a range of analytical techniques such as; FTIR-ATR, XRPD, Porosimmetry/BET and XPS (x-ray photoelectron spectroscopy).

In addition, non-doped frameworks will be subjected to impregnation techniques so that the dopant metal will be a nanoparticle positioned on the framework's surface, as opposed to being part of the framework. This will allow comparisons to be drawn in activity and potential leaching. In order to determine if the catalysts are indeed providing shape selectivity bulk materials will also be developed. For example, via wetness impregnation iron could be loaded onto bulk commercial TiO₂, or onto microporous TiO₂ synthesised following Antonelli's

protocol.¹⁴⁴ Then, from what we propose, iron could then be incorporated into the framework of TiO₂ by adding dopant material during Antonelli's described synthesis. Additionally, as zeolites are commercially available and the biggest rivals to this study, they too will be subjected to wet impregnation. This, in theory, will provide three materials; i) a metal nanoparticle located on a surface not confined in anyway (that is not embedded in the framework), ii) a metal nanoparticle sitting on a surface confined by a framework and iii) an active metal within a porous framework (and by definition confined). The resulting materials will then be applied to alkane oxidation so it can be determined; i) has shape selectivity been provided and ii) does this confinement/ incorporation of metal active sites lead to better selectivity to alcohols. Additionally, any metal/surface interactions can be resolved by comparisons to zeolites and between different microporous metal oxides (i.e. microporous TiO₂ and microporous Nb₂O₅).

As the production of bulk materials is significantly easier than microporous synthesis, these will be used for preliminary tests and benchmarks on alkane oxidation. Various parameters such as temperature, pressure and metal to substrate ratio will be tested with bulk material which is found to be active. This will allow the development of ideal conditions where the catalyst is most active and to determine how much conversion (if any) is from autoxidation.

However, in order to determine the activity of a catalyst accurate quantitative analytical methods need to be developed. Linear alkane oxidation will potentially lead to complex reaction mixtures. Therefore, distinguishing these products analytically so they may be quantified will also be a significant part of this project, as they will provide data for structure-activity correlation and in turn catalyst design. ¹H-NMR and GC-MS (gas chromatography mass spectrometry) will be used to determine if all the reaction products can be quantified and thus, can conversion and selectivity be accurately measured. Reaction mixtures will be from 'ideal' standards and 'actual' reaction mixtures from autoxidation/ where a catalyst has been used.

Finally, as linear alkane oxidation is a challenging task, cyclic alkane oxidation will also be tested. This is because activation of C-H bonds in cyclic alkanes is lower in energy and will allow a more straight forward proof of concept.

The ultimate goal of this project is to develop a fully characterised microporous metal oxide including a dopant metal which is capable of regio and chemo selective oxidation of linear alkanes to the primary alcohol, compared to commercial/ non-porous analogues, as determined from an accurate spectroscopic method.

1.8. References

- 1 S. E. Belanger, H. Sanderson, P. R. Fisk, C. Schäfers, S. M. Mudge, A. Willing, Y. Kasai, A. M. Nielsen, S. D. Dyer and R. Toy, *Ecotoxicol. Environ. Saf.*, 2009, **72**, 1006–1015.
- 2 K. Noweck and W. Grafahrend, in *Ullmann's Encyclopedia of Industrial Chemistry*, Wiley-VCH Verlag GmbH & Co. KGaA, Weinheim, 2012, pp. 117–141.
- 3 L. T. Cordova, J. Butler and H. S. Alper, *Metab. Eng. Commun.*, 2020, **10**, e00105.
- 4 J. Falbe, H. Bahrmann, W. Lipps, D. Mayer and G. D. Frey, in *Ullmann's Encyclopedia of Industrial Chemistry*, Wiley-VCH Verlag GmbH & Co. KGaA, Weinheim, Germany, 2013.
- 5 J. Julis and W. Leitner, *Angew. Chemie Int. Ed.*, 2012, **51**, 8615–8619.
- 6 S. Banerjee, S. H. Yalkowsky and S. C. Valvani, *Environ. Sci. Technol.*, 1980, **14**, 1227–1229.
- 7 C. D. Rutter and C. V. Rao, *Metab. Eng.*, 2016, **38**, 139–147.
- 8 E. Smulders, in *Laundry Detergents*, Wiley-VCH Verlag GmbH & Co. KGaA, Weinheim, FRG, 1st edn., 2002, pp. 38–98.
- 9 R. Varadaraj, J. Bock, P. Valint, S. Zushma and R. Thomas, *J. Phys. Chem.*, 1991, **95**, 1671–1676.
- 10 A. Kramer and G. Thodos, *J. Chem. Eng. Data*, 1988, **33**, 230–234.
- 11 J. Clayden, N. Greeves and S. Warren, in *Organic Chemistry*, Oxford University Press Inc., New York, 2nd edn., 2001, pp. 253–254.
- 12 E. Roduner, *Chem. Soc. Rev.*, 2014, **43**, 8226–8239.
- 13 R. Snoeckx and A. Bogaerts, *Chem. Soc. Rev.*, 2017, **46**, 5805–5863.

- 14 M. Bowker, *The Basis and Application of Heterogeneous Catalysis*, Oxford University Press Inc., New York, 1st edn., 1998.
- 15 C. R. Catlow, M. Davidson, C. Hardacre and G. J. Hutchings, *Philos. Trans. R. Soc. A Math. Phys. Eng. Sci.*, 2016, **374**, 20150089.
- 16 J. Falbe, H. Bahrmann and H. G. Gilde, *J. Chem. Educ.*, 1984, **61**, 961–967.
- 17 B. Cornils and W. A. Herrmann, *J. Catal.*, 2003, **216**, 23–31.
- 18 R. A. Sheldon, *J. Chem. Technol. Biotechnol.*, 1997, **68**, 381–388.
- 19 P. Christopher and S. Linic, *AIChE Annu. Meet. Conf. Proc.*, 2008, 11264–11265.
- 20 E. Gross, J. H. C. Liu, F. D. Toste and G. A. Somorjai, *Nat. Chem.*, 2012, **4**, 947–952.
- 21 J. P. Kehrer and S. S. Biswal, *Toxicol. Sci.*, 2000, **57**, 6–15.
- 22 Y. Lei, F. Mehmood, S. Lee, J. Greeley, B. Lee, S. Seifert, R. E. Winans, J. W. Elam, R. J. Meyer, P. C. Redfern, D. Teschner, R. Schlogl, M. J. Pellin, L. A. Curtiss and S. Vajda, *Science*, 2010, **328**, 224–228.
- 23 J. B. Reitz and E. I. Solomon, *J. Am. Chem. Soc.*, 1998, **120**, 11467–11478.
- 24 R. A. Sheldon, I. W. C. E. Arends and U. Hanefeld, in *Green Chemistry and Catalysis*, Wiley-VCH Verlag GmbH & Co. KGaA, Weinheim, 2007, pp. 1–47.
- 25 A. Podgoršek, M. Zupan and J. Iskra, *Angew. Chemie Int. Ed.*, 2009, **48**, 8424–8450.
- 26 R. Ciriminna, L. Albanese, F. Meneguzzo and M. Pagliaro, *ChemSusChem*, 2016, **9**, 3374–3381.
- 27 A. N. Campbell and S. S. Stahl, *Acc. Chem. Res.*, 2012, **45**, 851–863.
- 28 L. Chen, K. Zhu, L. H. Bi, A. Suchofar, M. Reicke, G. Mathys, H. Jaensch, U. Kortz and R. M. Richards, *Inorg. Chem.*, 2007, **46**, 8457–8459.
- 29 L. Chen, J. Hu and R. Richards, *J. Am. Chem. Soc.*, 2009, **131**, 914–915.

- 30 L. Chen, J. Hu and R. M. Richards, *ChemPhysChem*, 2008, **9**, 1069–1078.
- 31 R. A. Sheldon and J. K. Kochi, in *Metal-catalyzed Oxidations of Organic Compounds*, Elsevier, New York, 1st edn., 1981, pp. 17–32.
- 32 G. J. Ten Brink, I. W. C. E. Arends and R. A. Sheldon, *Science*, 2000, **287**, 1636–1639.
- 33 X. Tang, W. Wu, W. Zeng and H. Jiang, *Acc. Chem. Res.*, 2018, **51**, 1092–1105.
- 34 T. Punniyamurthy and L. Rout, *Coord. Chem. Rev.*, 2008, **252**, 134–154.
- 35 S. Mannam, S. K. Alamsetti and G. Sekar, *Adv. Synth. Catal.*, 2007, **349**, 2253–2258.
- 36 I. E. Markó, P. R. Giles, M. Tsukazaki, S. M. Brown and C. J. Urch, *Science*, 1996, **274**, 2044–2046.
- 37 O. Verho, M. D. V. Dilenstam, M. D. Kärkäs, E. V. Johnston, T. Åkermark, J.-E. Bäckvall and B. Åkermark, *Chem. Eur. J.*, 2012, **18**, 16947–16954.
- 38 M. À. Carvajal, S. Kozuch and S. Shaik, *Organometallics*, 2009, **28**, 3656–3665.
- 39 M. Schwarze, T. Pogrzeba, K. Seifert, T. Hamerla and R. Schomäcker, *Catal. Today*, 2015, **247**, 55–63.
- 40 C. Disser, C. Muennich and G. Luft, *Appl. Catal. A Gen.*, 2005, **296**, 201–208.
- 41 A. Peschel, B. Hentschel, H. Freund and K. Sundmacher, *Chem. Eng. J.*, 2012, **188**, 126–141.
- 42 F. Hebrard and P. Kalck, *Chem. Rev.*, 2009, **109**, 4272–4282.
- 43 B. Reuben and H. Wittcoff, *J. Chem. Educ.*, 1988, **65**, 605–607.
- 44 B. Fell, in *Anionic Surfactants: Organic Chemistry*, ed. H. Stache, Marcel Dekker, Inc., New York, 1st edn., 1995, pp. 20–25.
- 45 A. E. Shilov and G. B. Shul'pin, *Russ. Chem. Rev.*, 1987, **56**, 442–464.

- 46 J. A. Labinger and J. E. Bercaw, in *Higher Oxidation State Organopalladium and Platinum Chemistry. Topics in Organometallic Chemistry*, Springer, Berlin, Heidelberg, 2011, vol. 35, pp. 29–59.
- 47 R. H. Crabtree, *J. Organomet. Chem.*, 2004, **689**, 4083–4091.
- 48 A. E. Shilov and G. B. Shul'pin, *Chem. Rev.*, 1997, **97**, 2879–2932.
- 49 P. E. M. Siegbahn and R. H. Crabtree, *J. Am. Chem. Soc.*, 1996, **118**, 4442–4450.
- 50 M. Lin, C. Shen, E. A. Garcia-Zayas and A. Sen, *J. Am. Chem. Soc.*, 2001, **123**, 1000–1001.
- 51 R. Lloyd, R. L. Jenkins, M. Piccinini, Q. He, C. J. Kiely, A. F. Carley, S. E. Golunski, D. Bethell, J. K. Bartley and G. J. Hutchings, *J. Catal.*, 2011, **283**, 161–167.
- 52 G. Just, W. Pritzkow, M. Rudolf, T. D. Tien and V. Voerckel, *J. für Prakt. Chemie*, 1986, **328**, 469–474.
- 53 E. A. Elkhalifa and H. B. Friedrich, *Appl. Catal. A Gen.*, 2010, **373**, 122–131.
- 54 J. M. Thomas, R. Raja, G. Sankar and R. G. Bell, *Acc. Chem. Res.*, 2001, **34**, 191–200.
- 55 T. B. Gunnoe, in *Alkane C-H Activation by Single-Site Metal Catalysis*, ed. P. J. Pérez, Springer Netherlands, Dordrecht, 1st edn., 2012, vol. 38, pp. 1–15.
- 56 K. Kamata, K. Yonehara, Y. Nakagawa, K. Uehara and N. Mizuno, *Nat. Chem.*, 2010, **2**, 478–483.
- 57 L. Yu-Ran, *Comprehensive Handbook of Chemical Bond Energies*, CRC Press, Boca Raton, 1st edn., 2007.
- 58 K. Yamaguchi and N. Mizuno, *New J. Chem.*, 2002, **26**, 972–974.
- 59 S. Shinachi, M. Matsushita, K. Yamaguchi and N. Mizuno, *J. Catal.*, 2005, **233**, 81–

- 89.
- 60 L. Chen, K. Zhu, L. H. Bi, A. Suchopar, M. Reicke, G. Mathys, H. Jaensch, U. Kortz and R. M. Richards, *Inorg. Chem.*, 2007, **46**, 8457–8459.
- 61 L. Chen, J. Hu, S. S. Mal, U. Kortz, H. Jaensch, G. Mathys and R. M. Richards, *Chem. Eur. J.*, 2009, **15**, 7490–7497.
- 62 D. S. Gopala, R. R. Bhattacharjee and R. Richards, *Appl. Organomet. Chem.*, 2013, **27**, 1–5.
- 63 R.-Q. Meng, B. Wang, H.-M. Sui, B. Li, W. Song, L.-X. Wu, B. Zhao and L.-H. Bi, *Eur. J. Inorg. Chem.*, 2013, **2013**, 1935–1942.
- 64 D. G. Hendry, C. W. Gould, D. Schuetzle, M. G. Syz and F. R. Mayo, *J. Org. Chem.*, 1976, **41**, 1–10.
- 65 X. Liu, Y. Ryabenkova and M. Conte, *Phys. Chem. Chem. Phys.*, 2015, **17**, 715–731.
- 66 J. Betts, *Q. Rev. Chem. Soc.*, 1967, **25**, 265–288.
- 67 I. Hermans, J. Peeters and P. A. Jacobs, *Top. Catal.*, 2008, **50**, 124–132.
- 68 L. M. Slaughter, J. P. Collman, T. A. Eberspacher and J. I. Brauman, *Inorg. Chem.*, 2004, **43**, 5198–5204.
- 69 B. P. C. Hereijgers and B. M. Weckhuysen, *J. Catal.*, 2010, **270**, 16–25.
- 70 F. Garcia-Ochoa, J. Querol and A. Romero, *Ind. Eng. Chem. Res.*, 1990, **29**, 1989–1994.
- 71 L. Gómez-Hortigüela, F. Corà and C. R. A. Catlow, *ACS Catal.*, 2011, **1**, 1475–1486.
- 72 B. Modén, B. Z. Zhan, J. Dakka, J. G. Santiesteban and E. Iglesia, *J. Phys. Chem. C*, 2007, **111**, 1402–1411.
- 73 B. Z. Zhan, B. Modén, J. Dakka, J. G. Santiesteban and E. Iglesia, *J. Catal.*, 2007,

- 245**, 316–325.
- 74 M. G. Clerici, *Appl. Catal.*, 1991, **68**, 249–261.
- 75 M. Mitra, J. Lloret-Fillol, M. Haukka, M. Costas and E. Nordlander, *Chem. Commun.*, 2014, **50**, 1408–1410.
- 76 G. B. Shul'pin, *Comptes Rendus Chim.*, 2003, **6**, 163–178.
- 77 F. Cavani, *Catal. Today*, 2010, **157**, 8–15.
- 78 A. V. Biradar and T. Asefa, *Appl. Catal. A Gen.*, 2012, **435–436**, 19–26.
- 79 B. Modén, B. Z. Zhan, J. Dakka, J. G. Santiesteban and E. Iglesia, *J. Catal.*, 2006, **239**, 390–401.
- 80 C. Kim, K. Chen, J. Kim and L. Que, *J. Am. Chem. Soc.*, 1997, **119**, 5964–5965.
- 81 D. R. C. Huybrechts, L. De Bruycker and P. A. Jacobs, *Nature*, 1990, **345**, 240–242.
- 82 T. Tatsumi, M. Nakamura, S. Negishi and H. o. Tominaga, *J. Chem. Soc. Chem. Commun.*, 1990, **202**, 476–477.
- 83 V. Peneau, G. Shaw, R. D. Armstrong, R. L. Jenkins, N. Dimitratos, S. H. Taylor, H. W. Zanthoff, S. Peitz, G. Stochniol and G. J. Hutchings, *Catal. Sci. Technol.*, 2016, **6**, 7521–7531.
- 84 A. Corma, M. A. Camblor, P. Esteve, A. Martinez and J. Perezpariente, *J. Catal.*, 1994, **145**, 151–158.
- 85 C. Nozaki, C. G. Lugmair, A. T. Bell and T. D. Tilley, *J. Am. Chem. Soc.*, 2002, **124**, 13194–13203.
- 86 S. Tangestaninejad, V. Mirkhani, M. Moghadam, I. Mohammadpoor-Baltork, E. Shams and H. Salavati, *Ultrason. Sonochem.*, 2008, **15**, 438–447.
- 87 H. X. Yuan, Q. H. Xia, H. J. Zhan, X. H. Lu and K. X. Su, *Appl. Catal. A Gen.*, 2006,

- 304**, 178–184.
- 88 F. Farzaneh, M. Majidian and M. Ghandi, *J. Mol. Catal. A Chem.*, 1999, **148**, 227–233.
- 89 S. Klein, S. Thorimbert and W. F. Maier, *J. Catal.*, 1996, **163**, 476–488.
- 90 Y. Zhou, J. Long and Y. Li, *Chinese J. Catal.*, 2016, **37**, 955–962.
- 91 S. G. Burton, *Trends Biotechnol.*, 2003, **21**, 543–549.
- 92 S. G. Burton, D. A. Cowan and J. M. Woodley, *Nat. Biotechnol.*, 2002, **20**, 37–45.
- 93 S. Jemli, D. Ayadi-Zouari, H. Ben Hlima and S. Bejar, *Crit. Rev. Biotechnol.*, 2016, **36**, 246–258.
- 94 J. M. Woodley, *Biochem. Soc. Trans.*, 2006, **34**, 301–303.
- 95 M. Bordeaux, A. Galarneau and J. Drone, *Angew. Chemie Int. Ed.*, 2012, **51**, 10712–10723.
- 96 A. Weiss, in *Modern Biooxidation: Enzymes, Reactions and Applications*, Wiley-VCH Verlag GmbH & Co. KGaA, Weinheim, 2007, pp. 193–209.
- 97 B. Witholt, M. Desmet, J. Kingma, J. Vanbeilen, M. Kok, R. Lageveen and G. Eggink, *Trends Biotechnol.*, 1990, **8**, 46–52.
- 98 D. J. Koch, M. M. Chen, J. B. Van Beilen and F. H. Arnold, *Appl. Environ. Microbiol.*, 2009, **75**, 337–344.
- 99 J. B. van Beilen, E. G. Funhoff, A. van Loon, A. Just, L. Kaysser, M. Bouza, R. Holtackers, M. Rothlisberger, Z. Li and B. Witholt, *Appl. Environ. Microbiol.*, 2006, **72**, 59–65.
- 100 R. G. Mathys, A. Schmid and B. Witholt, *Biotechnol. Bioeng.*, 1999, **64**, 459–477.
- 101 A. Glieder, E. T. Farinas and F. H. Arnold, *Nat. Biotechnol.*, 2002, **20**, 1135–1139.

- 102 J. B. Van Beilen and E. G. Funhoff, *Curr. Opin. Biotechnol.*, 2005, **16**, 308–314.
- 103 J. M. Thomas and R. Raja, *Chem. Commun.*, 2001, **8**, 675–687.
- 104 L. Matachowski, K. Pamin, J. Połtowicz, E. M. Serwicka, W. Jones and R. Mokaya, *Appl. Catal. A Gen.*, 2006, **313**, 106–111.
- 105 P.-P. Knops-Gerrits, A. Verberckmoes, R. Schoonheydt, M. Ichikawa and P. A. Jacobs, *Microporous Mesoporous Mater.*, 1998, **21**, 475–486.
- 106 M. Halma, K. A. D. de F. Castro, V. Prévot, C. Forano, F. Wypych and S. Nakagaki, *J. Mol. Catal. A Chem.*, 2009, **310**, 42–50.
- 107 B. R. Cook, T. J. Reinert and K. S. Suslick, *J. Am. Chem. Soc.*, 1986, **108**, 7281–7286.
- 108 R. Raja and J. M. Thomas, *Chem. Commun.*, 1998, 1841–1842.
- 109 N. Herron and C. A. Tolman, *J. Am. Chem. Soc.*, 1987, **109**, 2837–2839.
- 110 S. Das, G. W. Brudvig and R. H. Crabtree, *Chem. Commun.*, 2002, **8**, 413–424.
- 111 B. Meunier, *Chem. Rev.*, 1992, **92**, 1411–1456.
- 112 P. A. Wright, *Microporous Framework Solids*, The Royal Society of Chemistry, London, 2008.
- 113 S. Goel, Z. Wu, S. I. Zones and E. Iglesia, *J. Am. Chem. Soc.*, 2012, **134**, 17688–17695.
- 114 R. Kumar, G. C. G. Pais, B. Pandey and P. Kumar, *J. Chem. Soc. Chem. Commun.*, 1995, 1315.
- 115 J. Y. Ying, C. P. Mehnert and M. S. Wong, *Angew. Chemie Int. Ed.*, 1999, **38**, 56–77.
- 116 P. B. Venuto, *Microporous Mater.*, 1994, **2**, 297–411.
- 117 M. Choi, H. S. Cho, R. Srivastava, C. Venkatesan, D. H. Choi and R. Ryoo, *Nat.*

- Mater.*, 2006, **5**, 718–723.
- 118 R. Raja, J. M. Thomas, M. Greenhill-Hooper and V. Doukova, *Chem. Commun.*, 2007, 1924–1926.
- 119 J. M. Thomas, R. Raja, G. Sankar and R. G. Bell, *Nature*, 1999, **398**, 227–230.
- 120 M. M. Pereira, L. D. Dias and M. J. F. Calvete, *ACS Catal.*, 2018, 10784–10808.
- 121 D. Mansuy, *Coord. Chem. Rev.*, 1993, **125**, 129–141.
- 122 L. N. Ji, M. Liu, A. K. Hsieh and T. S. A. Hor, *J. Mol. Catal.*, 1991, **70**, 247–257.
- 123 G. S. Machado, K. A. D. de Freitas Castro, F. Wypych and S. Nakagaki, *J. Mol. Catal. A Chem.*, 2008, **283**, 99–107.
- 124 E. Brulé and Y. R. De Miguel, *Org. Biomol. Chem.*, 2006, **4**, 599–609.
- 125 G. Simonneaux, P. Le Maux, Y. Ferrand and J. Rault-Berthelot, *Coord. Chem. Rev.*, 2006, **250**, 2212–2221.
- 126 B. Kerler, R. E. Robinson, A. S. Borovik and B. Subramaniam, *Appl. Catal. B Environ.*, 2004, **49**, 91–98.
- 127 G. J. de A. A. Soler-Illia, C. Sanchez, B. Lebeau and J. Patarin, *Chem. Rev.*, 2002, **102**, 4093–4138.
- 128 A. Corma, *Chem. Rev.*, 1997, **97**, 2373–2419.
- 129 Z. Kónya, V. F. Puentes, I. Kiricsi, J. Zhu, J. W. Ager, M. K. Ko, H. Frei, P. Alivisatos and G. A. Somorjai, *Chem. Mater.*, 2003, **15**, 1242–1248.
- 130 A. H. Janssen, A. J. Koster and K. P. De Jong, *J. Phys. Chem. B*, 2002, **106**, 11905–11909.
- 131 D. M. Antonelli and J. Y. Ying, *Chem. Mater.*, 1996, **8**, 874–881.
- 132 T. J. Barton, L. M. Bull, W. G. Klemperer, D. A. Loy, B. McEnaney, M. Misono, P. A.

- Monson, G. Pez, G. W. Schere, J. C. Vartuli and O. M. Yaghi, *Chem. Mater.*, 1999, **11**, 2633–2656.
- 133 M. Thommes, K. Kaneko, A. V. Neimark, J. P. Olivier, F. Rodriguez-Reinoso, J. Rouquerol and K. S. W. Sing, *Pure Appl. Chem.*, 2015, **87**, 1051–1069.
- 134 M. Kruk, M. Jaroniec, Y. Sakamoto, O. Terasaki, R. Ryoo and C. H. Ko, *J. Phys. Chem. B*, 2000, **104**, 292–301.
- 135 Z. Luan, C. F. Cheng, W. Zhou and J. Klinowski, *J. Phys. Chem.*, 1995, **99**, 1018–1024.
- 136 T. Sun and J. Y. Ying, *Nature*, 1997, **389**, 704.
- 137 S. R. Gajjela, K. Ananthanarayanan, C. Yap, M. Grätzel and P. Balaya, *Energy Environ. Sci.*, 2010, **3**, 838.
- 138 F. Jiao, J.-C. Jumas, M. Womes, A. V. Chadwick, A. Harrison and P. G. Bruce, *J. Am. Chem. Soc.*, 2006, **128**, 12905–12909.
- 139 D. M. Antonelli, *Adv. Mater.*, 1999, **11**, 487–492.
- 140 A. Ruplecker, F. Kleitz, E. L. Salabas and F. Schüth, *Chem. Mater.*, 2007, **19**, 485–496.
- 141 W. Yue and W. Zhou, *Prog. Nat. Sci.*, 2008, **18**, 1329–1338.
- 142 J. Shi, *Chem. Rev.*, 2013, **113**, 2139–2181.
- 143 T. Sun and J. Y. Ying, *Angew. Chemie Int. Ed.*, 1998, **37**, 664–667.
- 144 X. Hu, M. Trudeau and D. M. Antonelli, *Chem. Mater.*, 2007, **19**, 1388–1395.
- 145 Q. Dai, Z. Zhang, N. He, P. Li and C. Yuan, *Mater. Sci. Eng. C*, 1999, **8–9**, 417–423.
- 146 USOO5718878A, *US Pat. Appl. Publ.*, 1996.
- 147 D. M. Antonelli, A. Nakahira and J. Y. Ying, *Inorg. Chem.*, 1996, **35**, 3126–3136.

- 148 A. Lezau, M. Trudeau, G. M. Tsoi, L. E. Wenger and D. Antonelli, *J. Phys. Chem. B*, 2004, **108**, 5211–5216.
- 149 S. G. Lee, H. J. Lee, I. Song, S. Youn, D. H. Kim and S. J. Cho, *Sci. Rep.*, 2015, **5**, 12702.
- 150 A. Nakahira, T. Kubo and C. Numako, *Inorg. Chem.*, 2010, **49**, 5845–5852.
- 151 Y. Ma, W. Tong, H. Zhou and S. L. Suib, *Microporous Mesoporous Mater.*, 2000, **37**, 243–252.
- 152 M. Stöcker, *Microporous Mater.*, 1996, **6**, 235–257.
- 153 W. Jens, *Solid State Ionics*, 2000, **131**, 175–188.
- 154 N. Kosinov, C. Liu, E. J. M. Hensen and E. A. Pidko, *Chem. Mater.*, 2018, **30**, 3177–3198.
- 155 R. Murugavel and H. W. Roesky, *Angew. Chemie Int. Ed. English*, 1997, **36**, 477–479.
- 156 A. Corma, M. T. Navarro and J. P. Pariente, *J. Chem. Soc. Chem. Commun.*, 1994, 147–148.
- 157 P. T. Tanev and T. J. Pinnavaia, *Chem. Mater.*, 1996, **8**, 2068–2079.
- 158 H. H. Kung and M. C. Kung, *Catal. Today*, 2004, **97**, 219–224.
- 159 T. E. W. Nießen, J. P. M. Niederer, T. Gjervan and W. F. Hölderich, *Microporous Mesoporous Mater.*, 1998, **21**, 67–74.
- 160 J. Na, G. Liu, T. Zhou, G. Ding, S. Hu and L. Wang, *Catal. Letters*, 2013, **143**, 267–275.
- 161 M. T. Weller and S. E. Dann, *Curr. Opin. Solid State Mater. Sci.*, 1998, **3**, 137–143.
- 162 F. Fan, Z. Feng and C. Li, *Acc. Chem. Res.*, 2010, **43**, 378–387.
- 163 J. S. Beck, J. C. Vartuli, W. J. Roth, M. E. Leonowicz, C. T. Kresge, K. D. Schmitt, C.

- T. W. Chu, D. H. Olson, E. W. Sheppard, S. B. McCullen, J. B. Higgins and J. L. Schlenker, *J. Am. Chem. Soc.*, 1992, **114**, 10834–10843.
- 164 S. L. Burkett and M. E. Davis, *Chem. Mater.*, 1995, **7**, 920–928.
- 165 A. N. Fitch, H. Jobic and A. Renouprez, *J. Phys. Chem.*, 1986, **90**, 1311–1318.
- 166 T. Maschmeyer, F. Rey, G. Sankar and J. M. Thomas, *Nature*, 1995, **378**, 159–162.
- 167 A. Thangaraj, R. Kumar and P. Ratnasamy, *Appl. Catal.*, 1990, **57**, 4–6.
- 168 M. Guisnet and P. Magnoux, *Catal. Today*, 1997, **36**, 477–483.
- 169 M. Guisnet, L. Costa and F. R. Ribeiro, *J. Mol. Catal. A Chem.*, 2009, **305**, 69–83.
- 170 T. Naicker and H. B. Friedrich, *J. Porous Mater.*, 2013, **20**, 763–775.
- 171 J. Li, J. Yu and R. Xu, *Proc. R. Soc. A Math. Phys. Eng. Sci.*, 2012, **468**, 1955–1967.
- 172 L. Zhou, J. Xu, C. Chen, F. Wang and X. Li, *J. Porous Mater.*, 2008, **15**, 7–12.
- 173 J. M. L. Nieto, *Top. Catal.*, 2006, **41**, 3–15.
- 174 D. L. Vanoppen, D. E. De Vos, M. J. Genet, P. G. Rouxhet and P. A. Jacobs, *Angew. Chemie Int. Ed. English*, 1995, **34**, 560–563.
- 175 M. Hartmann and L. Kevan, *Res. Chem. Intermed.*, 2002, **28**, 625–695.
- 176 N. H. Phu, T. T. K. Hoa, N. Van Tan, H. V. Thang and P. Le Ha, *Appl. Catal. B Environ.*, 2001, **34**, 267–275.
- 177 K. Naicker, A. S. Mahomed, H. B. Friedrich and S. Singh, *J. Porous Mater.*, 2019, **26**, 301–309.
- 178 Q. H. Zhang, W. P. Deng and Y. Wang, *Chem. Commun.*, 2011, **47**, 9275–9292.
- 179 D. J. Stacchiola, S. D. Senanayake, P. Liu and J. A. Rodriguez, *Chem. Rev.*, 2013, **113**, 4373–4390.

- 180 E. Roduner, *Chem. Soc. Rev.*, 2006, **35**, 583–592.
- 181 M. C. Daniel and D. Astruc, *Chem. Rev.*, 2004, **104**, 293–346.
- 182 M. Haruta, *J. Catal.*, 1989, **115**, 301–309.
- 183 F. Shi, M. K. Tse, M.-M. Pohl, A. Brückner, S. Zhang and M. Beller, *Angew. Chemie Int. Ed.*, 2007, **46**, 8866–8868.
- 184 C. López and A. Corma, *ChemCatChem*, 2012, **4**, 751–752.
- 185 E. C. Tyo, C. Yin, M. Di Vece, Q. Qian, G. Kwon, S. Lee, B. Lee, J. E. Debartolo, S. Seifert, R. E. Winans, R. Si, B. Ricks, S. Goergen, M. Rutter, B. Zugic, M. Flytzani-Stephanopoulos, Z. W. Wang, R. E. Palmer, M. Neurock and S. Vajda, *ACS Catal.*, 2012, **2**, 2409–2423.
- 186 A. M. Gololobov, I. E. Bekk, G. O. Bragina, V. I. Zaikovskii, A. B. Ayupov, N. S. Telegina, V. I. Bukhtiyarov and A. Y. Stakheev, *Kinet. Catal.*, 2009, **50**, 830–836.
- 187 S. Guerrero, J. T. Miller and E. E. Wolf, *Appl. Catal. A Gen.*, 2007, **328**, 27–34.
- 188 S. Martínez-González, A. Gómez-Avilés, O. Martynyuk, A. Pestryakov, N. Bogdanchikova and V. C. Corberán, *Catal. Today*, 2014, **227**, 65–70.
- 189 J. M. Grau, J. C. Yori, C. R. Vera, F. C. Lovey, A. M. Condó and J. M. Parera, *Appl. Catal. A Gen.*, 2004, **265**, 141–152.
- 190 C. A. Wilde, Y. Ryabenkova, I. M. Firth, L. Pratt, J. Railton, M. Bravo-Sanchez, N. Sano, P. J. Cumpson, P. D. Coates, X. Liu and M. Conte, *Appl. Catal. A Gen.*, 2019, **570**, 271–282.
- 191 F. Regali, L. F. Liotta, A. M. Venezia, M. Boutonnet and S. Järås, *Appl. Catal. A Gen.*, 2014, **469**, 328–339.
- 192 M. S. Avila, C. I. Vignatti, C. R. Apesteguía and T. F. Garetto, *Chem. Eng. J.*, 2014, **241**, 52–59.

- 193 A. H. Lu, J. J. Nitz, M. Comotti, C. Weidenthaler, K. Schlichte, C. W. Lehmann, O. Terasaki and F. Schüth, *J. Am. Chem. Soc.*, 2010, **132**, 14152–14162.
- 194 N. Dimitratos, J. A. Lopez-Sanchez and G. J. Hutchings, in *Handbook of Advanced Methods and Processes in Oxidation Catalysis*, Imperial College Press, London, 2014, pp. 631–678.
- 195 C. Zhang, H. Huang, G. Li, L. Wang, L. Song and X. Li, *Catal. Today*, 2019, **327**, 374–381.
- 196 L. Coulier, J. A. R. Van Veen and J. W. Niemantsverdriet, *Catal. Letters*, 2002, **79**, 149–153.
- 197 Y. Chen, H. Zheng, Z. Guo, C. Zhou, C. Wang, A. Borgna and Y. Yang, *J. Catal.*, 2011, **283**, 34–44.
- 198 A. Harriman, I. J. Pickering, J. M. Thomas and P. A. Christensen, *J. Chem. Soc. Faraday Trans. 1 Phys. Chem. Condens. Phases*, 1988, **84**, 2795–2806.
- 199 R. Burch, D. J. Crittle and M. J. Hayes, *Catal. Today*, 1999, **47**, 229–234.
- 200 H. Gruber-Woelfler, P. F. Radaschitz, P. W. Feenstra, W. Haas and J. G. Khinast, *J. Catal.*, 2012, **286**, 30–40.
- 201 R. A. Sheldon, M. Wallau, I. W. C. E. Arends and U. Schuchardt, *Acc. Chem. Res.*, 1998, **31**, 485–493.
- 202 H. U. Blaser, A. Indolese, A. Schnyder, H. Steiner and M. Studer, *J. Mol. Catal. A Chem.*, 2001, **173**, 3–18.

CHAPTER 2: Experimental methods and techniques

Contents

CHAPTER 2: Experimental methods and techniques.....	72
Abbreviations	74
2.1. Materials	76
2.1.1. For bulk catalyst synthesis	79
2.1.2. For microporous synthesis	79
2.1.3. For template removal	80
2.1.4. For catalytic tests and calibration of equipment.....	80
2.2. Synthesis	81
2.2.1. Supported metals and metal oxides – working principles of deposition methods... 81	
2.2.1.1. Wetness impregnation.....	82
2.2.1.2. Deposition-precipitation	83
2.2.1.3. Coprecipitation	84
2.2.1.4. Sol-immobilisation	85
2.2.2. Supported metal oxides – actual preparation procedure(s)	86
2.2.2.1. Wetness impregnation.....	86
2.2.2.2. Hydrogenation	87
2.2.3. Microporous materials.....	87
2.2.4. Microporous titanium oxide	89
2.2.4.1. Antonelli's protocol	89
2.2.4.2. Dai's protocol	90
2.2.4.3. Zhang's protocol.....	90
2.2.4.4. Peptization	91
2.2.5. Microporous niobium oxide	92
2.2.5.1. Ying's protocol.....	92
2.2.5.2. Antonelli's protocol	93
2.3. Template removal	94
2.3.1. Microporous titanium oxide	94
2.3.1.1. Calcination	94
2.3.1.2. Solvent washes	94
2.3.1.3. Acidic washes	94
2.3.1.3.1. HNO ₃	94
2.3.1.3.2. <i>p</i> -TSA	95
2.3.1.4. Alternatives to acids	95

2.3.1.4.1.	H ₂ O ₂	95
2.3.1.4.2.	Phthalic anhydride	96
2.3.2.	Microporous niobium oxide (and microporous Fe/Nb ₂ O ₅).....	96
2.3.2.1.	Acidic washes	96
2.3.2.2.	Phthalic anhydride.....	97
2.4.	Catalytic tests	98
2.4.1.	<i>n</i> -decane.....	98
2.4.1.1.	Atmospheric tests.....	98
2.4.1.2.	Pressurised tests.....	98
2.4.2.	Cyclooctane.....	99
2.4.3.	Dried metal salt tests	99
2.5.	Analytical methods.....	100
2.5.1.	Quantitative analysis of hydrocarbon reaction mixtures	100
2.5.2.	¹ H-NMR	101
2.5.2.1.	¹ H-NMR <i>n</i> -decane and <i>n</i> -octane.....	102
2.5.2.2.	¹ H-NMR Cyclooctane	103
2.5.3.	Gas chromatography – mass spectrometry (GC-MS).....	103
2.5.4.	Fourier transform infrared – attenuated total reflectance (FTIR-ATR).....	105
2.5.5.	Thermogravimetric analysis (TGA).....	106
2.5.6.	X-ray powder diffraction (XRPD).....	107
2.5.6.1.	Determination of particle size	108
2.5.6.2.	Determination of pore size.....	108
2.5.7.	X-ray photoelectron spectroscopy (XPS)	109
2.5.8.	Brunauer-Emmett-Teller (BET)	110
2.5.9.	ICP-OES (Inductively coupled plasma optical emission spectroscopy)	111
2.6.	References	114

Abbreviations

BET – Brunauer-Emmett-Teller

COSHH – Control Of Substances Hazardous To Health

CP – Coprecipitation

DCM – Dichloromethane

DMF – Dimethylformamide

DP – Deposition Precipitation

EDTA – Ethylenediaminetetraacetic Acid

FTIR-ATR – Fourier Transform Infra-Red Attenuated Total Reflectance

GC-MS – Gas Chromatography – Mass Spectrometry

HPLC – High Performance Liquid Chromatography

ICP-OES – Inductively Coupled Plasma – Optical Emission Spectroscopy

IRE – Internal Reflection Element

IWI – Incipient Wetness Impregnation

MCM-41 – Mobil Composition of Matter #41

NIST – National Institute of Standards and Technology

NMR – Nuclear Magnetic Resonance

PO_2 – Pressure gauge O_2

p-TSA – *para* Toluene Sulphonic Acid

SI – Sol-immobilisation

TEM – Transmission Electron Microscopy

TEMPO – (2,2,6,6-Tetramethylpiperidin-1-yl)oxyl

TGA – Thermogravimetric Analysis

TMS-1 – Transition metal oxide molecular sieve #1

WI – Wetness impregnation

XPS – X-ray Photoelectron Spectroscopy

XRPD – X-ray Powder Diffraction

ZSM-5 – Zeolite Socony Material #5

2.1. Materials

A complete list of materials is shown below, table 2.1.1, materials used for a specific purpose are described under the relevant section headings.

Table 2.1.1: A complete list of materials used throughout the current work.

Name	Chemical formula	Supplier	Purity/ Grade/ Form
(2,2,6,6-Tetramethylpiperidin-1-yl)oxyl, TEMPO	C ₉ H ₁₈ NO	SLS	98%
1-decanol	C ₁₀ H ₂₂ O	Sigma-Aldrich	≥98%
2-decanol	C ₁₀ H ₂₂ O	Acros	98%
2-decanone	C ₁₀ H ₂₀ O	Aldrich	98%
3-decanol	C ₁₀ H ₂₂ O	Alfa Aesar	97%
3-decanone	C ₁₀ H ₂₀ O	Sigma-Aldrich	≥97%
4-decanol	C ₁₀ H ₂₂ O	Alfa Aesar	97+%
1-octanol	C ₈ H ₁₈ O	Merck	For synthesis
2-octanol	C ₈ H ₁₈ O	Merck	For synthesis
2-octanone	C ₈ H ₁₆ O	Merck	For synthesis
3-octanol	C ₈ H ₁₈ O	Merck	For synthesis
3-octanone	C ₈ H ₁₆ O	Aldrich	>98%
5-decanone	C ₁₀ H ₂₀ O	Alfa Aesar	99%
Aluminosilicate, mesostructured, MCM-41	SiO ₂ /Al ₂ O ₃	Aldrich	-
Cerium (IV) oxide	CeO ₂	Acros	99.9%, trace metal basis
Cyclooctane	C ₈ H ₁₆	Aldrich	≥99%
Decanal	C ₁₀ H ₂₀ O	Alfa Aesar	96%
Dodecylamine	C ₁₂ H ₂₅ N	Acros	98%
Dichloromethane, DCM	CH ₂ Cl ₂	Sigma	HPLC grade
Diethyl ether, Ether	C ₄ H ₁₀ O	Honeywell	≥99.8%
Dimethylformamide, DMF	C ₃ H ₇ NO	VWR	-
Deuterated chloroform	CDCl ₃	VWR	99.8% D
Ethanol	C ₂ H ₆ O	VWR	Absolute
Gold(III) chloride trihydrate	HAuCl ₄ ×3H ₂ O	Fluka	≥99% trace metal basis
Hexylamine	C ₆ H ₁₅ N	Acros	99%
Hydrochloric acid	HCl	VWR	35%
Hydrogen peroxide	H ₂ O ₂	Sigma	≥35%
Iron(III) acetylacetonate	Fe(C ₅ H ₇ O ₂) ₃	Acros	99+%
Iron(III) ethoxide	Fe(OEt) ₃	Alfa Aesar	99.6%, trace metal basis
Iron(III) isopropoxide	Fe(O ⁱ Pr) ₃	Alfa Aesar	98%

Iron(III) nitrate nonahydrate	$\text{Fe}(\text{NO}_3)_3 \cdot 9\text{H}_2\text{O}$	Acros	99+%
Iron(III) oxide powder	Fe_2O_3	Sigma	99.98%
Iron(0) powder	Fe	Acros	99%
Manganese(II) methoxide	$\text{Mn}(\text{OMe})_2$	Alfa Aesar	-
Manganese(II) nitrate tetrahydrate	$\text{Mn}(\text{NO}_3)_2 \cdot 4\text{H}_2\text{O}$	Sigma Aldrich	>97%
Methanol	CH_4O	Fisher	HPLC grade
Molecular sieves, titanium oxide based	TiO_2	Alfa Aesar	25 angstrom powder
<i>n</i> -decane	$\text{C}_{10}\text{H}_{22}$	Acros	99%
<i>n</i> -dodecane	$\text{C}_{12}\text{H}_{26}$	Fischer scientific	99%
<i>n</i> -octane	C_8H_{18}	Acros	99+%, extra pure
$\text{NH}_4\text{ZSM-5}$	$\text{NH}_4/\text{SiO}_2/\text{Al}_2\text{O}_3$	Alfa Aesar	$425\text{m}^2\text{ g}^{-1}$, 23:1 $\text{SiO}_2:\text{Al}_2\text{O}_3$
Niobium(V) ethoxide	$\text{Nb}(\text{OEt})_5$	Alfa Aesar	99.9%, metal basis
Niobium(IV) oxide	NbO_2	Alfa Aesar	99+%
Niobium(V) oxide	Nb_2O_5	Aldrich	99.9%, trace metal basis
Niobium(V) oxide	Nb_2O_5	Aldrich	99.99%, trace metal basis
Nitric acid	HNO_3	VWR	68%
Octanal	$\text{C}_8\text{H}_{16}\text{O}$	Aldrich	99%
Palladium(II) 2,4-pentanedionate	$\text{Pd}(\text{C}_5\text{H}_7\text{O}_2)_2$	Fisher	-
Palladium(II) nitrate hydrate	$\text{Pd}(\text{NO}_3)_2 \cdot x\text{H}_2\text{O}$	Acros	40% Pd
<i>para</i> toluene sulphonic acid monohydrate	$\text{C}_7\text{H}_8\text{O}_3\text{S} \cdot \text{H}_2\text{O}$	Sigma-Aldrich	98.50%
Phthalic anhydride	$\text{C}_8\text{H}_4\text{O}_3$	Sigma-Aldrich	$\geq 99\%$
Silica, mesostructured, MCM-41 type	SiO_2	Aldrich	-
Silicon(IV) dioxide	SiO_2	Aldrich	99.80%
Silver(I) 2,4-pentanedionate	$\text{AgC}_5\text{H}_7\text{O}_2$	Fisher	-
Silver(I) nitrate	AgNO_3	Sigma Aldrich	-
Sodium hydroxide	NaOH	VWR	$\geq 98\%$
Sodium iron EDTA	$\text{C}_{10}\text{H}_{12}\text{N}_2\text{FeNa}_2\text{O}_8 \cdot 3\text{H}_2\text{O}$	BioReagent	-
Tetradecylamine	$\text{C}_{14}\text{H}_{29}\text{N}$	Sigma-Aldrich	95%
Titanium(IV) (triethanolaminate)isopropoxide solution	$\text{C}_9\text{H}_{19}\text{NO}_4\text{Ti}$	Sigma-Aldrich	TYZOR® TE organic titanate
Titanium butoxide (IV)	$\text{Ti}(\text{O}^i\text{Bu})_4$	Aldrich	97%
Titanium (IV) ethoxide	$\text{Ti}(\text{OEt})_4$	Aldrich	Technical grade
Titanium (IV) isopropoxide	$\text{Ti}(\text{O}^i\text{Pr})_4$	Aldrich	99.999% trace metal basis
Titanium(IV) oxide	TiO_2	Acros	Aeroxide®, p-25

Titanium(IV) oxide	TiO ₂	Aldrich	Anatase, 99.8% trace metals basis
Titanium(IV) oxide	TiO ₂	Aldrich	Rutile, ≥99.9% trace metals basis
Toluene	C ₇ H ₈	Sigma	HPLC grade
Triethylamine	N(C ₂ H ₅) ₃	Sigma-Aldrich	≥99.5%
Zeolite 13X	-	Acros	Molecular sieves

2.1.1. For bulk catalyst synthesis

All materials used for bulk catalyst preparation are as follows: Iron(III) nitrate nonahydrate ($\text{Fe}(\text{NO}_3)_3 \cdot 9\text{H}_2\text{O}$, 99+%, Acros), Manganese(II) nitrate tetrahydrate ($\text{Mn}(\text{NO}_3)_2 \cdot 4\text{H}_2\text{O}$, >97%, Sigma Aldrich), Palladium(II) nitrate hydrate ($\text{Pd}(\text{NO}_3)_2 \cdot x\text{H}_2\text{O}$, 40% Pd, Acros), Gold(III) chloride trihydrate ($\text{HAuCl}_4 \cdot 3\text{H}_2\text{O}$, $\geq 99\%$ trace metal basis, Fluka), Silver(I) nitrate (AgNO_3 , Sigma Aldrich), Sodium iron EDTA ($\text{C}_{10}\text{H}_{12}\text{N}_2\text{FeNa}_2\text{O}_8 \cdot 3\text{H}_2\text{O}$, BioReagent), Titanium(IV) oxide (TiO_2 , aerioxide[®], p-25, Acros), Titanium(IV) oxide (TiO_2 , anatase, 99.8% trace metals basis, Aldrich), Titanium(IV) oxide (TiO_2 , rutile, $\geq 99.9\%$ trace metals basis, Aldrich), Molecular sieves, titanium oxide based, 25 angstrom powder (TiO_2 , Alfa Aesar), Silica, mesostructured, MCM-41 type (SiO_2 , Aldrich), Aluminosilicate, mesostructured, MCM-41 ($\text{SiO}_2/\text{Al}_2\text{O}_3$, Aldrich), $\text{NH}_4\text{ZSM-5}$ ($425\text{m}^2\text{ g}^{-1}$, 23:1 $\text{SiO}_2:\text{Al}_2\text{O}_3$, Alfa Aesar), Zeolite 13X (Molecular sieves, Acros), Cerium (IV) oxide (CeO_2 , 99.9%, trace metal basis, Acros), Silicon(IV) dioxide (SiO_2 , 99.8%, Aldrich), Niobium(IV) oxide (NbO_2 , 99+%, Alfa Aesar), Niobium(V) oxide (Nb_2O_5 , 99.9%, trace metal basis, Aldrich), Niobium(V) oxide (Nb_2O_5 , 99.99%, trace metal basis, Aldrich), Iron(0) powder (99%, Acros), Iron(III) oxide powder (Fe_2O_3 , 99.98%, Sigma).

Ovens used are: Genlab Mino 30/F/DIG for the initial drying of catalysts, Carbolite CWF 11/14 for calcination under static air and Carbolite MTF 12/38/250 for hydrogenation, all ovens were fitted with a Eurotherm temperature control.

Hydrogenation was conducted in the Carbolite MTF 12/38/250 furnace fitted with a quartz liner using Hydrogen 5%, Nitrogen 95% (H_2/N_2 , v/v%, BOC).

2.1.2. For microporous synthesis

All materials used for microporous TiO_2 and microporous Nb_2O_5 synthesis are as follows: Titanium (IV) isopropoxide ($\text{Ti}(\text{O}^i\text{Pr})_4$, 99.999% trace metal basis, Aldrich), Titanium (IV) ethoxide ($\text{Ti}(\text{OEt})_4$, technical grade, Aldrich), Titanium butoxide (IV) ($\text{Ti}(\text{O}^n\text{Bu})_4$, 97%, Aldrich), Titanium(IV) (triethanolaminate)isopropoxide solution ($\text{C}_9\text{H}_{19}\text{NO}_4\text{Ti}$, TYZOR[®] TE organic titanate, Sigma-Aldrich), Titanium(IV) oxide (TiO_2 , anatase, 99.8% trace metals basis, Aldrich)

Niobium(V) ethoxide ($\text{Nb}(\text{OEt})_5$, 99.9%, metal basis, Alfa Aesar) Iron(III) ethoxide ($\text{Fe}(\text{OEt})_3$, 99.6%, trace metal basis, Alfa Aesar), Iron(III) isopropoxide ($\text{Fe}(\text{O}^i\text{Pr})_3$, 98%, Alfa Aesar), Iron(III) acetylacetonate ($\text{Fe}(\text{C}_5\text{H}_7\text{O}_2)_3$, 99+%, Acros) Manganese(II) methoxide ($\text{Mn}(\text{OMe})_2$, Alfa Aesar), Silver(I) 2,4-pentanedionate ($\text{AgC}_5\text{H}_7\text{O}_2$, Fisher), Palladium(II) 2,4-pentanedionate ($\text{Pd}(\text{C}_5\text{H}_7\text{O}_2)_2$, Fisher), Hexylamine ($\text{C}_6\text{H}_{15}\text{N}$, 99%, Acros), Dodecylamine ($\text{C}_{12}\text{H}_{25}\text{N}$, 98%, Acros), Tetradecylamine ($\text{C}_{14}\text{H}_{29}\text{N}$, 95%, Sigma-Aldrich), Hydrochloric acid (HCl , 35%, VWR), Sodium hydroxide (NaOH , $\geq 98\%$, VWR), Methanol (CH_4O , HPLC grade, Fisher), Ethanol ($\text{C}_2\text{H}_6\text{O}$, absolute, VWR), Diethylether ($\text{C}_4\text{H}_{10}\text{O}$, Ether, $\geq 99.8\%$, Honeywell).

2.1.3. For template removal

Nitric acid 68% (HNO_3 , VWR), *para* toluene sulphonic acid monohydrate ($\text{C}_7\text{H}_8\text{O}_3\text{S}\cdot\text{H}_2\text{O}$, *p*-TSA. H_2O , 98.5%, ACS Sigma-Aldrich), Hydrogen peroxide $\geq 35\%$ (H_2O_2 , Sigma), Phthalic anhydride ($\text{C}_8\text{H}_4\text{O}_3$ $\geq 99\%$, Sigma-Aldrich) Dimethylformamide ($\text{C}_3\text{H}_7\text{NO}$, DMF, VWR), Triethylamine ($\text{N}(\text{C}_2\text{H}_5)_3$, $\geq 99.5\%$, Sigma-Aldrich), Hydrochloric acid (HCl , 35%, VWR).

Calcinations were conducted in a Carbolite CWF 11/14 oven fitted with a eurotherm temperature control.

2.1.4. For catalytic tests and calibration of equipment

All materials used during catalytic tests are as follows: *n*-octane (C_8H_{18} , 99+%, extra pure, Acros), 1-octanol ($\text{C}_8\text{H}_{18}\text{O}$, for synthesis, Merck), 2-octanol ($\text{C}_8\text{H}_{18}\text{O}$, for synthesis, Merck), 3-octanol ($\text{C}_8\text{H}_{18}\text{O}$, for synthesis, Merck), Octanal ($\text{C}_8\text{H}_{16}\text{O}$, 99%, Aldrich), 2-octanone ($\text{C}_8\text{H}_{16}\text{O}$, for synthesis, Merck), 3-octanone ($\text{C}_8\text{H}_{16}\text{O}$, $>98\%$, Aldrich), *n*-decane ($\text{C}_{10}\text{H}_{22}$, 99%, Acros), 1-decanol ($\text{C}_{10}\text{H}_{22}\text{O}$, $\geq 98\%$, Sigma-Aldrich), 2-decanol ($\text{C}_{10}\text{H}_{22}\text{O}$, 98%, Acros), 3-decanol ($\text{C}_{10}\text{H}_{22}\text{O}$, 97%, Alfa Aesar), 4-decanol ($\text{C}_{10}\text{H}_{22}\text{O}$, 97+%, Alfa Aesar), Decanal ($\text{C}_{10}\text{H}_{20}\text{O}$, 96%, Alfa Aesar), 2-decanone ($\text{C}_{10}\text{H}_{20}\text{O}$, 98%, Aldrich), 3-decanone ($\text{C}_{10}\text{H}_{20}\text{O}$, $\geq 97\%$, Sigma-Aldrich), 5-decanone ($\text{C}_{10}\text{H}_{20}\text{O}$, 99%, Alfa Aesar), *n*-dodecane ($\text{C}_{12}\text{H}_{26}$, 99%, Fischer scientific), Cyclooctane (C_8H_{16} , $\geq 99\%$, Aldrich) Dichloromethane (CH_2Cl_2 , DCM, HPLC grade,

Sigma), Toluene (C₇H₈, HPLC grade, Sigma) (2,2,6,6-Tetramethylpiperidin-1-yl)oxyl, (TEMPO, C₉H₁₈NO, 98%, SLS), Deuterated chloroform (CDCl₃, 99.8% D, VWR).

2.2. Synthesis

2.2.1. Supported metals and metal oxides – working principles of deposition methods

How a metal is doped onto a support may affect its catalytic activity.¹ Three main methods will be discussed: wetness impregnation (WI), precipitation (coprecipitation, CP and deposition-precipitation, DP) and sol-immobilisation (SI). A schematic summary of these techniques is shown in figure 2.2.1.1.¹⁻⁸ Microscopy images from a study of Pd/ZnO catalysts prepared by WI and Sol-immobilisation are shown side-by-side, figure 2.2.1.2,⁹ demonstrating the potential differences in particle size and distribution when different preparation methods are used.

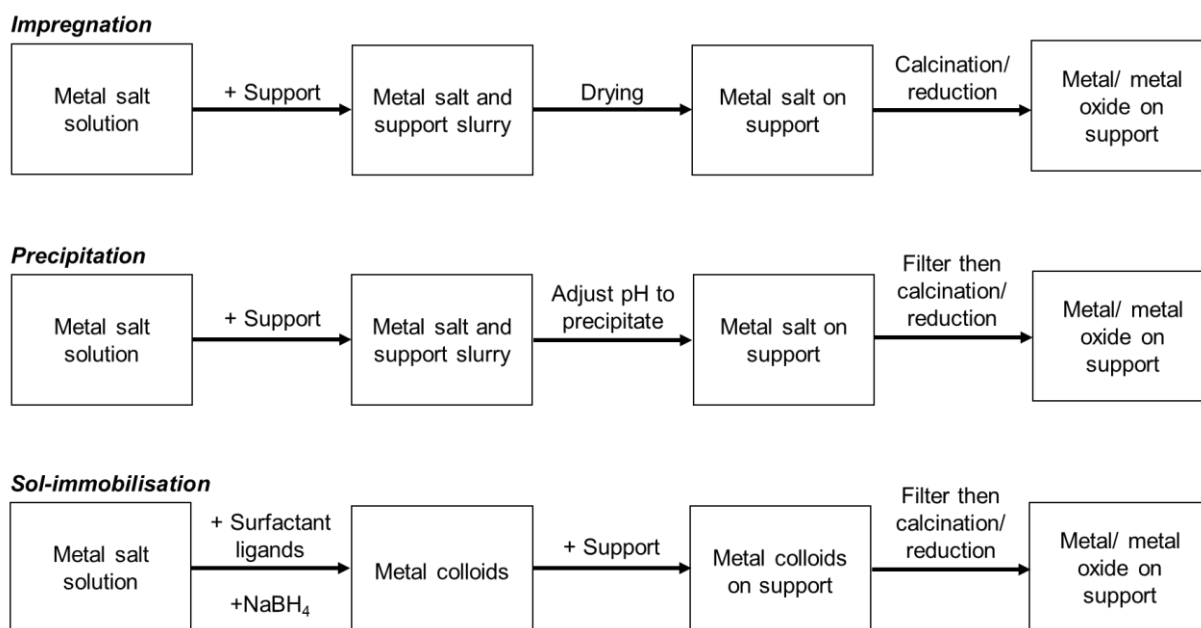


Figure 2.2.1.1 A brief summary of each of the three main deposition techniques for the preparation of metals or metal oxides on a support.¹⁻⁸

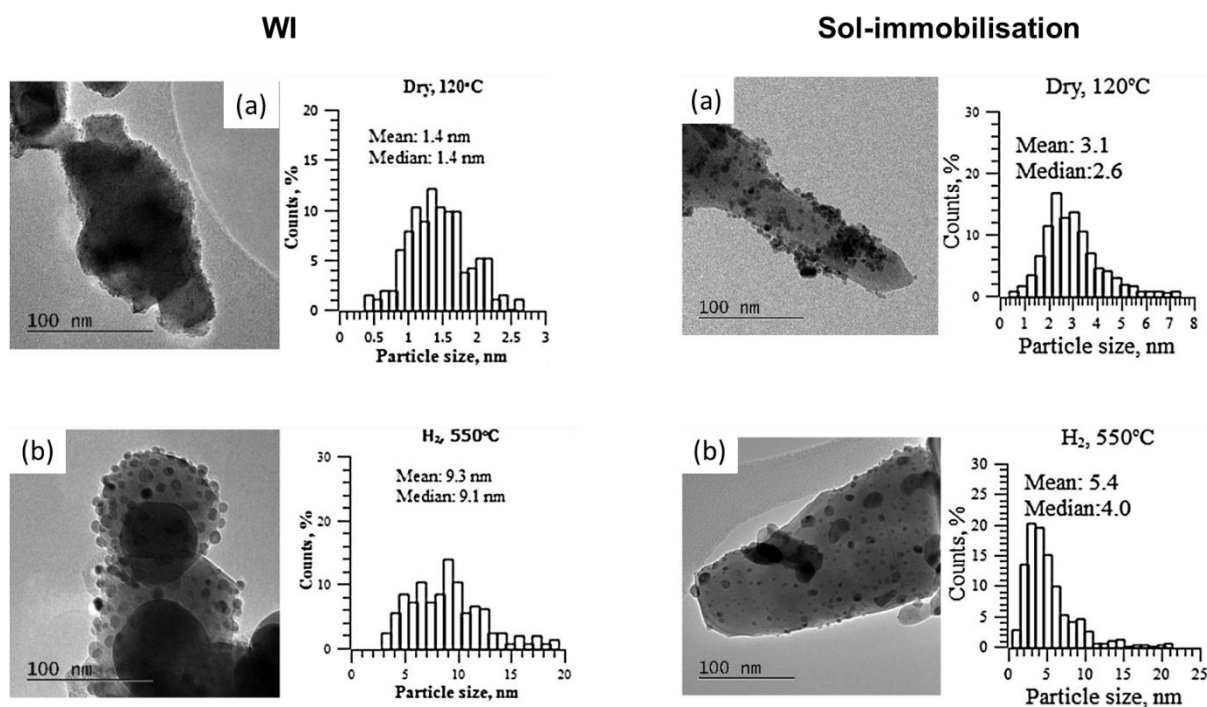


Figure 2.2.1.2: Transmission electron microscopy (TEM) images and corresponding particle size distribution of Pd/ZnO (1 wt% Pd) catalysts prepared by WI (left) and SI (right). (a) samples dried after synthesis at 120 °C, (b) samples annealed under hydrogen at 550 °C. Reproduced under a creative commons licence from *Bahruji et al.*⁹

2.2.1.1. Wetness impregnation

Wetness impregnation (WI) involves dissolving a metal precursor (e.g. a metal nitrate) in a solvent (typically water, or ethanol).¹⁰ The support (e.g. metal oxide, silica) is then added (with its amount varying on desired metal loading) to this solution often to form a slurry and the solvent is slowly dried through gentle heating below its boiling point. This leads to the metal precursor being dispersed across the support. The material is then often calcined to convert the precursor to the desired metal/ metal oxide (and reduced afterwards if required), figure 2.2.1.1.1.

A variant to this protocol is the 'incipient wetness impregnation' (IWI). This is where the solution's volume is equal to the pore volume of the support, this promotes the dopant metal to be deposited only within the pores of a support as opposed to the exterior.¹¹ IWI is often

preferred in industry because of a minimal requirement in the use of the solvent and as this promotes the nearly entire deposition of the metal into the support thus minimizing waste (especially in the case of precious metal deposition).

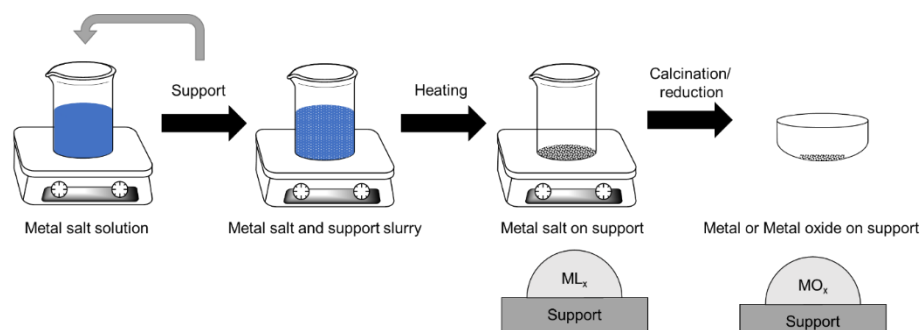


Figure 2.2.1.1.1: A schematic diagram to show the steps involved during wetness impregnation and composition of the dopant/support during some of the steps. Figure adapted from *L.Sun et al.* with permission.¹²

The incipient wetness protocol was shown to create active catalysts for the oxidation of alkanes. Iron oxide was dispersed on silica by using this method. These catalysts were capable of the oxidation of adamantane using hydrogen peroxide as an oxidant.¹³ Interestingly, the study compared the use of $Fe(NO_3)_3$ to FeEDTA as the metal salt precursor during the synthesis. It was found that using FeEDTA gave rise to ‘single-sites’ of iron due to much more dispersed material. The initial rate of the FeEDTA samples were significantly higher than those prepared by $Fe(NO_3)_3$ and is thought to be due to undercoordinated iron only found in small clusters. The study aptly illustrates how different nanomaterials may behave depending on their size and dispersion. Within this research we focused on wetness impregnation as the primary technique for loading metal oxides upon supports. We chose this method as it is easy to conduct practically and preliminary data of *n*-decane oxidation with Fe/TiO_2 gave sufficient conversion (~5%). Other loading techniques will be briefly mentioned here to demonstrate the possibilities and differences in the synthesis of loaded metal oxides.

2.2.1.2. Deposition-precipitation

This method is similar to that of wetness-impregnation, however, instead of drying the metal salt solution (leading to deposition) the pH of the solution is adjusted (this is typically done

with either sodium hydroxide or urea) until precipitation of the metal hydroxide occurs, thus depositing it onto the support.¹⁰ Unlike wetness impregnation, control on the properties of the final material are possible from varying pH of solution and duration of the precipitation process, however, the overall process is more complex.^{14–16} A summary of this process is shown in figure 2.2.1.2.1.

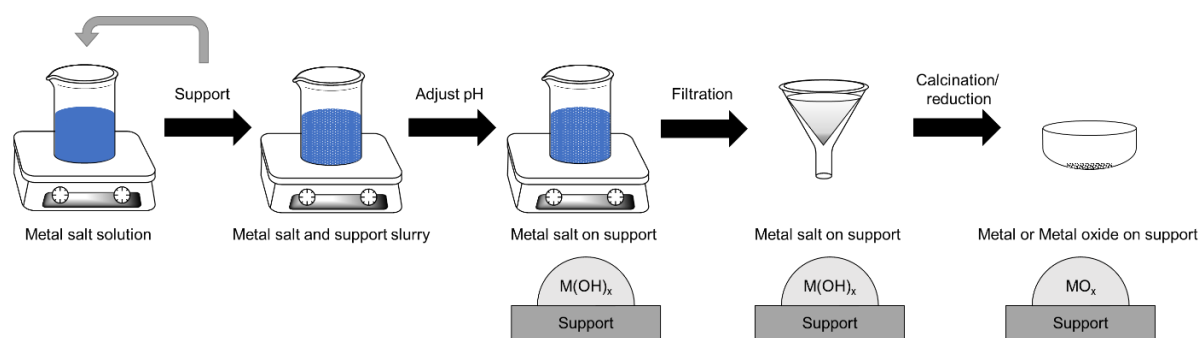


Figure 2.2.1.2.1: A schematic diagram to show the steps involved during deposition-precipitation and composition of the dopant/support during some of the steps.¹⁵

Catalysts prepared from deposition precipitation have been applied to alkane oxidation. For example, Xu *et al.* showed that gold deposited onto TiO_2/SiO_2 via deposition-precipitation is capable of cyclohexane oxidation. Conversions of 8 – 9% were observed for the oxidation of cyclohexane.¹⁷ Deposition-precipitation is an efficient method to achieve a smaller particle size distribution, but often leads to a lower metal loading as part of the metal remains in solution in the form of soluble non stoichiometric hydroxides.¹⁸

This method was trialled but did not yield significant conversion and was thus not pursued.

2.2.1.3. Coprecipitation

Coprecipitation involves dissolving a metal precursor into solution, where then a support precursor (the co-precipitate) is also added. Another solution is then added (e.g. sodium hydroxide) to form a precipitate of both the support and dopant metal, thus dispersing the dopant metal across the support. Any by-product is then washed away from the catalyst,

where then the catalyst may be calcined/reduced.^{19–22} This method is summarised in figure 2.2.1.3.1.

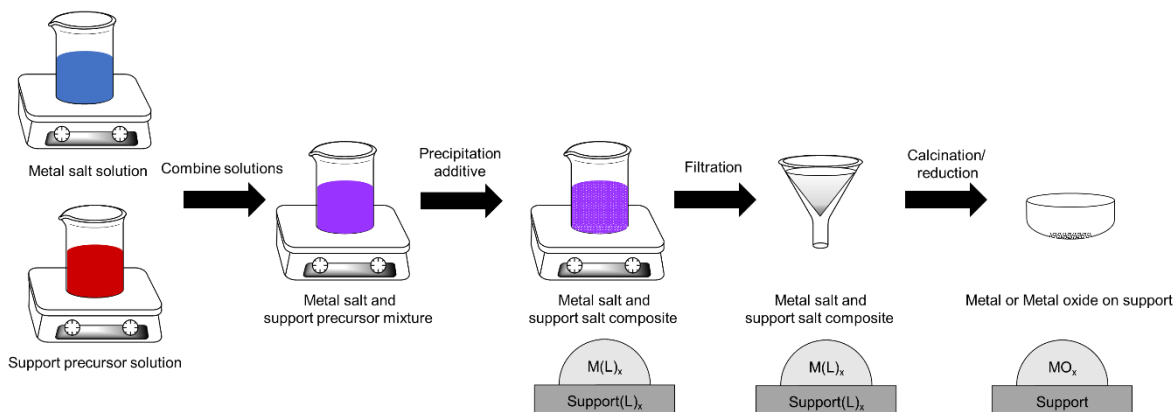


Figure 2.2.1.3.1: A schematic diagram to show the steps involved during coprecipitation and composition of the dopant/support during some of the steps.^{19–21}

This method may lead to significant dispersion of the dopant metal, however, the presence of the dopant metal during the support's formation may hinder its growth, leading to less desirable properties.¹⁰ This method was not used in this research, but for completeness it is mentioned here.

2.2.1.4. Sol-immobilisation

Sol-immobilisation is a technique where a metal nanoparticle is formed *in situ*, utilising ligands such as long-chain thiols.²³ A support is then added and the solvent is removed.²⁴ The main advantage of sol-immobilisation over other techniques is typically a narrower particle size distribution exists in the final product as the particles are formed as colloids prior to calcination.^{9,25–27} This is summarised in figure 2.2.1.4.1. It is a technique often used to optimise pre-existing catalysts for a more uniform distribution.²⁸

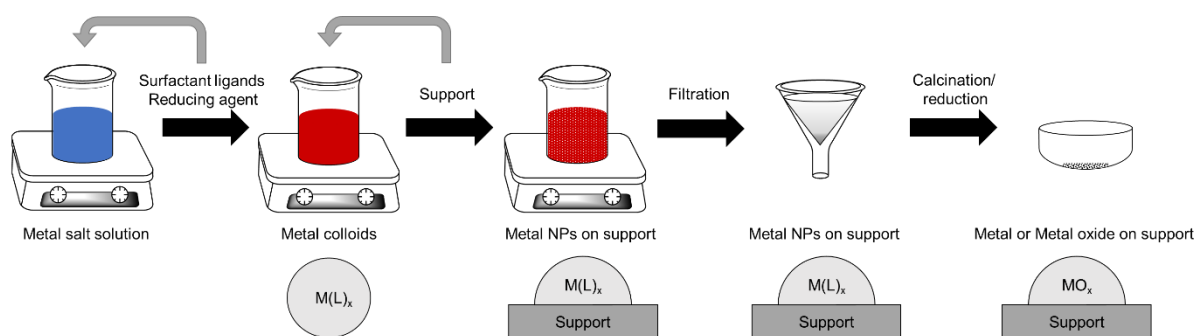


Figure 2.2.1.4.1: A schematic diagram to show the steps involved during sol-immobilisation and composition of the dopant/support during some of the steps.^{29,30}

Catalysts prepared through sol-immobilisation are therefore very common within the literature. For example, benzyl alcohol and CO can be oxidised using Au/MnO₂ prepared via sol-immobilisation. All methods mentioned thus far may lead to varying activity. This was shown in catalysts prepared by sol-immobilisation which gave the highest catalytic activity for benzyl alcohol conversion, whereas catalysts prepared via deposition-precipitation were best for CO oxidation.¹ As for catalysts used in alkane oxidation prepared via sol-immobilisation there are some significant examples. *G. Hutchings* has studied Au, Pd and Pt based catalysts where the metals are loaded onto a support (activated carbon, titania) via sol-immobilisation and their application to the oxidation of alkanes.^{7,8,31} The use of gold and palladium alkane oxidation catalysts gave scope for their use within this project. Similar to coprecipitation, this method was not conducted in this research, however, due to its significance in the literature, it is mentioned here.

2.2.2. Supported metal oxides – actual preparation procedure(s)

2.2.2.1. Wetness impregnation

Catalysts were prepared via wet impregnation. Here the preparation of the most extensively used catalyst in this research, Fe/TiO₂ 1 wt%, is described. Fe(NO₃)₃·9H₂O (0.145 g, 3.58·10⁻⁴ mol) was dissolved in distilled water (20 mL) followed by the addition of the support, TiO₂ (1.98 g). The mixture was then stirred at 80 °C in a 250 mL beaker. The water evaporated slowly leaving a damp orange solid, which was then further dried at 120 °C in a Genlab Mino

30/F/DIG for 16 h. The resulting material was then calcined (680 °C, 10 °C min⁻¹) in a Carbolite CWF 11/14 under static air. This procedure was identical across all other dopant metals (Mn, Pd, Ag, Au) and supports (Nb₂O₅, ZSM-5, MCM-41 etc.) used, with varying amounts so a desired wt% is obtained. Furthermore, varying calcination conditions (250 °C – 680 °C) and solvent (ethanol) were also trialled.

2.2.2.2. Hydrogenation

In a typical hydrogenation a sample (0.200 – 0.500g) was placed in a calcination boat, positioned in the centre of the tubular furnace lined with a quartz tube, this was then purged with nitrogen (1 bar, 100 mL min⁻¹, 10 min), followed by setting a flow of 5% H₂/N₂ (2 bar, 20 mL min⁻¹) and heated at the designated temperature (10 °C min⁻¹ ramp) for 30 min.

2.2.3. Microporous materials

Microporous metal oxides were synthesised utilising hydrothermal techniques. Microporous TiO₂ and microporous Nb₂O₅ are formed when a surfactant and metal alkoxide are mixed – with the surfactant displacing the alkoxide ligand. After the addition of water, the metal-surfactant complexes form micelles which align to form tubes. These tubes are then compiled from the pressure during the hydrothermal step to form a porous array of nanotubes (more information in section 1.5.1 and in the literature).³² The synthesis protocol of soft-templating synthesis via hydrothermal methods is summarised in figure 2.2.3.1. The advantages with this kind of synthesis is the ability to change the parameters (autoclave temperature, autoclave duration, template alkyl chain length) to fine tune the properties of the final material,^{32,33} however, the material must have the organic template removed which may affect porosity.³⁴

An alternative synthesis via peptization of bulk anatase was also conducted, see sections 1.5.1 and 2.2.4.4.³⁵

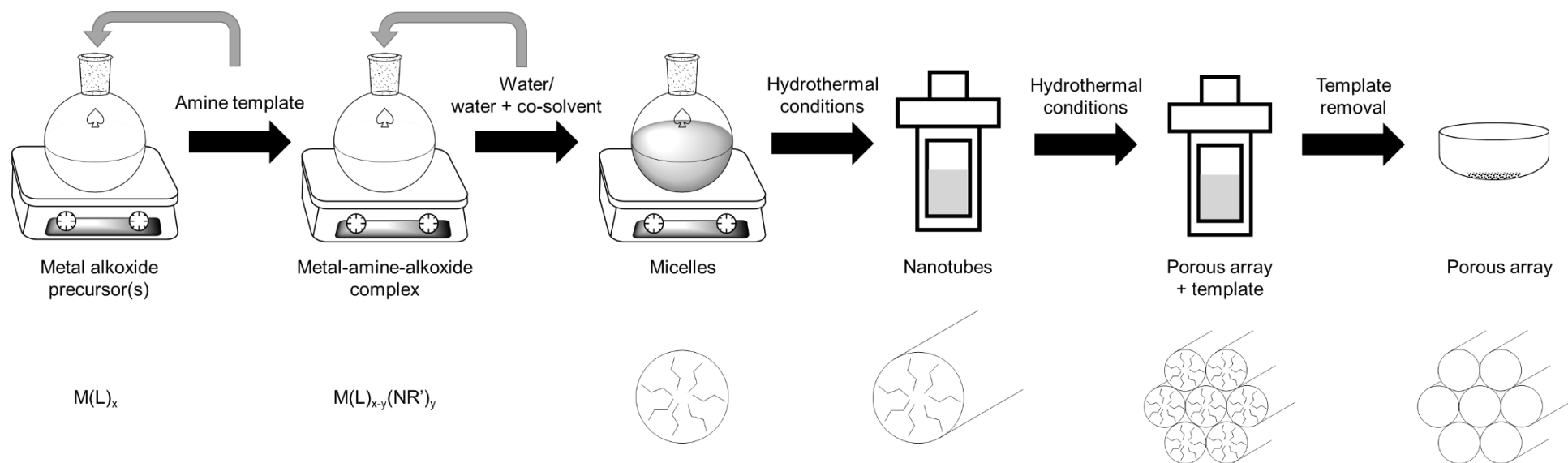


Figure 2.2.3.1: A general overview of microporous synthesis of porous metal oxides via a soft-templating approach, based on the literature sources used within this work.^{32,33,36–38}

2.2.4. Microporous titanium oxide

The synthesis of microporous titanium oxide was conducted several times during this research. Multiple modifications were made such as: autoclave step duration, autoclave temperature, titanium precursor and the presence of dopant metals. Therefore, specific examples are listed here, but are subject to differences in parameters where stated in the results section 5.2.

2.2.4.1. Antonelli's protocol

The synthesis is based on an adapted method from Antonelli *et al.*³⁷

Mesoporous titanium oxide

Hexylamine (0.823 mL, 6.26 mmol), was stirred between 40 – 50 °C followed by the addition of titanium(IV) isopropoxide in a 1:2 molar ration with respect to the template (3.71 mL, 12.5 mmol) and continued to stir for 10 min, forming a clear homogenous solution. Distilled water (17.8 mL) was then added, instantly forming a white precipitate. 35% HCl (0.054 mL, 0.63 mmol) was then added; the white precipitate was then crushed with a spatula and stirred gently, then left without agitation overnight. The mixture was then placed in a Teflon lined autoclave and heated at a designated temperature (60 °C – 120 °C) for 96 h. The resulting mixture was then filtered under vacuum, washed with water (3 x 50 mL), ethanol (3 x 50 mL) and then ether (3 x 50 mL). The remaining white solid was then dried in a vacuum desiccator for at least 2 days (48 h).

Note: For 1:1 hexylamine to titanium isopropoxide tests; tests where autoclave time/temperature were varied in the ranges 4-14 days/ 80 °C – 110 °C; and different titanium precursors were used, all other parameters were kept the same.

Mesoporous M/TiO₂

Hexylamine (0.823 mL, 6.26 mmol), was stirred between 40 – 50 °C followed by the addition of dopant metal precursor (2 mol%). To the solution titanium(IV) isopropoxide (3.51 mL, 12.3

mmol) was added and continued to stir for 10 min, forming a homogenous solution. Distilled water (17.8 mL) was then added, instantly forming a precipitate. 35% HCl (0.054 mL, 0.63 mmol) was then added; the precipitate was then broken up with a spatula and stirred gently then left without agitation overnight. The precipitate was then placed in a Teflon lined autoclave and heated at 80 °C for 96 h. The resulting mixture was then filtered under vacuum, washed with water (3 x 50 mL), ethanol (3 x 50 mL) and then ether (3 x 50 mL). The remaining solid was then dried in a vacuum desiccator for at least 2 days.

Note: The initial stirring temperature and time were varied (30 – 60 °C, 30 min – 2 h) in order to dissolve sparingly soluble precursors.

2.2.4.2. Dai's protocol

The synthesis is based on an adapted method from Dai *et al.*³³ Dai's protocol differed to Antonelli's reported here as a titanium ethoxide precursor is used instead of titanium isopropoxide. Furthermore, during the hydrolysis step where water is added in Antonelli's protocol, Dai's protocol differs as it uses an ethanol/water mixture (ethanol being a co-solvent) during the hydrolysis step. The time and temperature of the autoclave step was kept the same.

Hexylamine (0.823 mL, 6.26 mmol), was stirred between 40 – 50 °C followed by the addition of titanium(IV) ethoxide (2.63 mL, 12.5 mol) and continued to stir for 10 min, forming a clear homogenous solution. An ethanol (3.95 mL)/distilled water (11.9 mL) solution was then added, instantly forming a white precipitate. The white precipitate was then broken up with a spatula and stirred gently, then left without agitation overnight. The mixture was then placed in a Teflon lined autoclave and heated at 80 °C for 96 h. The resulting mixture was then filtered under vacuum, washed with water (3 x 50 mL), ethanol (3 x 50 mL) and then ether (3 x 50 mL). The remaining white solid was then dried in a vacuum desiccator for at least 2 days.

2.2.4.3. Zhang's protocol

The synthesis is based on a method reported by Zhang.³⁸ Zhang's protocol differs from Antonelli's and Dai's synthesis as it uses dodecylamine as the organic template, which is

longer than the hexylamine used in the other protocols. However, the key difference is Zhang's protocol reported no autoclave step, which is thought to be key in micelle formation (see section 1.5). Similar to Dai's protocol, Zhang's protocol also features an ethanol/water mixture for the hydrolysis step and similarly to Antonelli's protocol uses a titanium isopropoxide precursor.

Dodecylamine (0.703 g, 3.791 mmol), was dissolved in a 1:1 ethanol/water solution (14.1 mL) and stirred. To this solution, titanium(IV) isopropoxide (3.71 mL, 12.5 mmol) was added dropwise and continued to stir. The mixture was then left for 24 h, followed by filtration and solvent washes; H₂O (2 x 50 mL), ethanol (2 x 50 mL) ether (2 x 50 mL).

Note: An additional synthesis was conducted with an autoclave step (80 °C, 96 h) after the 24 h wait step. All other parameters were the same.

2.2.4.4. Peptization

This synthesis is based on a method reported by Lee *et al.*³⁵ The premise of this synthesis is marginally different to microporous synthesis mentioned thus far. Peptization causes changes in a pre-existing crystal structure via a peptizing agent reforming the morphology, and in this case, to a porous material. Figure 2.2.4.4.1 shows the proposed mechanism of how peptization can convert a bulk material into a porous one, see section (1.5.1). The disadvantage with this synthesis is the less discrete control and less variable parameters present with soft-templating approaches.

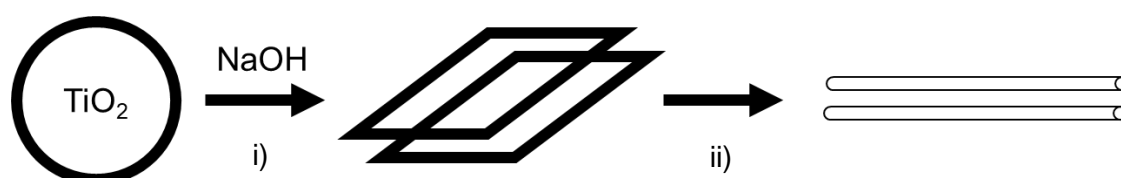


Figure 2.2.4.4.1: A schematic to show the steps involved during peptization under autoclave conditions. Adapted with permission from A. Nakahira *et al.* Copyright (2010) American Chemical Society.³⁹ In this example TiO₂ (anatase) is converted to microtubes via i) exfoliation and then ii) 'scrolling'.

The synthesis we performed is as follows, from *Lee et al.*:³⁵

To a Teflon lined autoclave NaOH solution (10 M, 20 mL) was added, followed by the addition of TiO₂, anatase (2.00 g) with a magnetic stirrer bar. The autoclave was then heated to 120 °C on a calibrated hotplate with stirring for 3 days. The resulting white paste was then washed with water (20 x 50 mL) and dried in a vacuum oven at 60 °C for 48 h.

2.2.5. Microporous niobium oxide

2.2.5.1. Ying's protocol

This synthesis is based on a method reported by Tao and Ying.³²

Microporous Nb₂O₅

A 1:1 acetone-ice bath had a round bottom flask added to it. To the round bottom flask, hexylamine (1.03 mL, 7.81 mmol) was added, followed quickly by Nb(OEt)₅ (1.96 mL, 7.79 mmol), which was then stirred for 30 mins. After raising the flask from the ice bath, H₂O (34 g) was then added dropwise initially until a white suspension was made, followed by the rest of the water which was then stirred for 1 h. The mixture was then placed in a Teflon lined autoclave, heated to 180 °C (10 °C min⁻¹ ramp) , and then held at 180 °C for 10 days. The resulting cream/yellow suspension was then separated from the crude mother liqueur (some of which retained for Nuclear magnetic resonance – NMR, gas chromatography-mass spectrometry – GC-MS and Inductively coupled plasma-optical emission spectroscopy – ICP-OES analysis) then the solid was washed with water (3 x 50 mL), ethanol (3 x 50 mL) and ether (3 x 50 mL). The solid was then dried at 120 °C for 16 h, yielding a cream/yellow solid.

Microporous Fe/Nb₂O₅

A 1:1 acetone-ice bath had a round bottom flask added to it. To the round bottom flask, hexylamine (1.03 mL, 7.81 mmol) was added, followed quickly by Fe(OEt)₃ (0.147 g, 7.70 mmol) and Nb(OEt)₅ (1.90 mL, 7.53 mmol), which was then stirred for 30 mins. The flask was then raised from the ice bath and stirred at room temperature for 30 mins, followed by heating

and stirring in an oil bath at 60 °C for 30 mins to give a dark brown solution. H₂O (34 g) was then added dropwise initially until a white suspension was made, followed by the rest of the water which was then stirred for 1 h. The mixture was then placed in a Teflon lined autoclave, heated to 180 °C (10 °C min⁻¹ ramp), and then held at 180 °C for 10 days. The resulting brown suspension was then separated from the crude mother liqueur (some of which retained for NMR and ICP-OES analysis) then the solid was washed with water (3 x 50 mL), ethanol (3 x 50 mL) and ether (3 x 50 mL). The solid was then dried at 120 °C for 16 h, yielding a brown solid.

2.2.5.2. Antonelli's protocol

This synthesis is based on a method reported by Antonelli and Ying.⁴⁰ The difference to Tao and Ying's protocol is a solvent, ethanol; and a longer organic template, tetradecylamine, are used in Antonelli's protocol. Furthermore, autoclave steps are used as opposed to a single temperature and time during the reaction mixture's duration in the autoclave.

Nb(OEt)₅ (5.00 g, 15.7 mmol) in ethanol (15 mL) had tetradecylamine (1.68g, 7.87 mmol) added to it and stirred for 1 h at 40 °C. H₂O (15 mL) was then added to create a cream precipitate, which was left overnight. The mixture was then added to a Teflon lined autoclave, where it was heated to 80 °C (24 h), 100 °C (24 h) and then 180 °C (7 days). The mixture became yellow with a white suspension, this was filtered and washed with water (3 x 50 mL), ethanol (3 x 50 mL) and ether (3 x 50 mL). The remaining white solid was then dried under vacuum at 80 °C.

2.3. Template removal

2.3.1. Microporous titanium oxide

The synthesis of microporous titanium oxide in this project required an organic template. Because the pores are required to be free of the template used in the synthesis for catalysis purposes, removal of the template was then conducted with a variety of methods.

2.3.1.1. Calcination

Typically, a sample of microporous titanium oxide (0.2 – 0.5 g), was placed in a static air or a dynamic tubular furnace and heated to a designated temperature (e.g. 250 °C – 550 °C) at 1-10 °C min⁻¹. Tests were conducted from no dwell times to 4 h.

2.3.1.2. Solvent washes

Typically, microporous TiO₂ (0.2 – 0.5 g) was refluxed with chosen solvent (e.g. ethanol, ether ~ 20 - 50 mL) and stirred vigorously for 1 h at just below the solvent's boiling point. The sample was then washed with the chosen solvent several times and then the reflux and wash steps were repeated if required. The sample was then dried for at least 2 days in a vacuum desiccator.

2.3.1.3. Acidic washes

2.3.1.3.1. HNO₃

Initial acid washes

Microporous TiO₂ (0.100 g) had nitric acid (100 mL, 0.626 mmol, pH 2.2) added to it and stirred for 1 h. The resulting solid was washed with water (3 x 50 mL) followed by ethanol (3 x 50 mL) and dried in a vacuum desiccator.

With indicator and pH-meter

Microporous TiO₂ (0.200 g) was added to distilled water (30 mL) and stirred vigorously. If a pH probe was being used, this was calibrated and placed into solution where pH was recorded.

An indicator was then added (e.g. methyl orange, 0.01% vol, approx. 100 μL) to give a coloured/colourless suspension. To this a stock solution of HNO_3 (0.063 mol dm^{-3} , pH 1.20) was added dropwise until a colour change was observed/ desired pH was reached. The suspension was then filtered under Buchner filtration, washed with distilled water (4 x 50 mL), ethanol (2 x 50 mL) and then distilled water again (2 x 50 mL). The powder was then dried for at least 2 days in a vacuum desiccator.

To determine pH curves, the procedure above was conducted, but until pH did not change after addition of acid.

2.3.1.3.2. *p*-TSA

Microporous TiO_2 (0.100 g) had aqueous *p*-TSA (varied moles, see section 5.2.6.2) or *p*-TSA dissolved in acetonitrile (0.626 mmol, pH 2.2 to pH 5.35) added to it and stirred for a given time (1 h to 24 h). The mixture was then filtered via Buchner filtration, washed with water (3 x 50 mL) and then ethanol (3 x 50 mL) and dried under vacuum.

2.3.1.4. Alternatives to acids

2.3.1.4.1. H_2O_2

Method adapted from Kidwai and Bhardwaj⁴¹ in combination with methods and scale factors from Gee and Williamson⁴² considered. Microporous TiO_2 (0.200 g) had hydrogen peroxide 30% (11 mL) added to it and stirred vigorously at a set temperature (40 $^\circ\text{C}$ to 108 $^\circ\text{C}$) under reflux apparatus for 24 h. This was then washed with distilled water (2 x 50 mL), and then ethanol (2 x 50 mL). For samples where another wash was conducted, the sample was then immediately washed with water again (2 x 50 mL) and then the procedure was repeated. Once washing was complete, the sample was then dried in a vacuum desiccator for at least 2 days.

2.3.1.4.2. Phthalic anhydride

Phthalic anhydride (0.186 g, 1.26 mmol) and triethylamine (2 μ L) were dissolved in DMF (25 mL). To this, microporous TiO₂ (0.200 g) was added and stirred overnight. The suspension was then filtered under vacuum and washed with acetone (2 x 50 mL) and ether (2 x 50 mL). The remaining pale-yellow solid was then dried in a vacuum desiccator for at least 48 h.

2.3.2. Microporous niobium oxide (and microporous Fe/Nb₂O₅)

2.3.2.1. Acidic washes

Ying and Tao – p-TSA

Microporous Nb₂O₅ (0.250 g) had methanolic *p*-TSA or aqueous *p*-TSA (0.1 mmol - 1 mmol amount also dependent on pH required) added to it and stirred at room temperature for 24 h. The mixture was then filtered via Buchner filtration, washed with water (3 x 50 mL) and then ethanol (3 x 50 mL) and dried under vacuum.

Ying and Tao – HNO₃

Microporous Nb₂O₅ (0.200 g) was placed in water (30 mL), where a calibrated pH probe was submerged. HNO₃ (0.0314 M) solution was added dropwise until pH 4 was reached. The pH was allowed to stabilise with each addition, until pH 4 was consistent. Once the desired pH was consistent, the solution was stirred for 10 minutes. The mixture was then filtered under vacuum and washed with water (2 x 50 mL), ethanol (2 x 50 mL) and then ether (2 x 50 mL). The solid was then dried in a vacuum desiccator for at least 48 h.

Note: An initial test was conducted where HNO₃ was added to the microporous niobium oxide suspension until the pH no longer changed in order to generate a pH curve.

Antonelli – HNO₃

Microporous Nb₂O₅ (0.500 g) was added to an ethanolic solution of nitric acid (pH 1.67) and stirred for 1 h. The solid was then filtered under vacuum and washed with water (3 x 50 mL),

ethanol (3 x 50 mL) and ether (3 x 50 mL). The solid was then dried in a vacuum desiccator for at least 48 h.

2.3.2.2. Phthalic anhydride

Phthalic anhydride (0.3274 g, 2.211 mmol) and triethylamine (4 μ L) were dissolved in DMF (25 mL). To this, microporous (Fe/Nb₂O₅) (0.500 g) was added and stirred overnight. The suspension was then filtered under vacuum and washed with acetone (2 x 50 mL) and ether (2 x 50 mL). The remaining pale-yellow solid was then dried in a vacuum desiccator for at least 48 h.

2.4. Catalytic tests

It should be noted here that safety considerations were paramount due to the characteristic flammable nature of hydrocarbons, for example the lower flammability limit of *n*-decane is as low as 2.1% in air under atmospheric conditions.⁴³ In order to operate safely, strict development of COSHH forms, risk assessment and standard operating procedure was conducted throughout the work reported here. When handling alkanes at high temperatures and under pressurised oxygen, care must always be given to ensure the risk of release of an alkane onto a hot surface is as low as possible. Furthermore, by conducting catalysis with relatively low volumes of substrate (i.e. < 5 mL) the risk of significant combustion from a large volume of substrate was also mitigated.

2.4.1. *n*-decane

2.4.1.1. Atmospheric tests

In a typical reaction, *n*-decane (3 mL, 15.4 mmol) in a round bottom flask with reflux apparatus had a catalyst (mass adjusted for loading to a specific metal to substrate ratio) added to it and heated to a given temperature while stirring, using a Radleys Starfish reactor set-up. The reaction mixture was stirred at the temperature for 24 h, and then allowed to cool. The mixture was then centrifuged to separate the solid catalyst. The separated supernatant solution was then used for analysis.

2.4.1.2. Pressurised tests

In a typical reaction *n*-decane (3 mL, 15.4 mmol), in a screw capped pressure resistant round bottom flask (ACE flask) fitted with a glass insert bubbler (ACE tube), had a catalyst (mass adjusted for loading) added to it. The mixture was then stirred under oxygen (PO_2 0.5 bar, where P is the pressure as read from the pressure gauge, in this case on an oxygen cylinder) for 5 minutes and then purged, this was repeated with increasing the pressure PO_2 0.5 bar a time until the designated pressure was met (note: for lower pressures, these steps were repeated twice so the number of washes remained constant across tests). The reaction

mixture was then heated to a given temperature while stirring by using a Radleys Starfish reactor set-up. The reaction mixture was stirred at the temperature for 24 h, and then allowed to cool. The mixture was then centrifuged to separate the solid catalyst. The resulting solution was then used for analysis.

2.4.2. Cyclooctane

The procedure for cyclooctane oxidation tests was identical to that of *n*-decane, however, cyclooctane (3 mL, 22.3 mmol) was used with a set pressure of PO_2 2 bar. The temperature used for all cyclooctane tests was 110 °C. All reaction mixture analysis was done via 1H -NMR.

2.4.3. Dried metal salt tests

Identical conditions for *n*-decane and cyclooctane oxidation (sections 2.4.1 and 2.4.2) were conducted with dried metal salts as a form of control test. However, prior to charging the round bottom flask with substrate, a metal salt solution (< 1 mL, concentration and volume adjusted for M:S ratio) was added to the flask. The flask was then stirred at 80 °C overnight, to give a dried metal salt on the surface of the round bottom flask, which then went on to the standard catalytic test procedures.

2.5. Analytical methods

2.5.1. Quantitative analysis of hydrocarbon reaction mixtures

It should be noted here that analysis of hydrocarbon mixtures is not a trivial task (sections 3.2.1 and 3.2.2).⁴⁴⁻⁴⁷ Due to the similar properties amongst the tens of potential products during oxidation, individual qualitative and quantitative characterisation requires significant in-depth analysis of reaction mixtures.⁴⁷

Furthermore, the presence of alkyl acids and hydroperoxides limits the amount of analytical techniques that can be used directly, or alternatively pre-preparation of reaction mixtures is required.^{17,44,48,49} This is because analysis of fatty acids typically requires them to be converted to esters.⁴⁹ Whereas hydroperoxides can decompose under the high temperatures typically used in injection steps during GC-MS to their corresponding alcohols and ketones (180 – 200 °C), figure 2.5.1.1, which is especially problematic when determining the relative amounts of each of these potential products.^{44,50,51} These requirements make analysis lengthy, with disagreements amongst authors about the capability of some catalysts.⁴⁴ The ideal analytical tool here would be ¹H-NMR as it is cheap, quick and can be run at room temperature, the latter relinquishing the chance of hydroperoxide decomposition leading to inaccurate quantification. However, ¹H-NMR can only be used if over oxidation is kept low, or for reaction mixtures at high conversion but also with high selectivity. This is because if the reaction mixture becomes too complex, then so will the NMR analysis from multiple overlaps and potential broad peaks from organic acids. The combinations of these two factors then hampers the capability of accurate quantitative determinations.



Figure 2.5.1.1: A simple equation to highlight the potential overall decomposition of alkyl hydroperoxides to the corresponding hydroxyl or carbonyl containing compounds under the conditions during GC-MS analysis which may lead to complications in quantification.^{44,51}

2.5.2. ¹H-NMR

Nevertheless, for a substantial part of this research project NMR has been used to analyse reaction mixtures and used especially as a fast screening tool. Then samples that were of high conversion and/or selectivity would go onto a more in-depth investigation were analysed also by GC-MS. ¹H-NMR quantification of conversion (eqs. 2.5.2.1, 2.5.2.2 and 2.5.2.3) and selectivity (eq. 2.5.2.4) were determined for reaction mixtures using the following equations (their development is described in section 3.2.1). It should be made explicit here that both conversion and selectivity will be strictly described as ‘observed’, as the equations rely on the assumption that all products are present in the reaction mixture analysed and fully quantified effectively. It is such that this is only correct if carbon mass balance is experimentally close to 100% (see section 3.2.1), which was indeed the case as determined by ¹H-NMR analysis of reaction mixtures with internal standards within the range of conversion observed.

$$\text{Conversion (\%)} = \frac{\sum_i n_{Pi}}{n_{R,f} + \sum_i n_{Pi}} \cdot 100 \quad (\text{eq. 2.5.2.1})$$

$$n_{Pi} \propto \frac{A_{Pi}}{m_H} \quad (\text{eq. 2.5.2.2})$$

Where n_{Pi} is the number of moles of a given product, $n_{R,f}$ is the number of moles of reactant left in the reaction mixture (or ‘final’ after a reaction time t), A_{Pi} is the area of a given product and m_H is the number of protons of the associated signal for that product or compound.

$$\text{Conversion (\%)} = \frac{\sum \frac{A_{Pi}}{m_H}}{\frac{A_{C_{Octane,corrected}}}{6} + \sum \frac{A_{Pi}}{m_H}} \cdot 100 \quad (\text{eq. 2.5.2.3})$$

$$\text{Selectivity}_{Pi}(\%) = \frac{n_{Pi}}{\sum_i n_{Pi}} \cdot 100 \quad (\text{eq. 2.5.2.4})$$

Here it can be seen in eq. 2.5.2.3, $A_{C_{Octane,corrected}}$ (the corrected peak area for remaining n -octane post reaction) is divided by six as n -octane’s characteristic peak is CH_3 , of which it has two ($2 \times \text{CH}_3$, $m_H = 6$). The peak had to be corrected as overlap from other products was

present. A more in-depth discussion on the development of these equations is present in section 3.2.1, particularly which NMR peak was chosen and thus individual m_H values are detailed, alongside discussions on correction factors.

All $^1\text{H-NMR}$ analysis was conducted on a Bruker Avance IIIHD 400 spectrometer, operating at 400 MHz. Samples were prepared by adding 50 μL of reaction mixture to an NMR tube and dissolved in CDCl_3 .

2.5.2.1. $^1\text{H-NMR}$ *n*-decane and *n*-octane

Characterisation of reaction mixture is as follows:

n-octane, $\text{CH}^{\text{a}_3}(\text{CH}^{\text{b}_2})_6\text{CH}^{\text{a}_3}$ (δ , ppm): 1.27 (m, 12H^b), 0.89 (t, 6H^a).

1-octanol, $\text{CH}^{\text{a}_3}(\text{CH}^{\text{b}_2})_6\text{CH}^{\text{c}_2}\text{OH}^{\text{d}}$ (δ , ppm): 3.56 (m, 2H^c), 2.51 (br, 1H^d), 1.52 - 1.24 (m, 12H^b), 0.84 (t, 3H^a).

2-octanol, $\text{CH}^{\text{a}_3}(\text{CH}^{\text{b}_2})_5\text{CH}^{\text{c}_2}\text{OH}^{\text{d}}\text{CH}^{\text{e}_3}$ (δ , ppm): 3.77 (m, 1H^c), 1.44 – 1.27 (m, 10H^b), 1.16 (d, 3H^e), 0.87 (t, 3H^a).

3-octanol, $\text{CH}^{\text{a}_3}(\text{CH}^{\text{b}_2})_4\text{CH}^{\text{c}_2}\text{OH}^{\text{d}}\text{CH}^{\text{b}_2}\text{CH}^{\text{e}_3}$ (δ , ppm): 3.50 (m, 1H^c), 1.52 – 1.22 (m, 10H^b), 0.92 (t, 3H^e), 0.87 (t, 3H^a).

Octanal, $\text{CH}^{\text{a}_3}(\text{CH}^{\text{b}_2})_4\text{CH}^{\text{c}_2}\text{CH}^{\text{d}_2}\text{C}(\text{O})\text{H}^{\text{e}}$ (δ , ppm): 9.75 (m, 1H^e), 2.40 (m, 2H^d), 1.61 (m, 2H^c), 1.27 (m, 8H^b), 0.86 (t, 3H^a).

2-octanone, $\text{CH}^{\text{a}_3}(\text{CH}^{\text{b}_2})_3\text{CH}^{\text{c}_2}\text{CH}^{\text{d}_2}\text{C}(\text{O})\text{CH}^{\text{e}_3}$ (δ , ppm): 2.39 (t, 2H^d), 2.10 (s, 3H^e), 1.54 (m, 2H^c), 1.25 (m, 6H^b), 0.85 (t, 3H^a).

3-octanone, $\text{CH}_3^{\text{a}}(\text{CH}^{\text{b}_2})_2\text{CH}^{\text{c}_2}\text{CH}^{\text{d}_2}\text{C}(\text{O})\text{CH}^{\text{d}_2}\text{CH}^{\text{e}_3}$ (δ , ppm): 2.38 (m, 4H^d), 1.55 (m, 2H^c), 1.26 (m, 4H^b), 1.02 (t, 3H^e), 0.86 (t, 3H^a).

n-decane, $\text{CH}^{\text{a}_3}(\text{CH}^{\text{b}_2})_8\text{CH}^{\text{a}_3}$ (δ , ppm): 1.27 (m, 16H^b), 0.89 (t, 6H^a).

1-decanol, $\text{CH}^{\text{a}_3}(\text{CH}^{\text{b}_2})_8\text{CH}^{\text{c}_2}\text{OH}^{\text{d}}$ (δ , ppm): 3.64 (m, 2H^c), 1.71 – 1.08 (m, 16H^b), 1.07 – 0.70 (m, 3H^a).

2-decanol, $\text{CH}_3^{\text{a}}(\text{CH}_2^{\text{b}})_7\text{CH}^{\text{c}}\text{OH}^{\text{d}}\text{CH}_3^{\text{a}}$ (δ , ppm): 3.80 (m, 1H^c), 1.71 – 1.08 (m, 14H^b), 1.07 – 0.70 (m, 6H^a) .

3-decanol, $\text{CH}_3^{\text{a}}(\text{CH}_2^{\text{b}})_6\text{CH}^{\text{c}}\text{OH}^{\text{d}}\text{CH}_2^{\text{b}}\text{CH}_3^{\text{a}}$ (δ , ppm): 3.53 (m, 1H^c), 1.71 – 1.08 (m, 14H^b), 1.07 – 0.70 (m, 6H^a).

Decanal, $\text{CH}_3^{\text{a}}(\text{CH}_2^{\text{b}})_7\text{CH}_2^{\text{c}}\text{C}(\text{O})\text{H}^{\text{d}}$: (δ , ppm): 9.78 (m, 1H^d), 2.45 – 2.31 (m, 2H^c), 1.71 – 1.08 (m, 14H^b), 1.07 – 0.70 (m, 3H^a).

2-decanone, $\text{CH}_3^{\text{a}}(\text{CH}_2^{\text{b}})_6\text{CH}_2^{\text{c}}\text{C}(\text{O})\text{CH}_3^{\text{d}}$ (δ , ppm): 2.41 (t, 2H^c), 2.12 (s, 3H^d), 1.55-1.27 (m, 12H^b), 0.87 (t, 3H^a).

3-decanone, $\text{CH}_3^{\text{a}}(\text{CH}_2^{\text{b}})_5\text{CH}_2^{\text{c}}\text{C}(\text{O})\text{CH}_2^{\text{d}}\text{CH}_3^{\text{d}}$ (δ , ppm): 2.45 – 2.31 (m, 4H^c), 2.13 (s, 3H^d), 1.71 – 1.08 (m, 10H^b), 1.07 – 0.70 (m, 3H^a)

2.5.2.2. ¹H-NMR Cyclooctane

Characterisation of reaction mixture is as follows:

Cyclooctane (δ , ppm): 1.2 – 2.3 (s, 16H).

Cyclooctanone (δ , ppm): 1.2 – 2.3 (m, 10 H), 2.43 (t, 4H).

Cyclooctanol (δ , ppm): 1.2 – 2.3 (m, 14H), 3.88 (m, 1H).

Cyclooctyl peroxide (δ , ppm): 1.2 – 2.3 (m, 14H), 4.15 (m, 1H).

1,2-cyclooctadione (δ , ppm): 1.2 – 2.3 (m, 8H), 2.68 (t, 4H).

Cis-9-oxabicyclononane (δ , ppm): 1.2 – 2.3 (14H), 2.89 (t, 4H)

2.5.3. Gas chromatography – mass spectrometry (GC-MS)

Gas chromatography (GC) and mass spectrometry (MS) can be combined into one powerful analytical tool.⁵² Sample is initially separated by passing over a stationary phase in the GC. In our case, this was a wax column (an Agilent DB-WAX-UI 30 m x 0.25 mm x 0.25 μm column) which separated samples based on polarity. MS is then used to determine the molecular

weights of both the compounds and the products of their fragmentation during analysis. For the purposes of our research, we sought to separate complex reaction mixtures of hydrocarbons for qualitative and quantitative analysis.

As with NMR, conversion can be defined with eq.2.5.2.1, section 2.5.2. However, with GC-MS $n_{R,f}$ could not be determined due to the remaining reactant in the reaction mixture being widely in excess and thus solvent stripping was required so products could be resolved. But assuming that carbon mass balance is experimentally equivalent to 100% (which we determined to be the case, see section 3.3), then conversion and selectivity can be defined as ‘observed’ in the following descriptions.

GC-MS quantification of conversion (eq. 2.5.3.1 and 2.5.3.2) and selectivity (eq. 2.5.3.3) was determined with the following equations, their development can be found in section 3.2.2. Note: as the amount of reactant after reaction cannot be determined via this method, these will be recorded as *observed* conversion and selectivity (see sections 3.2.1 and 3.2.2).

$$\text{Conversion (\%)} = \frac{\sum_i [p_i] \cdot r_f}{[R_i]} \cdot 100 \quad (\text{eq. 2.5.3.1})$$

$$[p_i] = [IS] \cdot \frac{\text{Area}_{p_i}}{\text{Area}_{IS}} \quad (\text{eq. 2.5.3.2})$$

$$\text{Selectivity (\%)} = \frac{[p_i] \cdot r_f}{\sum_i [p_i] \cdot r_f} \cdot 100 \quad (\text{eq. 2.5.3.3})$$

Where $[p_i]$ is the concentration of a given product, $[R_i]$ is the initial concentration of reactant, $[IS]$ is the concentration of internal standard and r_f is a retention factor as determined from a calibration curve.

GC-MS was conducted by taking an aliquot of reaction mixture (1 mL), adding dodecane (0.1 mL) as an internal standard and making this up to 10 mL with substrate (i.e. *n*-decane or *n*-octane). All analysis was performed using an Agilent 7200 accuratemass Q-TOF GC-MS fitted with either an Agilent DB-MS-UI 30 m x 0.25 mm x 0.25 μ m or an Agilent DB-WAX-UI 30 m x

0.25 mm x 0.25 μm column. Temperature ramping was conducted as follows: 50 $^{\circ}\text{C}$ to 90 $^{\circ}\text{C}$, 40 $^{\circ}\text{C min}^{-1}$; 90 $^{\circ}\text{C}$ to 120 $^{\circ}\text{C}$, 2 $^{\circ}\text{C min}^{-1}$; 120 $^{\circ}\text{C}$ to 250 $^{\circ}\text{C}$, 10 $^{\circ}\text{C min}^{-1}$ then held at 250 $^{\circ}\text{C}$ for 2 min.

Chromatograms of standard solutions with discussion can be found in section 3.2.2, typical positions of chemicals using the wax column method are as follows:

***n*-octane t_{R} :**

n-octane (min): 2.10; 1-decanol (min): 5.07; 1-octanol (min): 33.8; 2-octanol (min): 29.8; 3-octanol (min): 28.9; Octanal (min): 23.5; 2-octanone (min):23.2; 3-octanone (min): 21.1.

***n*-decane t_{R} :**

n-decane (min): 2.35; *n*-dodecane (min): 5.08; 1-decanol (min): 23.2; 2-decanol (min): 17.2; 3-decanol (min): 16.2; 4-decanol (min): 15.6; Decanal: 12.4; 2-decanone (min): 12.3; 3-decanone (min): 11.3.

4-octanol, 4-octanone, 5-decanol, 4-decanone and 5-decanone retention times were determined by qualitatively identifying these peaks amongst actual reaction mixtures via NIST (National Institute of Standards and Technology) functions available within the software.⁵³ GC-MS data are matched to the most probable identities of a substance from a spectral library database, this approach was required as these chemicals were not commercially accessible during the time of this research.^{54–57} All other components of the reaction mixture are grouped to determine the conversion and are titled as ‘other products’.

2.5.4. Fourier transform infrared – attenuated total reflectance (FTIR-ATR)

FTIR-ATR is a method in which a sample is placed on an internal reflection element (IRE). The evanescent wave from the IR source is almost completely reflected within the IRE, however, some of the radiation penetrates the sample at some depth where it is adsorbed by the sample, thus an absorption/transmission spectrum can be generated, summarised in figure 2.5.4.1.⁵⁸

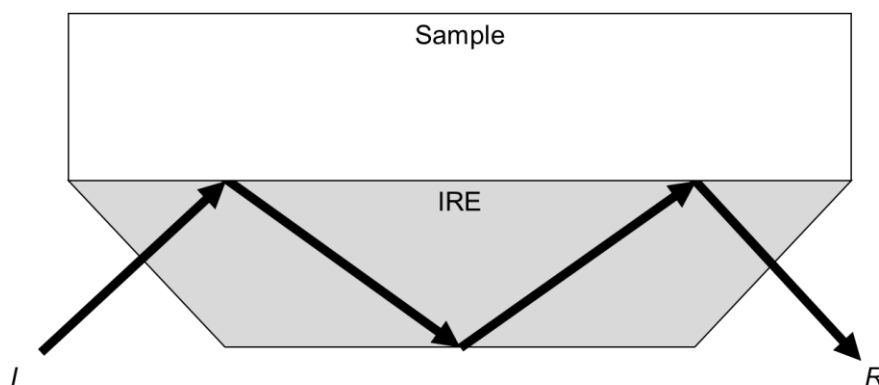


Figure 2.5.4.1: A simplified diagram to show how ATR-FTIR radiation is reflected (and partially adsorbed) at the interface between the sample and the IRE. *I* is the incident radiation and *R* is the reflected radiation. Adapted with permission from A. Hind *et al.*⁵⁸

FTIR-ATR has been used for several applications in microporous materials. These include; determination of surface acidity;⁵⁹ observation of adsorbates;^{60,61} and determining the presence of organic templates.⁶²

For the purpose of this research, FTIR-ATR was used prior to thermogravimetric analysis (TGA) as a preliminary test to determine if the organic template from microporous material synthesis was still present (and if there was any loss in intensity after template removal) by observing C-H stretches ($2700 - 3100 \text{ cm}^{-1}$).

FTIR-ATR analysis was conducted using a Bruker ALPHA-T fitted with an ALPHA-P platinum ATR scanned between $375 - 4000 \text{ cm}^{-1}$ with a resolution of 2 cm^{-1} over 64 scans.

2.5.5. Thermogravimetric analysis (TGA)

TGA is the method in which weight of a sample is measured as temperature is increased.⁶³ It has several applications in porous materials such as; determination of interlayer water;⁶⁴ quantification of adsorbates⁶⁵ and presence of residual surfactants from synthesis⁶⁶ (and their removal).³⁴

For the context of our research, TGA was primarily used both for quality control and qualitatively for determining the amount of surfactant present in as-synthesised material and how much had remained, if any, after template removal. Additionally, it was used to determine

possible changes in oxidation state during microporous niobium oxide calcination, as for this oxide a weight gain would be observed for the transformation $2\text{NbO}_2 + 1/2\text{O}_2 \rightarrow \text{Nb}_2\text{O}_5$.

TGA was conducted using a PerkinElmer Pyris 1 TGA operating between 25 °C (5 min hold) to 800 °C (5 min hold) with a 10 °C min⁻¹ ramp under air flow of 20 mL min⁻¹.

2.5.6. X-ray powder diffraction (XRPD)

According to Bragg's theory, when monochromatic X-rays are shone onto a sample, they are diffracted by the regular atomic layers, figure 2.5.6.1.⁶⁷ The angle of diffraction can thus determine the space between the layers when using Bragg's law (section 2.5.6.2). With XRPD, a diffraction pattern is generated, which provides information on what phases are present within the sample from diffraction peaks (and thus can reveal the presence of crystalline dopant species and even their oxidation state).

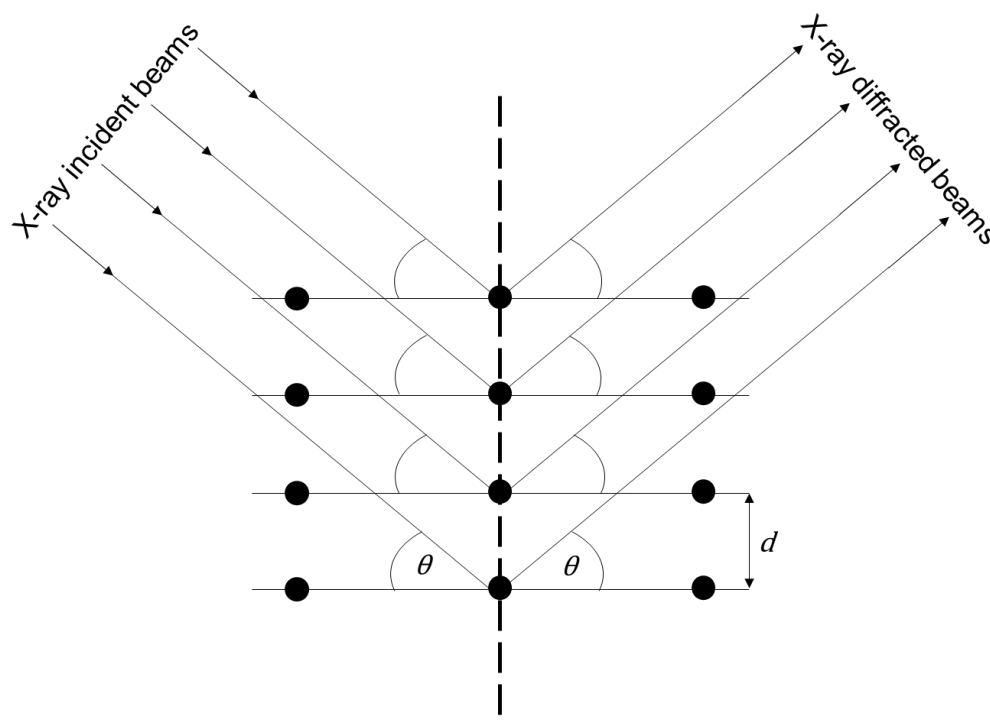


Figure 2.5.6.1: A simple schematic of how XRD occurs, according to Bragg's theory. The angle between incident beams and the normal to the lattice, θ , can be used to determine inter-layer spacing, d . Diagram reused with permission from *E. Ameh*.⁶⁷

XRPD was conducted using a Bruker D8 Advance powder diffractometer fitted with a LynxEye detector, using a CuK α X-ray source (operating at 40 kV and 40 mA) on a low-angle flat plate sample holder. Typical routine scanning is as follows:

- 1) 2θ : 1 – 15 °, t (per step): 0.2 s, primary opening, incident arm: 0.1 °, secondary opening, diffraction arm: 9.5 mm, no antiscatter slit
- 2) 2θ : 2 – 15 °, t (per step): 0.2 s, primary opening, incident arm: 0.3 °, secondary opening, diffraction arm: 9.5 mm, no antiscatter slit
- 3) 2θ : 2 – 80 °, t (per step): 0.6 s, primary opening, incident arm: 0.3 °, secondary opening, diffraction arm: 9.5 mm, no antiscatter slit

2.5.6.1. Determination of particle size

The particle size of the supported metal/ metal oxides can be determined via analytical techniques. These can be observed directly with TEM^{68–70} or estimated through XRPD using the Scherrer equation,^{71–73} eq. 2.5.6.1.1, which determines the *crystallite* size.

$$t = \frac{0.9\lambda}{\sqrt{B_M^2 - B_S^2 \cos^2 \theta}} \quad \text{eq. 2.5.6.1.1}$$

Where t is thickness of crystallite, λ is incident wavelength of X-ray, θ is the Bragg angle, B_M is the width of the peak and B_S is instrumental broadening at half maximum.^{73,74}

2.5.6.2. Determination of pore size

Crystalline porous materials can use small angle XRPD to determine pore diameter, this is achieved through Bragg's law: (eq.2.5.6.2.1)^{75,76}

$$n\lambda = 2d \sin \theta \quad \text{eq. 2.5.6.2.1}$$

Where n is an integer value, λ is the wavelength from the X-ray source, d is the interplanar distance and θ is the incident angle of the x-ray source with respect to the sample.

2.5.7. X-ray photoelectron spectroscopy (XPS)

XPS is a method of surface analysis based on the photoelectric effect. It is used to determine binding energies of core electrons used in bonding by measuring their kinetic energy after being emitted from a sample by X-ray radiation (summarised in figure 2.5.7.1 and eq. 2.5.7.1).⁷⁷

$$E_k = h\nu - E_b - \varphi \quad \text{eq. 2.5.7.1}$$

Where; E_k is the kinetic energy of emitted electron; E_b is the binding energy of the emitted electron; h is Planck's constant; ν is the frequency of incident X-ray and φ is the work function of the spectrometer.

XPS is strictly speaking a surface method, this is because the number of photoelectrons that can escape from a specimen decreases exponentially with depth,⁷⁸ this depth is known as the 'inelastic mean free path' of the photoelectrons. For this reason, XPS typically probes up to 10 nm in depth of the specimen.⁷⁹ Common practise during analysis is to have a relatively thick carbon (a ubiquitous element) layer on the surface of the sample which is in turn used as a reference for charge correction.⁸⁰

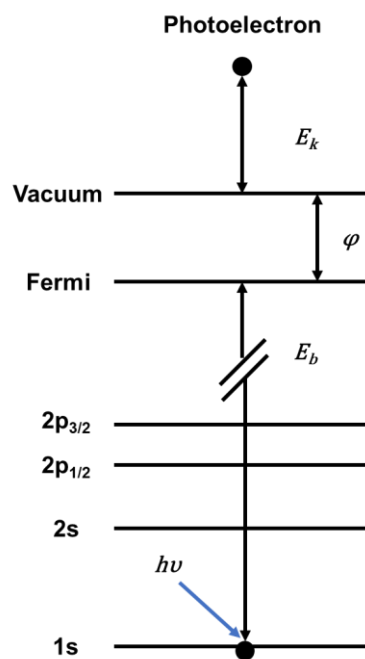


Figure 2.5.7.1: A simple diagram to show how the photoelectric effect is used to determine binding energies from emitted electrons in XPS. Adapted with permission from *M. Stöcker*.⁷⁷

XPS is a method used to determine a range of features in microporous materials, such as covalent/ionic character of species within a framework.⁸¹

XPS was used in our research in order to determine the oxidation states and environments around dopant metals on supports by comparing samples from wetness impregnation and hydrothermal synthesis. For example, with iron the Fe 2p_{3/2} peak could give information on iron's environment with Fe/TMS-1 compared to Fe/TiO₂ bulk.

XPS was conducted using a Kratos Axis Nova spectrometer via monochromatized AlK_α X-ray source (225 W), with an analyser pass energy of 160 eV for survey scans and 20 eV for high resolution scans. All spectra were charge corrected normalising the C1s component to 248.8 eV.

2.5.8. Brunauer-Emmett-Teller (BET)

BET theory can be used to generate isotherms from adsorbed gas within a sample. This is based on the Langmuir isotherm, but assumes multilayer coverage is possible.⁸² Using the

BET equation (eq.2.5.8.1) and the constant C, isotherms can be obtained to give information on; the type of physisorption isotherm;⁸³ pore sizes; pore volume and pore shape.^{34,84,85}

$$\frac{P/P_0}{n(1 - P/P_0)} = \frac{1}{n_m C} + \frac{C - 1}{n_m C} (P/P_0) \quad \text{eq. 2.5.8.1}$$

Where; C is the BET constant; n_m is the monolayer capacity of adsorbed gas; n is the specific amount of gas adsorbed at the relative pressure P/P_0 .⁸²

Practical BET analysis was conducted by using a Micromeritics 3Felex Gas Sorption System operating with liquid nitrogen at 77 K. Sample was degassed at 120 – 180 °C for 48 h before analysis.

2.5.9. Inductively coupled plasma optical emission spectroscopy (ICP-OES)

ICP-OES is an analytical tool used for elemental analysis.⁸⁶ Briefly, analysis is conducted by detecting emission (both wavelength and intensity are recorded) of elements in their excited states/collisions that occur when subjected to high temperatures in their gaseous phase.⁸⁷ For the context of this research, ICP-OES was used for the determination of metal ions in both reaction mixtures and mother liquors post hydrothermal synthesis of microporous metal oxides.

The effects of leaching, and the extent of how much material has leached can be monitored in several different ways. Gruber-Woelfler *et al.* displayed an extensive amount of analysis on leaching of immobilised palladium catalysts, summarised in table 2.5.9.1.⁸⁸ ICP-OES is an important tool as it allows potential quantification of leached material. Although it is typically limited to aqueous media, solvent extraction can be conducted to draw out any water-soluble leachates and thus provide insight into how robust the catalyst is. Ultimately, ICP-OES can give a strong indication if catalysis is occurring through the intended heterogeneous platform.

Samples were submitted directly from the collected mother liquor of hydrothermal synthesis, whereas catalytic tests underwent solvent exchange in order to draw out any aqueous metal

ions, where then the aqueous layer was submitted for analysis. A Spectro-Ciros-Vision ICP-OES was used for all analysis.

Table 2.5.9.1: A summary of tests conducted by Gruber-Woelfler for the analysis of leaching of immobilised palladium catalysts.⁸⁸

Test name	Method	Results obtained
Hot filtration	Removing the catalyst while the reaction proceeds	If the reaction proceeds in a similar manner to a parallel homogenous counterpart, it may be occurring due to leached material
ICP-OES	Separating the catalyst from the reaction mixture, drying the reaction mixture and detecting if any catalyst is present in the residue.	Directly detects whether the catalyst, or some form of it, is present in the reaction mixture after separation of the solid
Three-phase test	Adding a covalently supported reaction partner to a soluble reagent and then the supported catalyst	If leaching has occurred, the catalysed reaction would be detected as this means released catalyst has been able to move and therefore contact the covalently bound support
Catalyst reusability	Removing the catalyst from the reaction mixture and applying it to fresh substrate	If catalytic activity is dependent on the amount of catalyst present, leaching would cause a reduction in conversion seen after multiple runs due to less catalyst on the support applied to new substrate
Catalyst texture	Analysis of any physical changes in the support after reaction (BET)	This would show any deformation caused by the reaction conditions as surface area will decrease if pores have collapsed
Tests in different solvent	Using the catalyst in different solvent	A catalyst's activity and stability may vary in different solvents, therefore changes in conversion/ reusability will be detected if the catalyst has been affected
Catalyst poisons	Adding solid poisons to the reaction mixture	If any catalyst has leached the aqueous material will bind to the solid poison and thus a reduction in the catalysed reaction will be observed
TEM (Transmission electron microscopy)	Detecting any observable changes in particle size through microscopy	If any leaching has occurred, nanoparticle size of supported material may decrease in size

2.6. References

- 1 M. Alhumaimess, Z. Lin, Q. He, L. Lu, N. Dimitratos, N. F. Dummer, M. Conte, S. H. Taylor, J. K. Bartley, C. J. Kiely and G. J. Hutchings, *Chem. Eur. J.*, 2014, **20**, 1701–1710.
- 2 P. R. Ettireddy, N. Ettireddy, S. Mamedov, P. Boolchand and P. G. Smirniotis, *Appl. Catal. B Environ.*, 2007, **76**, 123–134.
- 3 G. R. Bamwenda, S. Tsubota, T. Nakamura and M. Haruta, *J. Photochem. Photobiol. A Chem.*, 1995, **89**, 177–189.
- 4 K. Naicker, A. S. Mahomed, H. B. Friedrich and S. Singh, *J. Porous Mater.*, 2019, **26**, 301–309.
- 5 S. S. R. Putluru, L. Schill, A. D. Jensen, B. Siret, F. Tabaries and R. Fehrmann, *Appl. Catal. B Environ.*, 2015, **165**, 628–635.
- 6 A. Wolf and F. Schüth, *Appl. Catal. A Gen.*, 2002, **226**, 1–13.
- 7 N. Dimitratos, J. A. Lopez-Sanchez, D. Morgan, A. F. Carley, R. Tiruvalam, C. J. Kiely, D. Bethell and G. J. Hutchings, *Phys. Chem. Chem. Phys.*, 2009, **11**, 5142–5153.
- 8 V. Peneau, G. Shaw, S. J. Freakley, M. M. Forde, N. Dimitratos, R. L. Jenkins, S. H. Taylor and G. J. Hutchings, *Catal. Sci. Technol.*, 2015, **5**, 3953–3959.
- 9 H. Bahruji, M. Bowker, G. Hutchings, N. Dimitratos, P. Wells, E. Gibson, W. Jones, C. Brookes, D. Morgan and G. Lalev, *J. Catal.*, 2016, **343**, 133–146.
- 10 R. J. White, R. Luque, V. L. Budarin, J. H. Clark and D. J. MacQuarrie, *Chem. Soc. Rev.*, 2009, **38**, 481–494.
- 11 P. Munnik, P. E. De Jongh and K. P. De Jong, *Chem. Rev.*, 2015, **115**, 6687–6718.
- 12 L. Sun, L. Jiang, X. Hua, Y. Zheng, X. Sun, M. Zhang, H. Su and C. Qi, *J. Alloys*

- Compd.*, 2019, **811**, 152052.
- 13 D. Prieto-Centurion and J. M. Notestein, *J. Catal.*, 2011, **279**, 103–110.
 - 14 Z. Wang, D. Brouri, S. Casale, L. Delannoy and C. Louis, *J. Catal.*, 2016, **340**, 95–106.
 - 15 R. Zanella, L. Delannoy and C. Louis, *Appl. Catal. A Gen.*, 2005, **291**, 62–72.
 - 16 L. Schill, S. S. R. Putluru, A. D. Jensen and R. Fehrmann, *Catal. Letters*, 2015, **145**, 1724–1732.
 - 17 L. X. Xu, C. H. He, M. Q. Zhu, K. J. Wu and Y. L. Lai, *Catal. Letters*, 2007, **118**, 248–253.
 - 18 R. Zanella, S. Giorgio, C. R. Henry and C. Louis, *J. Phys. Chem. B*, 2002, **106**, 7634–7642.
 - 19 V. Gandhi, R. Ganesan, H. H. Abdulrahman Syedahamed and M. Thaiyan, *J. Phys. Chem. C*, 2014, **118**, 9715–9725.
 - 20 H. Liang, J. M. Raitano, G. He, A. J. Akey, I. P. Herman, L. Zhang and S.-W. Chan, *J. Mater. Sci.*, 2012, **47**, 299–307.
 - 21 L. Lan, H. Li, S. Chen and Y. Chen, *J. Mater. Sci.*, 2017, **52**, 9615–9629.
 - 22 A. P. LaGrow, M. O. Besenhard, A. Hodzic, A. Sergides, L. K. Bogart, A. Gavriilidis and N. T. K. Thanh, *Nanoscale*, 2019, **11**, 6620–6628.
 - 23 R. R. Nasaruddin, T. Chen, N. Yan and J. Xie, *Coord. Chem. Rev.*, 2018, **368**, 60–79.
 - 24 A. Villa, D. Wang, G. M. Veith, F. Vindigni and L. Prati, *Catal. Sci. Technol.*, 2013, **3**, 3036–3041.
 - 25 J. Pritchard, L. Kesavan, M. Piccinini, Q. He, R. Tiruvalam, N. Dimitratos, J. A. Lopez-Sanchez, A. F. Carley, J. K. Edwards, C. J. Kiely and G. J. Hutchings, *Langmuir*,

- 2010, **26**, 16568–16577.
- 26 M. C. Daniel and D. Astruc, *Chem. Rev.*, 2004, **104**, 293–346.
- 27 N. Dimitratos, J. A. Lopez-Sanchez and G. J. Hutchings, in *Handbook of Advanced Methods and Processes in Oxidation Catalysis*, Imperial College Press, London, 2014, pp. 631–678.
- 28 C. A. Wilde, Y. Ryabenkova, I. M. Firth, L. Pratt, J. Railton, M. Bravo-Sanchez, N. Sano, P. J. Cumpson, P. D. Coates, X. Liu and M. Conte, *Appl. Catal. A Gen.*, 2019, **570**, 271–282.
- 29 J. A. Lopez-Sanchez, N. Dimitratos, P. Miedziak, E. Ntainjua, J. K. Edwards, D. Morgan, A. F. Carley, R. Tiruvalam, C. J. Kiely and G. J. Hutchings, *Phys. Chem. Chem. Phys.*, 2008, **10**, 1921.
- 30 P. Paalanen, B. M. Weckhuysen and M. Sankar, *Catal. Sci. Technol.*, 2013, **3**, 2869.
- 31 V. Peneau, Q. He, G. Shaw, S. A. Kondrat, T. E. Davies, P. Miedziak, M. Forde, N. Dimitratos, C. J. Kiely and G. J. Hutchings, *Phys. Chem. Chem. Phys.*, 2013, **15**, 10636–10644.
- 32 T. Sun and J. Y. Ying, *Nature*, 1997, **389**, 704.
- 33 Q. Dai, Z. Zhang, N. He, P. Li and C. Yuan, *Mater. Sci. Eng. C*, 1999, **8–9**, 417–423.
- 34 D. M. Antonelli and J. Y. Ying, *Chem. Mater.*, 1996, **8**, 874–881.
- 35 S. G. Lee, H. J. Lee, I. Song, S. Youn, D. H. Kim and S. J. Cho, *Sci. Rep.*, 2015, **5**, 12702.
- 36 X. Hu, B. O. Skadtchenko, M. Trudeau and D. M. Antonelli, *J. Am. Chem. Soc.*, 2006, **128**, 11740–11741.
- 37 X. Hu, M. Trudeau and D. M. Antonelli, *Chem. Mater.*, 2007, **19**, 1388–1395.

- 38 USOO5718878A, *US Pat. Appl. Publ.*, 1996.
- 39 A. Nakahira, T. Kubo and C. Numako, *Inorg. Chem.*, 2010, **49**, 5845–5852.
- 40 D. M. Antonelli and J. Y. Ying, *Angew. Chemie Int. Ed. English*, 1996, **35**, 426–430.
- 41 M. Kidwai and S. Bhardwaj, *Synth. Commun.*, 2011, **41**, 2655–2662.
- 42 J. C. Gee and R. C. Williamson, *J. Am. Oil Chem. Soc.*, 1997, **74**, 65–67.
- 43 C. Ding, Y. He, J. Yin, W. Yao, D. Zhou and J. Wang, *Ind. Eng. Chem. Res.*, 2015, **54**, 1899–1907.
- 44 B. P. C. Hereijgers and B. M. Weckhuysen, *J. Catal.*, 2010, **270**, 16–25.
- 45 F. Garcia-Ochoa, A. Romero and J. Querol, *Ind. Eng. Chem. Res.*, 1989, **28**, 43–48.
- 46 F. Garcia-Ochoa, J. Querol and A. Romero, *Ind. Eng. Chem. Res.*, 1990, **29**, 1989–1994.
- 47 S. Blaine and P. E. Savage, *Ind. Eng. Chem. Res.*, 1991, **30**, 2185–2191.
- 48 H. Pobiner, *Anal. Chem.*, 1961, **33**, 1423–1426.
- 49 M. A. Farajzadeh, N. Nouri and P. Khorram, *TrAC Trends Anal. Chem.*, 2014, **55**, 14–23.
- 50 J. D. Chen and R. A. Sheldon, *J. Catal.*, 1995, **153**, 1–8.
- 51 P. T. Wierzchowski and L. Wiesław Zatorski, *Chromatographia*, 2000, **51**, 83–86.
- 52 J. Sneddon, S. Masuram and J. C. Richert, *Anal. Lett.*, 2007, **40**, 1003–1012.
- 53 E. L. Schymanski, M. Bataineh, K.-U. Goss and W. Brack, *TrAC Trends Anal. Chem.*, 2009, **28**, 550–561.
- 54 C. Osorio, M. Alarcon, C. Moreno, A. Bonilla, J. Barrios, C. Garzon and C. Duque, *J. Agric. Food Chem.*, 2006, **54**, 509–516.

- 55 M. A. Sumathykutty, J. Madhusudana Rao, K. P. Padmakumari and C. S. Narayanan, *Flavour Fragr. J.*, 1999, **14**, 279–282.
- 56 K. Syed, A. Porollo, Y. W. Lam, P. E. Grimmett and J. S. Yadav, *Appl. Environ. Microbiol.*, 2013, **79**, 2692–2702.
- 57 M. K. Akhtar, H. Dandapani, K. Thiel and P. R. Jones, *Metab. Eng. Commun.*, 2015, **2**, 1–5.
- 58 A. R. Hind, S. K. Bhargava and A. McKinnon, *Adv. Colloid Interface Sci.*, 2001, **93**, 91–114.
- 59 S. Klein, S. Thorimbert and W. F. Maier, *J. Catal.*, 1996, **163**, 476–488.
- 60 V. Crupi, F. Longo, D. Majolino and V. Venuti, *J. Phys. Condens. Matter*, 2006, **18**, 3563–3580.
- 61 L. Ohlin, P. Bazin, F. Thibault-Starzyk, J. Hedlund and M. Grahn, *J. Phys. Chem. C*, 2013, **117**, 16972–16982.
- 62 D. M. Antonelli, *Adv. Mater.*, 1999, **11**, 487–492.
- 63 A. W. Coats and J. P. Redfern, *Analyst*, 1963, **88**, 906.
- 64 S. Ching, E. J. Welch, S. M. Hughes, A. B. F. Bahadoor and S. L. Suib, *Chem. Mater.*, 2002, **14**, 1292–1299.
- 65 G. Mirth, J. A. Lercher, M. W. Anderson and J. Klinowski, *J. Chem. Soc. Faraday Trans.*, 1990, **86**, 3039–3044.
- 66 M. Kruk, M. Jaroniec, Y. Sakamoto, O. Terasaki, R. Ryoo and C. H. Ko, *J. Phys. Chem. B*, 2000, **104**, 292–301.
- 67 E. S. Ameh, *Int. J. Adv. Manuf. Technol.*, 2019, **105**, 3289–3302.
- 68 A. V. Biradar and T. Asefa, *Appl. Catal. A Gen.*, 2012, **435–436**, 19–26.

- 69 D. S. Gopala, R. R. Bhattacharjee and R. Richards, *Appl. Organomet. Chem.*, 2013, **27**, 1–5.
- 70 F. Boccuzzi, A. Chiorino, M. Manzoli, P. Lu, T. Akita, S. Ichikawa and M. Haruta, *J. Catal.*, 2001, **202**, 256–267.
- 71 Y. Yalçın, M. Kılıç and Z. Çınar, *Appl. Catal. B Environ.*, 2010, **99**, 469–477.
- 72 Y. Zhou, J. Long and Y. Li, *Chinese J. Catal.*, 2016, **37**, 955–962.
- 73 Y. Zhou and J. A. Switzer, *J. Alloys Compd.*, 1996, **237**, 1–5.
- 74 M. T. Weller, *Inorganic Materials chemistry*, Oxford University Press Inc., New York, 1st edn., 1994.
- 75 H. Zhao, J. Zhou, H. Luo, C. Zeng, D. Li and Y. Liu, *Catal. Letters*, 2006, **108**, 49–54.
- 76 W. L. Bragg, *Proc. R. Soc. A Math. Phys. Eng. Sci.*, 1914, **89**, 468–489.
- 77 M. Stöcker, *Microporous Mater.*, 1996, **6**, 235–257.
- 78 M. Inagaki and F. Kang, in *Materials Science and Engineering of Carbon*, Elsevier Inc., Oxford, 2016, pp. 1–6.
- 79 R. R. Mather, in *Surface Modification of Textiles*, Woodhead Publishing Limited, Cambridge, 2009, pp. 296–317.
- 80 T. Yamashita and P. Hayes, *Appl. Surf. Sci.*, 2008, **254**, 2441–2449.
- 81 T. L. Barr, *Zeolites*, 1990, **10**, 760–765.
- 82 F. Ambroz, T. J. Macdonald, V. Martis and I. P. Parkin, *Small Methods*, 2018, **2**, 1800173.
- 83 M. Thommes, K. Kaneko, A. V. Neimark, J. P. Olivier, F. Rodriguez-Reinoso, J. Rouquerol and K. S. W. Sing, *Pure Appl. Chem.*, 2015, **87**, 1051–1069.
- 84 Z. Kónya, V. F. Puentes, I. Kiricsi, J. Zhu, J. W. Ager, M. K. Ko, H. Frei, P. Alivisatos

- and G. A. Somorjai, *Chem. Mater.*, 2003, **15**, 1242–1248.
- 85 A. H. Janssen, A. J. Koster and K. P. De Jong, *J. Phys. Chem. B*, 2002, **106**, 11905–11909.
- 86 T. W. Barnard, M. I. Crockett, J. C. Ivaldi, P. L. Lundberg, D. A. Yates, P. A. Levine and D. J. Sauer, *Anal. Chem.*, 1993, **65**, 1231–1239.
- 87 J. M. Fitzsimmons, D. G. Medvedev and L. F. Mausner, *J. Anal. At. Spectrom.*, 2016, **31**, 458–463.
- 88 H. Gruber-Woelfler, P. F. Radaschitz, P. W. Feenstra, W. Haas and J. G. Khinast, *J. Catal.*, 2012, **286**, 30–40.

CHAPTER 3: The autoxidation of alkanes and subsequent analysis of reaction mixtures

Contents

CHAPTER 3: The autoxidation of alkanes and subsequent analysis of reaction mixtures .	121
Abbreviations	122
3.1. Introduction	123
3.2. Results and discussion	126
3.2.1. Development of an ¹ H-NMR alkane oxidation quantification method.....	126
3.2.1.1. Application of ¹ H-NMR conversion calculator to the autoxidation of alkanes....	136
3.2.2. Development of a GC-MS <i>n</i> -decane oxidation quantification calculator	140
3.3. The autoxidation of <i>n</i> -decane and determination of ideal oxidation conditions	147
3.4. Conclusion and future work.....	151
3.5. References	152

Abbreviations

BDE – Bond Dissociation Energy

CMB – Carbon Mass Balance

FID – Flame Ionisation Detection

GC-MS – Gas Chromatography – Mass Spectrometry

NIST – National Institute of Standards and Technology

NMR – Nuclear Magnetic Resonance

3.1. Introduction

Alkanes are some of the most inert substrates within chemistry when referring to C-H bond activation.¹ Their reactivity is often used as a comparison to other compounds, for example methane has a pKa of >40, in comparison to water's pKa of 14.²⁻⁴ This exemplifies the acidity of the C-H bonds in methane and how difficult it is for these molecules to react, for example in acid/base catalysed or non-catalysed reactions. Similar arguments can be applied also for redox or radical pathways, as the typical bond dissociation energy (BDE) of the C-H bond for linear saturated hydrocarbons is largely in excess of 410 kJ mol⁻¹;⁵ whereas by comparison the BDE of a C-H bond of a carbonyl group is below 375 kJ mol⁻¹;⁵ and the BDE of C-Br bonds are usually assumed as relatively weak, being in the range of ca. 300 kJ mol⁻¹.⁵

However, alkanes have huge potential within applications in industry and academic research. As alkanes are a chemical feedstock – virtually all organic chemical compounds are obtained from them initially – it follows their functionalisation is a highly important research topic.⁶ Often dubbed the 'holy grail' of petrochemical and catalytic chemistry,⁷⁻⁹ selectively converting alkanes to a desired product, with minimal formation of by-products is the focus of this project. Specifically, the selective oxidation of long chain linear alkanes to their corresponding primary alcohols.^{10,11} As mentioned previously, this is challenging due to the potential for alternative, undesired products (e.g. secondary/tertiary alcohols, ketones, and products made from cracking).¹²

Catalysts therefore need to be selective in order to reduce waste products.^{11,13} To enable study on whether a catalyst is indeed selective an accurate and quantitative determination method (either spectroscopic or chromatographic) of the composition of the reaction mixture is required.

The complete characterization, both qualitatively and quantitatively, of a reaction mixture obtained from the oxidation of a hydrocarbon is not a trivial task.¹⁴⁻¹⁶ In fact typically tens of products can be obtained.¹⁶ A commonly used method to determine the composition of these reaction mixtures is via gas chromatography (GC, either using mass spectrometry - MS or

flame ionisation - FID as detection systems).¹⁷⁻¹⁹ However, despite their low detection limit (especially for GC-MS methods), these are tedious, require a long analysis time and crucially may not provide accurate results unless pre-preparation of the reaction mixture before analysis is carried out.^{20,21} In our case this specifically refers to the analysis of organic acids and alkyl hydro-peroxides.^{22,23} In fact, acids need to be converted to the corresponding ester (R(CO)OR')²¹ whereas alkyl hydroperoxides (R-OOH) can potentially decompose to ketones or alcohols under the injection of chromatography conditions (an injector typically operates at a temperature range of 180 – 200 °C to ensure full volatilization of the reaction mixture and its transfer to the chromatographic column).^{22,24,25} It follows that GC-MS or GC-FID methods can certainly have a low detection limit, but with the risk that the specimen analysed is not representative of the sample from a reaction mixture.

In view of this, as well as to cope with a large number of reaction mixtures to be analysed, we decided to develop a ¹H-NMR method (herein also referred to as a 'calculator') to quantify and characterize our reaction mixtures. In fact, as we expect low conversion, the amount of acids (which are known to be difficult to detect, due to proton exchange in NMR) to be very small. Furthermore, as NMR characterization is carried out at room temperature this should not induce any ROOH decomposition, and in turn also not require any pre-treatment of the sample. In addition, a single ¹H-NMR determination is relatively cheap and occurs in a matter of minutes, whereas chromatographic methods are by comparison expensive and time demanding (in relative terms up to 1 h per sample). Consequently, we want to use ¹H-NMR as a form of screening tool (materials or tests that are not active in NMR will also not be active in GC-MS), to quickly assess if a catalyst is active or not and gather preliminary information on its selectivity. Then for the most promising catalysts and corresponding tests these were subjected to GC-MS characterizations. We should underline though that in this work we attempted to use NMR entirely (because of its time and cost advantages) and in this perspective we carried out a method development for both NMR and chromatographic methods.

Initially, to test both NMR and GC methods we used an array of standards. Then once accurate quantification was available, it was applied to real reaction mixtures. These were carried out from the parallel study of the autoxidation of *n*-decane, as quantification of products in *standard* alkane reaction mixtures was developed alongside studying autoxidation. This is important as ideally little to no background reactions will be occurring and all activity will be due to the catalyst. Therefore, different autoxidation tests were carried out by varying temperature in order to determine the optimal or acceptable conditions where no autoxidation was occurring compared to tests and reaction mixtures in the presence of a catalyst.

3.2. Results and discussion

3.2.1. Development of an $^1\text{H-NMR}$ alkane oxidation quantification method

NMR allows rapid and cheap analysis of samples. However, as the oxidation of *n*-alkanes can typically lead to multiple products,¹⁶ it is important that the individual amounts of these can be accurately determined so that the conversion and selectivity amongst catalysts can be compared. Standards of *n*-octane and *n*-decane and their commercially available oxidation products were made in order to test $^1\text{H-NMR}$ as an appropriate tool. C_8 and C_{10} were chosen as they fit the description of 'linear fatty alkanes'²⁶ while having the lowest number of possible oxidation products compared to C_{12} and above. Therefore, these were an appropriate starting point to develop quantification via $^1\text{H-NMR}$. An overlay of the standards can be seen in figures 3.2.1.1 and 3.2.1.2.

Although fast and cheap, the use of NMR to characterize an alkane reaction mixture is by no means trivial. In fact, in 'standard' mono-dimensional NMR many NMR peaks appear to be overlapped. For our analysis the determination of a 'characteristic peak' for each compound of interest was chosen in the $^1\text{H-NMR}$ (see appendix for all individual spectra, also indications of characteristic peaks for *n*-octane and *n*-decane and corresponding oxidation products). This means that there should be no significant overlap of the integral between these peaks. The 1° alcohol seemingly had some overlap with the 3° and, in *n*-decane, the 4° alcohols. Although this may lead to issues in quantification, the method was pursued as ideally the catalyst would generate little amounts of $3^\circ - 5^\circ$ oxidised products. Please see later in this section and table 3.2.1.1 for characteristic peaks and corresponding chemical shifts.

With the characteristic peaks chosen, a method to determine conversion and selectivity was developed.

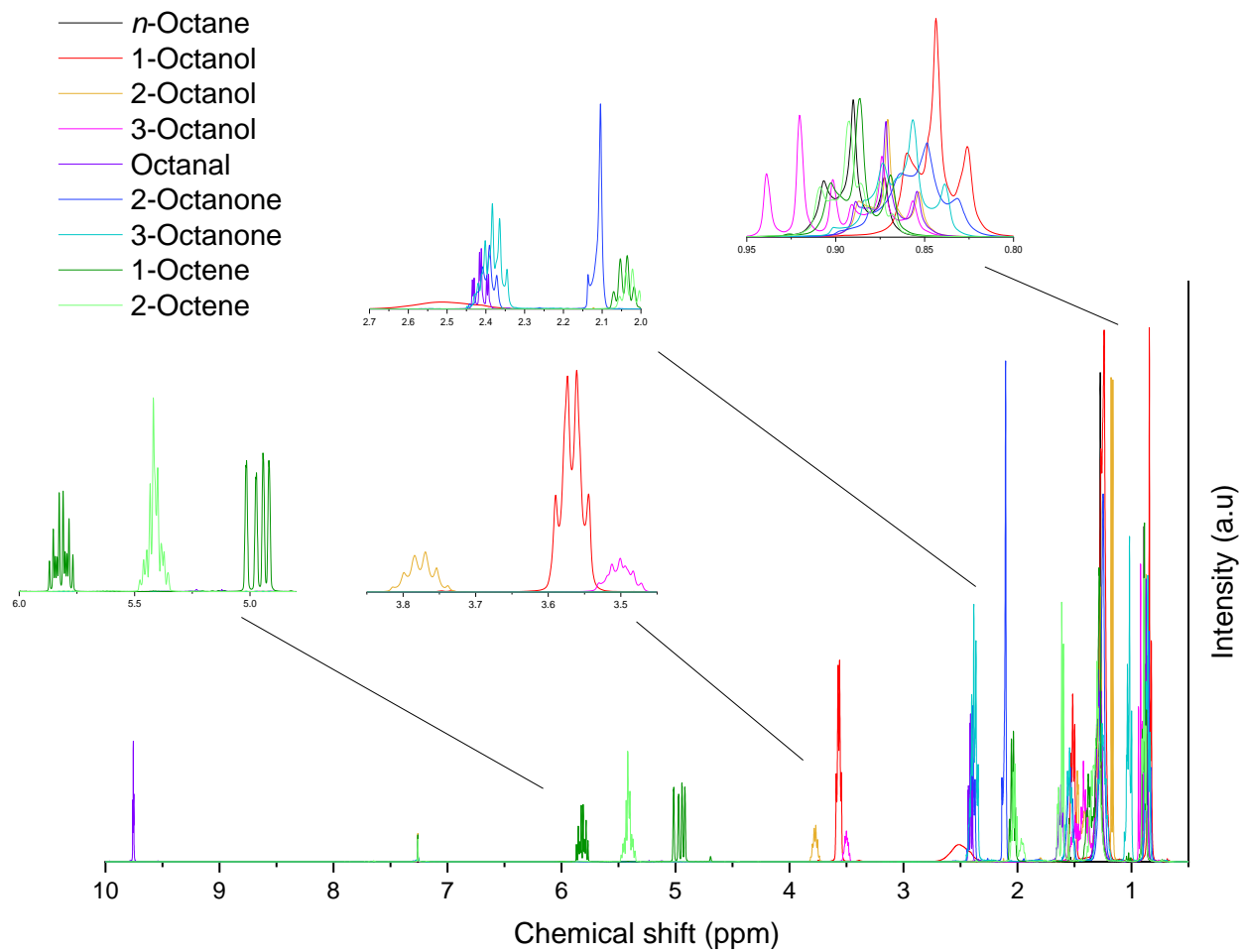


Figure 3.2.1.1: ^1H -NMR spectra of n -octane and commercially available oxidation products. Regions including characteristic peaks are highlighted.

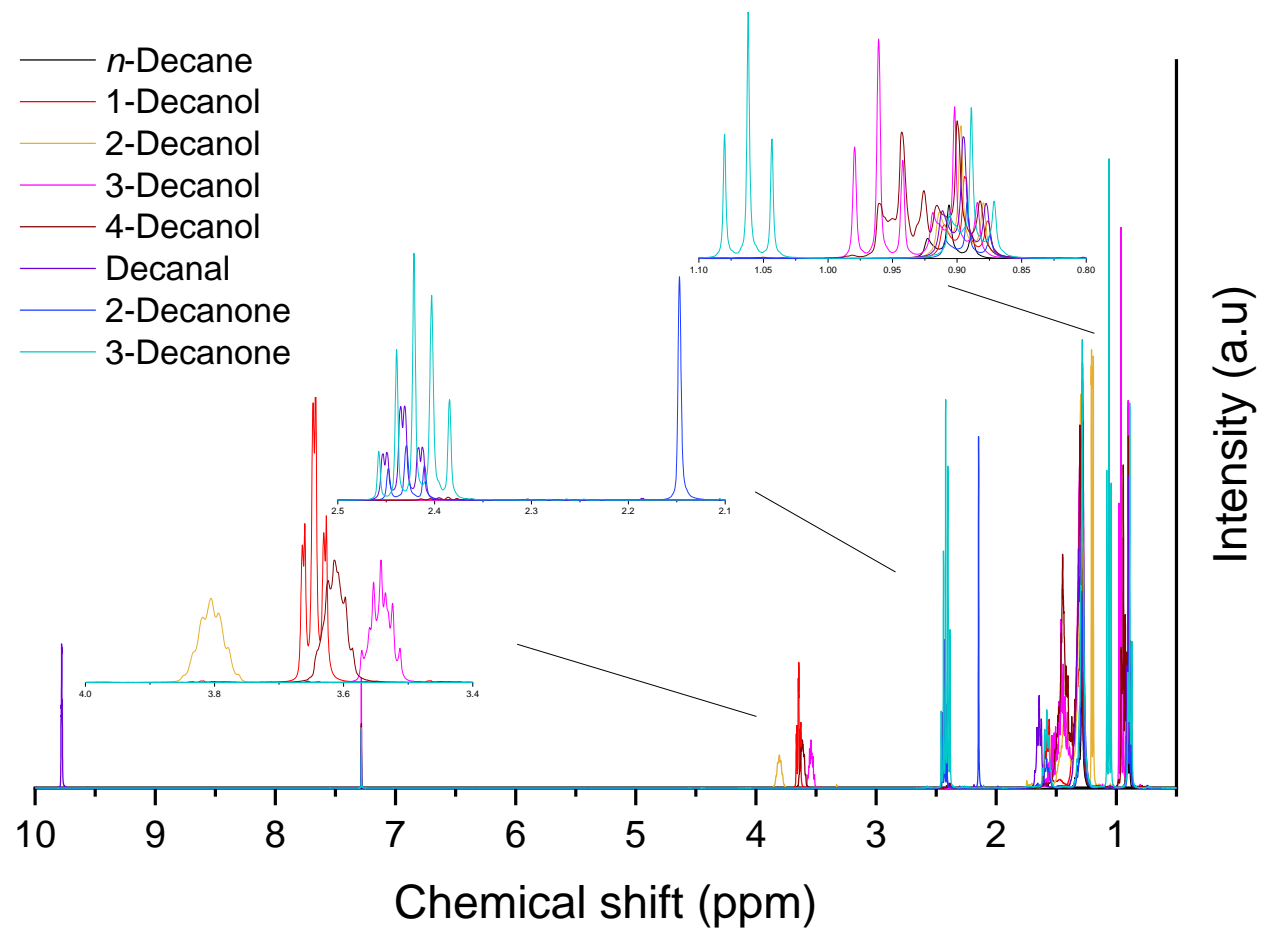


Figure 3.2.1.2: ^1H -NMR spectra of *n*-decane and commercially available oxidation products. Regions including characteristic peaks are highlighted.

Conversion, in our case *molar* conversion, is defined as the ratio between the number of moles, n , of reagent, R , that have been consumed during the reaction, $n_{R,c}$, and the initial number of moles of reagent, $n_{R,0}$ (eq. 3.2.1.1):²⁷

$$\text{Conversion} = \frac{n_{R,c}}{n_{R,0}} \quad (\text{eq. 3.2.1.1})$$

Or, as in our case if expressed in percentage (eq. 3.2.1.2):

$$\text{Conversion (\%)} = \frac{n_{R,c}}{n_{R,0}} \cdot 100 \quad (\text{eq. 3.2.1.2})$$

As this definition entirely relies on the reagent with no knowledge of the products this is also known as ‘absolute conversion’.

On the other hand, if the reaction has a carbon mass balance experimentally equal (i.e. within experimental error) to 100%, all reaction products are identified, and all the products are obtained per mole of reagent (i.e. the stoichiometric coefficient is 1) then eq.2 can be re-written as (eq. 3.2.1.3):

$$\text{Conversion (\%)} = \frac{\sum_i n_{Pi}}{n_{R,0}} \cdot 100 \quad (\text{eq. 3.2.1.3})$$

n_{Pi} , is the moles of a given product, i . However, as in NMR calibration curves are impractical (and in the absence of an internal standard), what we detect for R is the final number of moles, $n_{R,f}$, or moles left in the reaction mixture. We can calculate the conversion as (eq. 3.2.1.4):

$$\text{Conversion (\%)} = \frac{\sum_i n_{Pi}}{n_{R,f} + \sum_i n_{Pi}} \cdot 100 \quad (\text{eq. 3.2.1.4})$$

This equation (eq. 3.2.1.4) has been used as a basis for our calculations via NMR. It also follows that this kind of formula relies on the products that are actually observed. As a consequence, calculations based on these assumptions are also known as ‘observed conversion’ (and in turn there will also be an ‘observed’ selectivity).

However, in $^1\text{H-NMR}$ the signal obtained from NMR spectra is a consequence of the amount of substance, but also from the number of protons (with the latter practically acting as a response factor). In other words, the number of moles of a product, i , is proportional to the area, A , of a specific NMR signal divided by the number of protons, m , associated to that signal (eq. 3.2.1.5). The calculation requires the number of protons to be considered as n_{pi} is determined by an integral from a defined environment in the $^1\text{H-NMR}$. Therefore:

$$n_{pi} \propto \frac{A_{pi}}{m_H} \quad (\text{eq. 3.2.1.5})$$

Where A_{pi} is the area of a given product, and m_H equates to the number of protons for the integral chosen. This means that for n -octane (Octane) the signal associated to the two terminal CH_3 groups (6H) will need to be divided by 6; for 1-Octanol (1Ol) the signal associated to the $\text{CH}_2\text{-OH}$ (2H) will need to be divided by two and so on for the other products: 3-Octanol and 4-Octanol (3Ol and 4Ol respectively) the CH-OH (1H); Octanal (Ald) the C(O)-H (1H); 2-Octanone (2One) the C(O)-CH_3 (3H); 3-Octanone + 4-Octanone (3,4One) the $\text{CH}_2\text{-C(O)-CH}_2$ (4H); 1-Octene (1Ene) the HC=CH_2 (3H); 2-Octene (2Ene) the $\text{HC=CH(CH}_3)$ (2H). Note: the 3-Octanone and 4-Octanone do not have any additional characteristic peaks separate from the other products and are therefore grouped together. This gives in first approximation (eq. 3.2.1.6):

$$\text{Conversion (\%)} = \frac{\frac{A_{1Ol}}{2} + \frac{A_{2Ol}}{1} + \frac{A_{3Ol}}{1} + \frac{A_{4Ol}}{1} + \frac{A_{Ald}}{1} + \frac{A_{2One}}{3} + \frac{A_{3,4One}}{4} + \frac{A_{1Ene}}{3} + \frac{A_{2Ene}}{2}}{\frac{A_{Octane,f}}{6} + \left(\frac{A_{1Ol}}{2} + \frac{A_{2Ol}}{1} + \frac{A_{3Ol}}{1} + \frac{A_{4Ol}}{1} + \frac{A_{Ald}}{1} + \frac{A_{2One}}{3} + \frac{A_{3,4One}}{4} + \frac{A_{1Ene}}{3} + \frac{A_{2Ene}}{2} \right)} \cdot 100$$

(eq. 3.2.1.6)

Where A_{1Ol} is peak area for 1-octanol and in this instance is divided by two as the peak chosen has a m_H value of two (see table 3.2.1.1), A_{Ald} is the peak area for octanal, A_{2One} is the area for 2-octanone and so on.

However, this is a first approximation only as the signal associated to A_{Octane} overlaps with the signal from the CH_3 groups from all the other products. Therefore, each product's contribution

to this integral needs to be removed. Furthermore the $A_{3One} + A_{4One}$ integral contains a CH_2 group from 2-Octanone and Octanal. This induces some correction factors. The corrected value of 3-Octanone + 4-Octanone is ($A, c_{3,4One}$) (eq. 3.2.1.7):

$$A, c_{3,4One} = (A_{3,4One}) - 2\left(\frac{A_{2One}}{3}\right) - 2\left(\frac{A_{Ald}}{1}\right) \quad (\text{eq. 3.2.1.7})$$

The corrected integral area for n -octane can thus be determined (eq. 3.2.1.8a and eq. 3.2.1.8b):

$$A, c_{Octane,corrected} = (A_{Octane,observed}) - \sum m_{H'} \frac{A_{Pi}}{m_H} \quad (\text{eq. 3.2.1.8a})$$

$$\sum m_{H'} \frac{A_{Pi}}{m_H} = \left(3\left(\frac{A_{1Ol}}{2}\right) + 3\left(\frac{A_{2Ol}}{1}\right) + 6\left(\frac{A_{3Ol}}{1}\right) + 3\left(\frac{A_{Ald}}{1}\right) + 3\left(\frac{A_{2One}}{3}\right) + 6\left(\frac{A, c_{3,4One}}{4}\right) + 3\left(\frac{A_{1En}}{3}\right) + 3\left(\frac{A_{2En}}{2}\right)\right) \quad (\text{eq. 3.2.1.8b})$$

Where $m_{H'}$ is the number of protons of a species present in the overlapping ' CH_3 ' region of the spectra. For example, A_{1Ol} is divided by two as it has a m_H value of two from the peak chosen, it is then multiplied by three ($m_{H'}$) as this corresponds to the number of protons present in the overlapping peak with n -octane, see table 3.2.1.1 for a summary of all overlapping peaks.

Substituting these values into the equation gives the final conversion which can be calculated, or more appropriately we should say estimated, as (eq. 3.2.1.9):

$$\text{Conversion (\%)} = \frac{\frac{A_{1Ol}}{2} + \frac{A_{2Ol}}{1} + \frac{A_{3Ol}}{1} + \frac{A_{Ald}}{1} + \frac{A_{2One}}{3} + \frac{A, c_{3,4One}}{4} + \frac{A_{1En}}{3} + \frac{A_{2En}}{2}}{\frac{A, c_{Octane,corrected}}{6} + \frac{A_{1Ol}}{2} + \frac{A_{2Ol}}{1} + \frac{A_{3Ol}}{1} + \frac{A_{Ald}}{1} + \frac{A_{2One}}{3} + \frac{A, c_{3,4One}}{4} + \frac{A_{1En}}{3} + \frac{A_{2En}}{2}} \cdot 100 \quad (\text{eq. 3.2.1.9})$$

Also referred to in this chapter as the 'NMR conversion calculator'. Table 3.2.1.1 summarises all of the characteristic peaks discussed here used for n -octane and its corresponding oxidation products.

Table 3.2.2.1: A summary of NMR data of *n*-octane and its corresponding potential oxidation products with the characteristic (H^a) and overlapping (H^b for *A, c_{Octane,corrected}* overlap and H^c for *A, c_{3,4One}* overlap) peaks chosen for the conversion and selectivity calculators.

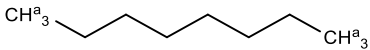
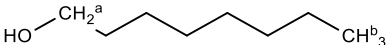
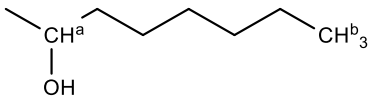
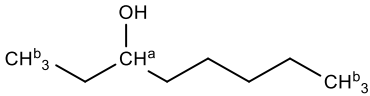
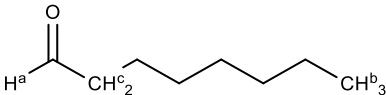
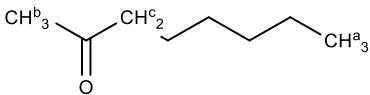
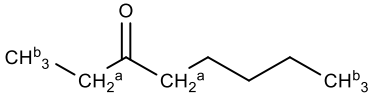
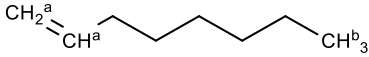
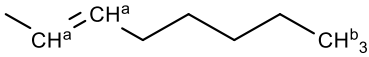
Compound	Characteristic peak (H^a) δ^a (ppm)	Overlapping peak(s) (H^b, H^c) δ^b, δ^c (ppm)
<i>n</i>-octane 	0.89 (CH ₃ , t, 6H)	-
1-octanol 	3.56 (CH ₂ , m, 2H)	0.83 (CH ₃ , t, 3H)
2-octanol 	3.78 (CH, m, 1H)	0.87 (CH ₃ , t, 3H)
3-octanol 	3.50 (CH, m, 1H)	0.87 (CH ₃ , t, 6H)
Octanal 	9.74 (CH, s, 1H)	0.86 (CH ₃ , t, 3H), 2.43 (CH ₂ , t, 2H)
2-octanone 	2.18 (CH ₃ , s, 3H)	0.86 (CH ₃ , t, 3H), 2.47 (CH ₂ , m, 2H)
3-octanone 	2.39 (CH ₂ , m, 4H)	1.02-0.86 (CH ₃ , t, 6H)

Table 3.2.2.1 (cont.)

Compound	Characteristic peak (H ^a) δ^a (ppm)	Overlapping peak(s) (H ^b , H ^c) δ^b, δ^c (ppm)
<p>1-octene</p> 	5.82-4.96 (CH and CH ₂ , m, 3H)	0.90 (CH ₃ , t, 3H)
<p>2-octene</p> 	5.45 (CH=CH, m, 2H)	0.91 (CH ₃ , t, 3H)

Similar arguments have been used to calculate or estimate the selectivity. Selectivity for a given product i (and with the assumptions in our case all products have a stoichiometric coefficient of 1) is (eq.3.2.1.10):

$$Selectivity_{Pi}(\%) = \frac{n_{Pi}}{\sum_i n_{Pi}} \cdot 100 \quad (eq. 3.2.1.10)$$

Where n_{Pi} is determined with the same considerations applied in the derivation of conversion.

For example, the selectivity of 1-octanol in a standard solution would be (eq.3.2.1.11):

$$Selectivity_{1Ol}(\%) = \frac{\frac{A_{1Ol}}{2}}{\frac{A_{1Ol}}{2} + \frac{A_{2Ol}}{1} + \frac{A_{3Ol}}{1} + \frac{A_{Ald}}{1} + \frac{A_{2One}}{3} + \frac{A_{c_{3,4One}}}{4} + \frac{A_{1Ene}}{3} + \frac{A_{2Ene}}{2}} \cdot 100 \quad (eq. 3.2.1.11)$$

The same principle has been applied to all the other products of our standards or reaction mixtures.

It should be noted, however, that preliminary results on known standards showed a systematic error within octanal, and therefore a calibration curve was conducted and determined that A_{Ald} required a correction factor. This is thought to arise from some areas of the characteristic peak being under the background and thus it cannot be quantified accurately. However, once the correction was applied the error of selectivity was found to be always less than 5%.

It should also be noted here that carbon mass balance (CMB) must be considered for accurate quantification. This is to ensure if not all, but the majority of product has been quantified and no losses of volatile material has occurred. CMB can be quantified as follows:²⁷

$$CMB_{\%} = \frac{c_R n_{R,f} + \sum_i c_i n_{P_i}}{c_R n_{R,0}} \cdot 100 \quad (\text{eq. 3.2.1.12})$$

Where c_R are the number of carbon atoms of reactant and c_i are the number of carbon atoms of product. For example, c_R for *n*-octane would be eight and c_i of 1-octanol would also be eight, whereas butanoic acid, one of the potential products from cracking, would have a c_i of four. CMB must be statistically identical to 100% to ensure our assumptions made for conversion and selectivity are permissible.

The conversion calculator was then trialled for a series of standards of varying predicted conversion and selectivity, the results are summarised in table 3.2.1.2.

The majority of errors reported here are below 10%, which is fully acceptable for our scope, especially considering overlap and integration errors of the method and given the large screening capabilities that this method allows. As a consequence, we have used NMR to initially characterize and screen our reaction mixtures.

Table 3.2.1.2: Data to display error associated with calculating conversion and selectivity of expected oxidation products of *n*-octane with varying degree of conversion.

Selectivity error (%)													
Conversion Expected (%)	Conversion Measured NMR (%)	Conversion Relative error (%)	1-Octanol	2-Octanol	3-Octanol	Octanal	2-Octanone	3-Octanone	1-Octene	2-Octene	A1/Atot	K2/Ktot	K/A
3.97	3.71	-6.62	-0.73	-2.75	-5.08	2.49	5.92	4.48	-3.07	-1.42	2.18	1.56	7.36
7.51	7.46	-0.60	12.2	5.44	0.23	-2.79	-2.58	-0.38	-7.23	-1.98	7.34	-0.86	-6.01
17.1	17.5	2.12	-1.17	4.46	24.1	-2.37	-5.70	-6.57	-	-	-9.42	-0.33	-13.3
45.7	44.9	-0.85	5.37	-0.25	2.37	4.77	3.31	-2.20	-7.06	-6.23	2.80	1.33	-0.53
55.4	53.8	-2.84	8.49	2.96	8.86	2.44	6.02	-2.71	-4.76	-3.84	1.61	4.03	-4.56
59.1	56.4	-4.59	0.09	-9.78	-0.33	4.38	4.30	-5.31	-0.39	3.28	3.46	1.52	6.21

3.2.1.1. Application of ¹H-NMR conversion calculator to the autoxidation of alkanes

Accurately determining the conversion and the selectivity for the autoxidation is essential. This is to provide a benchmark for what activity is occurring from the presence of a catalyst and any activity in its absence, the latter often referred to as 'background' activity or background reaction. In principle, three scenarios could occur: (i) either the catalyst is active via a non-autoxidation mechanism under mild conditions (i.e. is active at a specific temperature, where it is determined that background autoxidation is not occurring), (ii) The catalyst is active via a non-autoxidation mechanism where autoxidation would occur (i.e. the catalyst provides a dominating mechanism) or (iii) catalysis occurs through an autoxidation mechanism (but the catalyst induces selectivity to particular products).²⁸ To determine this, a study on how temperature effects autoxidation tests were conducted at different reaction conditions.

Although the NMR calculator was developed using *n*-octane standards, it can be applied to shorter and longer chain alkanes (e.g. *n*-hexane, *n*-decane etc.) by using exactly the same principles. This is essential as the project was planned to focus on substrates with varying alkyl chain lengths. Initial attempts of oxidation with no catalyst present found that autoxidation does not begin to occur until 125 °C and above. As the boiling point of *n*-octane is 125 °C, this made it a limited substrate to be studied with autoxidation if catalytic tests were carried out at atmospheric pressure, as we initially did. The use of non-pressurised systems was also selected at the initial stages of our project for screening purposes, despite previous explanations of alkanes' difficulty to activate. This initial choice was done on the following grounds: (i) the lab was equipped with reactor carousels allowing multiple tests at the same time, useful for screening and (ii) variation of temperature is known to affect a reaction much more than variation of pressure.²⁹⁻³¹ That said we also used pressurised systems following these results (see section 3.3). Therefore *n*-decane was chosen as the model substrate, having a boiling point of 175 °C gives scope for higher temperature reactions to be conducted if necessary.

With the $^1\text{H-NMR}$ conversion calculator proven to work, and substrate chosen, quantification of actual reaction mixtures was the next step to determine if it can indeed be applied to a 'real' example. Figure 3.2.1.1.1 shows a $^1\text{H-NMR}$ spectrum of a reaction mixture conducted at a temperature where autoxidation has occurred (140 °C).

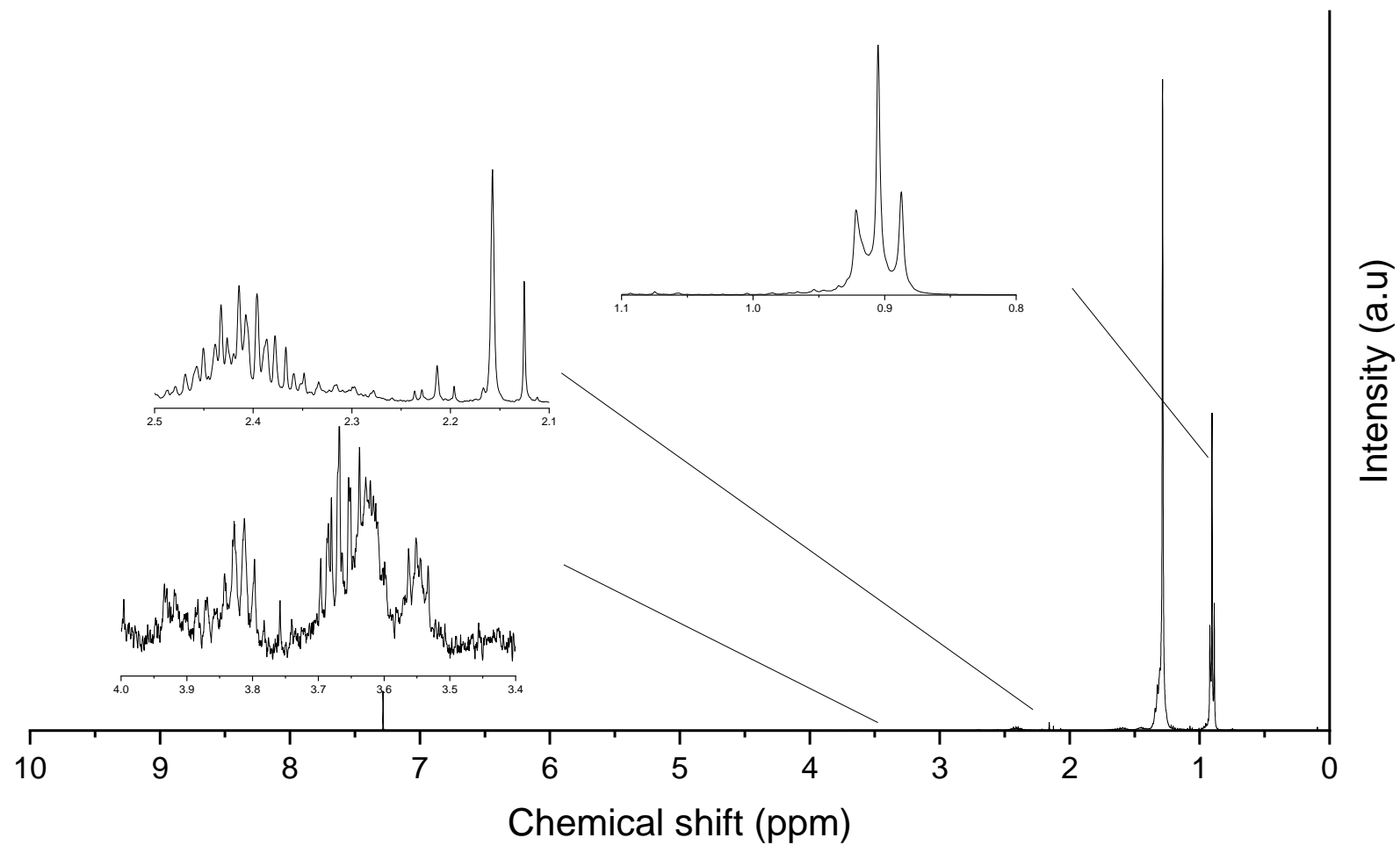


Figure 3.2.1.1.1: $^1\text{H-NMR}$ of a reaction mixture from *n*-decane oxidation, with no catalyst present. *n*-decane (3 mL), 140 °C, atmospheric pressure, 24 h.

NMR analysis of a real reaction mixture showed that there was significant overlap of the reaction's products. It should be stated that it *was expected* that some overlap would occur with by-products such as diones, acids and other over oxidised or cracked products.³² However, the extent actually observed was unexpected and characteristic peaks determined from standard solutions could not be integrated accurately.

As a consequence, instead of isolating single peaks, grouping peaks together to determine regions of the ¹H-NMR spectra (i.e. alcohols, ketones, other) was attempted. While this did give rough approximations for a catalyst's activity, exceptionally high conversions were calculated (in some cases >100%). This meant the calculation model was not appropriate for linear alkane oxidation where a significant number of by-products were made.

Therefore, we had to reconsider chromatographic methods (although slower) and an alternative quantification method was sought by using GC-MS.

3.2.2. Development of a GC-MS *n*-decane oxidation quantification calculator

Although a lengthy procedure, quantitative GC-MS is a powerful tool for analysis of complex mixtures.^{33,34} Distinct separation of peaks in the chromatogram is required for the oxidation products of long chain linear alkanes. However, as they all have similar boiling points, we switched from using an Agilent DB-MS-UI column to the wax-type column Agilent DB-WAX-UI so that the compounds would be separated on polarity.^{35,36} This was achieved with standard solutions of *n*-octane and *n*-decane and their commercially available oxidation products, as demonstrated in figures 3.2.2.2 and 3.2.2.3. Initial attempts of using solvents (e.g. toluene) for the reaction mixture yielded poorly resolved data from the overlap of peaks. Therefore, a solvent delay technique was utilised, treating the substrate as the solvent. This is where the detector is turned off during analysis when the solvent is expected to elute (often used to protect the detector).³⁷ As *n*-octane/*n*-decane are treated as the solvent they are not quantified due to their high concentration; however, products could be resolved. Although this does mean that the reacting substrate cannot be directly quantified post reaction, separate NMR analysis of the amount of alkane after reaction can be conducted. This will allow determination of an approximate amount of total reactant and products, alongside carbon mass balance.

Therefore, with the products in the standard being clearly defined, the following equations can be applied (eq. 3.2.2.1):

$$\text{Conversion (\%)} = \frac{\sum_i [p_i] \cdot r_f}{[R_i]} \cdot 100 \quad (\text{eq. 3.2.2.1})$$

In this case, $[p_i]$ is the concentration of a given product, $[R_i]$ is the concentration of the reactant before the reaction and r_f is the retention factor of a given product - as determined by its calibration curve. The concentration of products is determined through an internal standard (eq. 3.2.2.2):

$$[p_i] = [IS] \cdot \frac{\text{Area}_{p_i}}{\text{Area}_{IS}} \quad (\text{eq. 3.2.2.2})$$

Where $[IS]$ and $Area_{IS}$ are the concentration and area from the GC-MS of the internal standard (n -dodecane for n -decane analysis and 1-decanol for n -octane) respectively.

And finally, selectivity of a given product can be defined as (eq. 3.2.2.3):

$$Selectivity (\%) = \frac{[p_i] \cdot r_f}{\sum_i [p_i] \cdot r_f} \cdot 100 \quad (eq. 3.2.2.3)$$

The relative amounts of each product were determined through calibration curves, a selection is shown in figure 3.2.2.1. It should be noted here all lines are straight and thus the data is within the limits of linearity. Analogous to the approach used for NMR, a 'GC-MS calculator' was developed and then applied to a series of standards. The error of conversion for a selected range is shown in table 3.2.2.1.

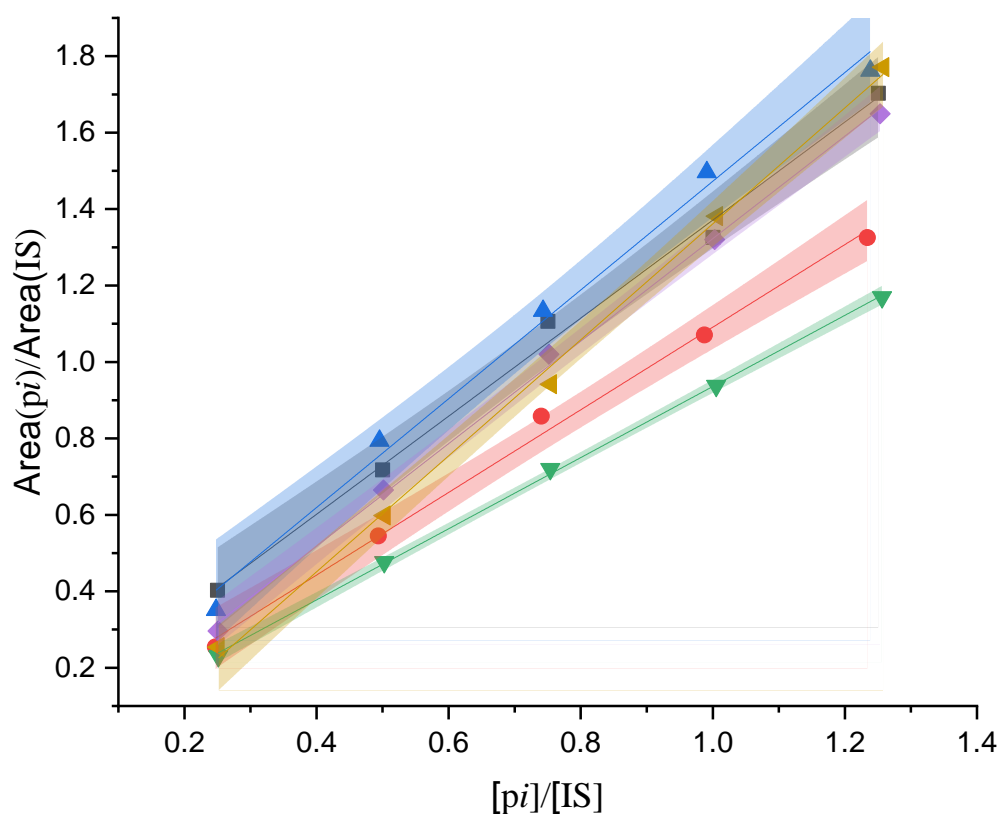


Figure 3.2.2.1: A sample of calibration curves for the various products used for the GC-MS calculator. Internal standard: 1-decanol. 1-Octanol (-■-), 2-Octanol (-●-), 3-Octanol (-▲-), Octanal (-▼-), 2-Octanone (-◆-), 3-Octanone (-▼-).

Table 3.2.2.1: A series of data showing the recorded conversion of *n*-octane standards from GC-MS compared to the actual amount, with the corresponding error and the error of selectivity of proposed oxidation products.

Conversion expected (%)	Conversion measured GC-MS (%)	Relative error (%)	Selectivity relative error (%)					
			1-Octanol	2-Octanol	3-Octanol	Octanal	2-Octanone	3-Octanone
15.1	15.0	0.6	35.2	1.3	7.7	-8.9	-7.5	-27.2
30.2	32.3	-6.4	14.6	13.8	3.1	0.4	-9.1	-22.4
45.3	48.2	-6.0	17.5	7.0	8.1	-9.6	-0.8	-21.6
60.4	64.1	-5.8	7.2	3.4	9.5	-11.0	0.6	-9.5
75.6	78.7	-3.9	-6.4	0.0	-10.3	3.6	2.1	11.2

Typically, the error is higher within GC-MS compared to that of NMR, and at lower conversions the error of selectivity for 1-octanol and 3-octanone starts to become significant. However, this can be rectified by making a more concentrated solution if a real reaction mixture's conversion was found to be too low. This is due to 1-octanol having a small tailing effect due to the nature of the wax-type column, which in turn, becomes harder to quantify at lower concentrations. Similarly, 3-octanone tends to have a broader peak shape and thus the sides of the peak start to become indistinguishable from the background, leading to a lower quantification. However, the error of conversion never exceeds 10% and thus the GC-MS calculator was deemed acceptable as an accurate tool for reaction mixture quantification. Most importantly, the peaks of a 'real' test were able to be distinguished and thus individual product selectivity could be determined.

Figure 3.2.2.4 shows the product distribution of *n*-decane autoxidation at 140 °C under atmospheric/reflux conditions. It reveals that a significant number of products other than the C₁₀ ketones and alcohols exist within the reaction mixture. This also shows why the corresponding NMR spectra contained many additional peaks and thus quantification was not possible. The additional products were primarily cracked products such as hexanol and hexanoic acid, but according to the NIST (National Institute of Standards and Technology) mass spec database,^{38,39} also contained some complex furanone-ester based compounds. These were possibly made from condensation reactions. Further study of the oxidation of *n*-decane via autoxidation is explored in section 3.3.

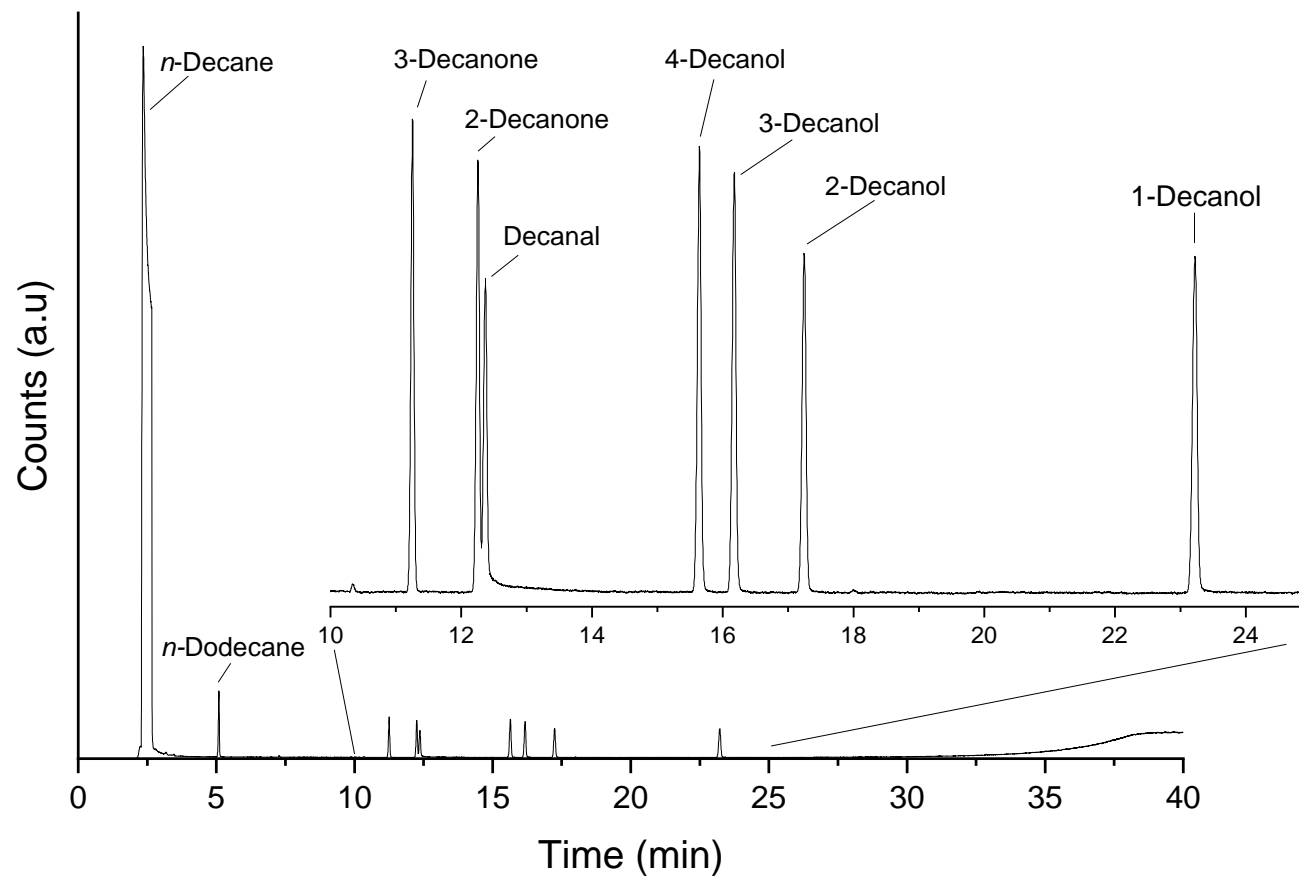


Figure 3.2.2.2: Chromatogram data to show the individual retention times of *n*-decane and its proposed oxidation products. Separation was successful by using a wax column which distinguished products from their polarities. *n*-dodecane is present as this was used as an internal standard.

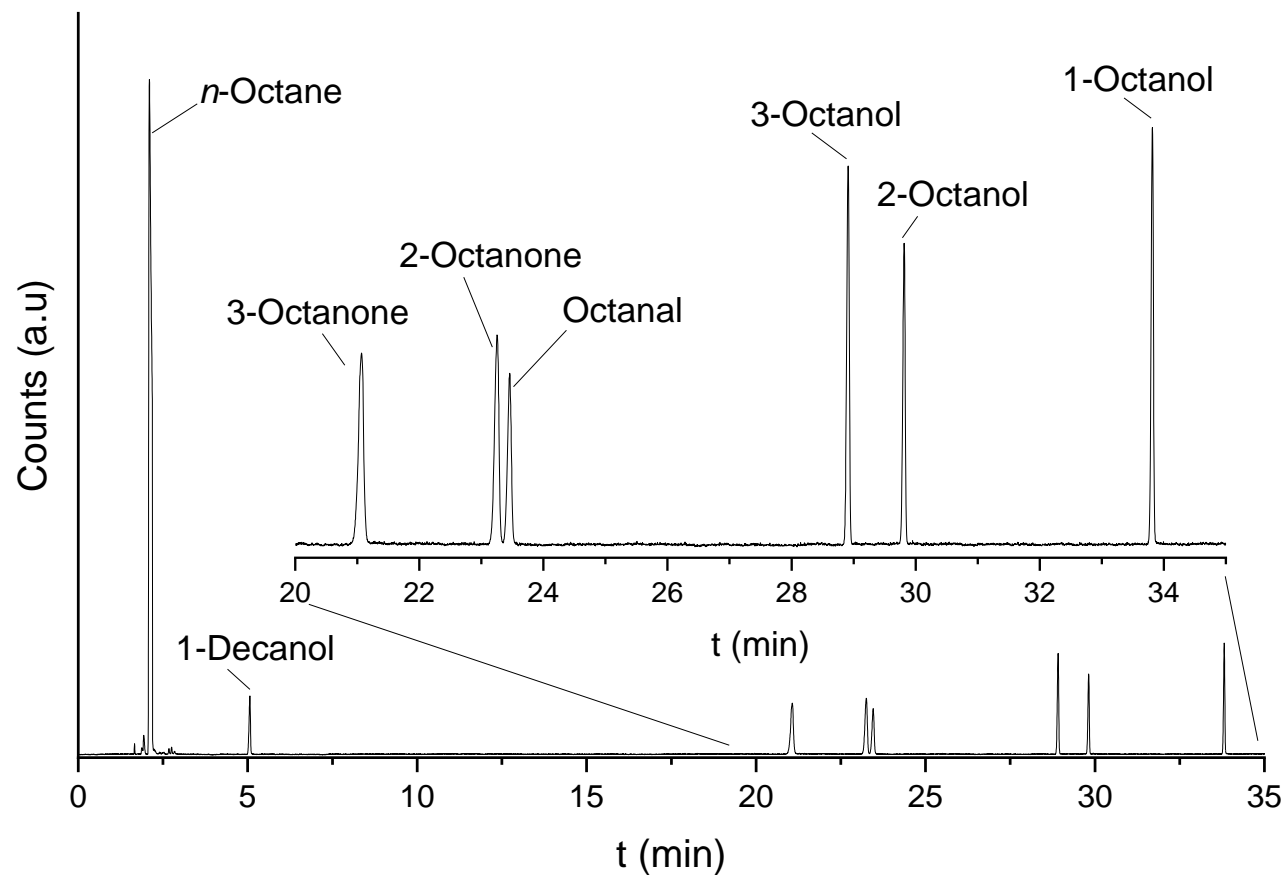


Figure 3.2.2.3: Chromatogram data to show the individual retention times of *n*-octane and its proposed oxidation products. Separation was successful by using a wax column which distinguished products from their polarities. 1-decanol is present as this was used as an internal standard.

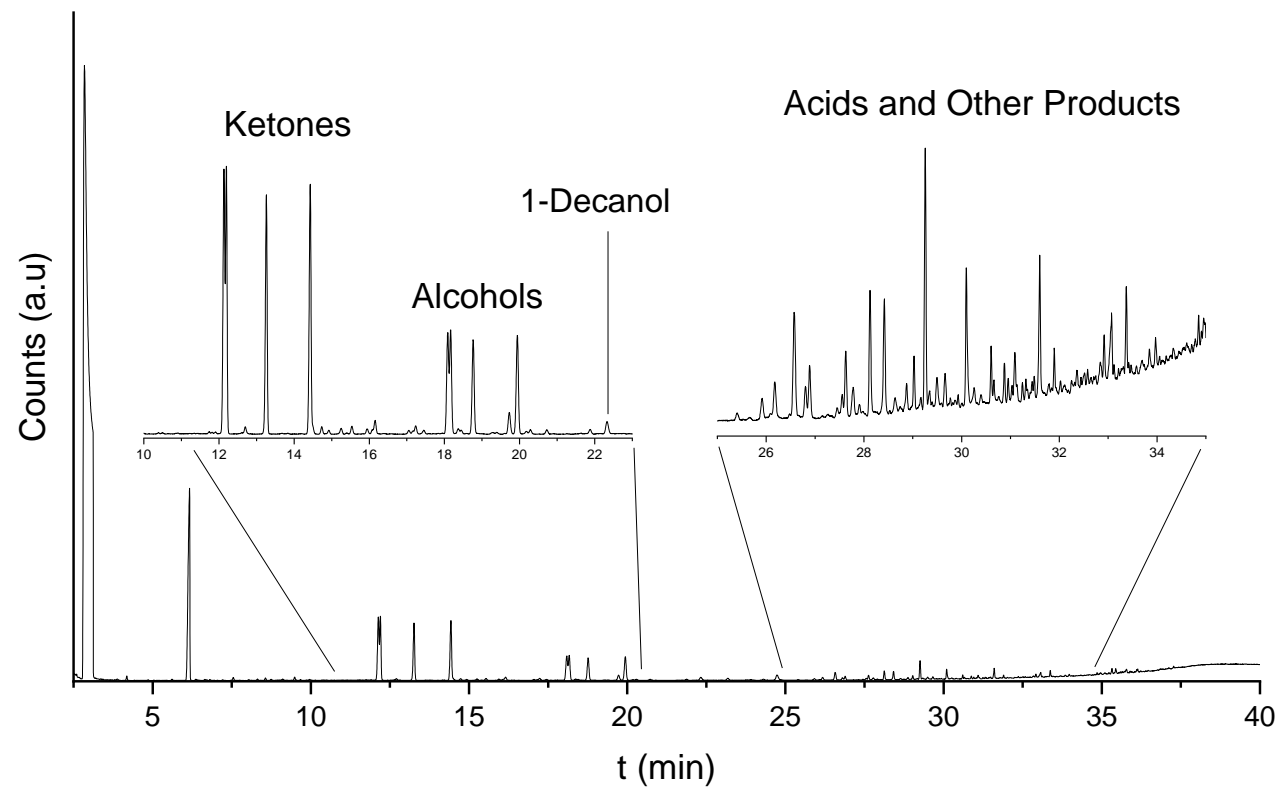


Figure 3.2.2.4: A chromatogram of the oxidation of *n*-decane under autoxidation conditions. Alongside the ketones (5-decanone, 4-decanone, 3-decanone, 2-decanone) and alcohols (5-decanol, 4-decanol, 3-decanol, 2-decanol, 1-decanol) acids from cracking and other products were identified. *n*-decane (3 mL), 140 °C, reflux, 24 h. Internal standard: *n*-dodecane.

3.3. The autoxidation of *n*-decane and determination of ideal oxidation conditions

Although theoretically reaction between a saturated hydrocarbon and molecular oxygen in its ground triplet state is spin forbidden, the reaction can still occur via a process known as 'autoxidation' or via combustion through higher temperatures.^{6,40} These reactions, by their own nature, are selective to products determined by the radicals generated only. However, this means that they are very challenging to drive towards specific and desirable products, like in our case, primary alcohols. This poses a challenge to this research as a catalyst must either:

- 1) Operate at temperatures where no autoxidation is occurring
- 2) Induce a different and 'dominating' mechanism and thus be so active it overcomes any autoxidation
- 3) Modify the autoxidation route so that the product distribution favours those desired (most often by inhibiting undesired reaction pathways)

The remainder of this chapter will focus on point 1) as to define where no autoxidation is occurring by systematically changing the reaction conditions. Information on when catalysts were used can be found in section 4.2. In principle, if a temperature and pressure is used where no autoxidation is occurring, but conversion does occur when a catalyst is present, this would suggest the catalyst is active and thus should have a different selectivity to that of the autoxidation route.

The simplest set up and thus the starting point of this research was the use of atmospheric pressure for the oxidation of *n*-decane. With an accurate quantification tool, the reaction mixture can be quantified over a series of temperature changes at atmospheric pressure to determine the point where autoxidation is occurring. Developing from there, pressurised systems were also tested as in theory these should provide higher conversions. The amount of oxygen used is defined here as ' PO_2 ', this is the reading of the pressure gauge from the oxygen cylinder. A set time of 24 h was chosen as this was found to be where an equilibrium was met from original tests with an approximate NMR quantification.

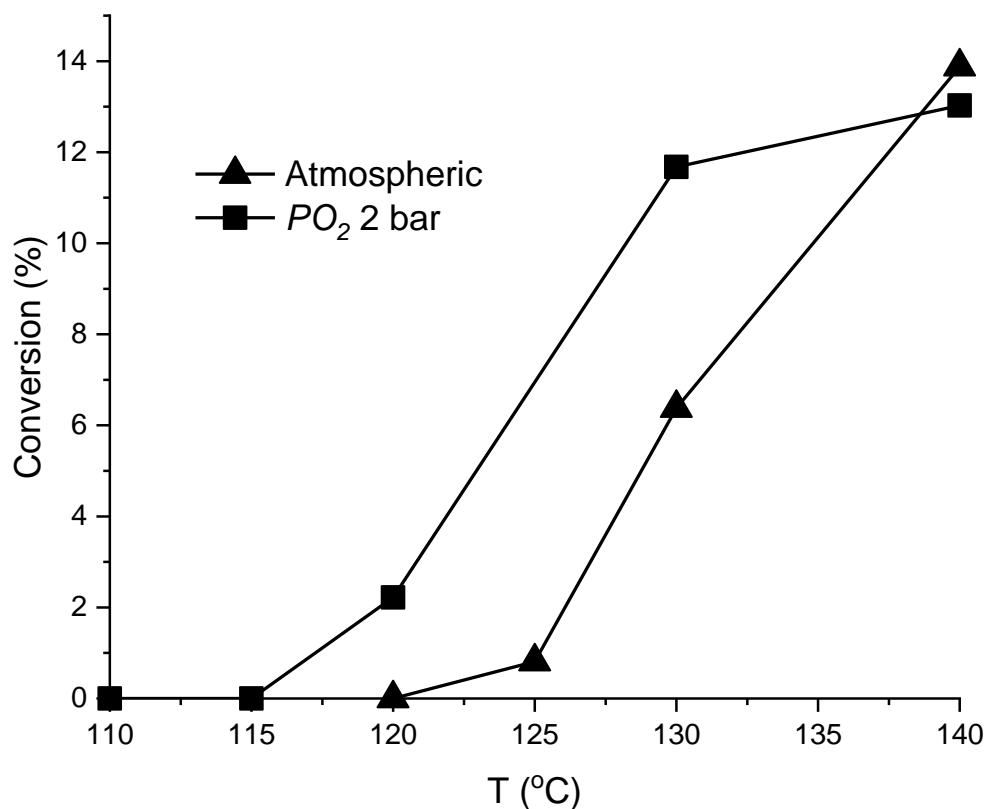


Figure 3.3.1: Conversion of *n*-decane to products quantified via GC-MS as a function of temperature. *n*-decane (3 mL), 24 h. *P* = Atmospheric (-▲-) and *PO*₂ 2 bar (-■-).

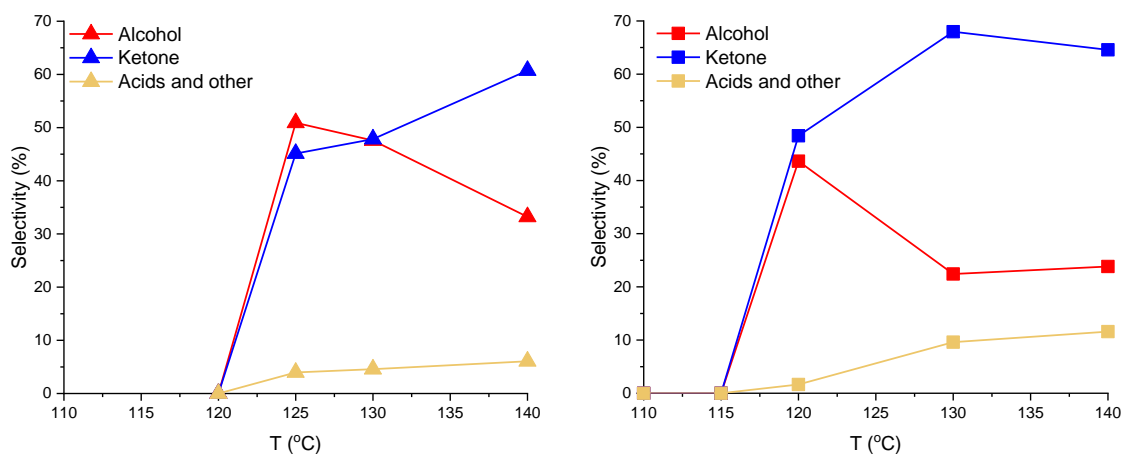


Figure 3.3.2: Selectivity data for alcohols, ketones and acids/other products as determined by GC-MS from the autoxidation of *n*-decane as a function of temperature. *n*-decane (3 mL), 24 h. *P* = Atmospheric (-▲-) and *PO*₂ = 2 bar (-■-).

As expected, atmospheric oxidation of *n*-decane did not occur until a higher temperature compared to that of the pressurised system (figure 3.3.1). Furthermore, at specific temperatures, the oxidation of *n*-decane is higher in pressurised systems than at atmospheric conditions until 140 °C, where the two lines meet. Temperatures higher than this were not conducted as this approached the boiling point of *n*-decane. In all cases, the carbon mass balance was determined via NMR to be >95% and thus no significant loss of volatile compounds was observed. At 140 °C it seems a maximum conversion is met, this is likely due to the limiting factor of oxygen solubility⁴¹ and the pressurised system has reached its limit of being beneficial.

The selectivity of products also fits loosely what is expected from literature studies (figure 3.3.2).⁴² In both atmospheric and pressurised conditions for oxidation there is a significant amount of alcohol at the lowest conversions, then a significant decrease of this class of products as temperature is increased. This is due to a further oxidation occurring where the oxidation of the alcohol yields the ketone or an aldehyde.⁴³ In fact the BDE of the C-H bond alpha to an OH group of an alcohol is ~125 kJ mol⁻¹ lower than the corresponding saturated hydrocarbon.⁵ In other words, the more the reaction progresses the more the products are easier to oxidise. This also explains why these reactions lead to a large number of by products and are so challenging to control in terms of selectivity.⁴⁴ Interestingly, decanal is never observed in the GC-MS. It is speculated that this is immediately converted to decanoic acid if ever present in the reaction mixture. Furthermore, the rise of acids and other condensation products occurs at higher temperatures. The alcohols, ketones and *n*-decane itself are being oxidised and/or cracked into over oxidised species due to more homolytic mechanisms occurring.⁴⁵ The pressurised system starts to show a higher selectivity for acids and other products and a lower selectivity to alcohols when compared to atmospheric conditions. As no further conversion is occurring and it is expected that oxygen diffusion is a limiting factor,⁴¹ the presence of a higher amount of by-products during the start of the reaction in the pressurised system could be affecting the multiple potential mechanisms occurring and thus leading to a

different selectivity. However, this is to some extent expected due to the complex nature of the radical components of the mechanisms (see section 1.3.1), these are summarised in figure 3.3.3:

3.3.3:

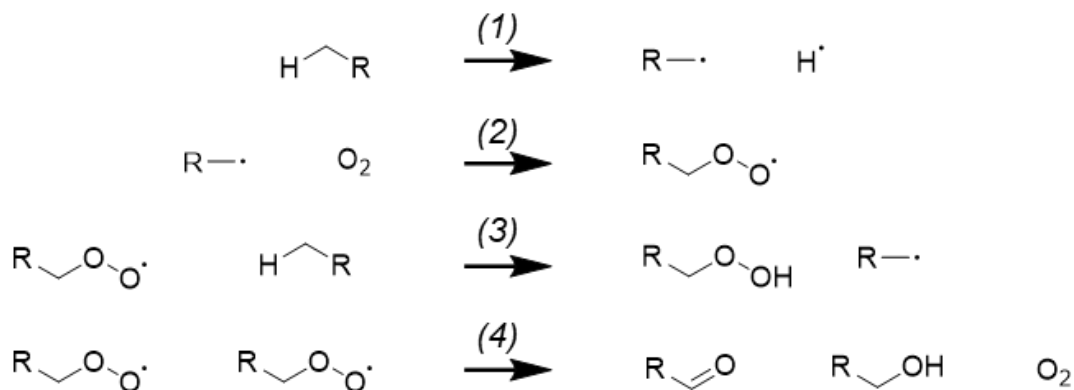


Figure 3.3.3: A sample of mechanistic steps occurring during autoxidation. Step (1) is an initiation step, steps (2) and (3) are propagation steps and step (4) is a termination step.⁶

Ultimately, this is useful for the proposed catalytic tests as it shows:

- 1) Where autoxidation does not occur. Therefore, a catalyst must be ideally active < 120 °C for pressurised systems and < 130 °C under atmospheric conditions. It should be noted, however, that this is a challenging and ambitious target as a temperature of 120 °C has to be considered very low for linear saturated hydrocarbons.
- 2) The extent and product distribution of autoxidation. If a catalyst is not active at lower temperatures, but changes in selectivity are observed compared to autoxidation conditions without a catalyst, then the catalyst still has an involvement in the reaction. In this specific case adsorbing a reaction intermediate.

3.4. Conclusion and future work

An efficient and accurate tool for the quantification of *n*-decane's and *n*-octane's oxidation products was developed. When using standard solutions both ¹H-NMR and using a wax-type column with GC-MS allowed adequate identification, quantification and separation of the compounds used to mimic a reaction mixture. ¹H-NMR, despite its intrinsic advantages like time of analysis, was unable to separate peaks in actual reaction mixtures due to the multitude of products formed and significant overlaps of their peaks. GC-MS on the other hand was capable of this and was set to be the primary tool for quantification of products in reaction mixtures, despite a much longer analysis time.

Furthermore, preliminary oxidation tests were conducted to study the autoxidation of *n*-decane. This determined a starting point for oxidation for a catalyst as no/minor conversion was seen < 120 °C under pressurised systems and < 130 °C under atmospheric conditions.

Finally, the results pave insight into how the autoxidation of *n*-decane behaves and thus conversion and selectivity can be compared to data at temperature ranges where catalysts will be used (section 4.2).

To further our understanding of autoxidation phenomena – kinetic experiments would be conducted to monitor the conversion and selectivity of alkane oxidation as a function of time and determine if there is a potential induction period. Additionally, radical scavenger experiments would be conducted to ensure the presence of radicals during specific autoxidation steps.

3.5. References

- 1 J. A. Labinger and J. E. Bercaw, *Nature*, 2002, **417**, 507–514.
- 2 K. Daasbjerg, *Acta Chem. Scand.*, 1995, **49**, 878–887.
- 3 A. E. Shilov and G. B. Shul'pin, *Chem. Rev.*, 1997, **97**, 2879–2932.
- 4 T. P. Silverstein and S. T. Heller, *J. Chem. Educ.*, 2017, **94**, 690–695.
- 5 L. Yu-Ran, *Comprehensive Handbook of Chemical Bond Energies*, CRC Press, Boca Raton, 1st edn., 2007.
- 6 X. Liu, Y. Ryabenkova and M. Conte, *Phys. Chem. Chem. Phys.*, 2015, **17**, 715–731.
- 7 J. B. Van Beilen and E. G. Funhoff, *Curr. Opin. Biotechnol.*, 2005, **16**, 308–314.
- 8 Q. H. Zhang, W. P. Deng and Y. Wang, *Chem. Commun.*, 2011, **47**, 9275–9292.
- 9 A. Sen, *Acc. Chem. Res.*, 1998, **31**, 550–557.
- 10 B. R. Cook, T. J. Reinert and K. S. Suslick, *J. Am. Chem. Soc.*, 1986, **108**, 7281–7286.
- 11 J. M. Thomas, R. Raja, G. Sankar and R. G. Bell, *Nature*, 1999, **398**, 227–230.
- 12 A. E. Shilov and G. B. Shul'pin, *Russ. Chem. Rev.*, 1987, **56**, 442–464.
- 13 F. Cavani, *Catal. Today*, 2010, **157**, 8–15.
- 14 F. Garcia-Ochoa, J. Querol and A. Romero, *Ind. Eng. Chem. Res.*, 1990, **29**, 1989–1994.
- 15 F. Garcia-Ochoa, A. Romero and J. Querol, *Ind. Eng. Chem. Res.*, 1989, **28**, 43–48.
- 16 S. Blaine and P. E. Savage, *Ind. Eng. Chem. Res.*, 1991, **30**, 2185–2191.
- 17 L. Chen, K. Zhu, L. H. Bi, A. Suchopar, M. Reicke, G. Mathys, H. Jaensch, U. Kortz and R. M. Richards, *Inorg. Chem.*, 2007, **46**, 8457–8459.

- 18 B. Modén, B. Z. Zhan, J. Dakka, J. G. Santiesteban and E. Iglesia, *J. Phys. Chem. C*, 2007, **111**, 1402–1411.
- 19 M. W. Peters, P. Meinhold, A. Glieder and F. H. Arnold, *J. Am. Chem. Soc.*, 2003, **125**, 13442–13450.
- 20 H. Pobiner, *Anal. Chem.*, 1961, **33**, 1423–1426.
- 21 M. A. Farajzadeh, N. Nouri and P. Khorram, *TrAC Trends Anal. Chem.*, 2014, **55**, 14–23.
- 22 B. P. C. Hereijgers and B. M. Weckhuysen, *J. Catal.*, 2010, **270**, 16–25.
- 23 L. X. Xu, C. H. He, M. Q. Zhu, K. J. Wu and Y. L. Lai, *Catal. Letters*, 2007, **118**, 248–253.
- 24 J. D. Chen and R. A. Sheldon, *J. Catal.*, 1995, **153**, 1–8.
- 25 P. T. Wierzchowski and L. Wiesław Zatorski, *Chromatographia*, 2000, **51**, 83–86.
- 26 K. Noweck and W. Grafahrend, in *Ullmann's Encyclopedia of Industrial Chemistry*, Wiley-VCH Verlag GmbH & Co. KGaA, Weinheim, 2012, pp. 117–141.
- 27 C. A. Wilde, Y. Ryabenkova, I. M. Firth, L. Pratt, J. Railton, M. Bravo-Sanchez, N. Sano, P. J. Cumpson, P. D. Coates, X. Liu and M. Conte, *Appl. Catal. A Gen.*, 2019, **570**, 271–282.
- 28 M. Hartmann and S. Ernst, *Angew. Chemie Int. Ed.*, 2000, **39**, 888–890.
- 29 H. X. Yuan, Q. H. Xia, H. J. Zhan, X. H. Lu and K. X. Su, *Appl. Catal. A Gen.*, 2006, **304**, 178–184.
- 30 J. Tong, Z. Li and C. Xia, *J. Mol. Catal. A Chem.*, 2005, **231**, 197–203.
- 31 J. Tong, L. Bo, Z. Li, Z. Lei and C. Xia, *J. Mol. Catal. A Chem.*, 2009, **307**, 58–63.
- 32 R. Lloyd, R. L. Jenkins, M. Piccinini, Q. He, C. J. Kiely, A. F. Carley, S. E. Golunski,

- D. Bethell, J. K. Bartley and G. J. Hutchings, *J. Catal.*, 2011, **283**, 161–167.
- 33 K. Buhr, S. Van Ruth and C. Delahunty, *Int. J. Mass Spectrom.*, 2002, **221**, 1–7.
- 34 T. C. S. Kanya, L. J. Rao and M. C. S. Sastry, *Food Chem.*, 2007, **101**, 1552–1557.
- 35 C. T. Peng, *J. Chromatogr. A*, 2000, **903**, 117–143.
- 36 C. Ragonese, D. Sciarrone, P. Q. Tranchida, P. Dugo, G. Dugo and L. Mondello, *Anal. Chem.*, 2011, **83**, 7947–7954.
- 37 X. R. Wang, J. Cassells and A. Z. Berna, *J. Chromatogr. B Anal. Technol. Biomed. Life Sci.*, 2018, **1097–1098**, 27–34.
- 38 C. Osorio, M. Alarcon, C. Moreno, A. Bonilla, J. Barrios, C. Garzon and C. Duque, *J. Agric. Food Chem.*, 2006, **54**, 509–516.
- 39 M. A. Sumathykutty, J. Madhusudana Rao, K. P. Padmakumari and C. S. Narayanan, *Flavour Fragr. J.*, 1999, **14**, 279–282.
- 40 I. Hermans, E. S. Spier, U. Neuenschwander, N. Turrà and A. Baiker, *Top. Catal.*, 2009, **52**, 1162–1174.
- 41 K. Fischer and M. Wilken, *J. Chem. Thermodyn.*, 2001, **33**, 1285–1308.
- 42 É. Danóczy, G. Vasvári and D. Gál, *J. Phys. Chem.*, 1972, **76**, 2785–2793.
- 43 B. Modén, B. Z. Zhan, J. Dakka, J. G. Santiesteban and E. Iglesia, *J. Catal.*, 2006, **239**, 390–401.
- 44 G. Just, W. Pritzkow, M. Rudolf, T. D. Tien and V. Voerckel, *J. für Prakt. Chemie*, 1986, **328**, 469–474.
- 45 J. A. Labinger, *J. Mol. Catal. A Chem.*, 2004, **220**, 27–35.

CHAPTER 4: Alkane oxidation with metal doped metal oxides and metal doped zeolites

Contents

CHAPTER 4: Alkane oxidation with metal doped metal oxides and metal doped zeolites .	155
Abbreviations	156
4.1. Introduction	157
4.2. Decane oxidation	158
4.2.1. Determination and optimization of oxidation conditions – avoiding autoxidation..	159
4.2.1.1. Effect of changes of temperature.....	159
4.2.1.2. Effect of changes of pressure	163
4.2.1.3. Effects of changes of stirrer speed	167
4.2.1.4. Changes of M:S (metal to substrate ratios) 1:2000 and 1:1000	170
4.2.1.5. ICP-OES analysis for the determination of leaching	173
4.2.1.6. Changes of metal loading wt%	174
4.2.2. Catalytic activity amongst different supports	176
4.2.3. Metal supported bulk TiO ₂	180
4.2.3.1. Wet impregnation metal-doped bulk TiO ₂	180
4.2.3.2. The effect of catalyst reduction on activity	185
4.2.4. Alternative supports for <i>n</i> -decane oxidation	189
4.2.4.1. Zeolite based catalysts	189
4.2.4.2. Niobium oxide-based catalysts	198
4.3. Cyclooctane oxidation.....	203
4.3.1. Cyclooctane oxidation with iron-based materials.....	204
4.3.2. Cyclooctane oxidation with noble metal-based materials	209
4.4. Conclusion and future work.....	211
4.5. References	214

Abbreviations

BDE – Bond Dissociation Energy

BET – Brunauer-Emmet-Teller

FTIR-ATR – Fourier-Transform Infrared – Attenuated Total Reflectance

ICP-OES – Inductively Coupled Plasma – Optical Emission Spectroscopy

KA Oil – Ketone-Alcohol oil

MCM-41 – Mobil Crystalline Material #41

M:S – Metal to substrate ratio

NMR – Nuclear Magnetic Resonance

PO_2 – Pressure Gauge O_2

SBA-15 – Santa Barbara Amorphous Type Material #15

TGA – Thermogravimetric Analysis

TEM – Transmission Electron Microscopy

TMS-1 – Transition Metal Oxide Molecular Sieve #1

WI – Wetness Impregnation

XRPD – X-ray Powder Diffraction

XPS – X-ray Photoelectric Spectroscopy

ZSM-5 – Zeolite Socony Mobil #5

4.1. Introduction

Catalyst design is a highly complex and challenging process. The active metal,¹⁻⁴ the support^{5,6} and how the metal is deposited onto the support⁷ are some of the common factors in catalyst synthesis, to name a few.⁸ Additionally, for porous materials, their pore diameter is paramount to this research. The concept of only a specific region of a molecule - in our case, a terminal methyl group of a long chain hydrocarbon - reaching an active site is dependent on the size of the pores and substrate.⁹ The identification and optimisation of all these parameters was a necessity to create an active and selective catalyst.

Two studies were conducted in parallel during this research: (i) (section 4.2) synthesis of bulk materials, where in this context bulk stands for non-porous (neither micro nor meso) metal oxides, and (ii) (sections 5.2 – 5.4 and 6.2 – 6.7) development or use of their micro- mesoporous counterparts. This approach was done in order to use materials in part (i) as a benchmark and comparison for part (ii), and to determine if the use and development of micro or meso porosity actually leads to an advantage, with respect to the chemistry of more established bulk metal oxides, either metal doped or not. This developed an understanding of how metal nanoparticles behave catalytically when different supports (e.g. TiO₂, Nb₂O₅ and zeolites) and post synthesis modifications (calcination and reduction) are used.

Additionally, this approach served for the identification and development of optimal conditions for *n*-decane oxidation with a catalyst. These were determined by using an active catalyst and systematically modifying parameters potentially affecting the catalytic activity like: temperature, pressure and stirring speed, until the highest conversion is found. Ultimately, the microporous materials from sections 5 and 6 would then be tested under these conditions and compared to the bulk materials. To put into context, a metal found to be active on bulk titanium oxide would be chosen as a contender to be included into the framework of microporous titanium oxide (and potentially niobium analogues). It should be noted, data from section 3.3 will be considered to ensure any catalytic activity observed is indeed due to the presence of a catalyst and not from background autoxidation.

Furthermore, commercial analogues of microporous materials will be tested here. Non-doped Ti-TMS1 (microporous titanium oxide) will be used to support metal nanoparticles added post-synthesis. Additionally, commercial zeolites will be tested as these are the biggest rival to microporous metal oxides. In summary, three types of catalysts will be developed i) metal nanoparticles on a bulk support, ii) an intra-framework active metal in a porous framework and iii) metal nanoparticles (extra framework species) on a porous framework.

Applying these catalysts to *n*-decane oxidation would allow us to determine the following; i) does the presence of pores increase regioselectivity? ii) does an active metal part of a framework give an advantage over doped commercial materials?

Ultimately, the goal of this chapter is to understand what variables lead to a catalyst most suited to selective oxidation.

4.2. Decane oxidation

Within the literature there are many examples of metal catalysed alkane oxidation reactions. For example iron,¹⁰ manganese,⁷ palladium¹¹ and gold⁵ have all been applied to alkane oxidation. Vanadium oxide is also prevalent in the literature but is primarily used for oxidative dehydrogenation and thus forms alkenes, which are not desired for our purposes.⁶ This gave scope for which metals should be prioritised.

Preliminary tests showed that iron on bulk titanium oxide (p-25), was catalytically active towards the oxidation of *n*-decane. p-25 is an anatase/rutile mix commonly used as a standard support for a range of applications.¹² Fe/TiO₂ was chosen to determine what are the most ideal conditions for *n*-decane oxidation. Therefore, reaction parameters were varied, and conversion and selectivity were determined. From this an optimal set of conditions would be developed and then kept unchanged for the numerous other catalysts to be tested and compared (i.e. both bulk and microporous materials).

4.2.1. Determination and optimization of oxidation conditions – avoiding autoxidation

In order to ensure any catalyst is indeed active and is at its most active, parameters were varied to ensure the highest possible conversion is achieved whilst also observing the effect of these parameters on the selectivity to alcohols, the desired product of this work. Temperature is possibly one of the most significant parameters to catalysis, especially within the context of autoxidation. This is important as it has been shown that within the literature some data initially thought to be catalyst centred oxidation was in fact autoxidation.¹³ Varying pressure, specifically O₂ pressure (PO_2) was also to be varied. This is important as this can allow understanding of the type of mechanism (i.e. Eley-Rideal or Langmuir-Hinshelwood) that is occurring on the surface of the catalyst. By understanding which mechanism is occurring and varying pressure, maximum conversion can be achieved.^{14,15} Furthermore to determine if the reaction is under a kinetic or a diffusion regime, stirrer speed and metal to substrate ratio were also varied. For significant comparison to be drawn between catalysts the system must be under a kinetic regime otherwise the limiting factor of the catalysis is diffusion of the substrate to the surface of the catalyst from mass transfer limitations – which may also, in turn, affect selectivity of a reaction.^{16,17} Once the ideal parameters have been determined these will be fixed and other factors such as wt% of metal; type of metal; type of support and porosity of support will be varied.

4.2.1.1. Effect of changes of temperature

Oxidation of an alkane under these solvent-free ‘mild conditions’ is not a trivial task.¹⁸ In both atmospheric and pressurised systems, Fe/TiO₂ was found to catalyse the oxidation of *n*-decane. Preliminary data showed that Fe/TiO₂ under pressurised oxygen was found to yield higher conversion (~ 5%) of *n*-decane in comparison to atmospheric conditions at lower temperatures (~ 2%). Therefore, catalytic testing under pressurised oxygen was a fixed parameter for this study.

A temperature range from 110 °C to 140 °C was explored. It can be seen that at 115 °C Fe/TiO₂ is catalytically active, as conversion of *n*-decane was observed. As a proof of concept, conversion was sought with bulk catalysts so that changes could be directly monitored from the parameters adjusted. Figure 4.2.1.1.1 shows the trend of temperature versus conversion with and without Fe/TiO₂ present. At 115 °C significant conversion (>2%) is observed with Fe/TiO₂, whereas when no catalyst is used no conversion occurs.

However, at higher temperatures the conversion data overlap where a catalyst is and is not present. The data follows a sigmoidal trend where a rapid increase in conversion follows a low gradient, commonly observed in oxidation reactions.¹⁹⁻²¹ This is because temperature is clearly a limiting factor < 120 °C, whereby >130 °C another limitation starts to hold back conversion.

By 120 °C the autoxidation has almost identical conversion and selectivity to when Fe/TiO₂ is used. Therefore, this means autoxidation is the dominating mechanism and the presence of Fe/TiO₂ does not affect the reaction under these conditions. Below 115 °C there is no conversion from either the autoxidation or Fe/TiO₂. This gives a very narrow temperature range of ~ 5°C where the reaction is catalysed and then there is either no activity at all or the reaction is taken over by autoxidation. Nevertheless, after repeating tests at 115 °C several times (>10 times over 3 different batches), it was found that autoxidation never occurs at this temperature whereas Fe/TiO₂ always yields conversion. Given these results we therefore considered Fe/TiO₂ a suitable catalyst for the identification of optimal reaction conditions and for further development of an improved catalytic system.

Furthermore, the goal of this project was the selective oxidation of alkanes to alcohols. The reaction mixture plummets in alcohol selectivity >120 °C, with increasing favour towards acids and other products and little change in ketone selectivity. This shows that the acids and other products are likely, at least in part, to come from alcohol oxidation. Although this is primarily due to autoxidation reactions, it is also crucial for catalytic testing. These data show that at

temperatures >120 °C alcohol decomposition is likely to occur, and thus are unsuitable for selective catalysis.

Therefore, 115 °C was fixed and chosen as a reference temperature. Other parameters were thus varied in order to optimise conversion.

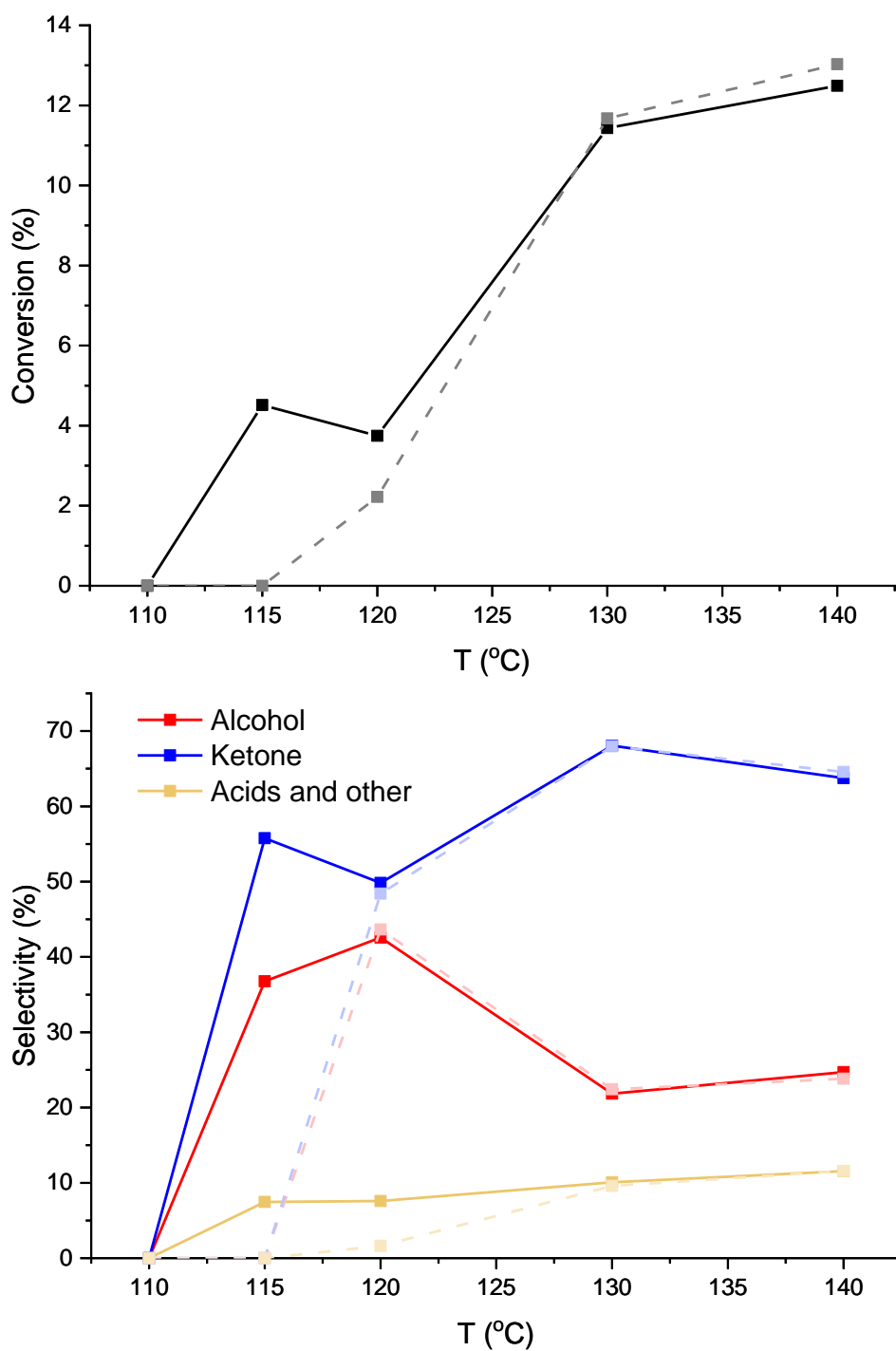


Figure 4.2.1.1.1: Top: Conversion data; Bottom: Selectivity data for *n*-decane oxidation with Fe/TiO₂ (1 wt%, bulk, wetness impregnation – WI), with varying temperature. Solid bold lines are where Fe/TiO₂ was used, dashed faded lines are blank reactions to serve as a background. *n*-decane (3 mL), Fe/TiO₂ (1 wt%, bulk, WI), M:S (metal to substrate ratio) = 1:2000, $PO_2 = 2$ bar, $t = 24$ h.

4.2.1.2. Effect of changes of pressure

As expected, it was found that changing from atmospheric to pressurised systems influences conversion in blank tests (section 3.3). Therefore, this gave scope to varying the O₂ pressure in order to maximise conversion of *n*-decane.

However, the effect of changing this parameter is not as trivial as it could sound. In theory, increasing the O₂ pressure would increase conversion until the amount of oxygen present in the reaction mixture is no longer a limiting factor.²² On the other hand if the reaction follows, for example, a Langmuir-Hinshelwood mechanism²³ or any mechanism with competitive adsorption between two reagents, we would expect that beyond a certain limit there is no gain by increasing the pressure of O₂. In fact, we would actually expect to observe a decrease in rate (and in turn conversion) as O₂ would occupy all of the catalyst's surface at the expense of the hydrocarbon.¹⁴ Catalytic tests were conducted where the temperature was fixed (115 °C) but the pressure was varied (both in pressurised air and O₂ systems) in order to determine an optimal oxygen pressure, the results are shown in figures 4.2.1.2.1 and 4.2.1.2.2.

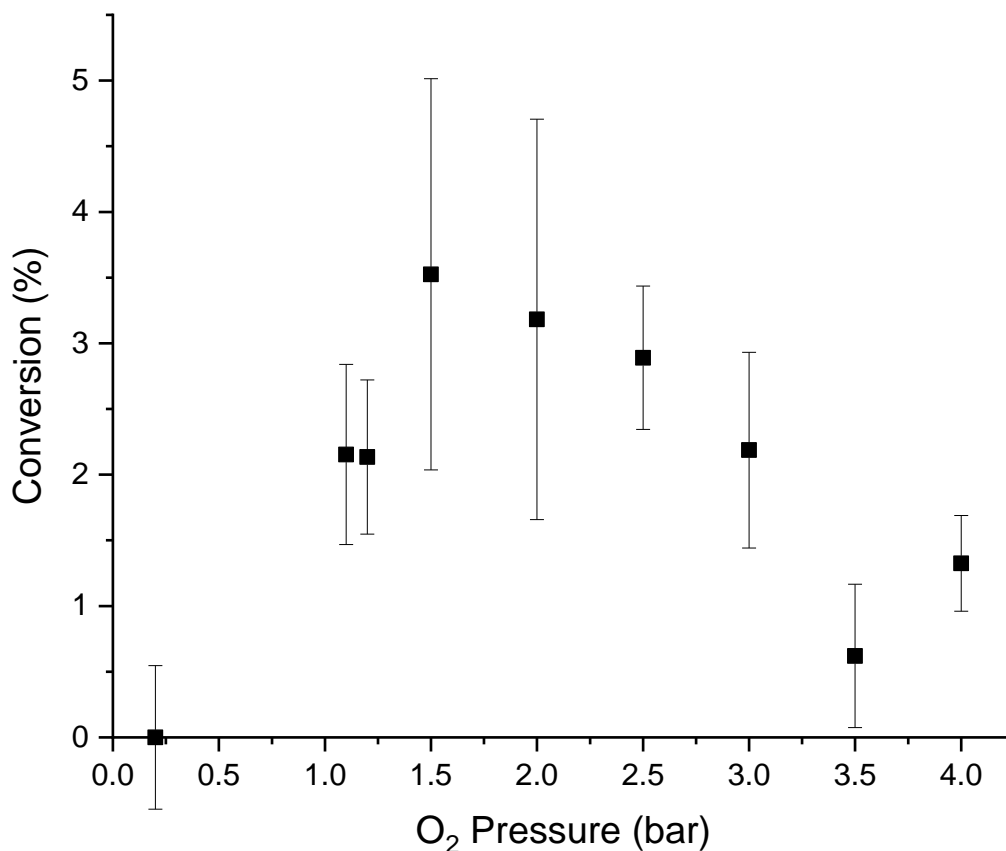


Figure 4.2.1.2.1: Conversion data of *n*-decane with Fe/TiO₂ (1 wt%, bulk, WI), with varying pressure. *n*-decane (3 mL), Fe/TiO₂ (1 wt%, bulk, WI), M:S = 1:2000, T = 115 °C, t = 24 h. Pressure is corresponding O₂ pressure. X-axis points 1.1 and 1.5 bar correspond to compressed air $P = 0.5$ and 1 bar respectively. Point 0.2 bar is atmospheric oxygen (i.e. under open reflux conditions) All other x-axis values are pressurised O₂ only.

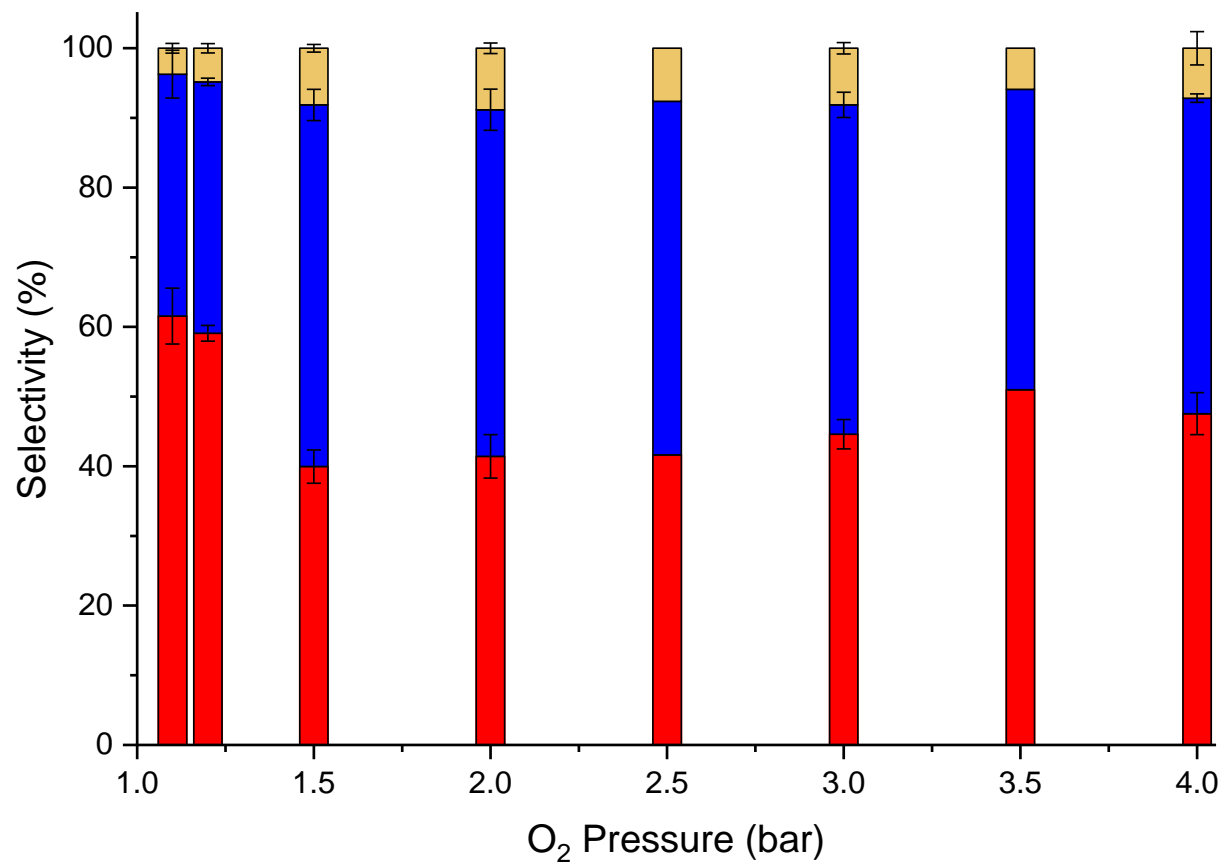


Figure 4.2.1.2.2: Selectivity data of *n*-decane with Fe/TiO₂ (1 wt%, bulk, WI), with varying pressure. *n*-decane (3 mL), Fe/TiO₂ (1 wt%, bulk, WI), M:S = 1:2000, T = 115 °C, t = 24 h. Pressure is corresponding O₂ pressure. Points 1.1 and 1.5 bar correspond to compressed air *P* = 0.5 and 1 bar respectively. All other x-axis values are pressurised O₂ only. (■) Alcohol, (■) Ketone, (■) Acids and other.

And in fact, a volcano-type plot typical of competitive adsorption was observed. Initially there is low conversion for low pressures of O₂, and as expected, as O₂ pressure increases so does the conversion, reaching a maximum between 1.5 and 2 bar ($PO_2 = 0.5$ and 1 bar respectively – i.e. pressure set on O₂ cylinder as opposed to local O₂ pressure). However, beyond 2 bar O₂ a decrease in conversion is observed. This would suggest a competitive adsorption process with too much oxygen causes, practically, an inhibition effect on the catalysts so that *n*-decane is incapable of being activated (a similar phenomenon is observed in tungsten carbides),²⁴ or the oxygen itself is hindering the reactivity of any radicals.²⁵ For completeness, other reasons could also include oxygen effecting the Fe surface, such as surface restructuring.²⁶

It should be noted that although oxygen pressure affects conversion, within pressurised oxygen systems selectivity is essentially unchanged. This means that the increased pressure of oxygen influences the number of available active sites, however, their nature remains unchanged. This further supports the hypothesis of competition between the alkane and oxygen during catalysis, as opposed to any fouling of the active sites.

On the other hand, when the oxidation is carried out using air, alcohols are selectively favoured compared to reactions under pure O₂. However, as technically selectivity can only be compared when tests have statistically similar conversion, the PO_2 set as 3 bar O₂ and 1.1 bar and 1.2 bar pressurised air can be compared. This enhanced selectivity to the alcohol could be due to less over oxidation occurring as less O₂ is present.^{27,28} Although alcohols were desired for this project, we nevertheless preferred to carry on with low pressure of pure O₂ in order to increase the conversion and in turn to obtain an appreciable yield.

Ultimately the results show oxygen pressures of 1.5 and 2 bar yield the highest conversion. Due to the ease of setting a higher pressure with our equipment, and in turn a higher stability of our reactor for long periods of time, 2 bar O₂ (PO_2 1 bar) was chosen as the optimum pressure for our tests.

4.2.1.3. Effects of changes of stirrer speed

Stirrer speed is an essential parameter during liquid phase catalysis.²⁹ This is because a uniform distribution of a solid catalyst within the reaction mixture is essential so that the catalyst and substrate are not limited by the slow mechanical motion of the mixture, which will lead to lower mass transfer.¹⁶ Stirring rates below 500 rpm were not creating a slurry, and above 900 rpm stirrer bars would not spin correctly. Therefore, the effect of 500 rpm to 900 rpm stirrer speeds were studied. As a control, 0 rpm was also tested.

From figure 4.2.1.3.1 it can be seen the highest conversion was obtained between 500 rpm and 700 rpm. Stirring at 900 rpm has significant error as at this speed the catalyst started to stick to the sides of the reaction vessel, and thus reaction uniformity is not consistent.

At 0 rpm conversion has still occurred, however, the absence of stirring is clearly a limiting factor and indicates that mass transfer limitation is operating. Interestingly, the selectivity at 0 rpm also changes (almost 1:1 ketone to alcohol, K:A, versus a typical ~2:1, figure 4.2.1.3.2). This suggests that selectivity is affected by diffusion in our system, commonly observed amongst other reactions.³⁰

Ultimately, neither conversion nor selectivity differed when using 500 rpm or 700 rpm. This indicated a true maximum had been reached and thus these conditions were chosen as optimal conditions.

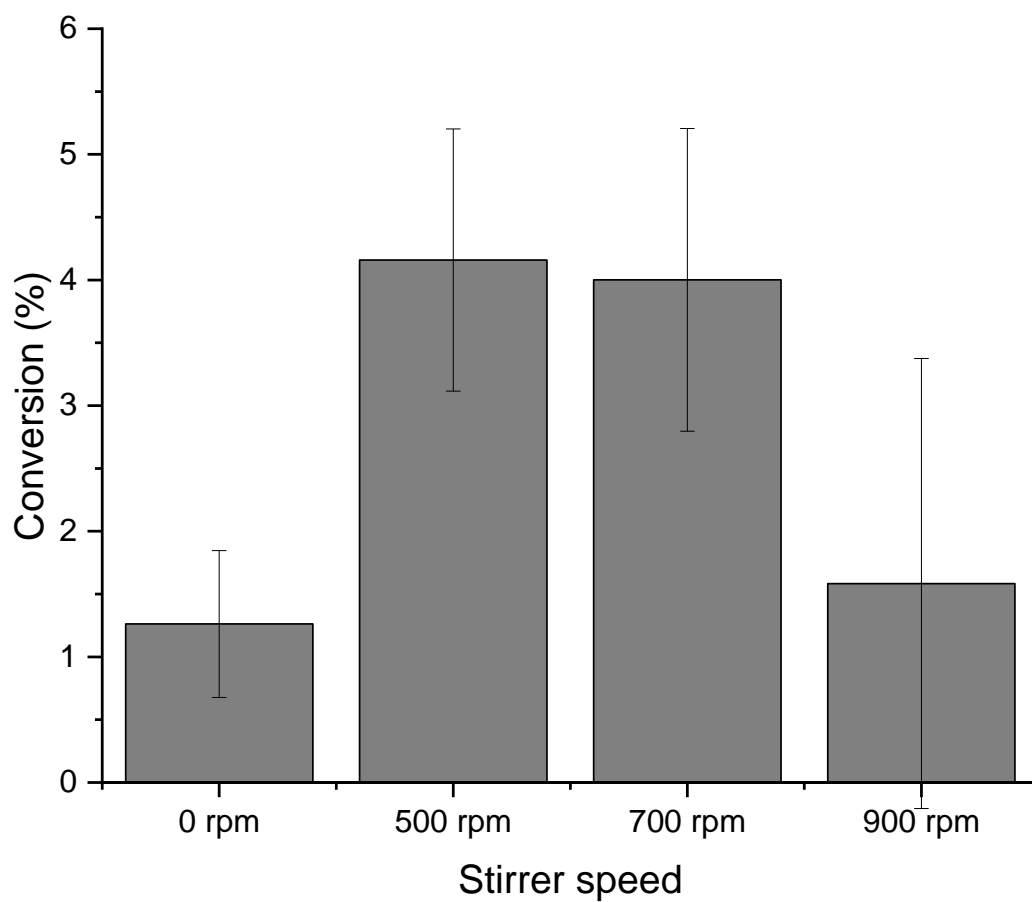


Figure 4.2.1.3.1: Conversion data of *n*-decane with Fe/TiO₂ (1 wt%, bulk, WI), with varying stirrer speed. *n*-decane (3 mL), Fe/TiO₂ (1 wt%, bulk, WI), M:S = 1:2000, T = 115 °C, P_{O₂} = 1 bar, t = 24 h.

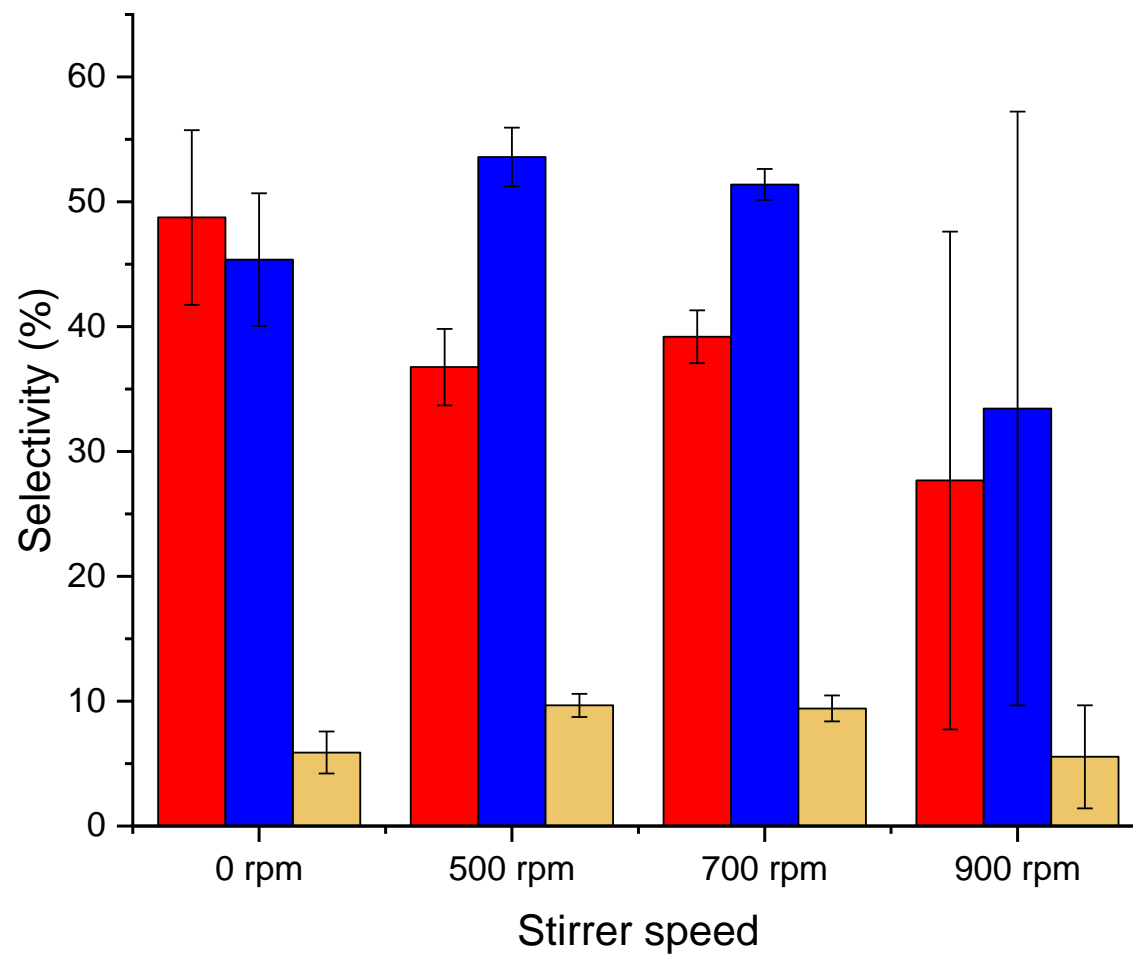


Figure 4.2.1.3.2: Selectivity data of *n*-decane with Fe/TiO₂ (1 wt%, bulk, WI), with varying stirrer speed. *n*-decane (3 mL), Fe/TiO₂ (1 wt%, bulk, WI), M:S = 1:1000, T = 115 °C, PO₂ = 1 bar, t = 24 h. (■) Alcohol, (■) Ketone, (■) Acids and other.

4.2.1.4. Changes of M:S (metal to substrate ratios) 1:2000 and 1:1000

Doubling the metal to substrate ratio does not necessarily double the conversion.²⁹ This is because multiple parameters (e.g. solubility of products,¹⁷ effect of by-products,³¹ etc.) could be affecting the complex mechanisms occurring during oxidation.^{17,31,32} Varying metal to substrate ratio can allow determination of i) mass transfer limitations occurring or ii) what is the minimum amount of catalyst that can be used. A metal to substrate ratio of 1:1000 was trialled and gave a slightly lower standard deviation. It was thought that this could affect the reaction in two ways: i) If metal to substrate ratio is a limiting factor, then conversion would increase and ii) if the catalyst distribution uniformity within the reaction mixture is improved, then the standard deviation would decrease. Metal to substrate ratios higher (with respect to amount of catalyst used) than 1:1000 were not trialled as a low amount of catalyst was desired from an economical perspective. Furthermore, a M:S of 1:500 led to a thick slurry which made practical separation more difficult.

It can be seen from figure 4.2.1.4.1 that M:S 1:1000 shows a higher conversion and slightly lower standard error. Therefore, an M:S of 1:2000 was a limiting factor and was also potentially leading to a higher standard deviation. The increase in conversion is likely from more active sites present as more catalyst is present and is a useful indicator that we are not carrying out reactions under a diffusion limited regime, as conversion may not increase in this regime. This in turn ensures that we can compare our catalysts under a kinetic regime of reactions over their surfaces.³⁰ In view of these factors we selected the metal to substrate ratio of 1:1000 as a fixed condition for comparison amongst catalysts.

It should be noted that selectivity does not change with metal to substrate ratio. Therefore, the additional active sites only effect conversion, and not selectivity. This suggests that the reaction is not limited by oxygen transfer into the reaction mixture. This further complements the data from varying the pressure of oxygen, and thus optimisation of this parameter was indeed at its maximum.

Within the parameters of the equipment used, optimum conditions for *n*-decane oxidation via Fe/TiO₂ were determined. The conversion and selectivity obtained from Fe/TiO₂ were set as a benchmark for all other catalysts to be tested. From here the goal was to find the most active metals (from high conversions/ selectivity) and thus determine which candidates were best to be incorporated into the proposed microporous titanium oxide (see section 5.2.4).

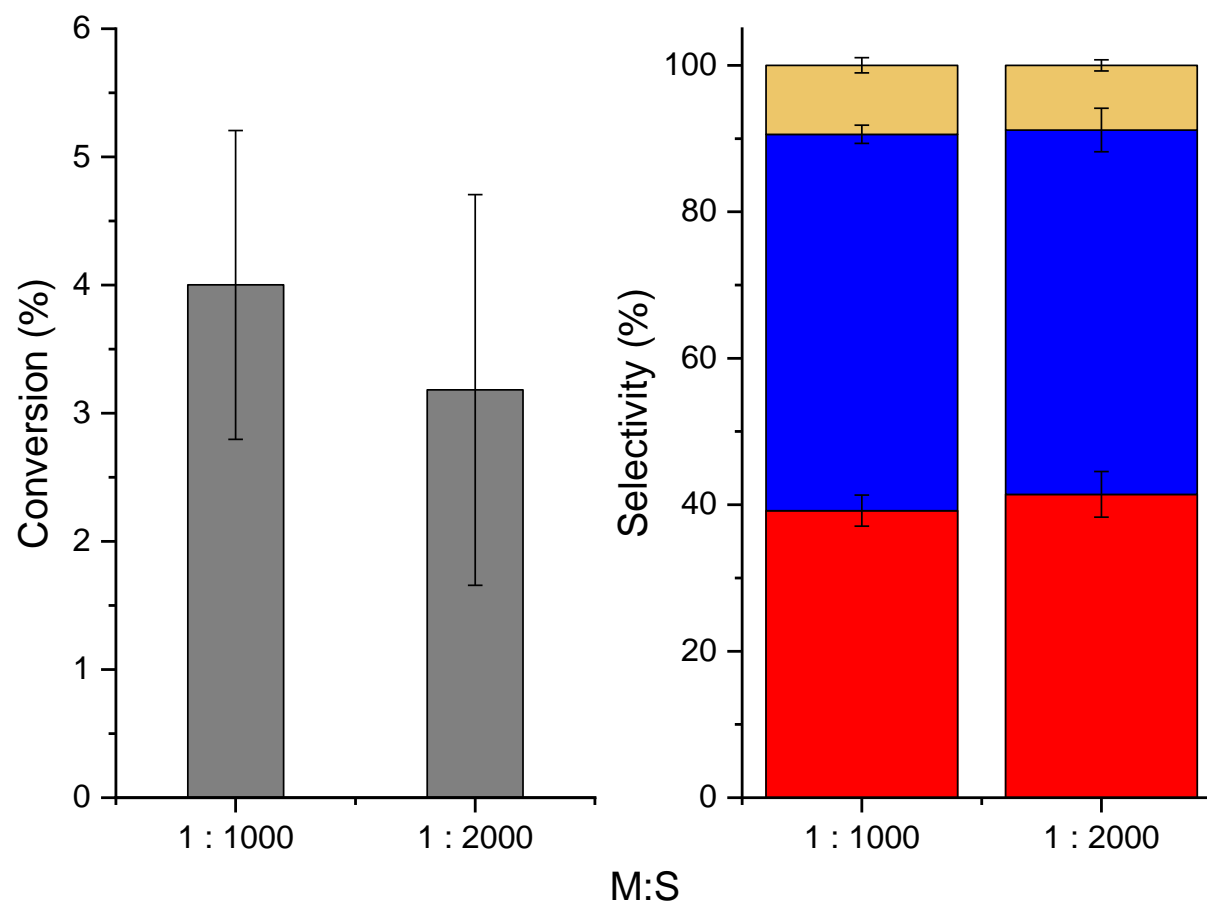


Figure 4.2.1.4.1: Conversion and selectivity data of *n*-decane with Fe/TiO₂ (1 wt%, bulk, WI), with different metal to substrate ratios. *n*-decane (3 mL), Fe/TiO₂ (1 wt%, bulk, WI), T = 115 °C, PO₂ = 1 bar, t = 24 h. (■) Conversion, (■) Alcohol, (■) Ketone, (■) Acids and other.

4.2.1.5. ICP-OES analysis for the determination of leaching

It is crucial that loaded metals (i.e. iron in Fe/TiO₂, bulk, WI) do not leach during catalytic conditions. This is important for heterogenous catalysts as their ease of reusability is their main advantage. Therefore, batch to batch, a loss of activity will be observed if significant leaching occurs.³³ Additionally, there is the potential of the leached metal to be active in solution.³⁴ This would lead to a degree of homogenous catalysis to occur (this has caused debates on mechanisms amongst palladium catalysts).³⁵ As the goal of this project is to produce a porous heterogenous catalyst with an active site geometrically confined, it follows non-confined leachates freely catalysing a reaction are highly undesirable.

ICP-OES (Inductively coupled plasma – optical emission spectroscopy) data was collected of the reaction mixture after a standard catalytic test (e.g. Fe/TiO₂, M:S = 1:1000, T = 115 °C, PO₂ = 1 bar, reaction time = 24 h). Fortunately, no iron is detected in the reaction mixture (< 0.01% relative to the original Fe amount in the catalyst). This means that all the iron has remained present on the surface, and thus, the catalytic activity is heterogenous in nature. Interestingly, relatively high amounts of sodium (1.2 μmol), silicon (45 nmol) and boron (130 nmol) were detected (table 4.2.1.5.1). Silicon and boron are suspected to come from the glassware used (borosilicate) for our reaction vessel.³⁶ Sodium is a ubiquitous element,³⁷ therefore its high abundance in the ICP could occur from the handling of the specimen. However, these elements are in low amounts compared to that of the original iron content and thus were disregarded.

Table 4.2.1.5.1: ICP-OES data from *n*-decane oxidation with Fe/TiO₂. Sample collected via solvent exchange with water. *n*-decane (3 mL), *n*-decane (3 mL), Fe/TiO₂ (1 wt%, bulk, WI) M:S = 1:1000, T = 115 °C, PO₂ = 1 bar, t = 24 h.

Element	Al	B	Na	Nb	Ba	Ca	Si	K
detected								
Amount (nmol)	4.9E+01	1.3E+02	1.2E+03	0.0E+00	6.9E+00	5.2E+01	4.5E+01	2.0E+01

4.2.1.6. Changes of metal loading wt%

Varying metal wt% is a crucial factor in catalyst design.³⁸ For the purposes of this project, metal nanoparticles were desired to be loaded onto a support (if the support is a bulk metal oxide/ commercially available porous support), or for the active metal to be part of a framework (for porous metal oxides). The corresponding wt% of the metal can determine how close the nanoparticles are to each one another on the support.³⁹ If an excessive amount of metal is loaded then space between nanoparticles will be less, which will eventually form a bulk monolayer.⁴⁰ A monolayer may behave differently to its nanoparticle counterpart, and thus lead to an inactive catalyst, or lead to a catalyst capable of different activity.⁴¹ Ultimately, a lower wt% would be a desirable target so less material can be used, this is especially significant when using precious metals. Therefore, varying wt% of loaded metal was trialled for Fe/TiO₂.

Preliminary data of *n*-decane oxidation with 1, 2 and 5 wt% Fe/TiO₂ showed no difference in conversion or selectivity. However, in order to gather possible structural differences between these materials, XRPD (x-ray powder diffraction) patterns were collected and analysed. Figure 4.2.1.6.1 shows that at 5 wt% a small additional peak at 33 ° 2θ is observed compared to WI-p-25 (a WI where no dopant metal salt is added); and 1 wt% and 2 wt% Fe/TiO₂. This reflection is consistent with the (104) facet of Fe₂O₃.⁴² This detection is possible precisely because of the higher metal loading, and in turn a higher exposed fraction of metal oxide capable to generate diffraction. However, this peak was too small to estimate the particles size of Fe₂O₃ by using the Scherrer equation in a reliable manner.

While no advantages were observed for varying metal wt% the data shows that varying wt% of Fe in Fe/TiO₂ tested at this scale is not a limiting factor. In this case, by following the principle of using the lowest metal loading as possible (see precious metals), a 1 wt% catalyst was used in our study.

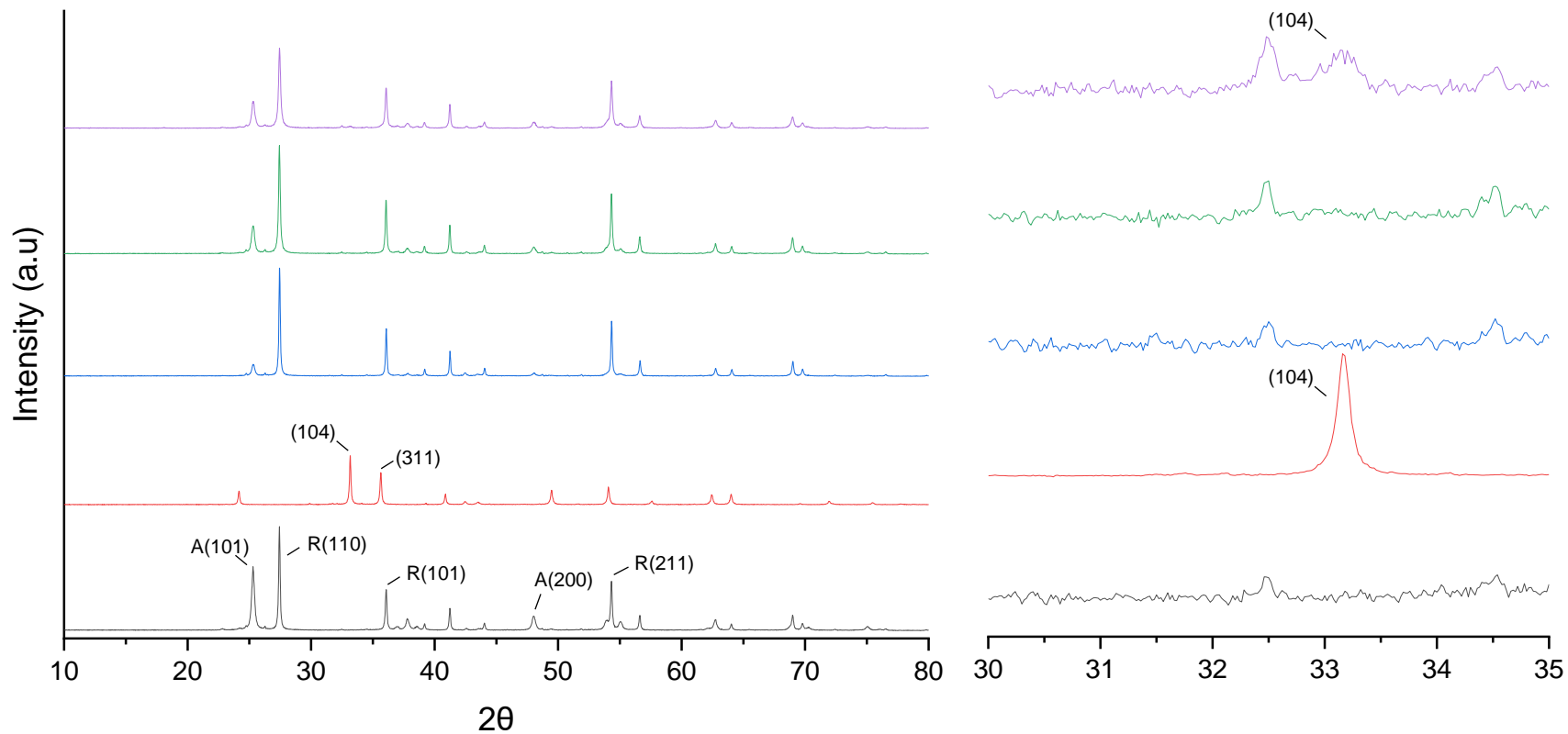


Figure 4.2.1.6.1: XRPD patterns of Fe/TiO₂ WI, 680 °C with varying Fe wt%. A magnification of a reflection consistent with Fe₂O₃ is present is included (right). Undoped TiO₂ calcined at 680 °C and commercial Fe₂O₃ are included for comparison. Undoped TiO₂ 680 °C (-), commercial Fe₂O₃ (-), Fe/TiO₂ WI 680 °C 1 wt% (-), 2 wt% (-), 5 wt% (-). The most intense peaks of the patterns are assigned from literature, where in undoped TiO₂ 'A' is Anatase and 'R' is Rutile.⁴²⁻⁴⁶

4.2.2. Catalytic activity amongst different supports

Ideally for the scope of selective oxidation a support will not be active itself during catalysis. Shape selectivity arises from the isolated nature of the dopant metal within the support,⁴⁷ therefore it is not desired for the support to provide additional unwanted catalysis. In principle if the support is active and the active site is not restricted in anyway then by-products could be formed where no shape selectivity has taken place. It is therefore essential that all catalytic activity is from the isolated metal within a porous framework in order to induce geometrical constraints capable of selectivity control.

Table 4.2.2.1 contains a range of supports and their corresponding conversion when applied to *n*-decane oxidation. Bulk TiO₂ and a commercially available Ti-TMS1 show no conversion during *n*-decane oxidation (where Fe/TiO₂, bulk, WI, showed a modest conversion). This is advantageous as it means that the catalytic activity observed when using Fe/TiO₂ is indeed due to the iron and not the TiO₂. Furthermore, alongside the ICP data from section 4.2.1.5, this concludes that the catalytic activity has occurred specifically on the iron on the titanium oxide heterogeneously (i.e. no catalysis from the support nor leached iron). Additionally, the commercial Ti-TMS1 shows no conversion. This means that the framework of porous titanium oxide is also inert towards *n*-decane oxidation under our chosen conditions.

On the other hand, the catalytic behaviour of the other supports proved interesting. Predominantly, the zeolite-based supports showed no conversion, apart from MCM-41 (commercial mesostructured silica). This is somewhat unexpected as the MCM-41 should not contain any catalytically active material. This could be due to a small amount of autoxidation occurring (however, blank tests at this temperature always showed no conversion), or an unknown metal impurity has led to minor oxidation. Perhaps most surprising is the oxidation of *n*-decane with niobium oxide (a support used within the research group for mechanistic studies on ethylbenzene oxidation). To our knowledge there are no instances where undoped niobium oxide has been applied to *n*-decane oxidation. Different manufacturer purity grades and samples from different lots were tested to determine if the presence of any undetected

impurities were causing conversion (table 4.2.2.2). As it can be seen in all instances the niobium oxide is indeed active. Furthermore, it was found to be active under atmospheric conditions at the same temperature, also yielding higher conversion (~7% versus ~2%) where no other catalysts were active. Presently these results are still being interpreted and are beyond the scope of this project. However, as doped microporous niobium oxide is proposed to be synthesised and applied to alkane oxidation, the results from the bulk material will make interesting and crucial comparisons for understanding how the alkane is oxidised (see section 4.2.4.2 for further study of bulk niobium oxide as a support and section 6.7 for data on microporous niobium oxide).

Table 4.2.2.1: A summary of results for *n*-decane oxidation with a varied selection of supports. *n*-decane (3 mL), M:S (1:1000, based on a nominal 1 wt% Fe), T = 115 °C, P_{O_2} = 1 bar, t = 24 h.

	Selectivity (%)			
	Conversion (%)	Alcohol	Ketone	Acids and other
TiO₂ (p-25, Commercial)	0	0	0	0
MCM-41 (SiO₂, Commercial)	0.7	54	38	8
MCM-41 (SiO₂/Al₂O₃, Commercial)	0	0	0	0
Ti-TMS1 (Commercial)	0	0	0	0
TiO₂ (WI)	0	0	0	0
ZSM-5 (Commercial)	0	0	0	0
Nb₂O₅ 99.99 (Commercial)	1.9	46	45	8.5
Nb₂O₅ (WI)	1.8	46	46	8.2
Nb₂O₅ (WI, reduced)	0	0	0	0
Nb₂O₅ 99.9 Batch 1 (Commercial)	3	42	50	8.5
NbO₂ (Commercial)	1.3	46	48	6.2

Table 4.2.2.2: A summary of results for *n*-decane oxidation with a varied selection of supports. *n*-decane (3 mL), M:S (1:1000, based on theoretical 1 wt% Fe), T = 115 °C, P = atmospheric (reflux), t = 24 h.

	Selectivity (%)			
	Conversion (%)	Alcohol	Ketone	Acids and other
Nb₂O₅ 99.99 (Commercial)	4.6	45	49	5.9
Nb₂O₅ 99.9 Batch 1 (Commercial)	5.6	42	52	5.9
Nb₂O₅ 99.9 Batch 2 (Commercial)	5	46	49	4.7
Nb₂O₅ (WI)	7.2	41	53	6.4
CeO₂ (Commercial)	2	43	48	9
SiO₂ (Commercial)	0	0	0	0

4.2.3. Metal supported bulk TiO₂

4.2.3.1. Wet impregnation metal-doped bulk TiO₂

Bulk TiO₂ was selected as an appropriate support for adding dopant metals. This is because bulk TiO₂ is inert with regards to *n*-decane oxidation. An array of TiO₂ catalysts were hence forth developed to determine which metals were active towards *n*-decane oxidation. This will allow prioritisation and expectations of activity to be made for dopant metals in microporous TiO₂.

Figure 4.2.3.1.1 shows the conversion data for varying metals on TiO₂, bulk metal oxides and dried metal salts. Fe/TiO₂ is the most active for all metals on TiO₂ (M/TiO₂) based catalysts. Pure iron and iron nitrate are capable of oxidising *n*-decane, however, Fe₂O₃ powder shows no conversion. This shows that the morphology of Fe₂O₃ on Fe/TiO₂ is different to that of bulk Fe₂O₃ powder. This suggests that the dopant Fe₂O₃ is indeed a nanoparticle (or nanosized) as this would explain the difference in reactivity. Furthermore, the crystallite size of bulk Fe₂O₃ powder was found to be in the range of ~52 nm, this is significantly larger than the expected ~1-10 nm of Fe₂O₃ when deposited onto a support in this manner,^{5,48-50} complementing the catalytic data.

The Fe/TiO₂ shows a significantly higher conversion to that of Fe powder and Fe(NO₃)₃. This demonstrates that it is advantageous to use a support to enhance iron's activity in order to avoid the sintering of small Fe₂O₃ particles.

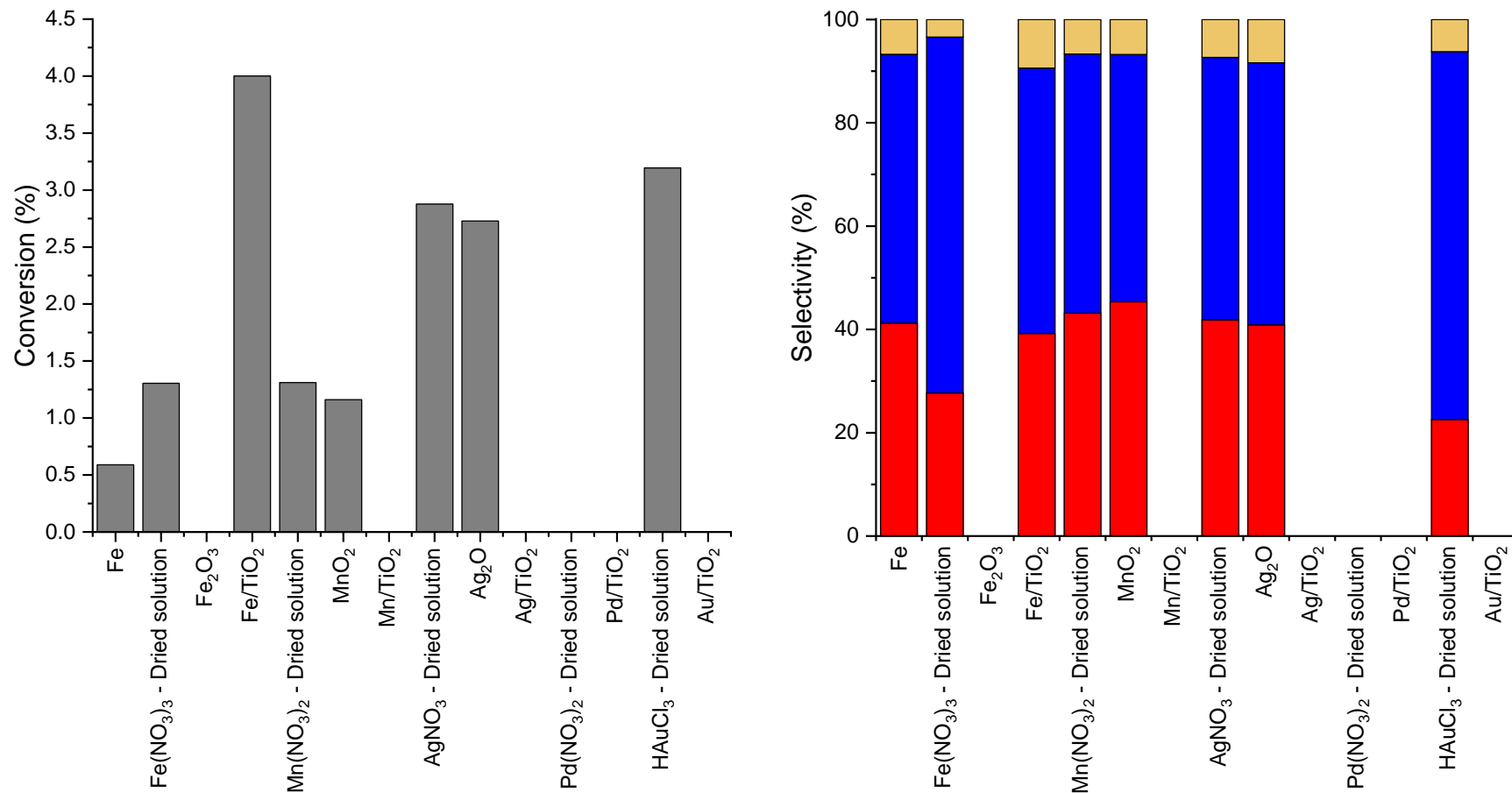


Figure 4.2.3.1.1: Conversion (left) and selectivity data (right) for *n*-decane oxidation with varying metal, oxidation state of metal, and metal loaded onto bulk TiO₂. *n*-decane (3 mL), M:S = 1:1000, T = 115 °C, PO₂ = 1 bar, t = 24 h. (■) Conversion, (■) Alcohol, (■) Ketone, (■) Acids and other. Dried metal salts prepared via drying a standard solution onto glassware prior to catalytic tests.

On the other hand, manganese shows the opposite effect to iron. Dried $\text{Mn}(\text{NO}_3)_2$ solution and bulk MnO_2 powder are active towards *n*-decane oxidation, whereas the TiO_2 supported manganese shows no conversion at all. This could be due to unfavourable metal-support interactions, the manganese being in an inactive oxidation state, or alternatively the manganese oxide nanoparticle is inactive towards *n*-decane oxidation. However, this is somewhat unexpected due to the extensive literature of manganese oxidation catalysis.^{7,10,51,52} The same effect is also seen in silver, both the dried nitrate salt (AgNO_3) and bulk oxide (Ag_2O) are capable of *n*-decane oxidation, whereas the supported metal oxide on TiO_2 is incapable of oxidation. Supported silver's lack of activity could be due to the same reason as manganese's lack of activity. Palladium shows no conversion in either the metal salt or the titanium oxide supported material. This is somewhat unexpected as palladium is a well-known oxidation catalyst.^{35,53} However, owing to the inert nature of linear alkanes,⁵⁴ they may be too difficult to oxidise under our relatively mild conditions (< 150 °C and P ca. 2 bar) and thus also explain why the palladium, silver and manganese are inactive. Lastly, gold supported on titanium oxide is also inactive. However, the dried metal salt HAuCl_4 is active yielding the second highest conversion of the series. The different activity could be due to multiple reasons explained in other examples where the salt/bulk is active, and the supported metal is not. Furthermore, the chloride ligands will influence gold's activity also.⁵⁵ However, this is not desired as only the metal/metal oxide will be present in our proposed catalysts. This is because oxidising conditions during catalysis and potential catalyst recycling at calcination temperatures may convert the gold chloride into the oxide, Au_2O_3 , and thus make it inactive.

It should be noted from the XRPD of all the M/TiO_2 (figure 4.2.3.1.2), no additional peaks were observed compared to that of undoped TiO_2 . As explained in section 4.2.1.6, this is expected as the weight loading of active metal of these catalysts is too low to detect any reflections, or the existence of particle sizes below 5 nm, or both these factors. There is a difference in the TiO_2 peaks in Mn/TiO_2 and Fe/TiO_2 compared to the other catalysts as a higher calcination temperature was used. The additional peaks indicate a shift from an anatase/rutile mix to

predominately rutile.⁵⁶ However, as preliminary tests indicated there was no difference in activity when iron supported anatase and iron supported rutile were used, this should not cause any inhibition effects.

Ultimately, iron on titanium oxide showed the highest conversion. Therefore, this will be prioritised for the incorporation into a porous framework (sections 5.2 and 6.2). However, the data from other metals is crucial to this project as it has shown how different oxidation states and how the bulk versus nanosized phases have a profound effect on *n*-decane oxidation. Although many supported metals on titanium oxide were inactive, their literature presence as oxidation catalysts still makes them potential candidates to be incorporated into a porous framework. In theory, the environment around these intra-framework metals will be different to that of the bulk,⁵⁷ and once tested will allow comparisons to be made (and determine if their incorporation into a framework is advantageous).

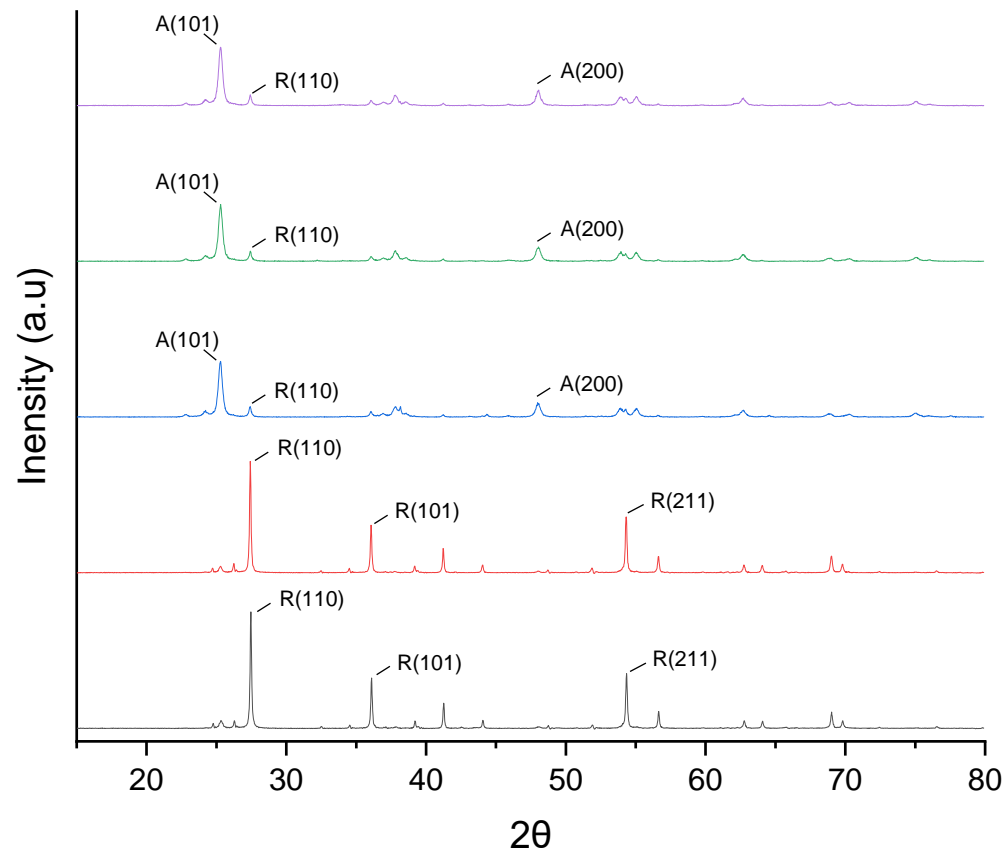


Figure 4.2.3.1.2: XRPD patterns of M/TiO₂ 1 wt%, WI with varying dopant metal. From bottom to top: Fe/TiO₂ 680 °C (-), Mn/TiO₂ 680 °C (-), Au/TiO₂ 450 °C (-), Ag/TiO₂ 180 °C (-), Pd/TiO₂ 450 °C (-). The most intense peaks of the patterns are assigned from literature, where 'A' is Anatase and 'R' is Rutile.^{44–46}

4.2.3.2. The effect of catalyst reduction on activity

Thus far all catalysts have been used directly after calcination and are likely to be in their most stable oxidation state. Therefore, to determine if conversion and/or selectivity can be boosted with varying oxidation state, all catalysts were subjected to reduction with H₂.

It was found that Ag, Au, Pd and Mn supported on TiO₂ showed no conversion after reduction. This is somewhat unexpected due to a strong literature presence of these metals as oxidation catalysts.^{53,58–61} However, this could be due to a number of reasons; the metals have inhibiting metal-surface interactions with titanium oxide (as seen in zirconia supports),⁶² or the thermal reduction treatment (180 °C - 450 °C, 2% H₂/N₂, 10 ml min⁻¹, 30 min) may have led to an increase or partial sintering of the supported metal nanoparticles, thus making them inactive.

On the other hand, iron is still active post reduction (figures 4.2.3.2.1). However, this is most likely due to the reactivity of Fe⁰ towards oxygen even at room temperature, and the sample most likely contains Fe₂O₃ domains. In fact, the conversion for 'reduced' Fe/TiO₂ is statistically the same as the corresponding as synthesised Fe/TiO₂. Furthermore, the selectivity between the two catalysts is also identical. As iron in its elemental form is readily converted to the corresponding oxide, it is likely this has occurred *in situ* and thus the active catalyst is identical in composition to that of Fe/TiO₂ post calcination.

XRPD (figures 4.2.3.2.2a and 4.2.3.2.2b) of the reduced catalysts showed no differences before and after reduction. As the metal loading is too low to observe any reflections from the doped metal, this data reveals information only about the support. Therefore, as there are no differences, this means that the support remains unchanged after reduction. Although the crystallinity of the TiO₂ support has been shown to not affect the conversion of *n*-decane, it is important to know how this behaves under calcination and reduction conditions for potential recycling tests.

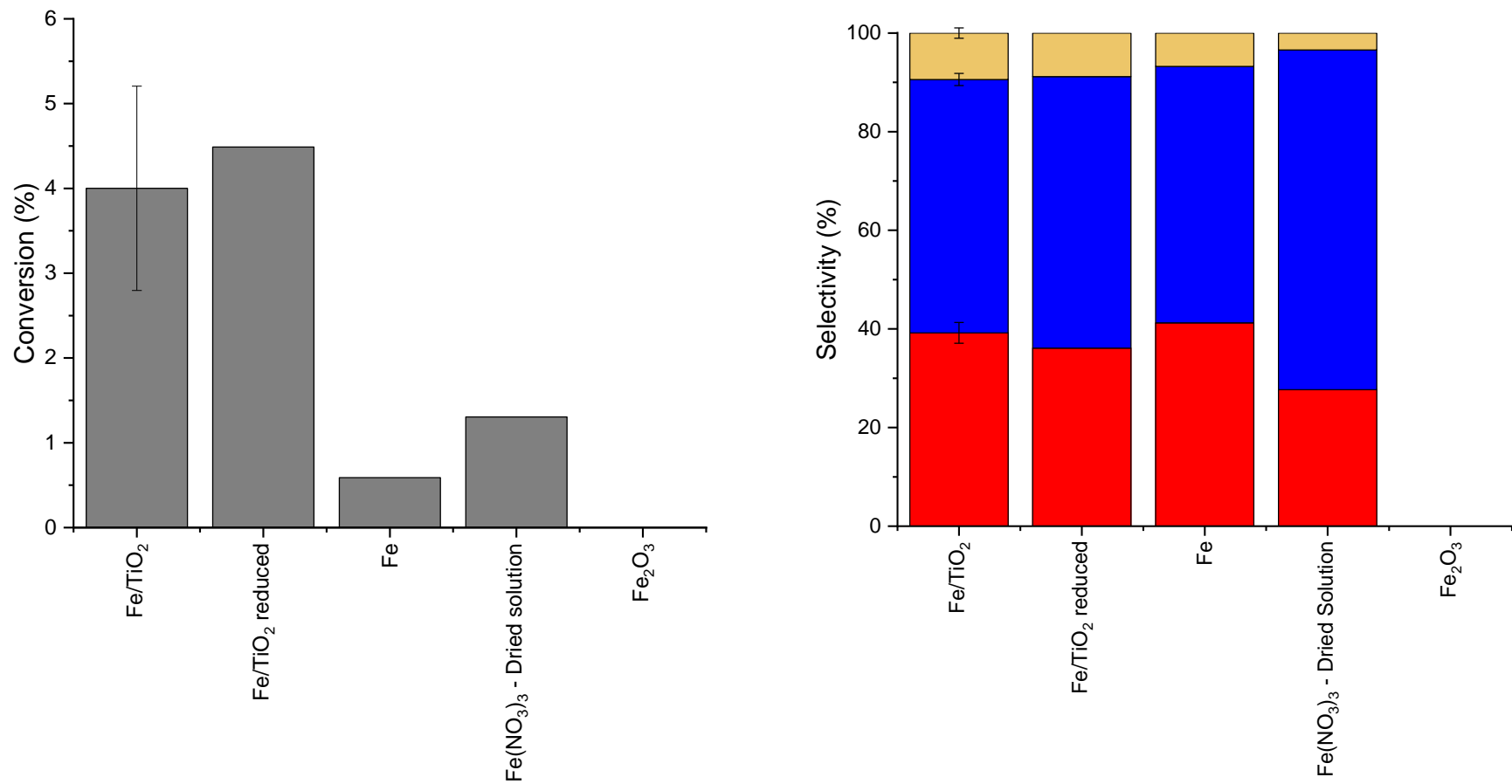


Figure 4.2.3.2.1: Conversion (left) and selectivity data (right) for *n*-decane oxidation with varying iron species. *n*-decane (3 mL), M:S = 1:1000, T = 115 °C, PO_2 = 1 bar, t = 24 h. (■) Conversion, (■) Alcohol, (■) Ketone, (■) Acids and other. Dried metal salts prepared via drying a standard solution onto glassware prior to catalytic tests.

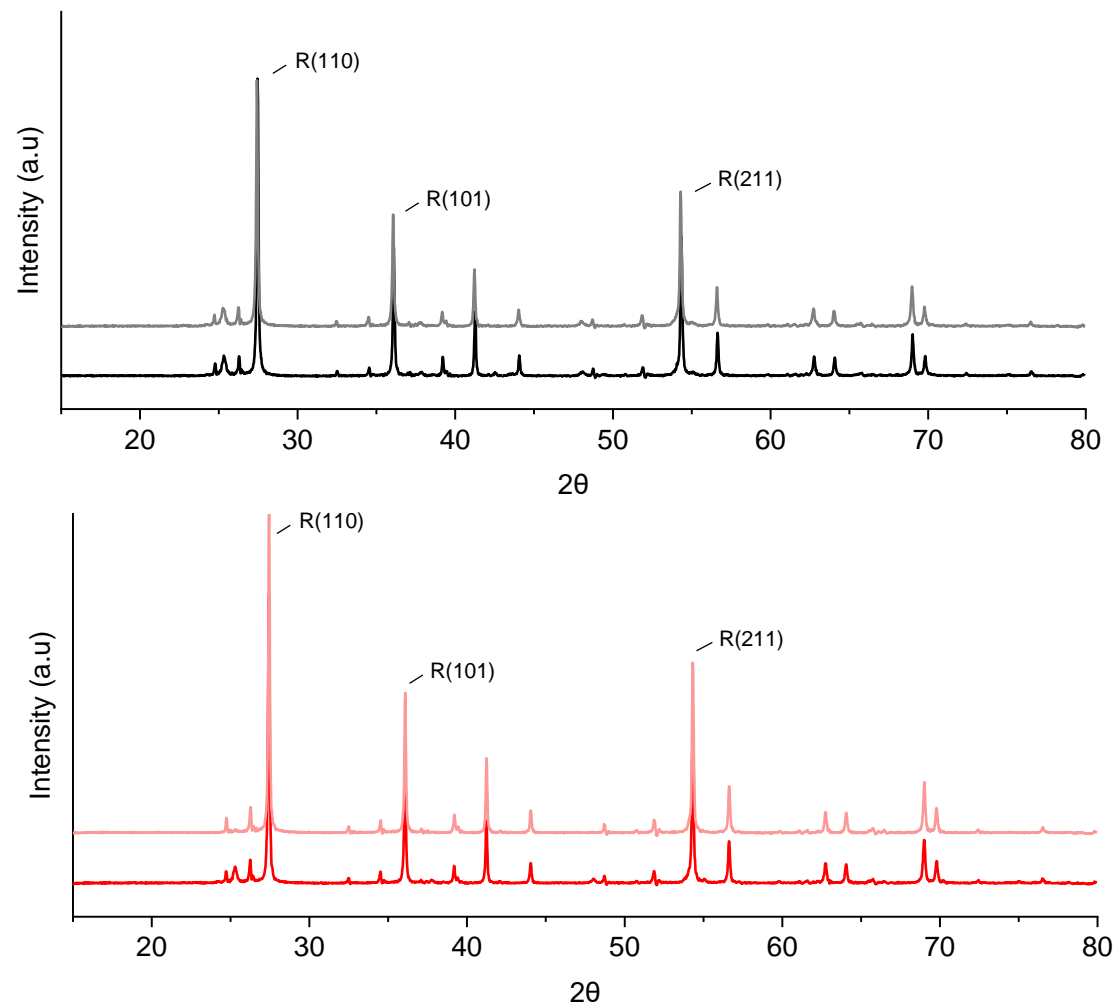


Figure 4.2.3.2a: XRPD patterns of M/TiO₂ 1 wt%, WI with varying dopant metal and corresponding reduced M/TiO₂. Fe/TiO₂ 680 °C, H₂ 450 °C (-), Mn/TiO₂ 680 °C, H₂ 450 °C (-). The most intense peaks of the patterns are assigned from literature, where 'R' is Rutile.⁴⁴⁻⁴⁶

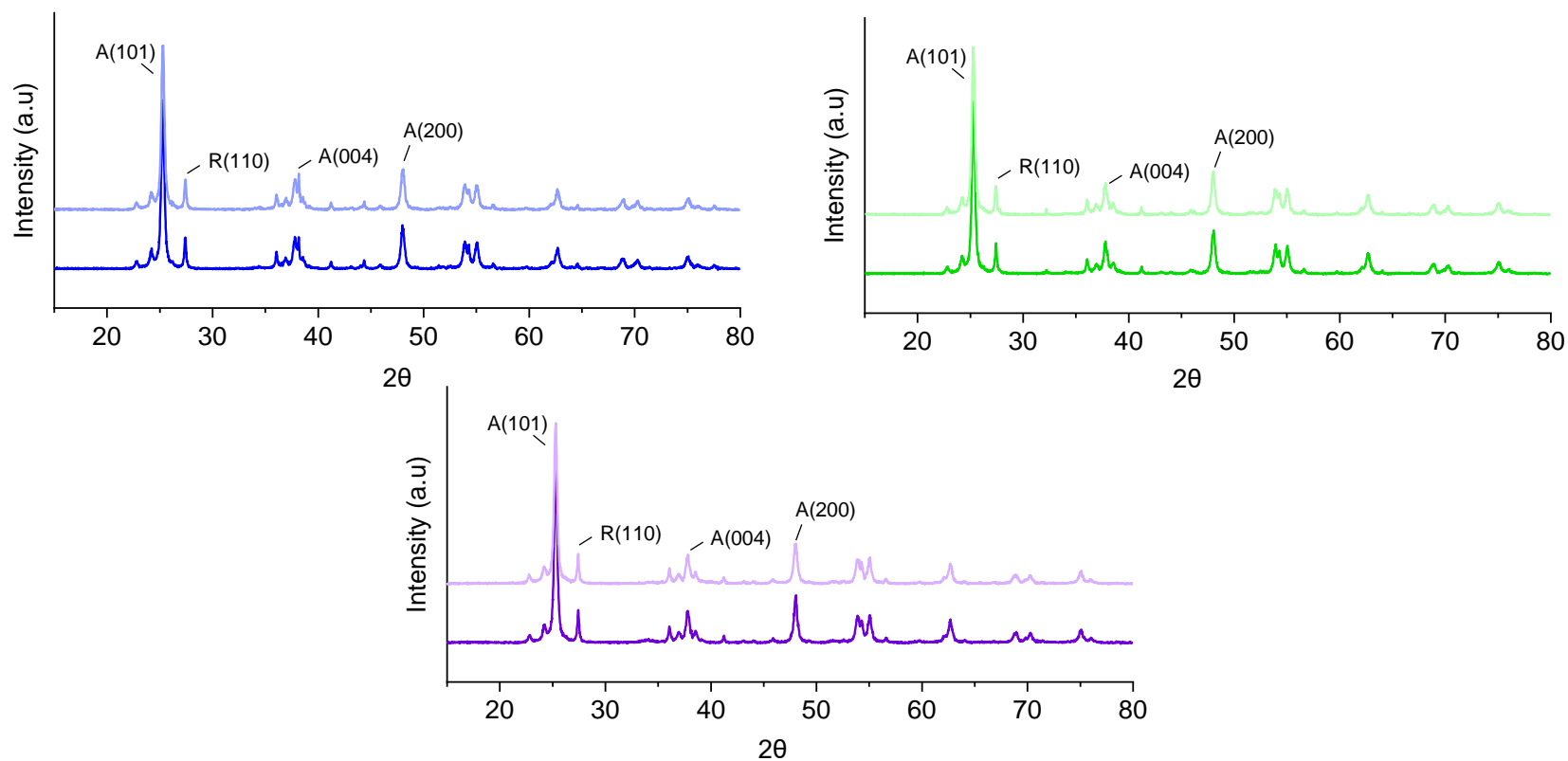


Figure 4.2.3.2.2b: XRPD patterns of M/TiO₂ 1 wt%, WI with varying dopant metal and corresponding reduced M/TiO₂. Au/TiO₂ 450 °C, H₂ 450 °C (-), Ag/TiO₂ 180 °C, H₂ 200 °C (-), Pd/TiO₂ 450 °C, H₂ 450 °C (-). The most intense peaks of the patterns are assigned from literature, where 'A' is Anatase and 'R' is Rutile.⁴⁴⁻

4.2.4. Alternative supports for *n*-decane oxidation

Thus far a range of metals on TiO₂ have been applied to *n*-decane oxidation. Metals with a strong literature presence on alkane oxidation were found to be poorly active at best. As this lack of activity was suspected, in part, to be due to inhibiting metal-support interactions, alternative supports are tested here. Furthermore, zeolite-based supports would allow determination of any confinement effects through desired shape selective oxidation.⁶³

4.2.4.1. Zeolite based catalysts

Two predominant zeolites were chosen as supports for *n*-decane oxidation. MCM-41^{60,64–66} and ZSM-5^{11,61,67} were chosen due to their presence within the literature as supports for metals and their appropriate pore sizes. In principle, only parts of the *n*-decane molecule will have access to the metal doped support, as the support itself will provide a degree of confinement.^{34,68} The result of this will show selectivity to specific products (i.e. differences in selectivity of positional isomers) if steric confinement of an active site has occurred.¹¹

From figure 4.2.4.1.1 the iron doped zeolites were found to be not as active as the corresponding iron doped TiO₂ and dried metal salt solution. Fe/MCM-41 shows conversion, whereas Fe/ZSM-5 shows no conversion at all. It is thought this could be due to two possible reasons: i) inhibiting metal/support interactions and ii) diffusion limitations of the substrate to the active site. As the catalysts were synthesised via a wetness impregnation technique, it is highly likely that the dispersion of nanoparticles results in a proportion being present on the exterior of the pores of the zeolite catalysts.^{11,67} Therefore, in principle, the substrate should have access to these sites and thus be activated (without any confinement). This means that point i), where unfavourable metal/support interactions are present, is likely to be the main reason why these catalysts are not as active. Figure 4.2.4.1.1 also shows there is no advantage on selectivity towards alcohols and figure 4.2.4.1.2 shows no regioselectivity has occurred when MCM-41 was used as a support (i.e. due to having identical selectivity to that of bulk Fe/TiO₂ and the dried metal salt solution). This indicates that the activity that has occurred in Fe/MCM-41 is likely to be due to active sites on the exterior of the porous

framework, or the pores are too large to induce enough confinement for selectivity. Finally, it should be noted for completeness, that acidity of these materials may be having an effect on conversion as ZSM-5 and MCM-41 may have differing Si/Al ratios and interactions when doped with Fe and in turn active sites.⁶⁹⁻⁷¹

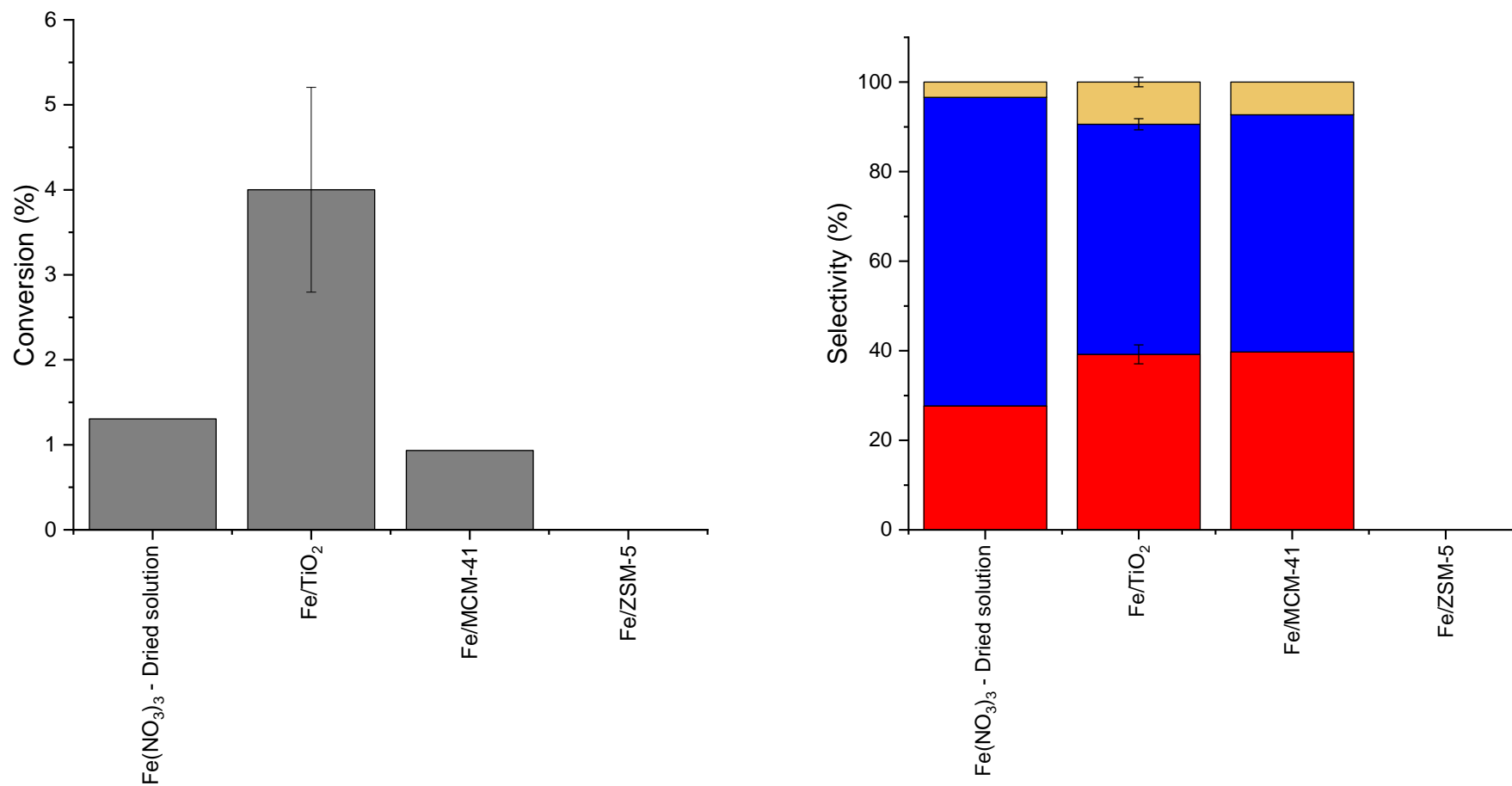


Figure 4.2.4.1.1: Conversion (left) and selectivity data (right) for *n*-decane oxidation with iron doped zeolites, with dried Fe(NO₃)₃ solution and Fe/TiO₂ bulk as a comparison. *n*-decane (3 mL), M:S = 1:1000, T = 115 °C, PO₂ = 1 bar, t = 24 h. (■) Conversion, (■) Alcohol, (■) Ketone, (■) Acids and other.

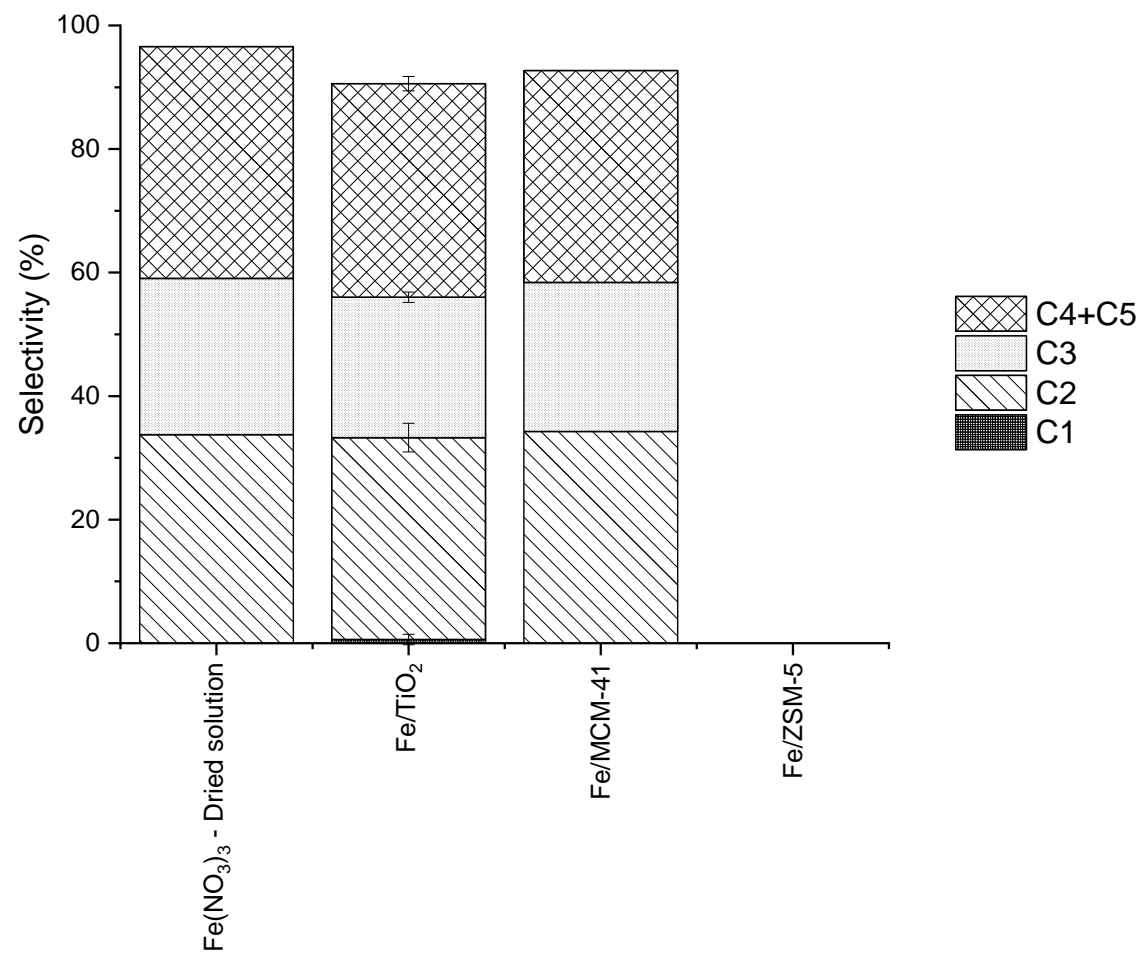


Figure 4.2.4.1.2: Positional selectivity data for *n*-decane oxidation with iron doped zeolites, with dried Fe(NO₃)₃ solution and Fe/TiO₂ bulk as a comparison. Selectivity is based on the sum of alcohol and ketone for a given position (e.g. C₃ = 3-Decanol + 3-Decanone). *n*-decane (3 mL), M:S = 1:1000, T = 115 °C, P_{O₂} = 1 bar, t = 24 h.

Figures 4.2.4.1.3 and 4.2.4.1.4 show that the pores within MCM-41 are indeed still present (and likely to be accessible) after WI with iron. Although a drop in the crystallinity of the pores is observed (a decrease in intensity to $\sim 1/3$), pores are still present after calcination. Furthermore, pore width and pore volume distribution remain almost identical (figure 4.2.4.1.4) alongside the hysteresis loops. This data concludes that pores are indeed still present, but as the product distribution from *n*-decane oxidation is identical to Fe/TiO₂, it is likely that any conversion has occurred without steric confinement.

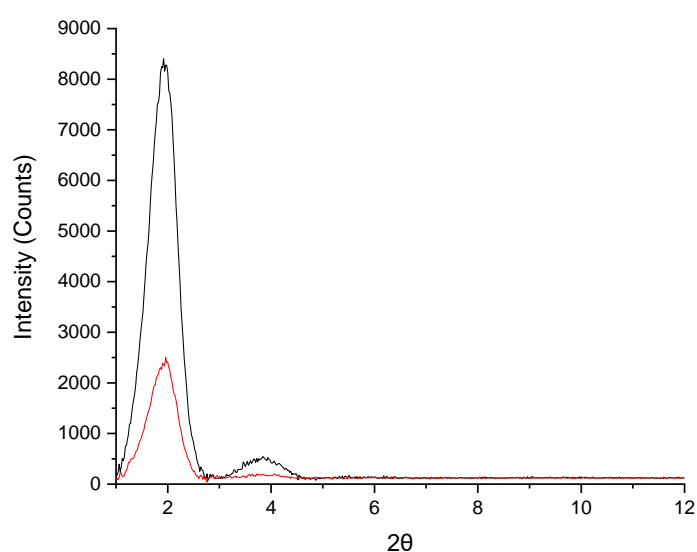


Figure 4.2.4.1.3: XRPD patterns of MCM-41 before and after wetness impregnation with iron. MCM-41 (-) d-spacing = 46.2 Å, Fe/MCM-41 (-) 1 wt% WI, 680 °C d-spacing = 46.2 Å.

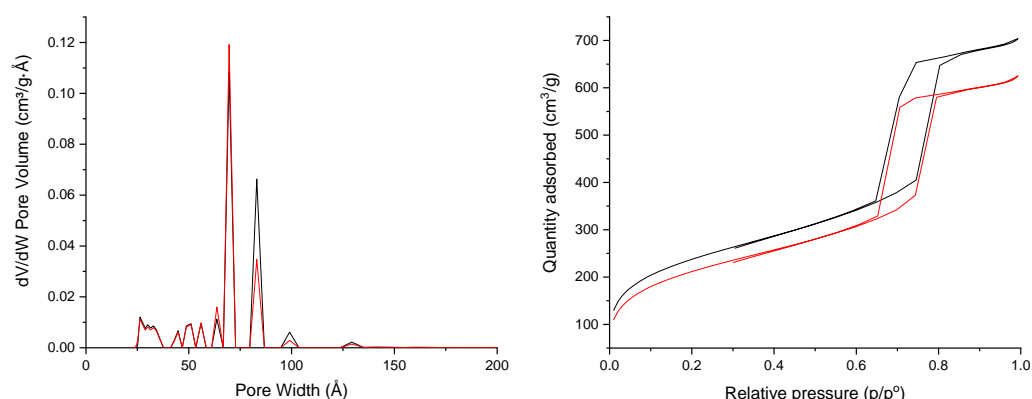


Figure 4.2.4.1.4: Porosimmetry data of MCM-41 before and after wetness impregnation with iron. MCM-41 (-), Fe/MCM-41 (-) 1 wt% WI 680 °C.

It has been seen in this data that metal/surface interactions have a dramatic effect on conversion. Therefore, active metals from the literature and those previously trialled with TiO₂ were doped onto MCM-41 and subsequently tested towards *n*-decane oxidation.

Interestingly, metals previously shown to be inactive towards *n*-decane oxidation on TiO₂ were found to be active on MCM-41 (figure 4.2.4.1.5). Gold on MCM-41 was found to be active, even the calcined and reduced catalysts were also active, unlike any of the Au/TiO₂ catalysts. This suggests that MCM-41 can support an active metal which is inactive on TiO₂, indicative of varying metal-support interactions.^{72,73}

Furthermore, palladium was found to be active on MCM-41. Palladium nitrate on MCM-41 showed the highest *n*-decane conversion amongst all the noble metals tested on MCM-41. However, reduced Pd/MCM-41 and the unsupported palladium nitrate salt showed no conversion. This data further complements the evidence of metal/support interactions affecting catalytic activity. Palladium nitrate on MCM-41 shows that Pd(II) is a promising contender for being doped into porous materials.

However, in all instances there is no significant selectivity towards alcohols, with most catalysts having similar/identical product distributions. This is apart from gold, which shows a preference for ketones. Although this is not desired for linear alkanes, and thus for the specific purpose of our research (terminal or primary alcohols), a process where ketones are produced from alkanes (e.g. KA oil, a Ketone-Alcohol mixture, from the oxidation of cyclic hydrocarbons)⁷⁴ could make use of these catalysts.

Finally, no regioselectivity is evident from the observed product distributions (figure 4.2.4.1.6). The data shows that the distribution of products in *n*-decane oxidation was identical amongst metal salts and doped metals onto MCM-41. Similar to the Fe/MCM-41 results, the data suggests that the WI technique for doping metals is not appropriate for generating isolated active sites. This is likely to be creating a significant number of active sites on the exterior of the porous framework, thus leading to oxidation of all positions of the *n*-decane molecule. This

further demonstrates the need for intra-framework metals, which are the primary focus of this project (see section 1.5).

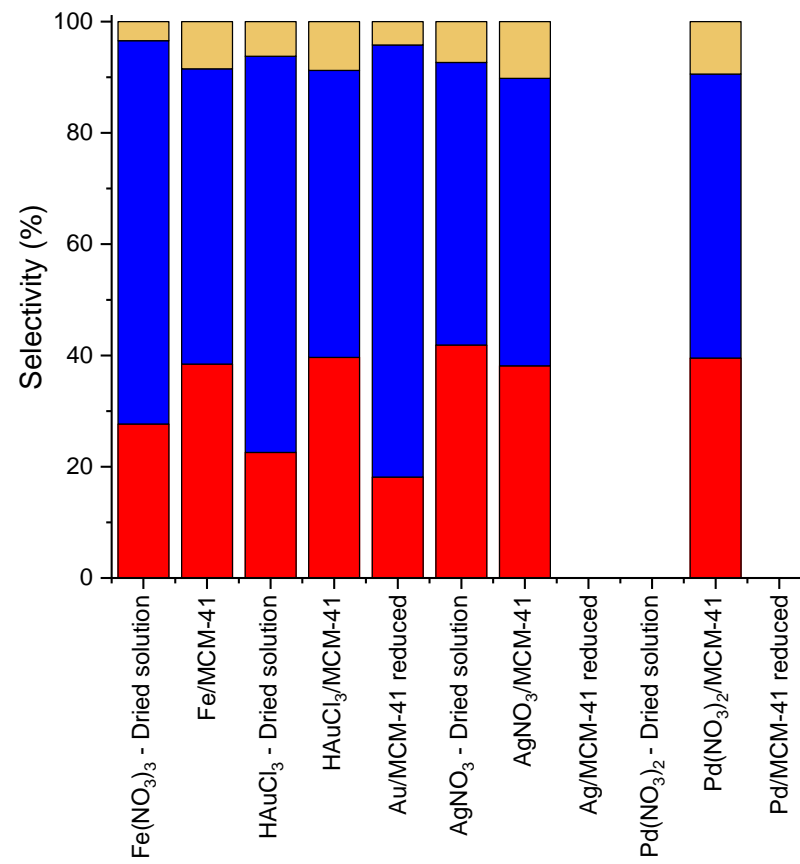
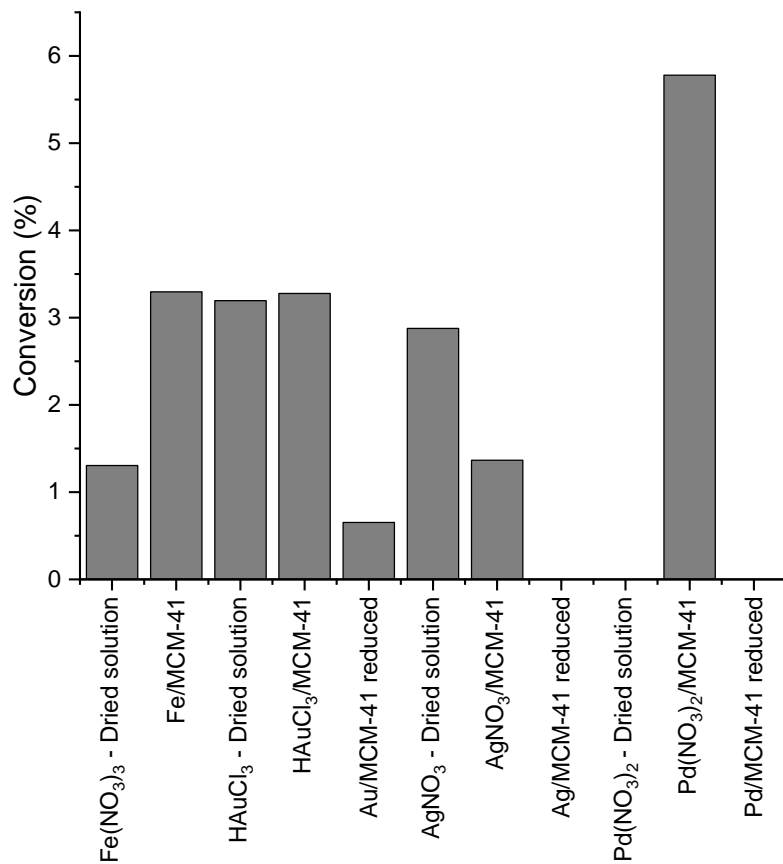


Figure 4.2.4.1.5: Conversion (left) and selectivity data (right) for *n*-decane oxidation with metal doped MCM-41, with dried metal salt solutions shown as a comparison. *n*-decane (3 mL), M:S = 1:1000, T = 115 °C, *P*O₂ = 1 bar, t = 24 h. (■) Conversion, (■) Alcohol, (■) Ketone, (■) Acids and other.

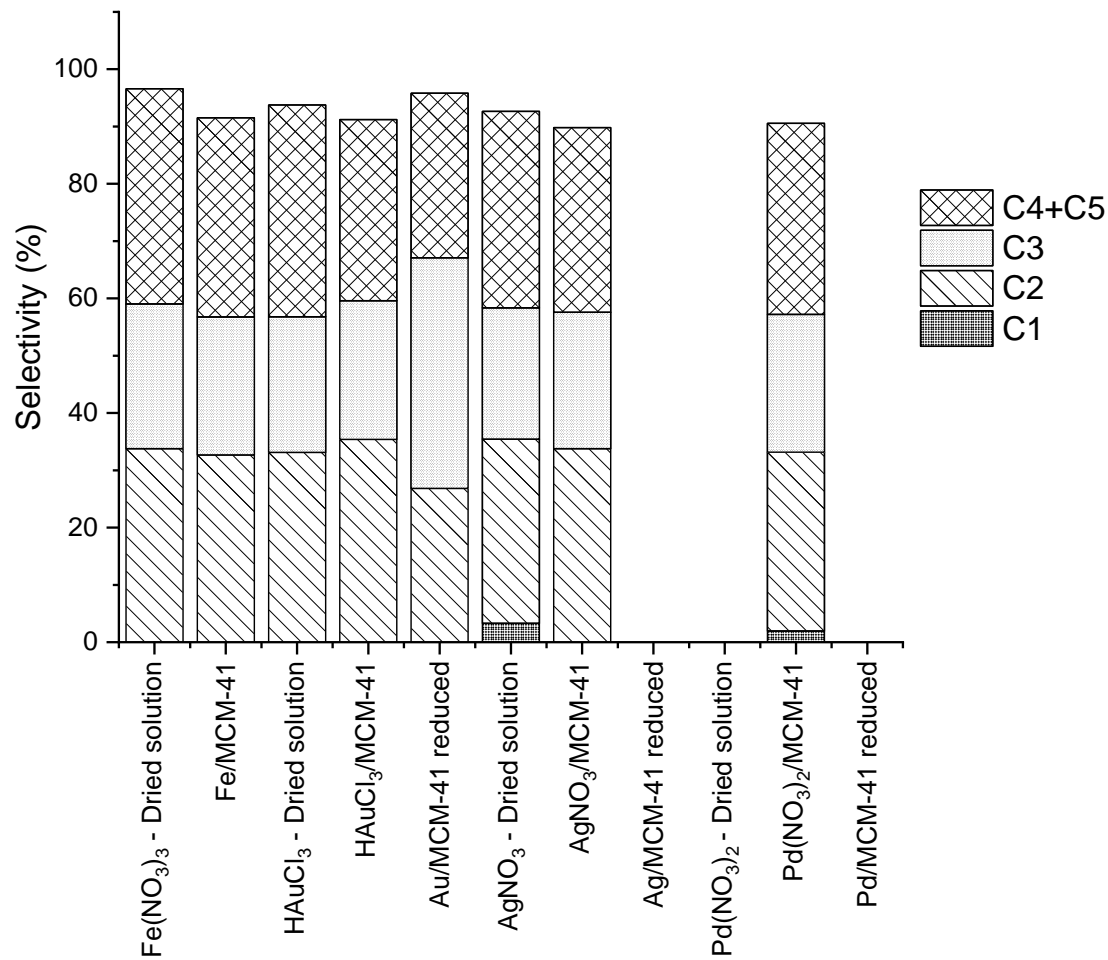


Figure 4.2.4.1.6: Positional selectivity data for *n*-decane oxidation with metal doped MCM-41, with corresponding dried metal salt solutions shown as a comparison. Selectivity is based on the sum of alcohol and ketone for a given position (e.g. C₃ = 3-Decanol + 3-Decanone). *n*-decane (3 mL), M:S = 1:1000, T = 115 °C, P_{O₂} = 1 bar, t = 24 h.

4.2.4.2. Niobium oxide-based catalysts

As previously mentioned, (section 4.2.2) niobium oxide was capable of significant oxidation of *n*-decane (2 – 7% conversion). This result was surprising as to the best of our knowledge no examples of bulk niobium oxide acting as a linear alkane oxidation catalyst are present in the literature. In principle, a support is required to be inert towards the catalytic process to avoid undesired parallel reactions and in turn more by-products. If, however, a support is capable in leading desired reactions, this is certainly noteworthy of further investigations. Nb₂O₅ did cause interest in the product distribution of the supports, this prompted us to determine if this could be altered with an additional active metal. Active metals were chosen from previous data and their literature presence. Data collected here will be crucial for comparisons to microporous niobium oxide (section 6.7).

Figure 4.2.4.2.1 shows the conversion of *n*-decane and selectivity data of various metals doped onto Nb₂O₅. Firstly, the wetness impregnation technique has no effect on the conversion of Nb₂O₅. From the XRPD pattern (figure 4.2.4.2.2) the crystallinity of the material is also unaffected. The material is yet to be indexed, to determine the crystalline phases present, however, it can be seen from the patterns they completely overlap. This suggests that the impregnation technique has essentially left the material unchanged. On the other hand, treatment of Nb₂O₅ with hydrogen led to complete loss of activity. This is interesting as the XRPD patterns again show no observable differences before and after reduction. The inactivity could be from a small number of surface species which were initially active and then become inactive (and inhibiting, see later in discussion) upon reduction, which cannot be detected via XRD as this is a bulk method.

Additional loaded metals change the activity of Nb₂O₅ in most instances. Manganese, gold and palladium doped niobium oxide show no catalytic activity. This is peculiar as it suggests that these metals are somewhat inhibiting conversion. This could be due to two reasons: i) The metal itself may be deactivating the mechanism that niobium is initiating; however, some minor products would be expected to be observed here. Furthermore gold was found to be

active on MCM-41, suggesting that the Nb-Au interaction is the source of the inhibition (in Au/Nb₂O₅) or ii) The active sites in the undoped niobium oxide have been blocked by the dopant metal nanoparticles; however, this would suggest the relatively low 1 wt% loading is enough to cover a significant proportion of the surface active sites. Niobium inhibiting oxidation (to an extent) is present within the literature,⁷⁵⁻⁷⁷ but does not provide an explanation why the presence of these metals inhibit niobium oxide's own activity. We speculate the most likely explanation might be active site blocking.

On the other hand, dopant silver provides a significant increase in activity (around 3 times as much compared to the undoped Nb₂O₅). It is still uncertain what this could be due to. Potentially the silver and niobium are acting independently, and the conversion observed is the sum of the niobium's and silver's own conversion. Alternatively, the silver or niobium could be acting as a promoter to one another.^{78,79}

Besides this, iron doped niobium oxide shows no difference in activity to undoped Nb₂O₅. This is somewhat unexpected as iron is always the most active metal within the series when doped on other supports reported above. The conversion of Fe/Nb₂O₅ is identical to that of the dried iron salt (and similar to that of the undoped niobium oxide). However, the product distribution is identical to that of the undoped material. This suggests that active sites are located on the surface of the niobium oxide, and these could be, for example, oxygen vacancies, edges, or corners on the oxide at atomic level. Therefore, these are the dominating species responsible for the catalytic activity in this support and potentially the iron is not responsible for any conversion.

Finally, reduction of doped niobium oxide almost always leads to inactivity. As with the undoped material, iron and silver doped niobium oxide show no conversion after reduction. As mentioned previously, this could be due to speculated active species on the surface of the niobium oxide becoming inactive (and in this case inhibiting) after reduction. However, palladium does not fit this trend (and actually has the opposite effect). Palladium thus far has been predominantly inactive on supports (except for Pd(NO₃) on MCM-41). After reduction

Pd/Nb₂O₅ becomes active. This means that any inhibition from the support previously seen in other metals is surpassed by the palladium nanoparticles. It is still uncertain why this the case is but certainly demonstrates the necessity for testing other supports (both bulk and porous).

Ultimately, this data could lead to a whole new project studying the surface of the niobium oxide-based materials. However, for the context of this project the data has shown how changes to a synthesis can have a significant effect on the activity of a catalyst. This will be crucial information for understanding any differences in activity in porous materials.

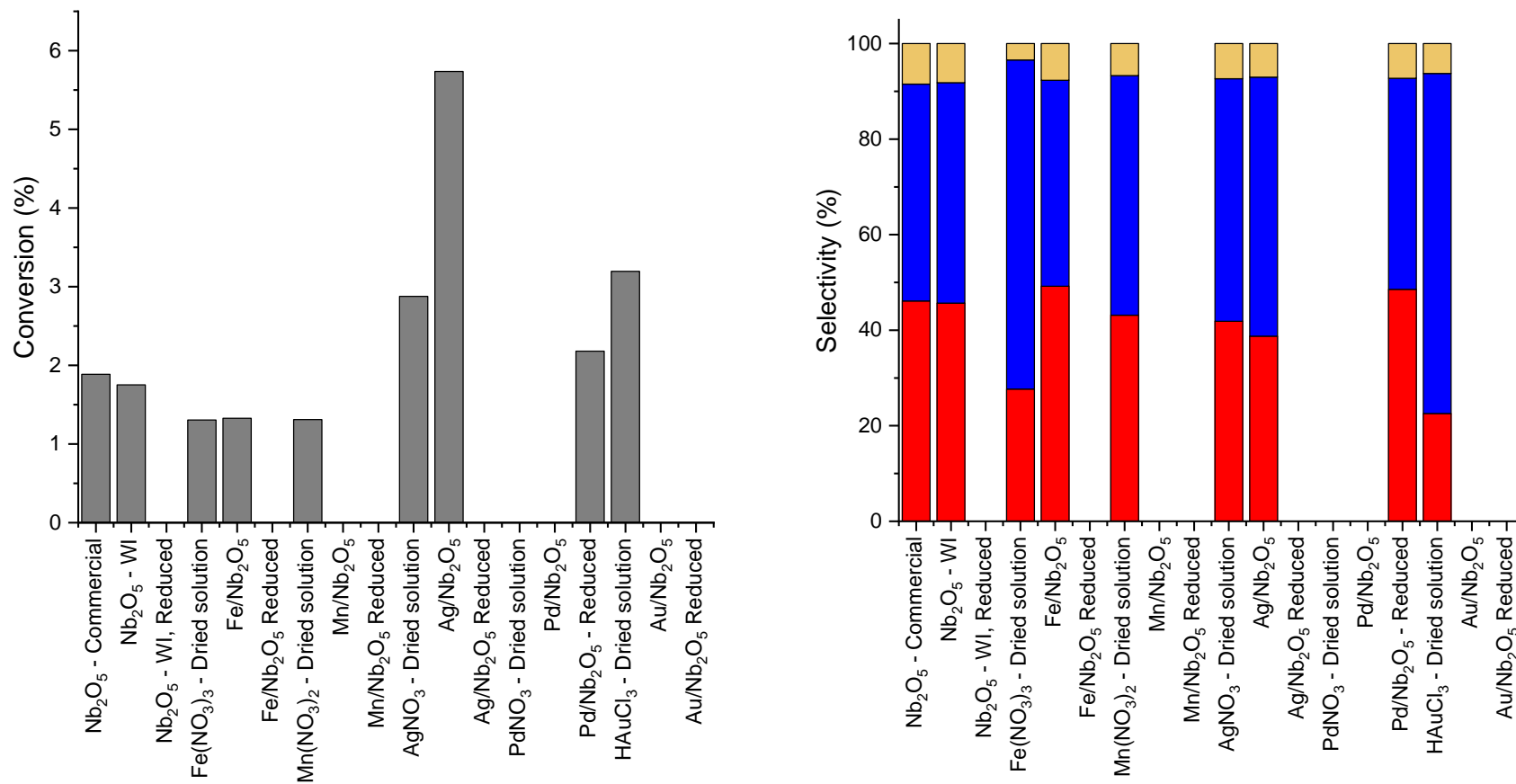


Figure 4.2.4.2.1: Conversion (left) and selectivity data (right) for *n*-decane oxidation with metal doped Nb₂O₅, with dried metal salt solutions shown as a comparison. *n*-decane (3 mL), M:S = 1:1000, T = 115 °C, PO₂ = 1 bar, t = 24 h. (■) Conversion, (■) Alcohol, (■) Ketone, (■) Acids and other.

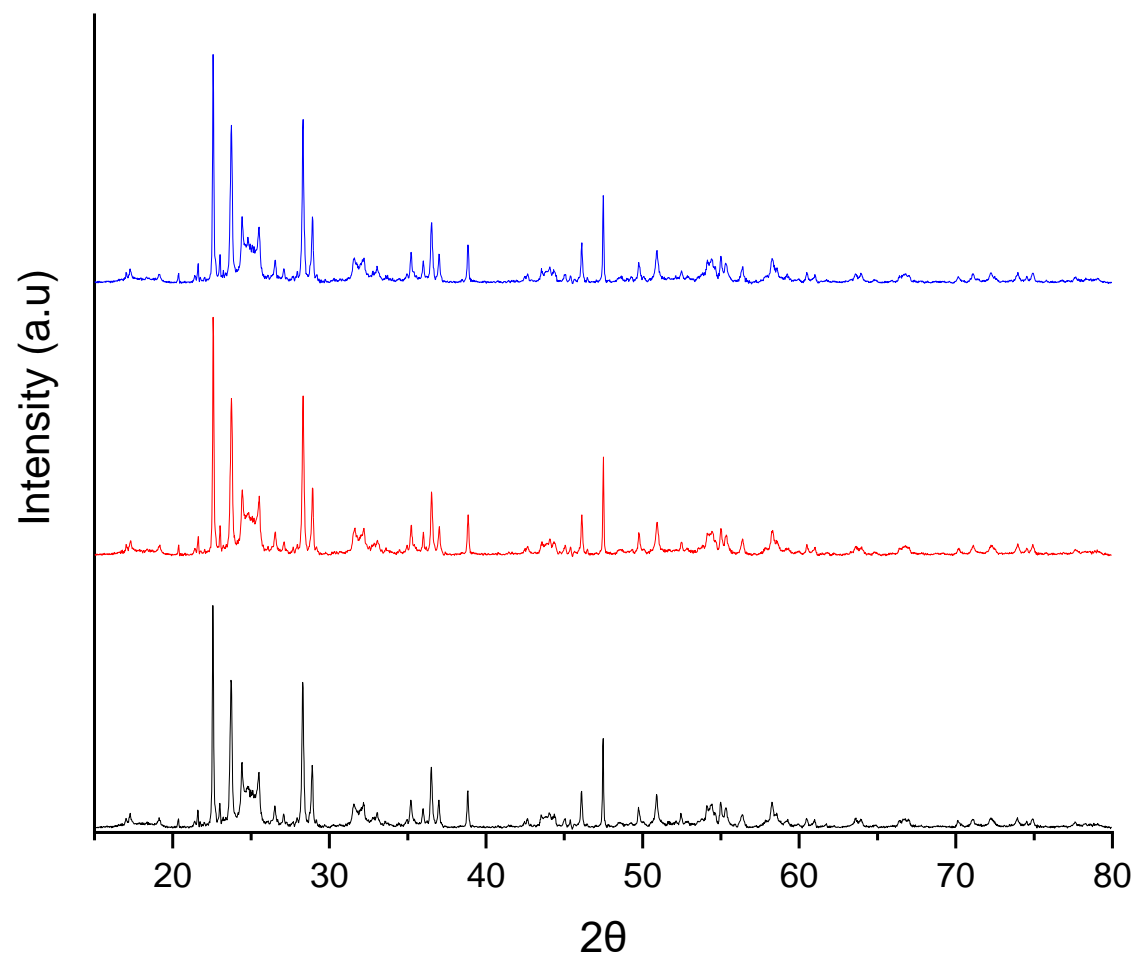


Figure 4.2.4.2.2: XRPD patterns of commercial Niobium oxide (99.99%, Sigma), and corresponding samples from wetness impregnation (i.e. with no dopant metal) and reduction. (■) Nb_2O_5 Commercial, 99.99% (■) Nb_2O_5 WI, 680 °C (■) Nb_2O_5 WI, 680 °C, 450 °C H_2 30 min, 10 ml min^{-1} .

4.3. Cyclooctane oxidation

As *n*-decane has been difficult to activate, an alternative hydrocarbon was tested for catalytic oxidation. Cyclooctane was chosen as because it is cyclic it will have a lower C-H activation energy than similar linear alkanes (a difference up to $\sim 84 \text{ kJ mol}^{-1}$).^{80,81} Furthermore, cyclooctane oxidation is analogous to cyclohexane oxidation, an industrially relevant reaction which requires selectivity and provides sought after products.⁷⁴ This allowed an easier 'proof of concept' that a catalyst can indeed activate a C-H bond compared to using *n*-decane. Catalysts which were shown to be active with *n*-decane and those with a strong literature presence were tested. Furthermore, particular interest was paid to the support ZSM-5. This is because its pore size (5.6 \AA)⁶⁷ is almost identical to that of cyclooctane's approximate kinetic diameter of ca. $5.5\text{-}5.7 \text{ \AA}$.⁸² Therefore, some shape selectivity may be induced by the catalyst (whereas in *n*-decane's oxidation, Fe/ZSM-5 was found to be inactive).

Like with *n*-decane, ideal conditions and a conversion calculator were required to be developed. This was done previously within the research group, and it was found that $110 \text{ }^\circ\text{C}$, PO_2 2 bar, 24 h were ideal for the study of cyclooctane oxidation. Furthermore, as the product distribution of cyclooctane oxidation is significantly lower than *n*-decane oxidation (i.e. less individual products and by-products), $^1\text{H-NMR}$ was able to be employed as the main technique for product and reactant quantification (alongside the several advantages of NMR previously mentioned).⁸³ A detailed description of the development of these analytical tools is not reported here, as it is beyond the scope of the current thesis work.

Although the goal of this project was to oxidise linear alkanes, cyclooctane oxidation tests are crucial in ruling out if a catalyst is totally inactive to hydrocarbon oxidation, or simply not active enough for linear alkanes.

4.3.1. Cyclooctane oxidation with iron-based materials

As mentioned previously, the reactivity of cyclooctane is expected to be markedly different to that of *n*-decane. This is due to cycloalkanes having a lower BDE (bond dissociation energy) than that of corresponding linear alkanes.^{80,81} Therefore, a series of catalysts previously tested with *n*-decane were applied to cyclooctane oxidation. As iron has proved to be the most active when applied to *n*-decane oxidation, it was prioritised for cyclooctane oxidation. Figures 4.3.1.1 and 4.3.1.2 show a summary of cyclooctane oxidation with all the iron-based catalysts utilised.

Firstly, cyclooctane can be activated much more readily than *n*-decane. Furthermore, across the series the conversion is significantly higher (by around a factor of 10) for all catalysts. For example, Fe/Nb₂O₅ has a conversion close to 70%, whereas with *n*-decane, conversions barely exceeded 5%. The data is agreeable with the principle that the BDE of cycloalkanes are lower than linear alkanes, and thus are easier to activate.^{80,81} Consequently supports that were inactive with *n*-decane show significant conversion with cyclooctane. For example, commercial TiO₂ and ZSM-5-WI (no dopant metal) are capable of relatively high conversions of cyclooctane, where with *n*-decane no conversion is seen. This result is crucial as if the active sites are on the outside of the pores of these materials (and with TiO₂ which is not porous, thus is likely the case), then catalysis can be occurring with no steric confinement. Niobium oxide also shows a significant conversion with no dopant metal. This is somewhat unexpected as to our knowledge no examples of bulk niobium oxide exhibiting such high conversions of hydrocarbon exist. This is ongoing in investigation.

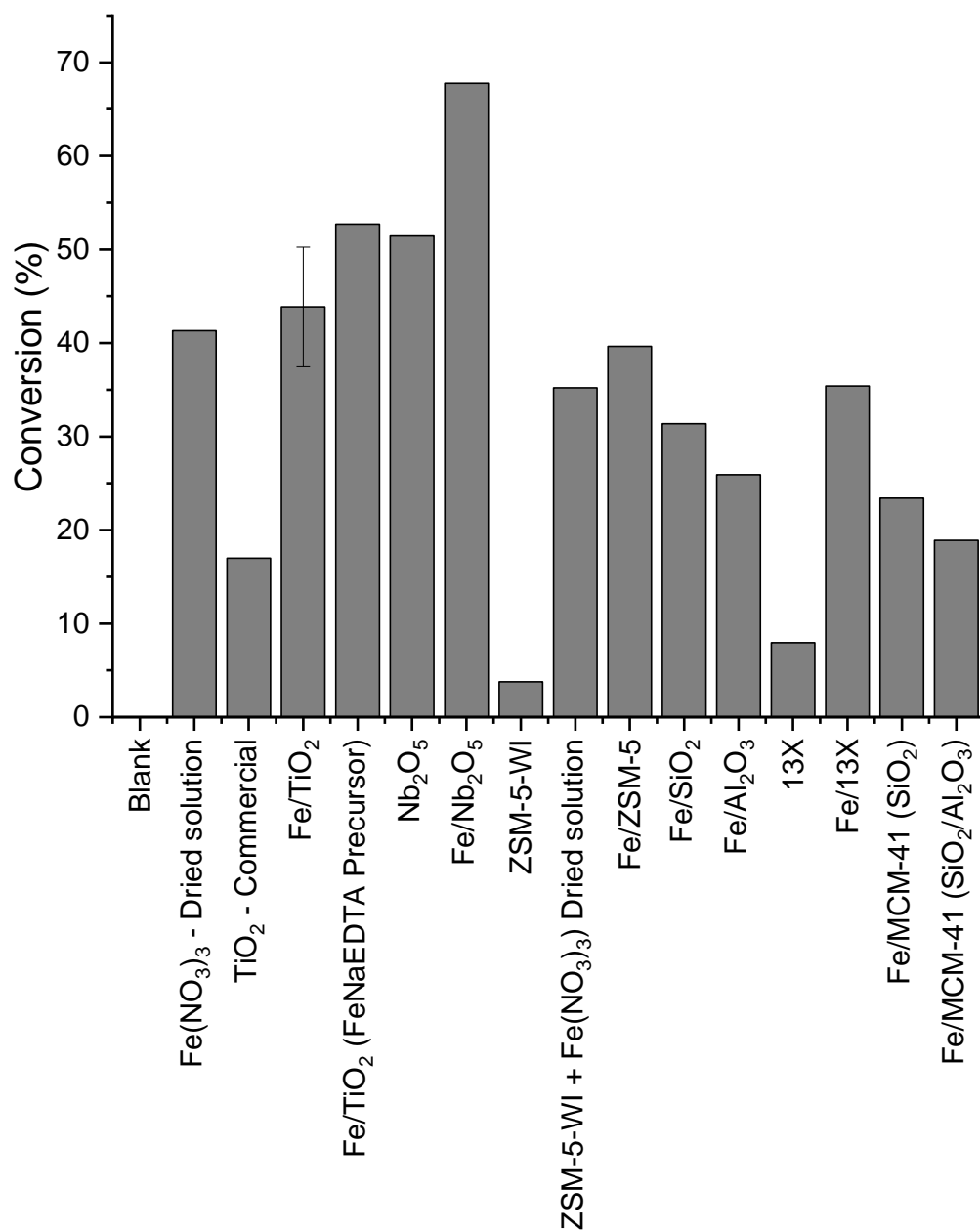


Figure 4.3.1.1: Cyclooctane conversion data with varying iron-based catalysts and corresponding supports. Cyclooctane (3 mL), M:S = 1:1000, T = 110 °C, PO₂ = 2 bar, t = 24 h.

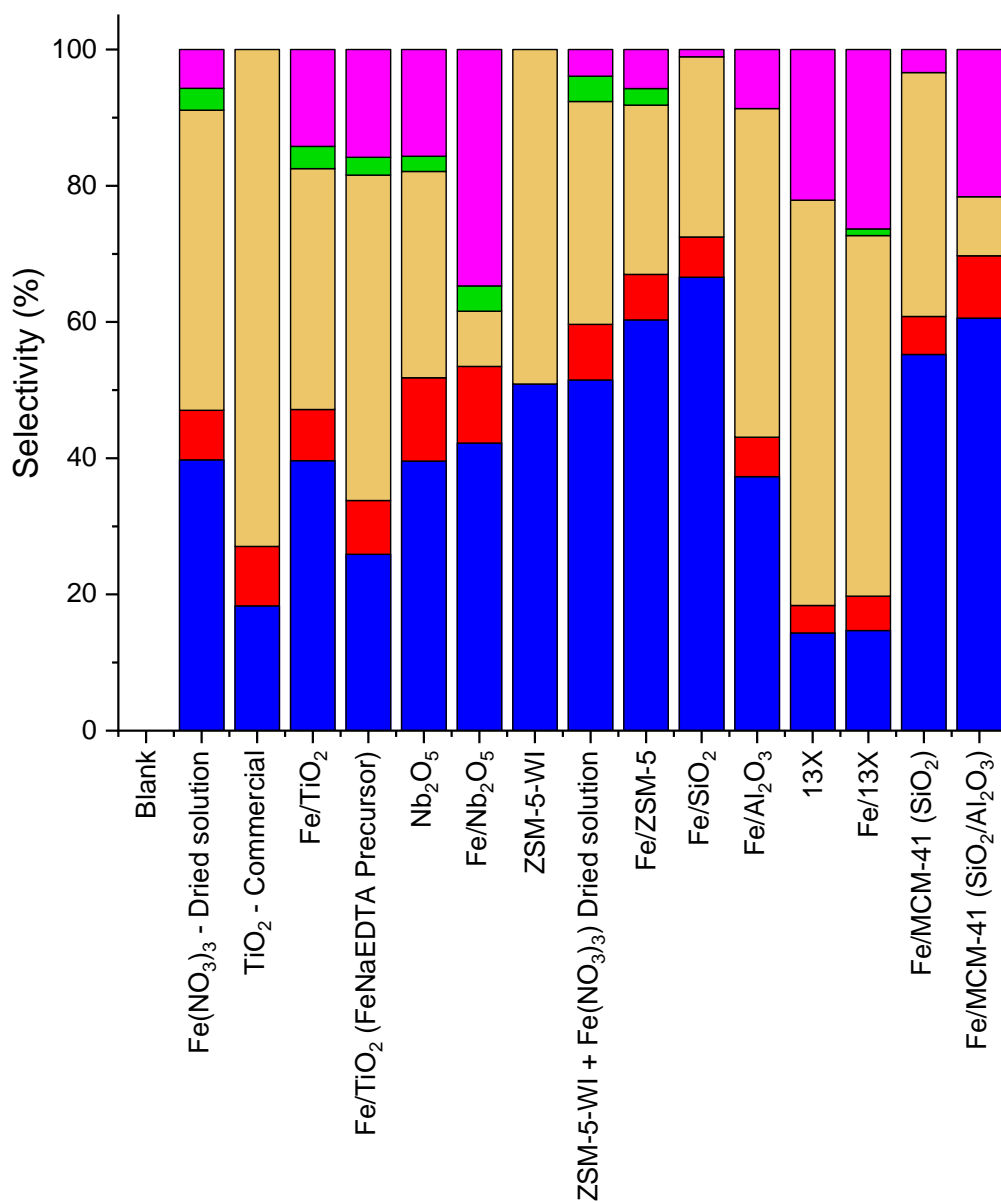


Figure 4.3.1.2: Cyclooctane selectivity data with varying iron-based catalysts and corresponding supports. Cyclooctane (3 mL), M:S = 1:1000, T = 110 °C, PO₂ = 2 bar, t = 24 h. Cyclooctanone (■), Cyclooctanol (■), Cyclooctyl hydroperoxide (■), other products (■), unknown products (■).

With the conversion of supports determined, it was then possible to see how the presence of iron affects oxidation. In all instances the presence of iron increases cyclooctane conversion. For example, Fe/TiO₂ has a conversion of 44% compared to undoped TiO₂ with 17%. This suggests that the iron is indeed capable of activating the cyclooctane. To try and further the conversion an alternative iron precursor was trialled. It was found in the literature that WI with FeNaEDTA gave significantly more disperse nanoparticles, which yielded active sites not found with Fe(NO₃)₃ and better catalytic activity.⁸⁴ In our case, indeed an increase in conversion is seen (53% compared to 44%). Additionally, a difference in selectivity is observed. A shift to almost 1.5 times more peroxide and 1.5 times less ketone is seen when FeNaEDTA was used as the precursor. This suggests a potentially different mechanism, or adsorption of the alkyl hydroperoxide over the catalyst surface is occurring with this material. However, as the alcohol and ketone were desired for our scope, tests with FeNaEDTA were not pursued. Interestingly, the dried iron nitrate salt had an almost identical conversion to that of iron doped titanium oxide. Both the conversion and selectivity of all products were within experimental error of the two tests. This contrasts with *n*-decane where supported iron was significantly more active than the dried salt. This could be due to cyclooctane's inherently lower BDE^{80,81} leading to iron's dispersion not being a limiting factor in its activation. It was speculated that the high conversions could be due to potential leaching of Fe from Fe/TiO₂ and thus all catalysis occurs homogeneously; however, this was not the case as ICP-OES data showed no presence of iron in solution.

Additionally, the presence of iron on niobium oxide showed an increase in conversion. Undoped niobium oxide already showed significant conversion (even higher than iron doped TiO₂), but when iron is added, an additional 15% conversion is observed. The presence of more unknown products when using Fe/Nb₂O₅ suggests either over oxidation or an alternative mechanism is occurring due to iron's presence. Although more ketone and alcohol were desired, these results will be used to compare to porous material where iron is within the porous framework.

Next, the use of ZSM-5 was trialled for cyclooctane oxidation. Mirroring Fe/TiO₂ and Fe/Nb₂O₅, Fe/ZSM-5 shows a significant increase in conversion to that of the undoped support. The result of the selectivity observed towards cyclooctanone is important. It seems the presence of ZSM-5 causes an increase in cyclooctanone selectivity compared to when iron is loaded onto TiO₂ (~1.5 times as much). From an industrial view, this is advantageous as the ketone is the most desired product for fibres-based manufacture.⁸⁵ It was speculated that the ZSM-5's acidic properties may have caused this via alkyl hydroperoxide cleavage. This is demonstrated as when dried Fe(NO₃)₃ with ZSM-5 were tested together it can be seen that the conversion is identical to that of when only Fe(NO₃)₃ is used. However, Fe/ZSM-5 selectively catalyses the reaction to produce ketones. This suggests that this difference is not due to potential metal/support interactions or confinement of nanoparticles, and instead, iron is catalysing one part of the mechanism and ZSM-5 another. This is interesting as this adds an additional contribution which must be considered when testing porous materials where the dopant metal is part of the framework. Fe/SiO₂ and Fe/Al₂O₃ were also tested as bulk comparisons to the zeolite. Fe/SiO₂ showed the highest selectivity to cyclooctanone of the series with significant conversion. Although out of the scope of this project, these results could be furthered for the industrial production of KA oil.

Finally, as ZSM-5's pore size (~5.5 Å)⁶⁷ is almost equal to cyclooctane's kinetic diameter, other zeolites with differing pore sizes were tested. Iron doped zeolite 13X (~11 Å)⁸⁶ and MCM-41 (~46 Å) were applied to cyclooctane oxidation. Fe/13X has a similar conversion to that of Fe/ZSM-5, and Fe/MCM-41 shows a lower conversion (~20% versus ~40%). This is of particular interest as in principle, ZSM-5 may have some diffusion limitation compared to the other, larger pore zeolites. However, the data shows ZSM-5 has the highest conversion. This does not necessarily mean the smaller pores are responsible for this, as multiple factors such as crystal size,⁸⁷ Si/Al ratios⁸⁸ etc. will be different amongst the supports. The data also represents how these differences have a profound effect on selectivity. Comparing Fe/ZSM-5 and Fe/13X, as they have similar conversions, Fe/13X significantly favours cyclooctyl peroxide

formation (53%) compared to Fe/ZSM-5 (25%). The difference in selectivity was attributed to the multiple parameters mentioned throughout this chapter. Ultimately, the data shows the intricate details which may affect conversion and selectivity.

4.3.2. Cyclooctane oxidation with noble metal-based materials

Silver and palladium on ZSM-5 were prioritised for cyclooctane oxidation due to their potential demonstrated in results mentioned previously. Figure 4.3.2.1 shows the conversion and selectivity of these catalysts. Surprisingly, palladium is inactive. Thus far all catalysts applied to cyclooctane oxidation, which were inactive/ of low conversion with *n*-decane, were found to be active. This suggests that palladium oxide nanoparticles prepared via wet impregnation in this way are not active towards alkane oxidation. However, palladium is known to be a common oxidation catalyst¹¹ and potentially if it is incorporated into a framework, its properties may be different. This is explored in section 5.2.

Silver on ZSM-5 showed modest activity towards cyclooctane oxidation. Although not as active as the corresponding Fe/ZSM-5 (23% versus 40% respectively), the data shows that silver is indeed an active metal towards hydrocarbon oxidation. Thus far, silver nitrate salt, Ag₂O, Ag/Nb₂O₅ and now Ag/ZSM-5 have been demonstrated as active catalysts. This gives scope for silver/ silver oxide supported microporous catalysts (section 5.4).

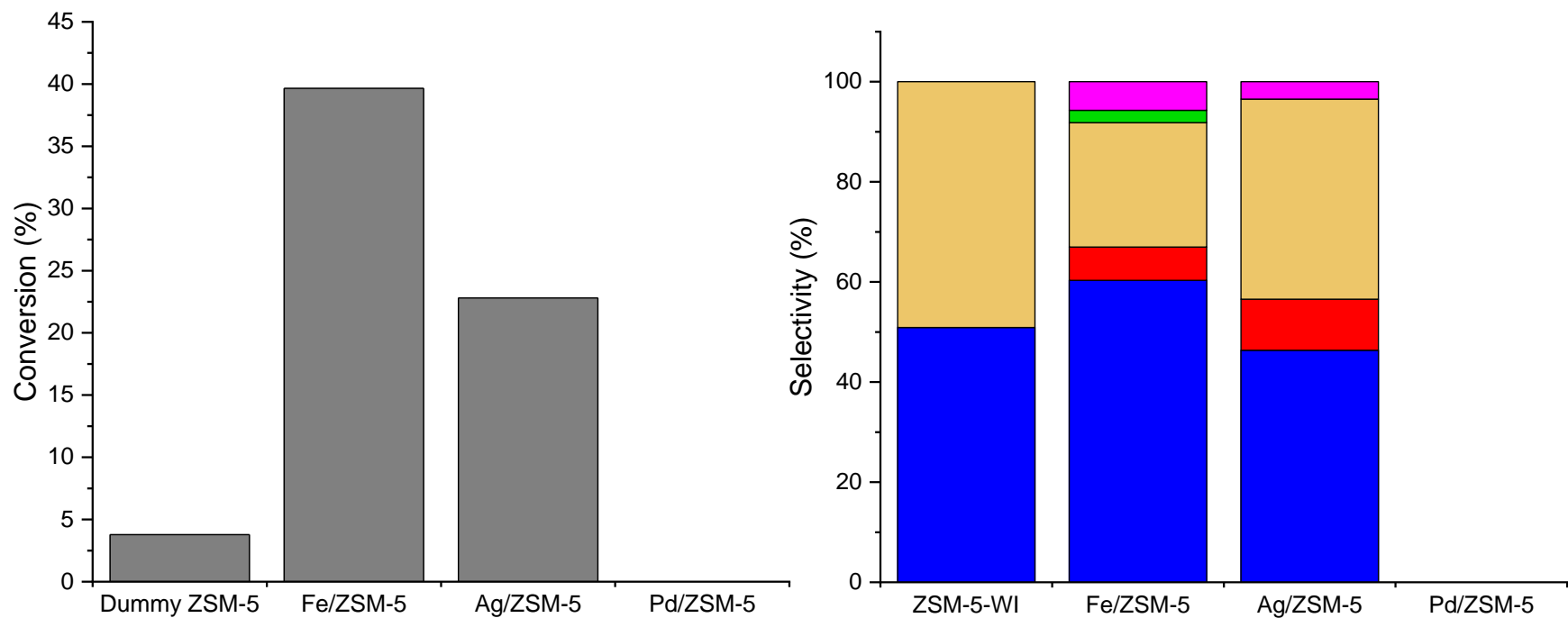


Figure 4.3.2.1: Cyclooctane conversion and selectivity data with varying noble metal doped ZSM-5 catalysts with WI-ZSM-5 and Fe/ZSM-5 present as comparison. Cyclooctane (3 mL), M:S = 1:1000, T = 110 °C, $PO_2 = 2$ bar, t = 24 h. Cyclooctanone (■), Cyclooctanol (■), Cyclooctyl hydroperoxide (■), other products (■), unknown products (■).

4.4. Conclusion and future work

The selective oxidation of hydrocarbons is a challenging task. Numerous parameters must be considered to achieve the narrow sweet spot between no activation at all to over oxidation. Here it has been demonstrated that catalyst design for application to alkane oxidation reflects this difficulty. Active metals within literature; supports leading to more/less activity and the type of hydrocarbon which is activated have led to a spectrum of results.

Nevertheless, it was found that iron is capable of significant oxidation of *n*-decane and cyclooctane. Optimum conditions were developed for the oxidation of *n*-decane with Fe/TiO₂, where no autoxidation was occurring. These conditions were then applied to an array of synthesised catalysts to find a metal capable of significant conversion or selectivity. The data revealed that iron would always be the most active metal for a series of dopant metals on a support (except when doped onto niobium oxide). Silver and palladium also showed in some cases the metals were active but suffered from metal support interactions leading to some inactive catalysts, dependent on the support used. Surprisingly, manganese never showed any activity, despite significant literature on its use as an oxidation catalyst. This could be due to inhibiting metal/support interactions also, or manganese oxide being in an inactive oxidation state.

Future work would be heavily focused on further catalyst characterization with a combination of the analytical techniques available.^{26,89} This would be used to determine a trend of properties that makes a catalyst active or not. For example, further elucidation of surface properties and edges between the metal nanoparticle and support would be one way to further understand these materials. This would allow determination of how metal salts are bound to a surface compared to the corresponding metal oxide, and does the choice of precursor affect metal particle morphology (and does this effect conversion). Specifically, for some catalysts, TEM (transmission electron microscopy) would be used to determine the particle size of the catalysts as this is crucial for catalysis. For example, Fe/TiO₂ 1 wt% - 5 wt% could not have the active Fe₂O₃ crystallite size determined from XRPD due to the lower loading used,

therefore TEM could be used to determine if particle size changes at all across this higher loadings, and even if particle size changes depending on the support used. This could also be used to determine if the particle size of the noble metals is the reason for their inactivity. Further surface analysis techniques (e.g. Raman, X-ray absorption spectroscopy, etc.) would also be beneficial in determining the reasons behind the activity of niobium oxide as analysis within the present work was unable to observe any differences between active and inactive niobium oxide based catalysts.

Additionally, it was found in cyclooctane oxidation selectivity towards ketones was greatly increased in the presence of acidic sites. Specifically, Fe/ZSM-5 and Fe/SiO₂ showed great selectivity towards cyclooctanone (60% and 67% respectively), an industrially relevant product used in the fibre sector. Perhaps obtaining Fe/ZSM-5 where pore size is fixed but decreasing the Si/Al ratio (i.e. increasing the acidity) would lead to even greater yields of ketones, and thus make these catalysts contenders for industrial scale production of KA oil.

Furthermore, future work would also focus more on the kinetics of the reactions described here. Similar to section 3, time online experiments would be conducted to determine the kinetics of alkane oxidation, comparisons would ultimately be made between autoxidation and reactions where a catalyst is present to help determine how conversion and selectivity vary over time. Additionally, extra data points throughout the work could help guide focus to higher conversions and selectivity, for example; more data points for varying PO_2 , stirrer speed and M:S ratio, the latter two would also support discussions on kinetic/diffusion regimes. This information may also allow further comparisons between catalysts. For example, many catalyst selectivities could not be compared due to differences in conversion, as comparisons can only be made at statistically identical conversion. Therefore, if equivalent conversions were found then the selectivity of the wider range of catalysts could then be compared.

Ultimately, the results obtained in this chapter allowed a proof of concept that hydrocarbon oxidation, albeit difficult, is possible with metal nanoparticles on supports. It also demonstrated

that an active metal may be inactive on different supports, a crucial concept for sections 5.2 and 6.2 where metals will be included within a porous framework.

4.5. References

- 1 J. M. Thomas, R. Raja, G. Sankar and R. G. Bell, *Nature*, 1999, **398**, 227–230.
- 2 T. Machej, J. Haber, A. M. Turek and I. E. Wachs, *Appl. Catal.*, 1991, **70**, 115–128.
- 3 J. A. Rodriguez and D. Stacchiola, *Phys. Chem. Chem. Phys.*, 2010, **12**, 9557–9565.
- 4 F. Farzaneh, M. Majidian and M. Ghandi, *J. Mol. Catal. A Chem.*, 1999, **148**, 227–233.
- 5 S. Martínez-González, A. Gómez-Avilés, O. Martynyuk, A. Pestryakov, N. Bogdanchikova and V. C. Corberán, *Catal. Today*, 2014, **227**, 65–70.
- 6 V. D. B. C. Dasireddy, S. Singh and H. B. Friedrich, *Appl. Catal. A Gen.*, 2013, **456**, 105–117.
- 7 K. Naicker, A. S. Mahomed, H. B. Friedrich and S. Singh, *J. Porous Mater.*, 2019, **26**, 301–309.
- 8 M. A. Bañares and I. E. Wachs, *J. Raman Spectrosc.*, 2002, **33**, 359–380.
- 9 J. M. Thomas and R. Raja, *Chem. Commun.*, 2001, **8**, 675–687.
- 10 B. R. Cook, T. J. Reinert and K. S. Suslick, *J. Am. Chem. Soc.*, 1986, **108**, 7281–7286.
- 11 N. Herron and C. A. Tolman, *J. Am. Chem. Soc.*, 1987, **109**, 2837–2839.
- 12 T. Ohno, K. Sarukawa, K. Tokieda and M. Matsumura, *J. Catal.*, 2001, **203**, 82–86.
- 13 B. Modén, B. Z. Zhan, J. Dakka, J. G. Santiesteban and E. Iglesia, *J. Phys. Chem. C*, 2007, **111**, 1402–1411.
- 14 M. S. Avila, C. I. Vignatti, C. R. Apesteguía and T. F. Garetto, *Chem. Eng. J.*, 2014, **241**, 52–59.
- 15 A. Dejoz, J. M. López Nieto, F. Melo and I. Vázquez, *Ind. Eng. Chem. Res.*, 1997, **36**,

- 2588–2596.
- 16 C. Resini, F. Catania, S. Berardinelli, O. Paladino and G. Busca, *Appl. Catal. B Environ.*, 2008, **84**, 678–683.
 - 17 A. Villa, N. Janjic, P. Spontoni, D. Wang, D. S. Su and L. Prati, *Appl. Catal. A Gen.*, 2009, **364**, 221–228.
 - 18 L. Chen, K. Zhu, L. H. Bi, A. Suchopar, M. Reicke, G. Mathys, H. Jaensch, U. Kortz and R. M. Richards, *Inorg. Chem.*, 2007, **46**, 8457–8459.
 - 19 A. Schwartz, L. L. Holbrook and H. Wise, *J. Catal.*, 1971, **21**, 199–207.
 - 20 D. E. Gawthrope, A. F. Lee and K. Wilson, *Phys. Chem. Chem. Phys.*, 2004, **6**, 3907–3914.
 - 21 T. F. Garetto, E. Rincón and C. R. Apesteguía, *Appl. Catal. B Environ.*, 2007, **73**, 65–72.
 - 22 K. Fischer and M. Wilken, *J. Chem. Thermodyn.*, 2001, **33**, 1285–1308.
 - 23 R. J. Baxter and P. Hu, *J. Chem. Phys.*, 2002, **116**, 4379–4381.
 - 24 F. H. Ribeiro, M. Boudart, R. A. Dalla Betta and E. Iglesia, *J. Catal.*, 1991, **130**, 498–513.
 - 25 A. Bravo, H. R. Bjorsvik, F. Fontana, F. Minisci and A. Serri, *J. Org. Chem.*, 1996, **61**, 9409–9416.
 - 26 J. Haber, J. H. Block and B. Delmon, in *Handbook of Heterogeneous Catalysis*, Wiley-VCH Verlag GmbH & Co. KGaA, Weinheim, Germany, 2008, pp. 1230–1258.
 - 27 V. S. Arutyunov, R. N. Magomedov, A. Y. Proshina and L. N. Strekova, *Chem. Eng. J.*, 2014, **238**, 9–16.
 - 28 D. I. Iordanoglou, A. S. Bodke and L. D. Schmidt, *J. Catal.*, 1999, **187**, 400–409.

- 29 S. Demirel-Gülen, M. Lucas and P. Claus, *Catal. Today*, 2005, **102–103**, 166–172.
- 30 J. R. Bourne, *Org. Process Res. Dev.*, 2003, **7**, 471–508.
- 31 A. Dubey, V. Rives and S. Kannan, *J. Mol. Catal. A Chem.*, 2002, **181**, 151–160.
- 32 L. N. Ji, M. Liu, A. K. Hsieh and T. S. A. Hor, *J. Mol. Catal.*, 1991, **70**, 247–257.
- 33 H. Gruber-Woelfler, P. F. Radaschitz, P. W. Feenstra, W. Haas and J. G. Khinast, *J. Catal.*, 2012, **286**, 30–40.
- 34 R. A. Sheldon, M. Wallau, I. W. C. E. Arends and U. Schuchardt, *Acc. Chem. Res.*, 1998, **31**, 485–493.
- 35 H. U. Blaser, A. Indolese, A. Schnyder, H. Steiner and M. Studer, *J. Mol. Catal. A Chem.*, 2001, **173**, 3–18.
- 36 N. Noguchi, Y. Morinaga, T. Kajio, E. Yogarajah and T. Nawa, *J. Am. Ceram. Soc.*, 2018, **101**, 4549–4559.
- 37 D. Wildhagen, V. Krivan, B. Gercken and J. Pavel, *J. Anal. At. Spectrom.*, 1996, **11**, 371–377.
- 38 F. Regali, L. F. Liotta, A. M. Venezia, M. Boutonnet and S. Järås, *Appl. Catal. A Gen.*, 2014, **469**, 328–339.
- 39 J. Speder, L. Altmann, M. Bäumer, J. J. K. Kirkensgaard, K. Mortensen and M. Arenz, *RSC Adv.*, 2014, **4**, 14971–14978.
- 40 L. Salvati, L. E. Makovsky, J. M. Stencel, F. R. Brown and D. M. Hercules, *J. Phys. Chem.*, 1981, **85**, 3700–3707.
- 41 T. Kim and I. E. Wachs, *J. Catal.*, 2008, **255**, 197–205.
- 42 M. Aronniemi, J. Lahtinen and P. Hautojärvi, *Surf. Interface Anal.*, 2004, **36**, 1004–1006.

- 43 V. A. J. Silva, P. L. Andrade, M. P. C. Silva, A. Bustamante D., L. De Los Santos Valladares and J. Albino Aguiar, *J. Magn. Magn. Mater.*, 2013, **343**, 138–143.
- 44 J. Du and H. Sun, *ACS Appl. Mater. Interfaces*, 2014, **6**, 13535–13541.
- 45 X. An, H. Liu, J. Qu, S. J. A. Moniz and J. Tang, *New J. Chem.*, 2015, **39**, 314–320.
- 46 X. Jiang, M. Manawan, T. Feng, R. Qian, T. Zhao, G. Zhou, F. Kong, Q. Wang, S. Dai and J. H. Pan, *Catal. Today*, 2018, **300**, 12–17.
- 47 J. M. Thomas, R. Raja, G. Sankar and R. G. Bell, *Acc. Chem. Res.*, 2001, **34**, 191–200.
- 48 A. H. Lu, J. J. Nitz, M. Comotti, C. Weidenthaler, K. Schlichte, C. W. Lehmann, O. Terasaki and F. Schüth, *J. Am. Chem. Soc.*, 2010, **132**, 14152–14162.
- 49 R. J. White, R. Luque, V. L. Budarin, J. H. Clark and D. J. MacQuarrie, *Chem. Soc. Rev.*, 2009, **38**, 481–494.
- 50 N. Perkas, Y. Koltypin, O. Palchik, A. Gedanken and S. Chandrasekaran, *Appl. Catal. A Gen.*, 2001, **209**, 125–130.
- 51 R. Raja and J. M. Thomas, *Chem. Commun.*, 1998, 1841–1842.
- 52 L. M. Slaughter, J. P. Collman, T. A. Eberspacher and J. I. Brauman, *Inorg. Chem.*, 2004, **43**, 5198–5204.
- 53 M. Aryafar and F. Zaera, *Catal. Letters*, 1997, **48**, 173–183.
- 54 J. A. Labinger and J. E. Bercaw, *Nature*, 2002, **417**, 507–514.
- 55 M. Bowker, A. Nuhu and J. Soares, *Catal. Today*, 2007, **122**, 245–247.
- 56 G. Yudoyono, N. Ichzan, V. Zharvan, R. Daniyati, H. Santoso, B. Indarto, Y. H. Pramono, M. Zainuri and Darminto, in *AIP Conference Proceedings*, 2016, vol. 1725.
- 57 N. H. Phu, T. T. K. Hoa, N. Van Tan, H. V. Thang and P. Le Ha, *Appl. Catal. B*

- Environ.*, 2001, **34**, 267–275.
- 58 P. Gallezot, *Catal. Today*, 1997, **37**, 405–418.
- 59 W.-X. Li, C. Stampfl and M. Scheffler, *Phys. Rev. Lett.*, 2003, **90**, 256102.
- 60 H. Zhao, J. Zhou, H. Luo, C. Zeng, D. Li and Y. Liu, *Catal. Letters*, 2006, **108**, 49–54.
- 61 R. Lloyd, R. L. Jenkins, M. Piccinini, Q. He, C. J. Kiely, A. F. Carley, S. E. Golunski, D. Bethell, J. K. Bartley and G. J. Hutchings, *J. Catal.*, 2011, **283**, 161–167.
- 62 R. Burch, D. J. Crittle and M. J. Hayes, *Catal. Today*, 1999, **47**, 229–234.
- 63 M. G. Clerici, *Appl. Catal.*, 1991, **68**, 249–261.
- 64 J. Poltowicz, K. Pamin, L. Matachowski, E. M. Serwicka, R. Mokaya, Y. Xia and Z. Olejniczak, *Catal. Today*, 2006, **114**, 287–292.
- 65 E. Armengol, A. Corma, V. Forne, H. Garcõ and J. Primo, *Appl. Catal. A Gen.*, 1999, **181**, 305–312.
- 66 J. Na, G. Liu, T. Zhou, G. Ding, S. Hu and L. Wang, *Catal. Letters*, 2013, **143**, 267–275.
- 67 T. Naicker and H. B. Friedrich, *J. Porous Mater.*, 2013, **20**, 763–775.
- 68 N. Kosinov, C. Liu, E. J. M. Hensen and E. A. Pidko, *Chem. Mater.*, 2018, **30**, 3177–3198.
- 69 H. Kosslick, G. Lischke, B. Parltitz, W. Storek and R. Fricke, *Appl. Catal. A Gen.*, 1999, **184**, 49–60.
- 70 Y. Furumoto, Y. Harada, N. Tsunoji, A. Takahashi, T. Fujitani, Y. Ide, M. Sadakane and T. Sano, *Appl. Catal. A Gen.*, 2011, **399**, 262–267.
- 71 B. Chakraborty and B. Viswanathan, *Catal. Today*, 1999, **49**, 253–260.
- 72 C. A. Wilde, Y. Ryabenkova, I. M. Firth, L. Pratt, J. Railton, M. Bravo-Sanchez, N.

- Sano, P. J. Cumpson, P. D. Coates, X. Liu and M. Conte, *Appl. Catal. A Gen.*, 2019, **570**, 271–282.
- 73 S. J. Tauster, S. C. Fung and R. L. Garten, *J. Am. Chem. Soc.*, 1978, **100**, 170–175.
- 74 H. X. Yuan, Q. H. Xia, H. J. Zhan, X. H. Lu and K. X. Su, *Appl. Catal. A Gen.*, 2006, **304**, 178–184.
- 75 S. Guerrero, J. T. Miller and E. E. Wolf, *Appl. Catal. A Gen.*, 2007, **328**, 27–34.
- 76 O. Desponds, R. L. Keiski and G. A. Somorjai, *Catal. Letters*, 1993, **19**, 17–32.
- 77 R. R. C. M. Silva, H. A. Oliveira, A. C. P. F. Guarino, B. B. Toledo, M. B. T. Moura, B. T. M. Oliveira and F. B. Passos, *Int. J. Hydrogen Energy*, 2016, **41**, 6763–6772.
- 78 W. X. Huang, J. W. Teng, T. X. Cai and X. H. Bao, *Stud. Surf. Sci. Catal.*, 2000, **100**, 1409–1414.
- 79 I. Nowak and M. Ziolk, *Chem. Rev.*, 1999, **99**, 3603–3624.
- 80 R. D. Bach and O. Dmitrenko, *J. Am. Chem. Soc.*, 2004, **126**, 4444–4452.
- 81 L. Yu-Ran, *Comprehensive Handbook of Chemical Bond Energies*, CRC Press, Boca Raton, 1st edn., 2007.
- 82 C. J. Stephenson, J. T. Hupp and O. K. Farha, *Inorg. Chem. Front.*, 2015, **2**, 448–452.
- 83 B. P. C. Hereijgers and B. M. Weckhuysen, *J. Catal.*, 2010, **270**, 16–25.
- 84 D. Prieto-Centurion and J. M. Notestein, *J. Catal.*, 2011, **279**, 103–110.
- 85 *US patent.*, *US2857364*, 1954.
- 86 D. P. Bezerra, R. S. Oliveira, R. S. Vieira, C. L. Cavalcante and D. C. S. Azevedo, *Adsorption*, 2011, **17**, 235–246.
- 87 M. Sugimoto, H. Katsuno, K. Takatsu and N. Kawata, *Zeolites*, 1987, **7**, 503–507.
- 88 B. Xu, S. Bordiga, R. Prins and J. A. van Bokhoven, *Appl. Catal. A Gen.*, 2007, **333**,

245–253.

- 89 J. Haber, J. H. Block and B. Delmon, *Pure Appl. Chem.*, 1995, **67**, 1257–1306.

CHAPTER 5: The synthesis of micro and mesoporous titanium oxide, varying template removal techniques and subsequent catalytic testing

Contents

CHAPTER 5: The synthesis of micro and mesoporous titanium oxide, varying template removal techniques and subsequent catalytic testing.....	221
Abbreviations	222
5.1. Introduction	223
5.2. Antonelli's protocol for the synthesis of microporous titanium oxide	225
5.2.1. Change of ratio of titanium precursor to amine template	233
5.2.2. Varying autoclave conditions	234
5.2.3. Varying titanium alkoxide precursor	237
5.2.4. Introduction of dopant metals during synthesis	239
5.2.5. Thermal resistance and calcination for template removal.....	243
5.2.6. Template removal: Acidification	246
5.2.6.1. Acidification via HNO ₃	246
5.2.6.2. Acidification with <i>p</i> -TSA.....	252
5.2.7. Summary of template removal attempts – calcination and acidification	252
5.2.8. Template removal: Alternatives to acid	253
5.2.8.1. Hydrogen peroxide	253
5.2.8.2. Phthalic anhydride.....	257
5.2.9. Reaction resistance and catalytic tests	259
5.3. Dai and Zhang synthesis of microporous titanium oxide.....	261
5.3.1. Alternative synthesis of microporous titanium oxide with amine templates.....	262
5.3.2. Template removal - Zhang	263
5.4. Non-template synthesis method: Peptization	265
5.4.1. Synthesis and subsequent metal loading	265
5.4.2. Catalytic testing	267
5.4.2.1. <i>n</i> -decane	267
5.4.2.2. Cyclooctane	268
5.5. Conclusions and future work	271
5.6. References	272

Abbreviations

BET – Brunauer-Emmet-Teller

CTAB – Cetyltrimethylammonium Bromide

DMF – Dimethylformamide

FTIR-ATR – Fourier Transform Infra-Red – Attenuated Total Reflectance

GC-MS – Gas Chromatography – Mass Spectrometry

ICP-OES – Inductively Coupled Plasma – Optical Emission Spectrometry

MCM-41 – Mobil Composition of Matter #41

M:S – Metal to substrate ratio

PO_2 – Pressure Gauge O_2

p-TSA – *para* Toluene Sulfonic Acid

TGA – Thermogravimetric Analysis

TMS-1 – Transition Metal Oxide Molecular Sieve #1

TS-1 – Titanium Silicate #1

XRPD – X-ray Powder Diffraction

XPS – X-ray Photoelectron Spectroscopy

ZSM-5 – Zeolite Socony Mobil #5

5.1. Introduction

The hydrothermal synthesis of mesoporous and microporous metal oxides is a highly complex process from a chemical perspective, despite the relative low difficulty of practical techniques used to synthesise these materials. In fact, the synthesis of these materials involves self-assembly steps¹ which once started are not under the control of the operator anymore. The challenge of the synthesis arises from what conditions should be used from the multitude possible, all of which will have an effect during the delicate pore formation. The goal of this project was to synthesise a highly porous, uniform, and chemically resistant material, with any template removed from the final product. The parameters for making these materials, as well as the effects of these parameters to the synthesis, are explored here.

As mentioned previously titanium oxide has been chosen as the focal material due to its theoretical desired properties which will be applied during alkane oxidation. Examples of microporous titanium oxide within literature are relatively limited; however, several authors have published its synthesis and subsequent template removal, each with their own 'ideal conditions' for maximum porosity and uniformity. These different methods were conducted and altered in order to achieve the optimum material.

The two main analytical methods used to determine porosity throughout the literature are XRPD (x-ray powder diffraction) and BET (Brunauer-Emmett-Teller)/porosimetry. XRPD is used to identify reflections within the regions of $1 - 15^\circ 2\theta$ (this will be referred to as the 'porous region', as reflections in this range correspond to interlunar distances of 8.8 to 0.6 nm). If there are any reflections here, the 2θ value can be used to determine the pore diameter (see section 2.5.6). Furthermore, it is used to determine if any other reflections are present beyond this region as this would suggest crystallinity in other phases (and thus it can be determined if any unwanted phases are present). For example, the polymorphs rutile and/or anatase would be present if titanium oxide crystallised into bulk TiO_2 .² BET/porosimetry is used to determine surface area, pore size and pore volume.³ Out of the two methods XRPD was chosen to be a primary indicator for porosity as this would show if the material has

reflections in the porous region (and is not just amorphous) as: (i) it is quicker and easier to run than BET, and (ii) XRPD is sensitive to highly crystalline phases, unlike BET/porosimetry which can be applied to amorphous systems too. And as we were interested in crystalline porous materials, XRPD was serving these two scopes in a more practical manner.

Once the material has been synthesised successfully, the challenge of template removal arises.^{4,5} This is a very general problem involved in the synthesis of micro or meso- porous materials. In fact, the template must be removed as diffusion of molecules in and out of the pores must not be limited, nor can the active sites be blocked. However, as the template is chemically bound to the titanium, its removal can cause pore collapse (analogous to removing the inner supports from a tunnel), possibly rendering the material unsuitable for shape-selective catalysis. Therefore, delicate tweaking of template removal was conducted in order to optimise the properties of the final material.

5.2. Antonelli's protocol for the synthesis of microporous titanium oxide

Antonelli and co-workers have done significant research into the synthesis of multiple types of porous metal oxides.^{1,6-9} Due to a few papers reporting successful synthesis and template removal, the synthesis of microporous titanium oxide was considered to be a good starting point for this project. Specifically, the synthetic protocol where titanium isopropoxide and hexylamine were utilised as precursors and the template was removed through solvent washes.^{6,9} However, despite initially replicating the protocol in full in our laboratory, the material yielded did not have any reflections in the XRPD pattern as reported in literature (figure 5.2.1).

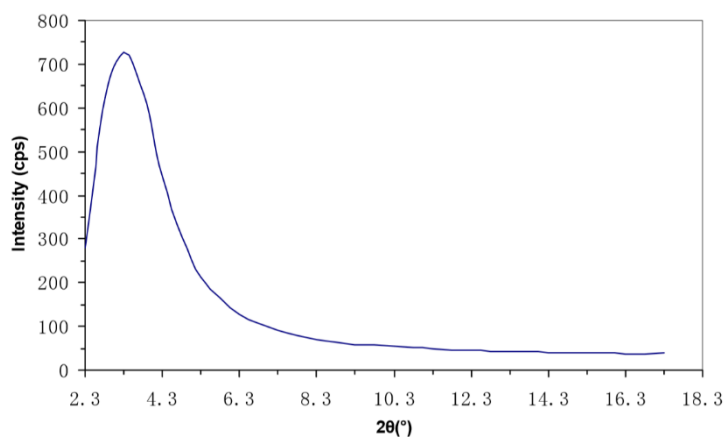


Figure 5.2.1: An XRPD pattern of microporous titanium oxide from D.M Antonelli *et al.* to show the reflection corresponding to the material's porosity. Figure reproduced here with permission from *X. Hu et al.*⁹

Therefore, the synthesis was conducted several times but stopping and retrieving samples at specific points (figure 5.2.2).

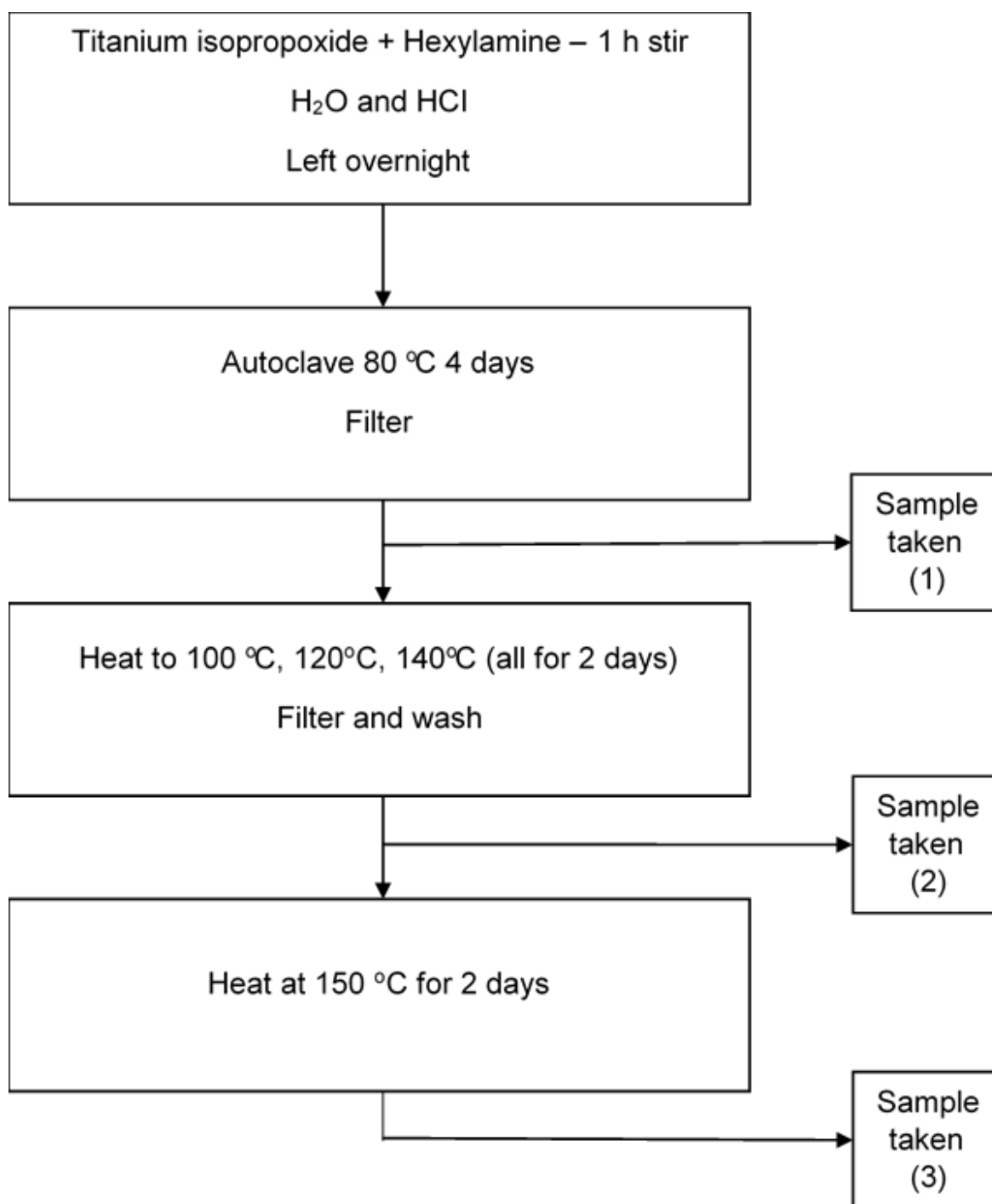


Figure 5.2.2: A diagram to show steps in the synthesis of mesoporous titanium oxide as reported by Antonelli. Samples were taken at specified steps for analysis (specifically XRPD) to determine the presence of pores and template.

Following all the steps as reported in the synthesis yielded non-porous material, however, porosity *is* present in the initial steps. The sample taken after heating at 100 °C – 140 °C and the sample after the final drying step at 150 °C (samples 2 – 3) were found to be non-porous via XRPD, whereas the initial 80 °C autoclave (sample 1) gave porous titanium oxide, which will be referred to as ‘Ti-TMS1’, see figure 5.2.3.

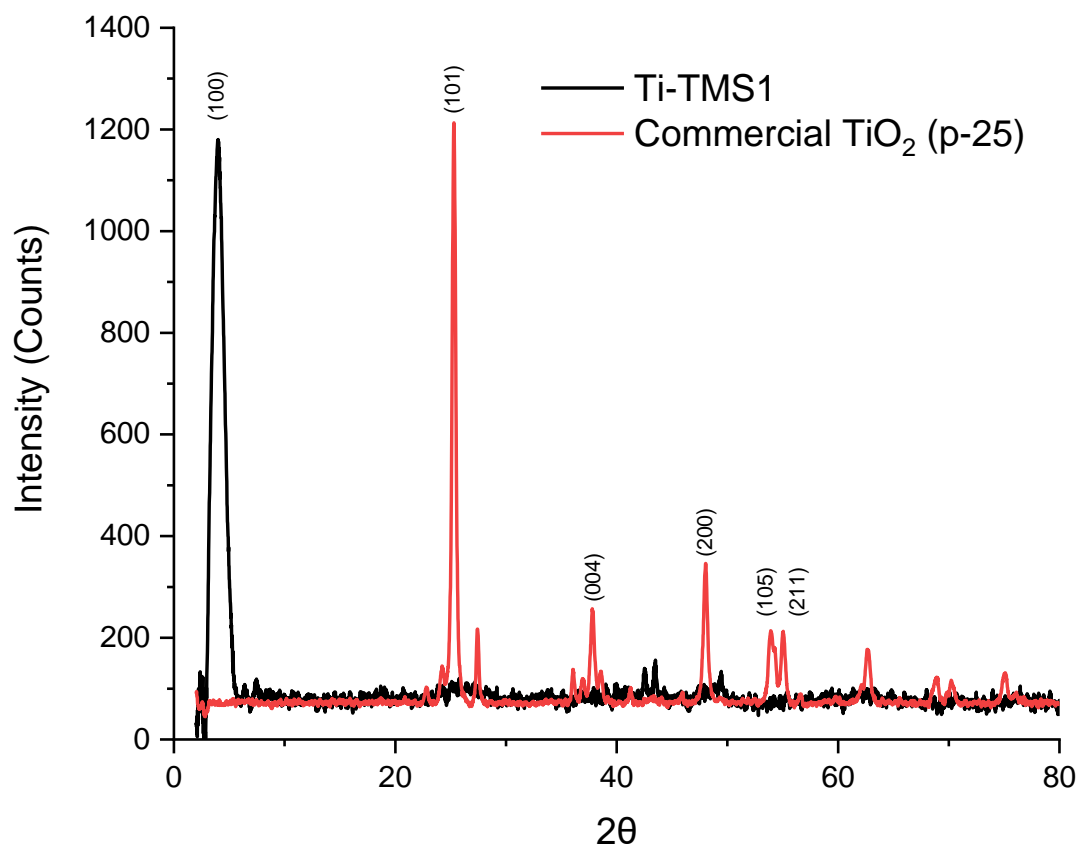


Figure 5.2.3: XRPD patterns of as-synthesised mesoporous titanium oxide with commercial p-25 (y-axis normalised) included as a term of comparison. A single reflection ($d = 22.1 \text{ \AA}$) due to the presence of pores can be seen in the mesoporous titanium oxide pattern with relatively no crystallinity in the bulk phase. (-) Mesoporous titanium oxide: $\text{Ti}(\text{O}i\text{Pr})_4$ and hexylamine (2:1) Autoclave 80 °C, 96 h, washed with H_2O (3 x 50 mL), MeOH (3 x 50 mL) and Et_2O (3 x 50 mL), (-) Commercial TiO_2 (p-25). The most intense peaks of the anatase pattern are assigned from literature,¹⁰⁻¹² and the microporous peak of titanium oxide.^{13,14}

A single relatively broad peak is observed in the mesoporous titanium oxide XRPD pattern. This signifies the existence of crystalline pores corresponding to a pore diameter of 22.1 \AA , which is larger than the reported pore size (12 \AA).⁹ However, as this is on the cusp of being microporous the material is still within the desired range for shape selective catalysis of

alkanes. Pentylamine and butylamine were not utilised as templates as they are reported to lead to poorer crystalline samples.¹³ As pore sizes of ~2 nm were desired for the application of shape-selective catalysis for our scope¹⁵⁻¹⁷ hexylamine remained as the template of choice. Although templates of longer chain lengths may lead to better micelle formation, they would also, in theory, lead to larger undesired pore sizes (see section 5.3 for discussions on the use of longer templates). The broadness of the peak and its Gaussian shape suggests that a distribution of pores exist, and 22.1 Å would represent the average for this sample. Comparing the rest of the pattern no other peaks, besides two small peaks at 42-45° 2 θ , are present within the mesoporous titanium oxide sample. This was desired as little to no crystallinity in the bulk phase means that only reflections from the pores exist.

This result was complemented with porosimetry (figure 5.2.4), showing most of the pores lying around 2 nm, gradually tailing off to broader pores. This material was synthesised a large number of times (>20) across the entire project, giving an average pore size of 22.4 (\pm 0.3) Å determined through XRPD analysis, which before template removal has to be considered a highly reproducible and statistically robust preparation method.

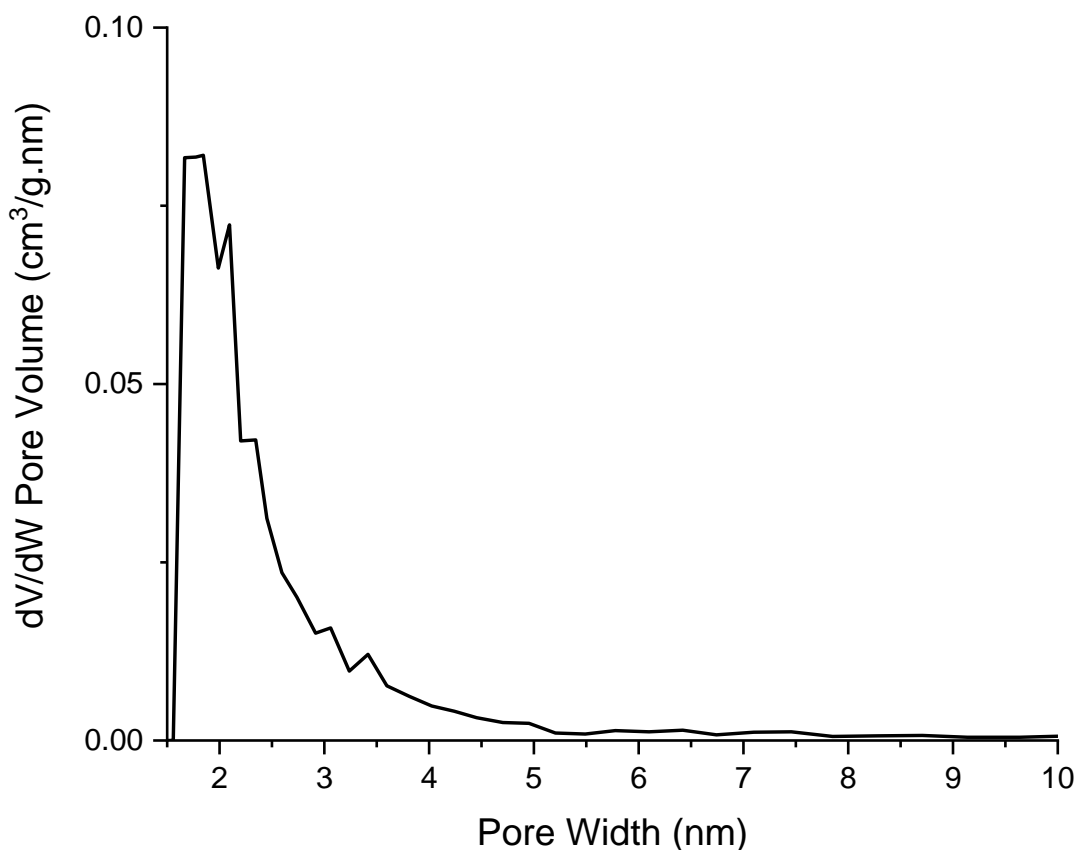


Figure 5.2.4: Porosimetry data showing the trace of as-synthesised mesoporous titanium oxide. The area under the graph is focused at 2 nm and exponentially decreases beyond this suggesting most pores have a diameter of 2 – 2.5 nm. Mesoporous titanium oxide as synthesised: Ti:Hexylamine = 2:1, Autoclave: 80 °C, 96 h, washed with H₂O (3 x 50 mL), MeOH (3 x 50 mL) and Et₂O (3 x 50 mL).

The ATR-FTIR (attenuated total reflectance – Fourier transform infrared) (figure 5.2.5) showed the presence of organic material. As no template removal has been conducted at this point, it was expected the hexylamine would still be present within the porous structure. The C-H stretch (2700 – 3100 cm⁻¹) and a broad O-H stretch (~2750 – 3500 cm⁻¹) can be seen in the spectra, with additional unassigned peaks.¹⁸ The additional peaks (1250 – 1700 cm⁻¹) were attributed to the N-H bond,¹⁹ potential lattice vibrations commonly observed in zeolites^{20,21} and adsorbed water¹⁸.

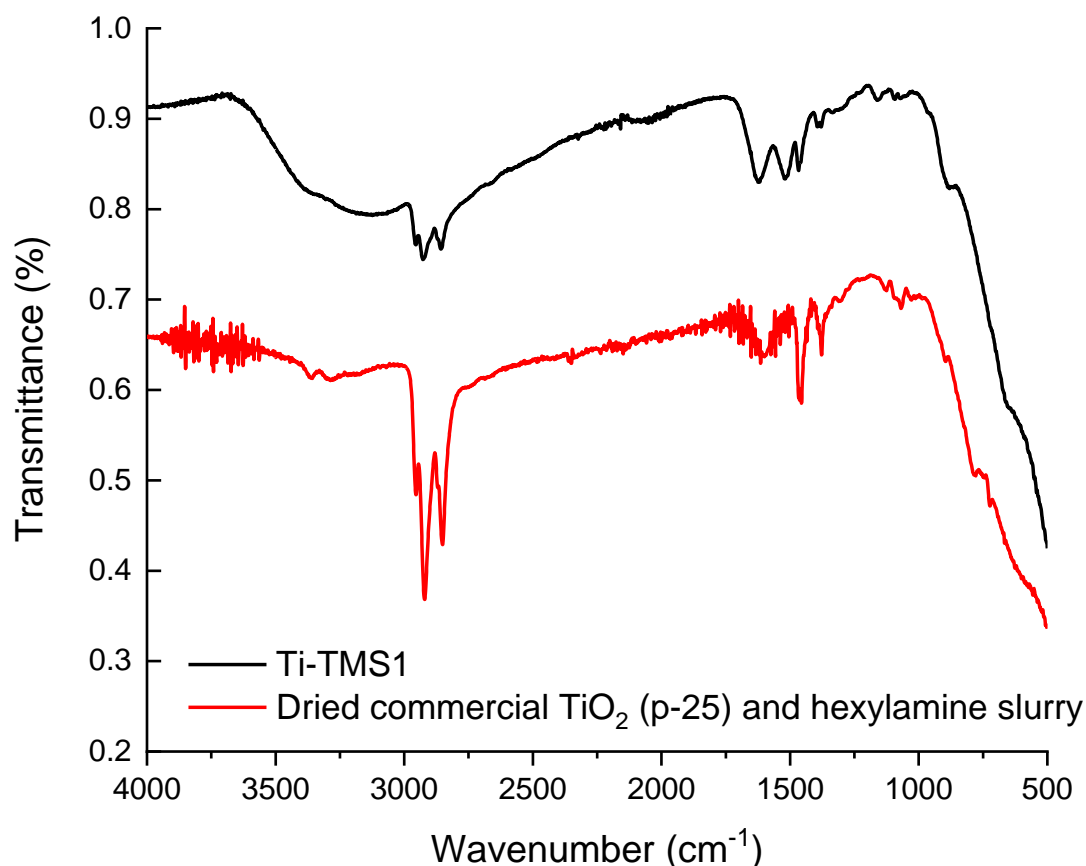


Figure 5.2.5: ATR-FTIR spectra of as-synthesised mesoporous titanium oxide with dried commercial p-25 and hexylamine slurry as a means of comparison. The C-H stretch (2700 – 3100 cm^{-1}), O-H stretch (~2750 – 3500 cm^{-1}) and potentially additional hexylamine N-H/lattice vibration peaks (1250 – 1700 cm^{-1}) can be seen. (-) Mesoporous titanium oxide as synthesised: Ti:Hexylamine = 2:1, Autoclave: 80 °C, 96 h, washed with H_2O (3 x 50 mL), MeOH (3 x 50 mL) and Et_2O (3 x 50 mL) (-) Dried Commercial TiO_2 (p-25) and hexylamine slurry (based on Ti:Hexylamine = 2:1).

The TGA (thermogravimetric analysis) (figure 5.2.6) also showed the significant presence of the amine template. An initial mass loss of 5 wt% at ca. 120 °C is water, 28 wt% is hexylamine from 300 °C to 520 °C¹⁸ and the remainder of the material is TiO_2 . A control test by using commercial titanium oxide with hexylamine, to confirm the weight loss is indeed our template (prepared by drying a slurry with water), shows the shape of the TGA profile was virtually overlapping with the mesoporous sample. The mass loss being significantly lower in the dried slurry is expected as the amine would not bind to the titanium oxide and instead just be dried onto the surface.

The expected wt% of amine is not present in the as synthesised mesoporous titanium oxide. An expected 38 wt% compared to an observed 28 wt% suggests that a proportion of template is lost during the synthesis. This is due to all the template not binding to the titanium isopropoxide and washed away with solvent. It was expected that all the amine would be bound to the metal alkoxide according to literature reporting analogous proposed mechanisms.^{1,7,14}

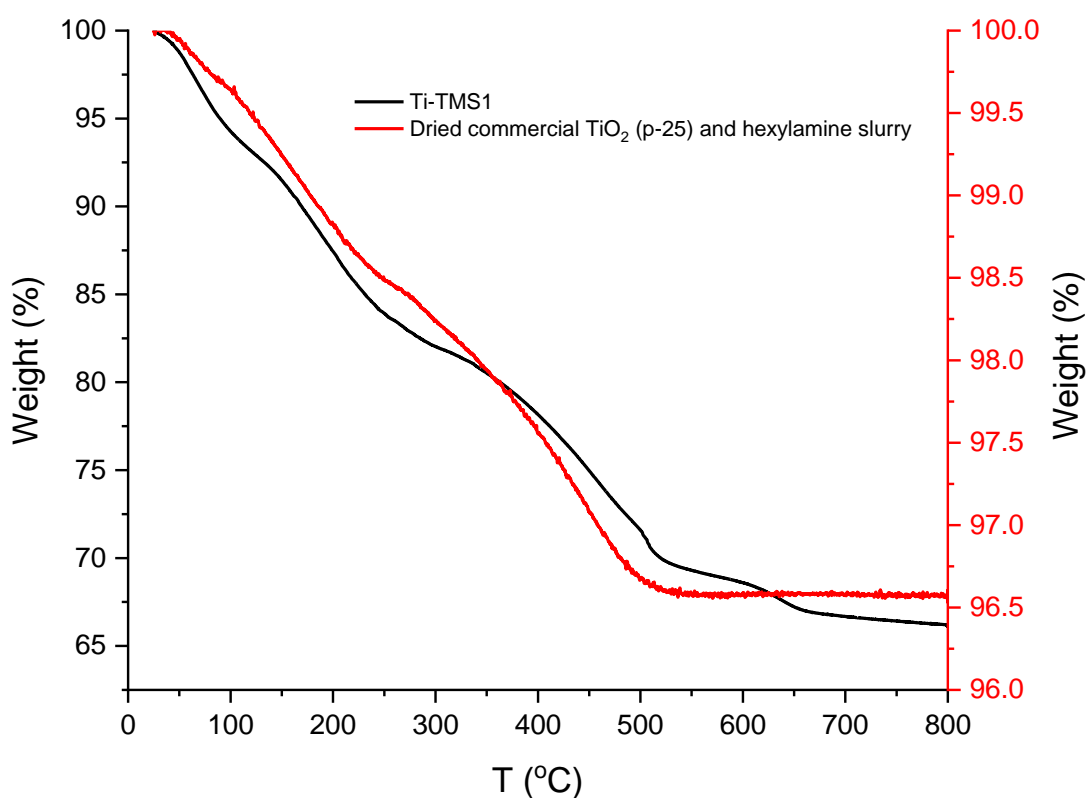


Figure 5.2.6: TGA of as-synthesised mesoporous titanium oxide with commercial p-25 and hexylamine (prepared via a dried slurry) for comparison. An initial mass loss from water/solvents from the synthesis is seen initially, followed by organic material decomposition from around 300 °C to 520 °C. (-) Mesoporous titanium oxide as synthesised: Ti:Hexylamine = 2:1, Autoclave: 80 °C, 96 h, washed with H₂O (3 x 50 mL), MeOH (3 x 50 mL) and Et₂O (3 x 50 mL). (-) Dried Commercial TiO₂ (p-25) and hexylamine slurry (based on Ti:Hexylamine = 2:1).

It was concluded that the synthesis conditions when conducted on a 1 g scale were in need of optimisation. This was reasoned as the material could not withstand elevated temperatures (both within the autoclave and during calcination, see sections 5.2.2 and 5.2.5 where this was further explored and quantified). This led to a series of modifications to the synthesis to try and optimise pore formation and the material's robustness and thermal resistance.

After washing several times with solvents (via filtration 3 x 50 mL with ethanol, methanol and ether as reported in the original protocol) and gentle heating (stirring sample with solvent near its corresponding boiling point < 80 °C), it was found that the template remained present and the material was not as resilient as initially expected based on the literature available.^{6,9} Because of this, the project focused on optimising the conditions for the synthesis of microporous titanium oxide and subsequent template removal by implementing systematic changes to the protocols available in literature.

5.2.1. Change of ratio of titanium precursor to amine template

Various literature has studied the effect of changing metal alkoxide precursor to amine template ratios when synthesising porous metal oxides.^{1,8,22-24} The mechanism for micelle formation in the synthesis suggests that the amine binds to the alkoxide in a 1:1 ratio. Furthermore, it was found with mesostructured Fe oxide that the samples with the largest porosity (from XRPD determinations) were those synthesised with an amine:alkoxide ratio of 1:1,⁸ this same molar ratio was therefore applied to improve porosity.

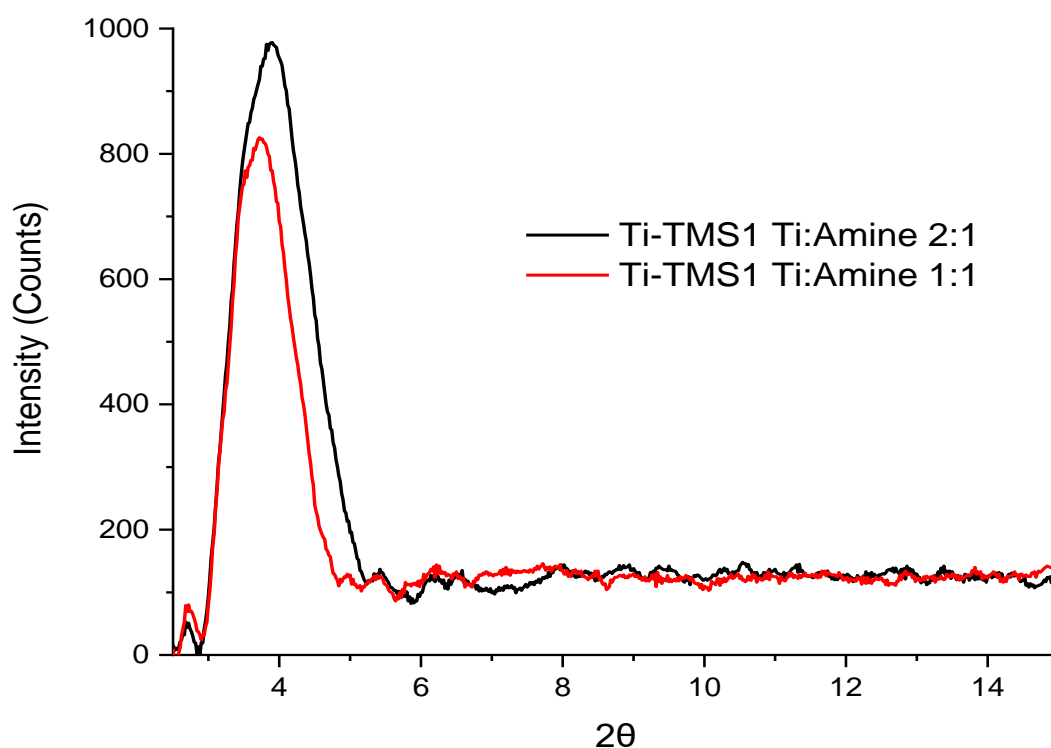


Figure 5.2.1.1: XRPD patterns of as-synthesised mesoporous titanium oxide with two examples where different ratios of titanium to hexylamine template were conducted.
(-) Mesoporous titanium oxide: $\text{Ti}(\text{O}^i\text{Pr})_4$ and hexylamine (molar ratio 2:1) Autoclave 80 °C, 96 h
(-) Mesoporous titanium oxide: $\text{Ti}(\text{O}^i\text{Pr})_4$ and hexylamine (molar ratio 1:1) Autoclave 80 °C, 96 h

From the XRPD (figure 5.2.1.1) alone it can be seen the intensity corresponding to the porous peak is slightly lower in 1:1 than that of the 2:1 sample. As no clear advantage was seen using a 1:1 ratio, the literature method of 2:1 was maintained. This is likely to be due to the template having a more complex role during the hydrothermal step and, for example, potentially forming a multitude of different phases depending on the amine concentration^{1,7,14}

5.2.2. Varying autoclave conditions

Temperature is a crucial parameter during the hydrothermal step of any microporous material synthesis. Not only does it provide energy to the reactants, but also changes the pressure within the sealed container. A low temperature may lead to no crystallisation at all, where high temperatures may lead to crystallisation in the bulk/undesired phases. Therefore, varying temperature was systematically trialled for the synthesis.

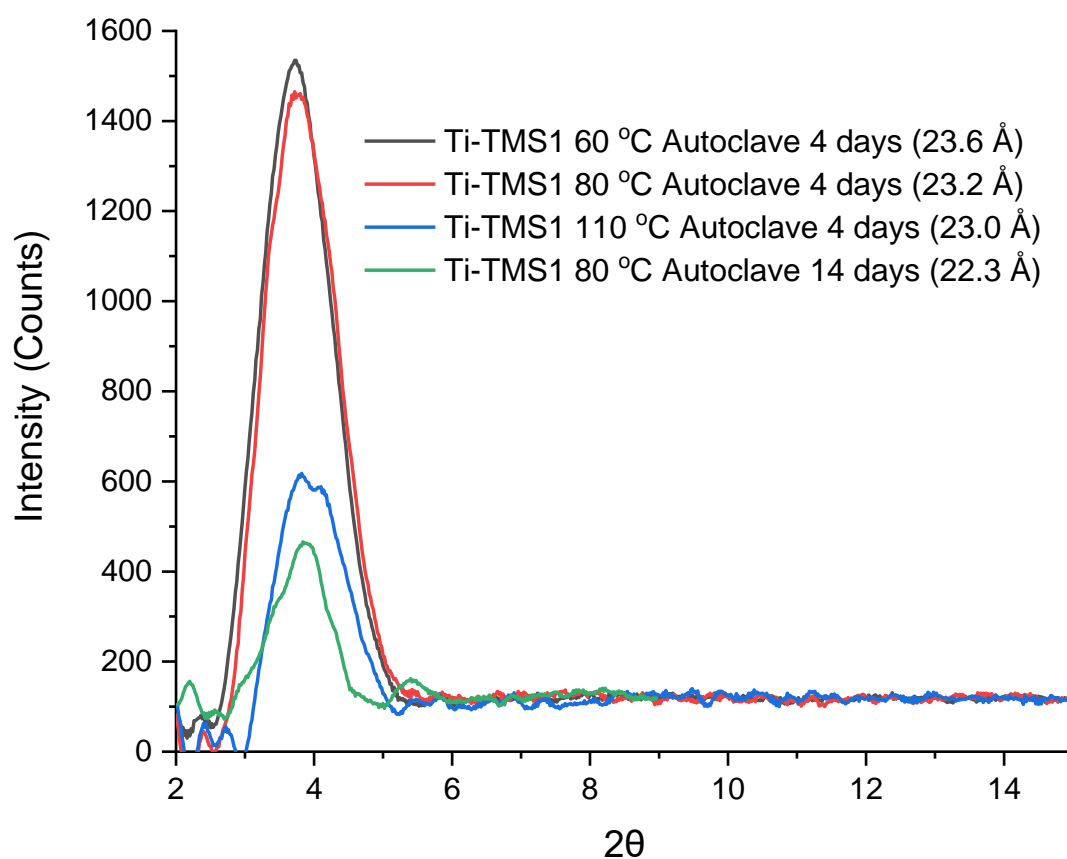


Figure 5.2.2.1: An overlay of XRPD patterns focusing on the characteristic reflection of porosity within mesoporous titanium oxide with varying temperature of the autoclave step and length of time within the autoclave. Autoclave temperature and hydrothermal step time: (-) 60 °C, 4 days, (-) 80 °C, 4 days, (-) 110 °C, 4 days, (-) 80 °C, 14 days.

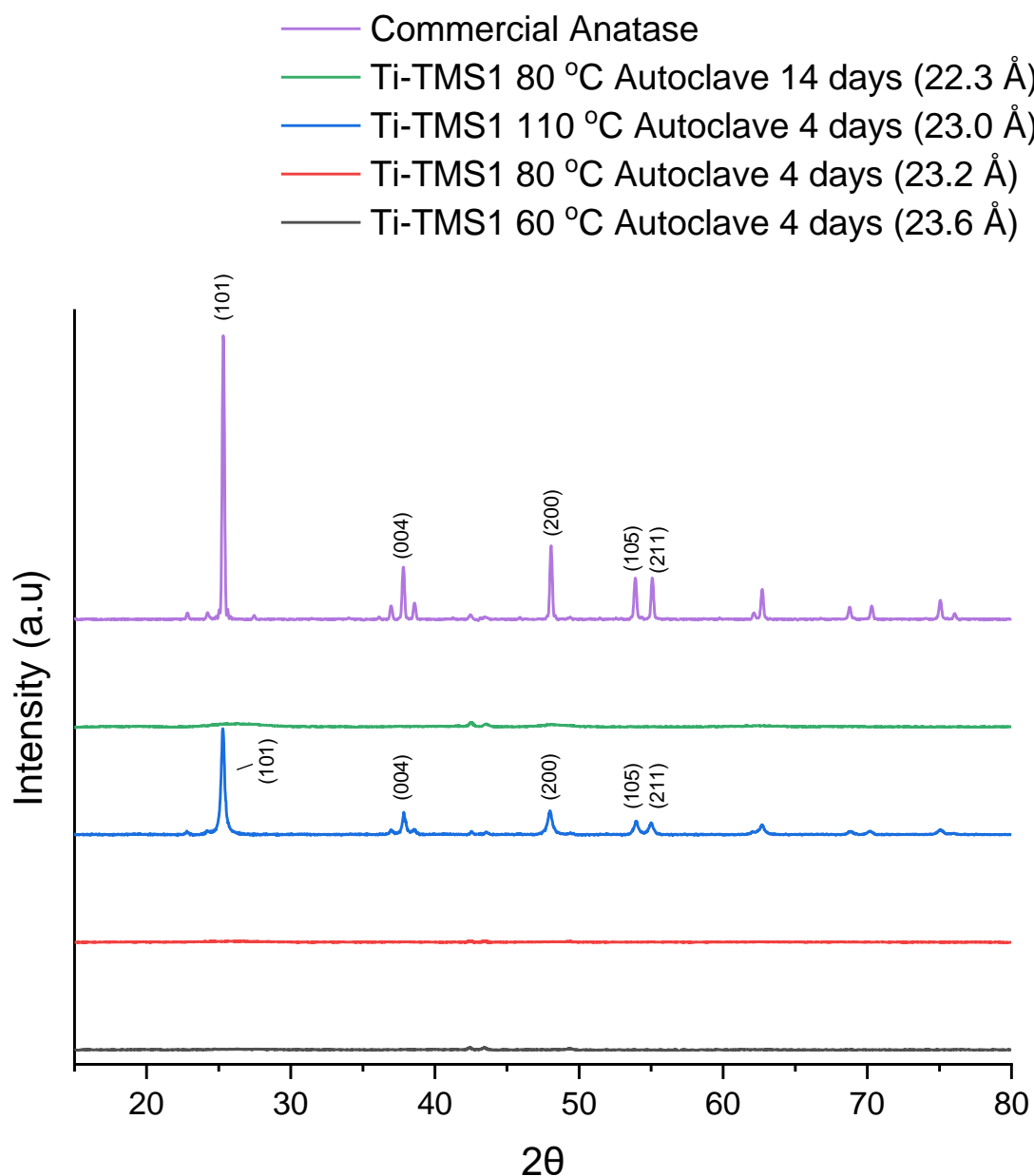


Figure 5.2.2.2: An overlay of XRPD patterns of mesoporous titanium oxide focusing on the bulk region with varying temperature of the autoclave step and length of time within the autoclave. The XRPD of commercial anatase is included as means of comparison to the crystallinity observed beyond 2θ in the 110 °C autoclave sample. From top to bottom XRPD patterns obtained from materials treated at: (-) 60 °C, 4 days, (-) 80 °C, 4 days, (-) 110 °C, 4 days, (-) 80 °C, 14 days. (-) Commercial anatase. The most intense peaks of anatase within the patterns are assigned from literature.¹⁰⁻¹²

Antonelli's study reported that 140 °C was the upper temperature limit of the autoclave step.⁶ However, it was found that drying samples at 120 °C overnight led to pore collapse. Therefore, temperatures of 60 °C, 80 °C and 110 °C were chosen to identify suitable conditions for the hydrothermal synthesis. Figures 5.2.2.1 and 5.2.2.2 show an autoclave step with 110 °C is unsuitable as crystallisation to anatase has occurred with a significantly lower intensity for the porous peak (~2½ times less than that when 80 °C was used). Whereas samples synthesised with 60 °C and 80 °C are identical and therefore 80 °C was chosen as the optimal condition, as this can be more easily controlled with our set-up.

To try and promote further crystallisation of our materials and pore formation, a synthesis with a longer aging time was conducted, as typically aging is done for 7 – 14 days for other microporous materials.^{1,14,24}

The sample synthesised via a 14-day autoclave step showed no difference in the bulk phase of the XRPD compared to the 4-day sample. However, porosity is significantly lower in the 14-day sample. This suggests that prolonged autoclave steps for longer aging causes crystallinity to decay to amorphous material.

Therefore, for the synthesis of mesoporous titanium oxide, an autoclave step was set at 4 days at 80 °C as standard procedure. Other parameters such as choice of alkoxide, implementing dopant metals and the various proposed template removal techniques were then explored.

5.2.3. Varying titanium alkoxide precursor

Micelle formation is an important part of the synthesis of microporous metal oxides. As this is dependent on the binding of the template to the precursor, varying titanium alkoxides were tested. Titanium isopropoxide exists as a monomer and therefore should be best suited for addition from an amine as the isopropyl ligands will be substituted. However, it was speculated that multiple substitutions could be occurring, leading to a potential tetraamine substituted titanium species. This could lead to the possibility of micelles not forming as effectively as they would in a mono-substituted species. To determine these possible effects titanium ethoxide (which exists as a tetramer) and a chelated titanium alkoxide, where only one position was available for substitution, were chosen as alternative candidates for the metal alkoxide precursor (see figure 5.2.3.1).

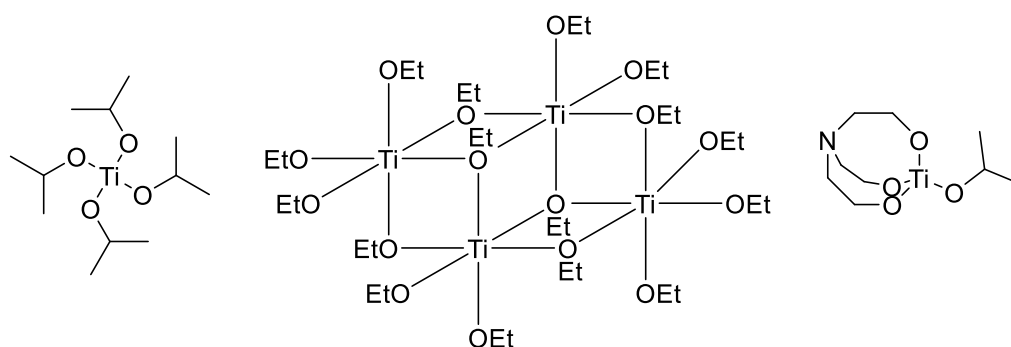


Figure 5.2.3.1: The titanium alkoxides trialled for microporous titanium oxide synthesis. Left: Titanium(IV) isopropoxide, which exists as a monomer; middle: Titanium(IV) ethoxide, which exists as a tetramer; right: Titanium(IV) (triethanolaminate)isopropoxide, which was chosen for its single substitution site (the isopropyl ligand) achieved from the chelate ligand being theoretically harder to displace.

All other conditions were maintained to determine the effect of the varying ligands.

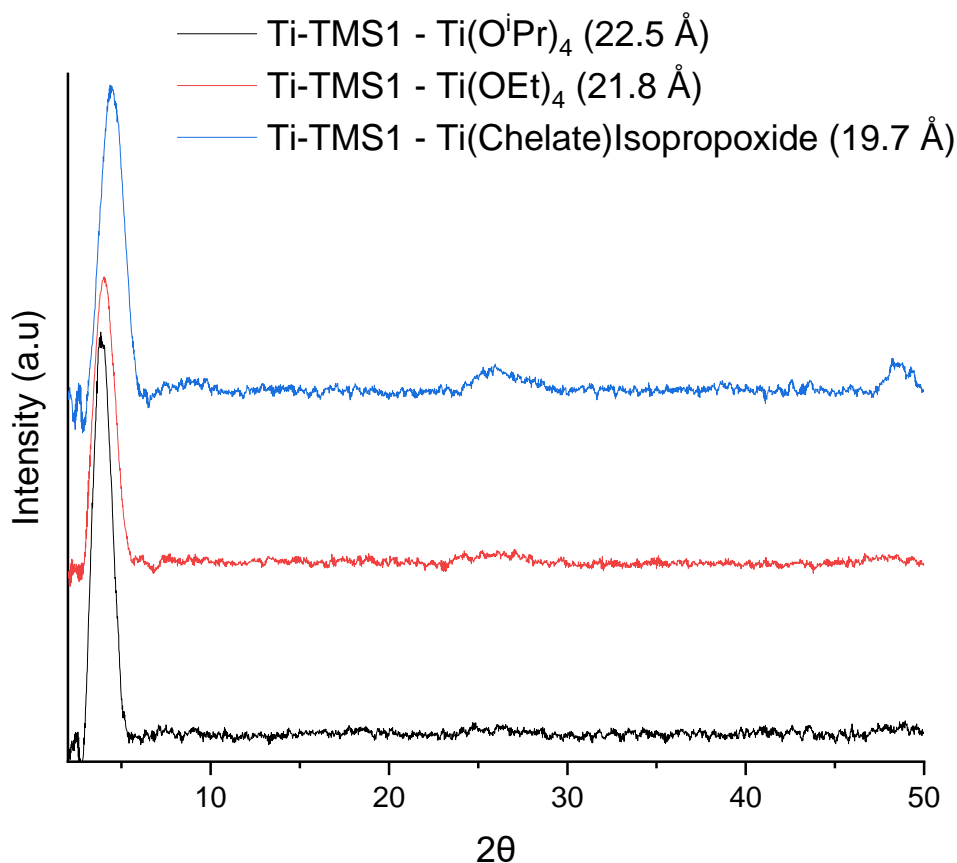


Figure 5.2.3.2: XRPD patterns for mesoporous and microporous titanium oxide as synthesised with varying metal alkoxide precursors. The patterns show the reflection from the micro/mesopores between 2° and 10° 2θ and the absence of reflections beyond 10° 2θ . Ti:Hexylamine 2:1, autoclave: 80°C , 96 h.

It can be seen from figure 5.2.3.2 that a variation in titanium alkoxide precursors does not significantly affect the porosity of the structure, at least for the precursors that we have selected. The intensity of the porous reflection is highest in the sample synthesised from titanium isopropoxide and the pore size only varies by 3 \AA amongst the samples. The only observable difference was the amount of water required to hydrolyse the titanium chelate isopropoxide during the pre-autoclave step. Usually observable hydrolysis (i.e. solid formation) occurs after one drop of water is added to the initial titanium alkoxide/ amine mixture when using $\text{Ti(IV)(O}^i\text{Pr)}_4$. Whereas in the chelated titanium alkoxide, hydrolysis did not occur until a significant amount of the water (ca. 3-4 mL from the 15 mL used) was added. This is likely due to hydrolysis being more difficult due to the chelate effect.

Due to no clear advantage when using the alternative alkoxides, titanium isopropoxide was maintained as the primary alkoxide used, as it is most prevalent in the literature. However, to the best of our knowledge this is the first example of the synthesis of microporous titanium oxide utilising a chelate ligand in the alkoxide precursor.

5.2.4. Introduction of dopant metals during synthesis

The main aim of this project was to synthesise materials where the active metal for catalysis is incorporated into the structure of the porous support. Therefore, metals which were active when doped onto bulk commercial supports (see section 4.2 – 4.3) and those which were prevalent oxidation catalysts throughout the literature were chosen to be incorporated during the initial introduction of titanium alkoxide and the template.

Incorporation was achieved by including a desired mol% of dopant metal precursor (i.e. a metal alkoxide or acetylacetonate) which would then bind to the amine like the titanium alkoxide, and thus ultimately be incorporated into the porous framework.

Figure 5.2.4.1 shows the XRPD patterns for the porous samples when a dopant metal is included. The characteristic reflection diagnostic of a mesoporous solid at ca. $4^\circ 2\theta$ in the diffraction pattern is present in all samples synthesised. Although no additional reflections are observed in the XRPD patterns, this does not necessarily mean all the dopant metals are part of the micro or meso-porous framework as intra-framework species, that is, part of a Ti-O-M-O-Ti structure where M is the dopant metal. In fact dopant metal could also exist, in principle, as small metal oxide clusters outside the pores of the mesoporous framework - a common occurrence, for example, in zeolites.²⁵⁻²⁷ In view of this, and because usually these small clusters are often observed in the case of a metal loading >5 wt%, control tests on bulk titanium oxide with large Fe content were carried out (see section 4.2.1.6). The additional peak present in mesoporous Ag/Ti-TMS1 at $38^\circ 2\theta$ is likely from metallic silver²⁸ and could be due to early hydrolysis (i.e. prior to micelle formation) of the precursor owing to its instability. To our knowledge these are the first examples of materials where a dopant metal has been included

into a porous titanium oxide framework during template synthesis, where titanium oxide is exclusively the framework, as opposed to TS-1 (titanium silicate-1).²⁹

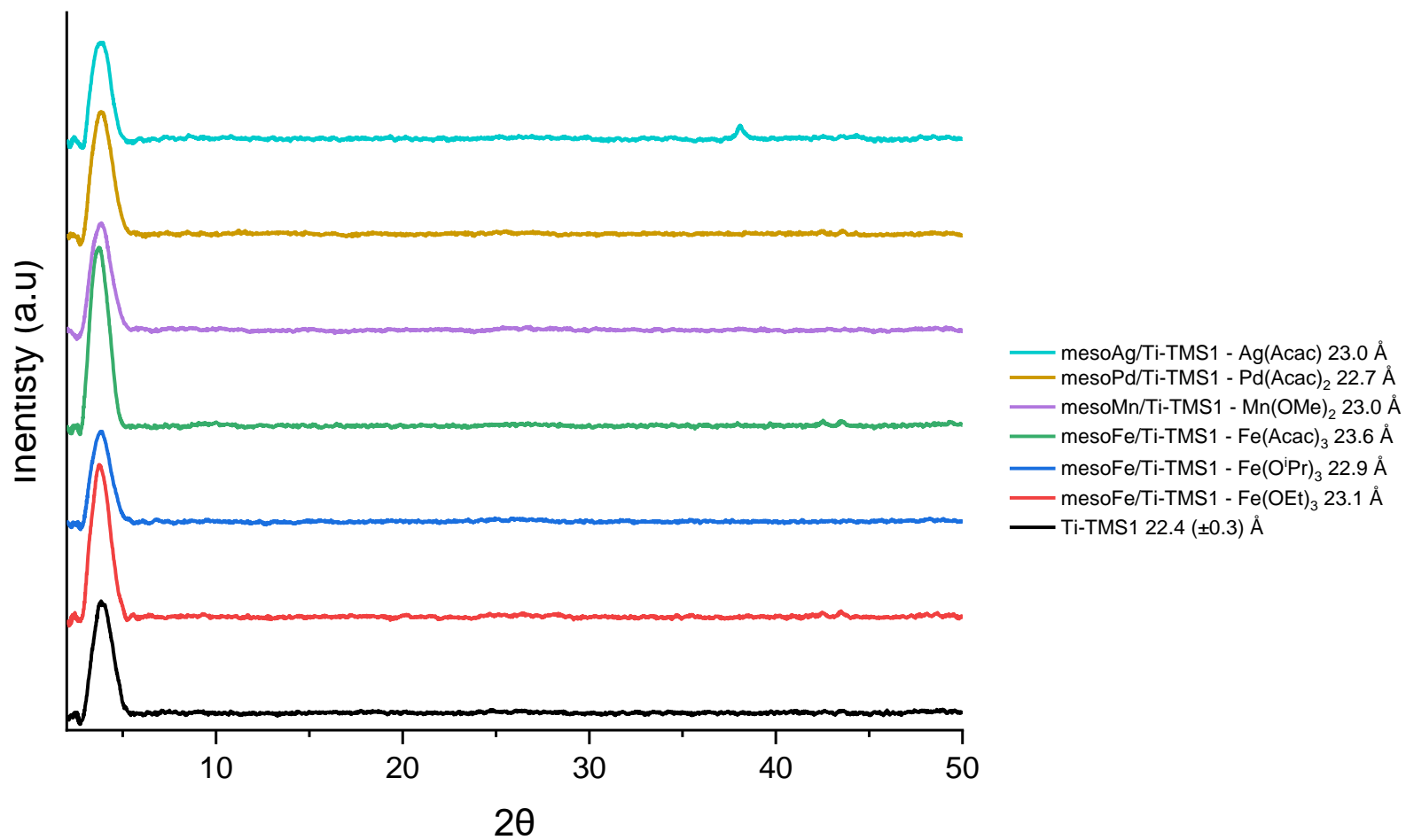


Figure 5.2.4.1: XRPD patterns of mesoporous titanium oxide, where a dopant metal has been incorporated into the synthesis. For all samples: dopant metal 2 mol%, Ti: Hexylamine 2:1, hydrothermal step: T= 80 °C, t = 96 h.

In order to gather additional structural information on our material and importantly to determine the chemical environment around the dopant metal present in these samples, XPS (x-ray photoelectron spectroscopy) was carried out. However, this method did not prove to be particularly informative with our samples. Mesoporous Fe/Ti-TMS1 was analysed, however, iron could not be detected in any of the samples. The control tests of bulk Fe/TiO₂ WI 1 wt% and Fe/MCM-41 WI 1 wt% also did not show any presence of iron. There are multiple reasons for this. For the porous materials it was speculated that most of the iron could be within the pores and therefore as XPS is a surface technique³⁰ the iron cannot be detected. However, as iron is not seen on the bulk TiO₂, this could be due to an inhomogeneous sample (and therefore the iron nanoparticles were not detected in the areas selected) or alternatively the metal loading is too low to be detected, with respect to the surface area of our materials (as observed in the literature where iron was not detected in Fe/SBA-15 1 wt%, for example).³¹ XPS did reveal the presence of adventitious carbon, and nitrogen from the amine template within the as synthesised mesoporous titanium oxide samples though.

5.2.5. Thermal resistance and calcination for template removal

From the TGA of as synthesised material, it was shown that calcination in air, above 500 °C combusts all organic material. Initial attempts were made to calcine as-synthesised mesoporous titanium oxide material at 550 °C with varying ramping rates and dwell times. The template was completely removed; however, the reflection at ca. 4° 2 θ in the XRPD pattern associated to micro or meso porosity was also lost. In order to investigate this phenomenon more in detail, and gather ranges of temperature resistance for our materials, *in situ* XRPD was used (figures 5.2.5.1 and 5.2.5.2).

From the *in situ* XRPD analysis it was found that the material was not as thermally robust as originally thought. Beyond 160 °C, the porous reflection starts to drop in intensity, and beyond 190 °C, the 2 θ region becomes completely flat. Whilst observing the bulk phase, the (101) facet from anatase starts to crystallise from 440 °C onwards. However, as catalytic tests were found to be optimal at 115 °C (see section 4.2.1.1) the material was still theoretically capable of withstanding the temperatures required. The results show that the material is likely to be in a metastable crystalline phase which crystallises to anatase with calcination.

To the best of our knowledge this is the first time *in situ* XRPD analysis has been conducted on mesoporous titanium oxide to assess the thermal stability, and this might be the reason why these materials are not found in gas phase reactions, as they would not be able to withstand the needed reaction conditions.

On the other hand, this same experimental observation also meant that for complete template removal, an alternative to calcination must be sought.

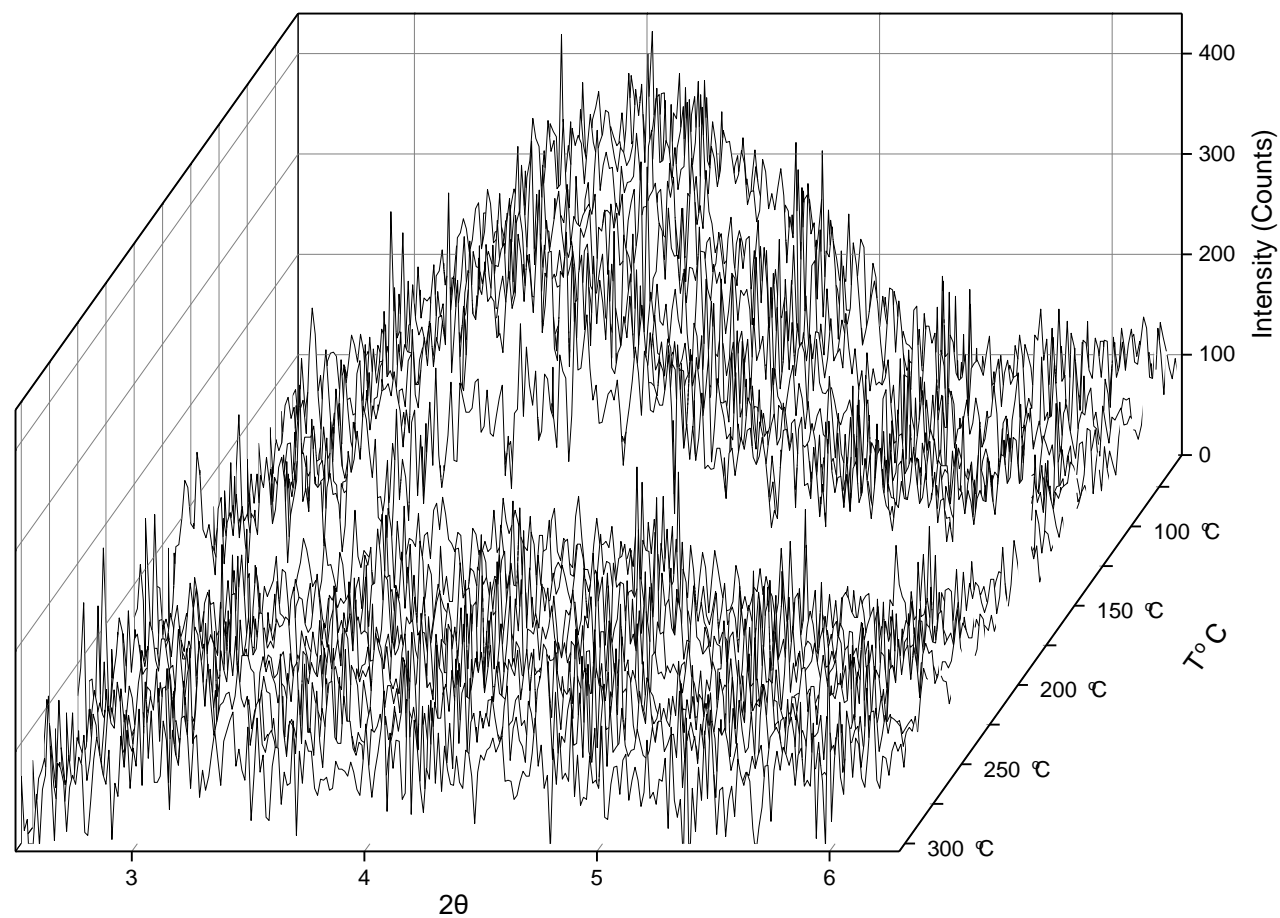


Figure 5.2.5.1: *In situ* XRPD analysis of as synthesised mesoporous titanium oxide, focusing on the porous region. Pore collapse indicated from loss of intensity in the reflection starts to occur 150-160 °C, and all porosity is lost beyond 190 °C shown by the absence of the reflection. Air flow 10 ml min⁻¹, T = 10 °C min⁻¹.

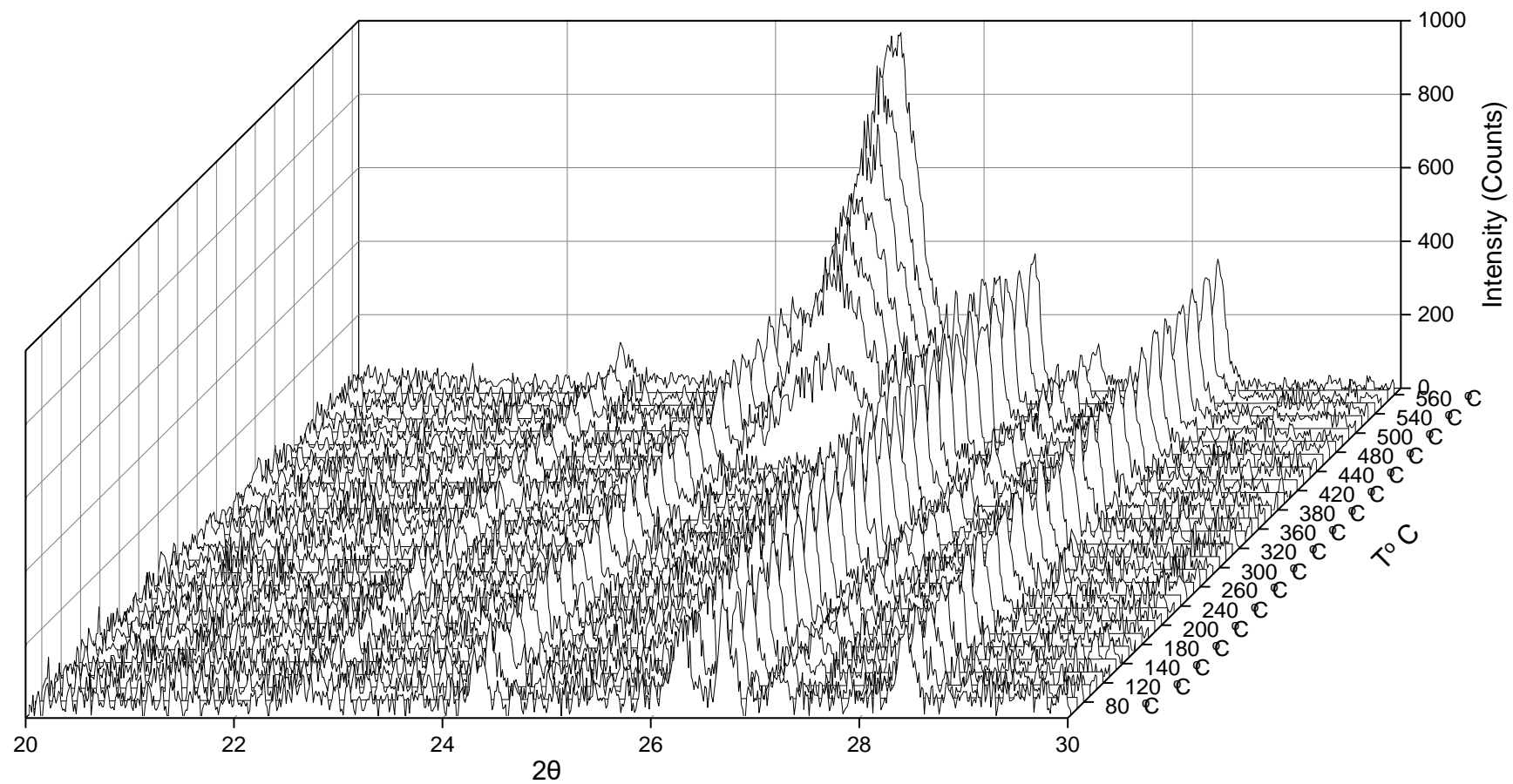


Figure 5.2.5.2: *In situ* XRPD analysis of as synthesised mesoporous titanium oxide, focusing on (101) facet. Crystallinity in the bulk phase is indicated by the presence of a reflection at $25^{\circ} 2\theta$ which occurs from 440 $^{\circ}\text{C}$ and gradually becomes more intense. Air flow 10 ml min^{-1} , $T = 10 \text{ }^{\circ}\text{C min}^{-1}$.

5.2.6. Template removal: Acidification

Although calcination methods are by far the most common to remove a template, within the literature another common method of template removal is done through acidification. The template (as in our case is a base) being removed relies on the protonation of the amine group, which will then dissociate from the porous structure and then be completely removed via washing. The most common acid used is HNO_3 , in ethanol or methanol with pH ranging from 1-2 (typically using a 1:1 ratio of initial hexylamine to acid).^{13,14} Initial attempts were made with these conditions, and although the template was removed, the material lost its porosity. This is due to the acid attacking the porous framework leading to decomposition of crystalline material, or alternatively a collapse of the pore structure occurs without the template being present.

Therefore, a milder approach for template removal via acidification was sought.

5.2.6.1. Acidification via HNO_3

The optimal pH for template removal was required as a starting point for controlled template removal. Control tests were conducted with the expected amount of hexylamine with HNO_3 , this was compared to a pH plot with mesoporous titanium oxide (figure 5.2.6.1.1). As it can be seen the characteristic shape for acid-base titrations is present with hexylamine and p-25 and HNO_3 . Whereas when HNO_3 is added to mesoporous titanium oxide containing hexylamine, instead a more gradual decrease is seen in pH. This could be due to the gradual release of the template from the porous structure. Multiple points of interest on the curve are marked and here repeat tests were conducted, stopping at these points and analysing the material.

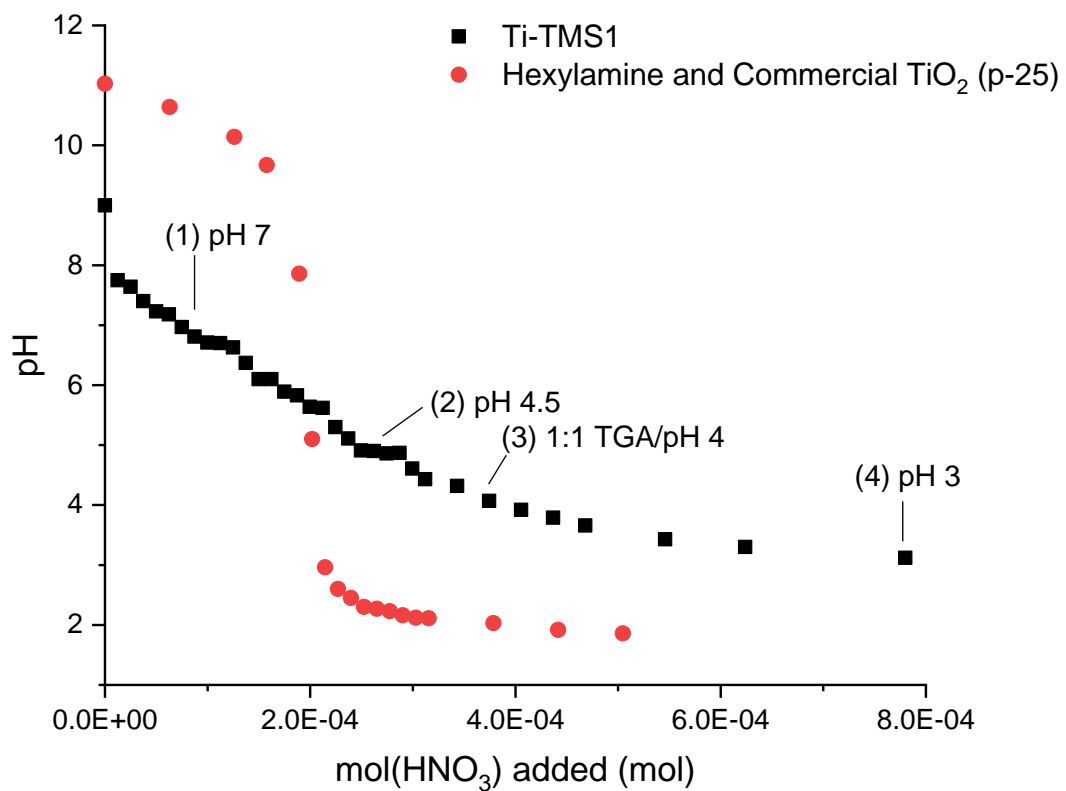


Figure 5.2.6.1.1: pH curves from the addition of HNO₃ to mesoporous titanium oxide (-) and a control comprised of commercial TiO₂ (p-25) and hexylamine (-). Points where the addition of acid was halted and sample collected are shown.

Table 5.2.6.1.1: Quantification of parameters on the degree of porosity and the amount of template removed from mesoporous titanium oxide with increasing acidity of HNO₃ solution utilising a range of analytical techniques.

Summary of results					
Test conducted	As synthesised	pH 7	pH 4.5	1:1 TGA (pH 4)	pH 3
XRPD (Porosity and pore size)	Porous 22.4 Å	Porous (intensity loss) 22.1 Å	Porous (intensity loss) 21.5 Å	Porous (intensity loss) 22.5 Å	Not porous
ATR-FTIR (C-H peak present)	Template present	Template present	Template present	Very minor peaks	Template removed
TGA (Ti:Hexylamine molar ratio)	5:1	6.4:1	7.7:1	< 5 wt%	Template removed
Porosimetry (BET surface area)	258 m ² g ⁻¹	186 m ² g ⁻¹	296 m ² g ⁻¹	470 m ² g ⁻¹	485 m ² g ⁻¹

Table 5.2.6.1.1 shows a summary of the results from dropwise addition of HNO_3 to mesoporous titanium oxide. From the XRPD there is no visible trend in pore size as acid is added. This suggests that no pore shrinkage occurs *during* template removal instead, as intensity is lost the pore's structure is broken apart (figure 5.2.6.1.2).

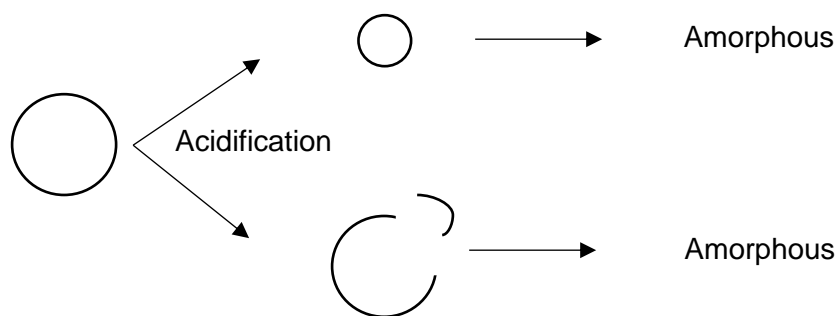


Figure 5.2.6.1.2: Two possible routes to loss of porosity as acid attacks the porous structure. Top: Pore shrinkage leading to amorphous materials. Bottom: Stripping of the framework walls until all crystallinity is removed.

Additional control tests were carried out using TGA and FTIR. The TGA and ATR-FTIR show, as expected, a stoichiometric amount of HNO_3 is required before complete template removal is achieved. However, the amount which is removed is not proportional to the amount of acid added. This leaves a narrow range where if slightly too little acid is added, the template is still quantifiable, and if too much is added, complete pore collapse occurs. However, this postulates a trade-off could be met where if a significant amount of material is 'template free' and still porous, then this may still be suitable for catalytic tests.

Interestingly, the BET surface area increases even after the $4^\circ 2\theta$ reflection in the XRPD is lost. The trend is an initial drop in surface area, followed by an increase to higher than the as-synthesised sample. The initial drop could be due to blockage of the pores from the template which has been dislodged, but not completely removed by washing. As expected, the BET increases as more template is removed as this means more surface area is capable of being occupied. However, even when the sample is no longer porous, it has the largest surface area. The shape of the hysteresis loops are identical for all samples (figure 5.2.6.1.3), showing a H4 type shape, as defined by IUPAC.³² The H4 shape is indicative of the presence of

micropores and is often found in aggregated crystals of zeolites. This is further complemented by the pore distribution data, figure 5.2.6.1.4, which show a pore distribution around 2-3 nm, tailing off towards higher pore volumes for all samples either with or without crystalline pores.

The porosimetry results could suggest that some pores are indeed still present after template removal but are not uniform. Although this is an interesting result, it is unwanted for this research as regular, ordered pores are desired for single-site shape selective oxidation catalysis. Furthermore, if this was to be pursued, batch to batch reproducibility may cause variation and ambiguity in active sites, leading to potential differences in catalytic behaviour.

In summary, by combining all of these data, pH 4 was chosen as the optimum condition for template removal. However, when this was conducted on larger scales (>0.5 g) required for catalyst synthesis the material did not retain porosity. This is possibly due to the fragile nature of acid addition and the porous structure. Because of this, inorganic acids were no longer pursued as candidates for template removal due to significant attack on the porous structure and organic acids were explored.

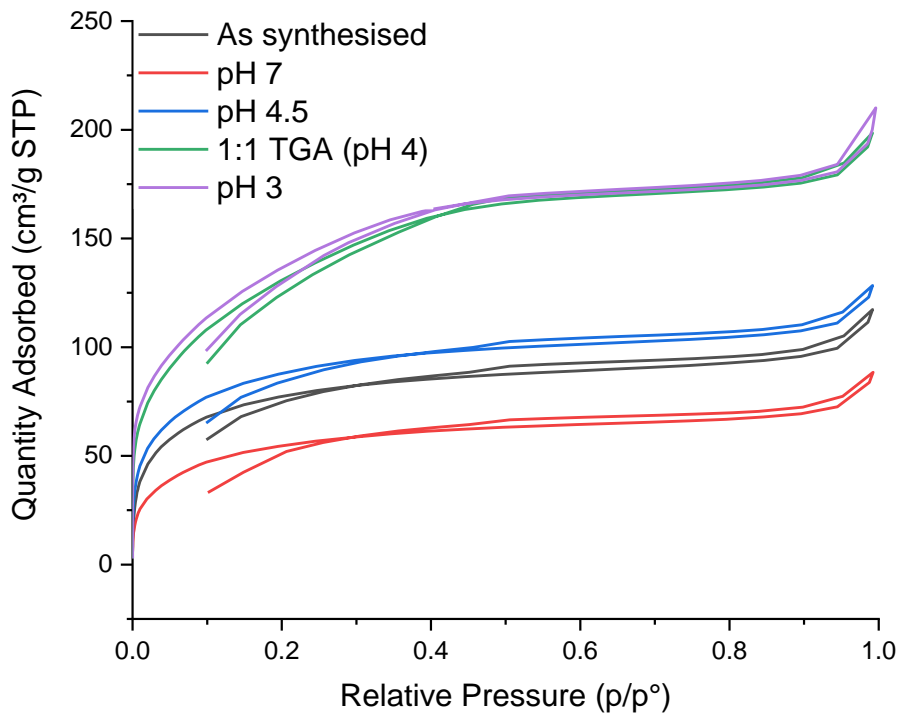


Figure 5.2.6.1.3: A collection of porosimetry traces of HNO₃ washed mesoporous titanium oxide. The hysteresis loop in all samples match the H4 type shape, indicative of micropores being present.

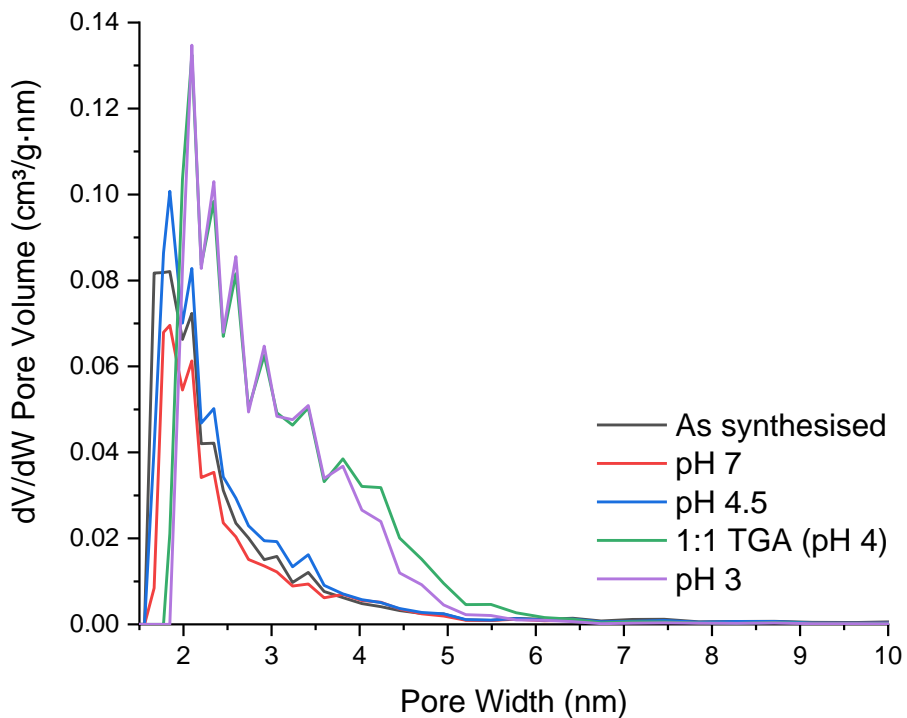


Figure 5.2.6.1.4: A collection of pore width versus pore volume data of HNO₃ washed mesoporous titanium oxide.

5.2.6.2. Acidification with *p*-TSA

In view of this, para toluene sulphonic acid (*p*-TSA) was used for template removal.³³ Acidic solutions with pH up to 5.35 were tested with *p*-TSA, however, although the template was always removed, complete loss of porosity was observed. This suggests that even when organic acids are used the inorganic framework is either attacked directly, or the amine template is the only scaffold keeping the structure together. Therefore, alternatives to acids were sought to determine if the template can be removed without affecting the porous framework and avoiding methods which may attack the framework directly.

5.2.7. Summary of template removal attempts – calcination and acidification

All attempts of template removal using conventional methods thus far have led to pore collapse. It is uncertain why exactly this is, despite the use of known and accepted protocols in literature. On the other hand, a closer inspection of the current literature very rarely reports, for these materials, data after template removal. And in fact we have found only one author replicating a synthesis where alkyl phosphates were used as the template for mesoporous titanium oxide, who also found that any attempts of template removal led to complete pore collapse.⁴ It might be the 'architecture' of Ti-O-Ti rings constituting the walls of our material are too strained to stand the removal of the template that, in our case, would act as a 'scaffolding'. On the other hand, as this project's drive is the template free microporous titanium oxide, it was decided that other, unconventional removal techniques were to be explored, without the use of acids.

5.2.8. Template removal: Alternatives to acid

To avoid the addition of acid altogether, alternative methods for amine removal were trialled. This was to avoid chemicals and harsh conditions that may attack the porous framework and exclusively interact with the amine template.

5.2.8.1. Hydrogen peroxide

As our template is an amine, this ligand could in principle detach from a metal not necessarily by protonating it, but by converting it into an oxide. This is in fact a mechanism of ligand loss for phosphine-based ligands.³⁴ By applying this same principle to our amine, it is possible to identify literature where the oxidation of alkyl amines is prevalent.^{35,36} It was postulated that if the oxidation of the amine template leads to an amine oxide (figure 5.2.8.1.1), this would lead to a weaker bond/ bond cleavage from the titanium oxide framework (the premise of acidification of the template) and thus yield template-free porous titanium oxide.

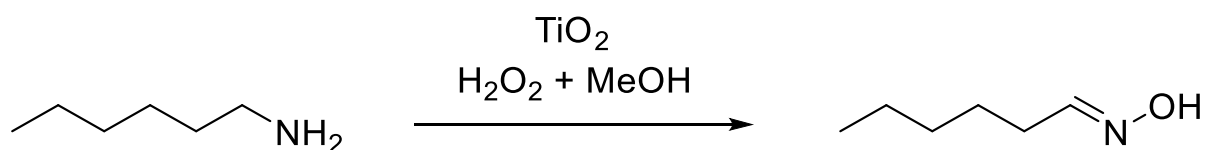


Figure 5.2.8.1.1: A reaction scheme to show the conversion of hexylamine to its corresponding oxime as reported by S. Bhardwaj.³⁶ In their study, hexylamine was in solution and TiO₂ (anatase) was used as a catalyst. The proposed scheme was envisioned to occur within the mesoporous titanium oxide, and thus remove the template and retain the porous structure.

Several attempts with varying reaction conditions including temperature, reaction time and solvent choice were conducted. The most successful of which are summarised in figure 5.2.8.1.2. After refluxing with hydrogen peroxide for 24 h the intensity of the organic peaks in the IR have reduced and the porous structure is still present (and some pore collapse has occurred, suggesting a different mechanism to template removal with acidification). When the necessary additional washes were repeated however, they led to complete pore collapse and the amine was still present. This might be due to the titanium oxide not activating the hydrogen peroxide as its crystal structure is different to anatase, originally reported in the literature.

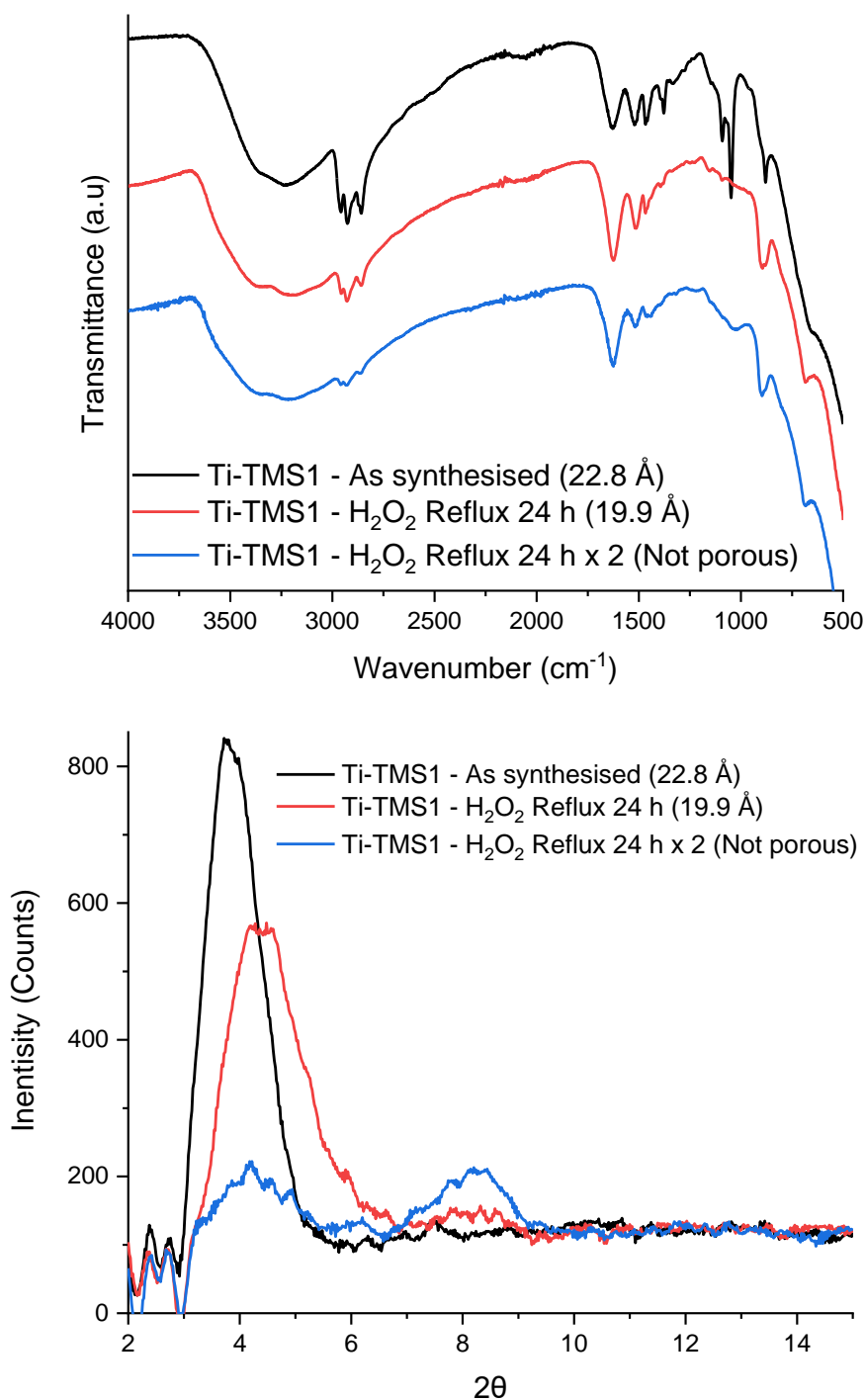


Figure 5.2.8.1.2 Top: ATR-FTIR spectra of mesoporous titanium oxide to show how the amine template reduces in intensity after the treatment with hydrogen peroxide, as shown through the decrease in C-H stretch (2500 – 3000 cm⁻¹). Bottom: Corresponding XRPD patterns focusing on how the intensity of the reflection corresponding to porosity varies with the hydrogen peroxide treatment. H₂O₂ 30 v/v%, XS, reflux, 24 h (-), 2 x 24 h (-).

Iron can generate radical species from hydrogen peroxide.^{37,38} To try and promote the generation of radical species, Fe/Ti-TMS1 was subjected to hydrogen peroxide treatment. In theory the hydrogen peroxide should break down to form hydroxy free radicals through Fenton chemistry in the presence of iron. The resulting radicals would then attack the hexylamine template. However, it can be seen in figure 5.2.8.1.3 the amine template is still present after washing with hydrogen peroxide. Although the pores are still observed in the XRPD patterns, the template is desired to be completely removed so no obstructions to substrates occur. Therefore, a further different method for template removal was sought.

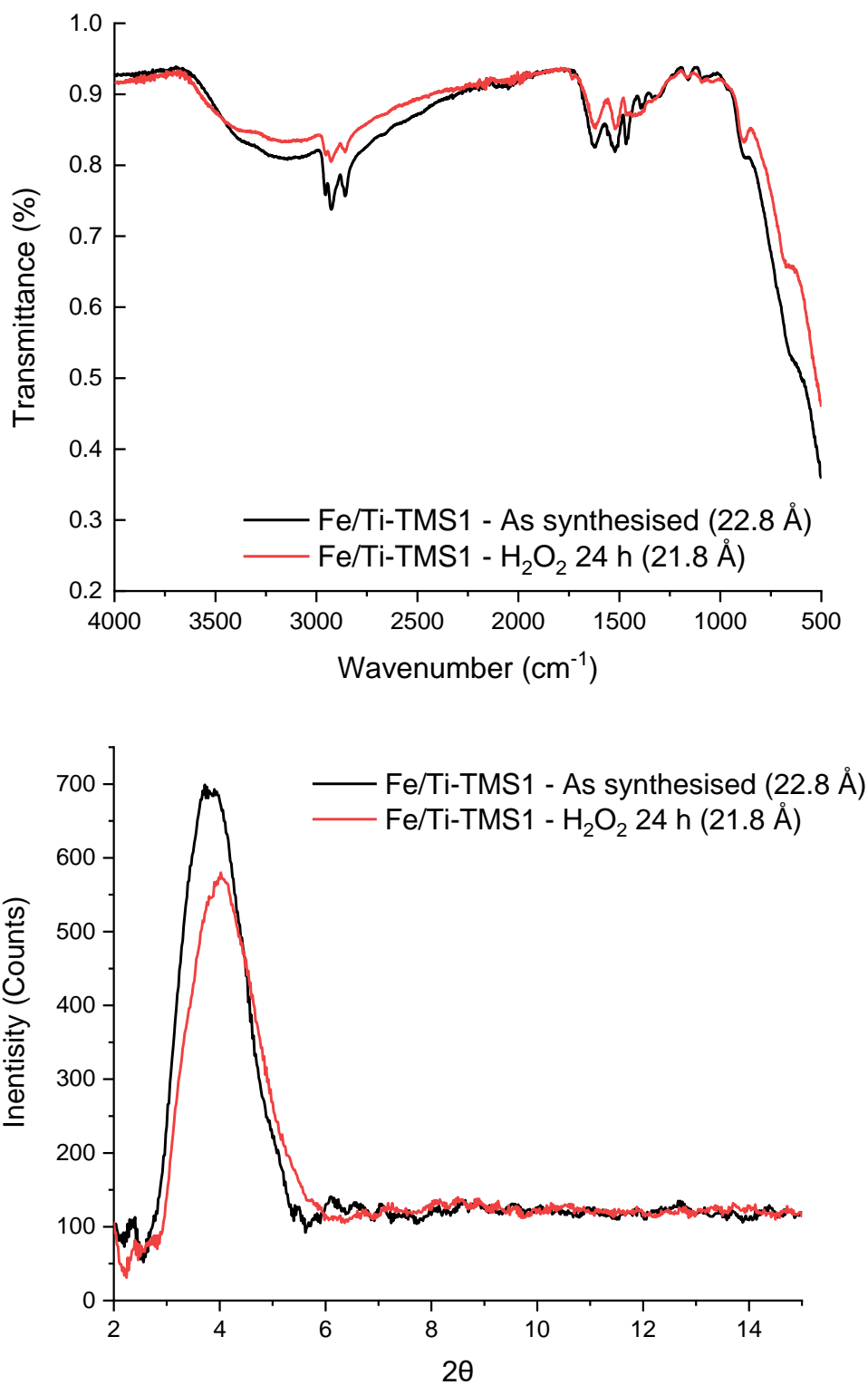


Figure 5.2.8.1.3 Top: ATR-FTIR spectra of Fe/Ti-TMS1 2 mol% to show how the amine template reduces in intensity after the treatment with hydrogen peroxide, as shown through the C-H stretch (2500 – 3000 cm⁻¹). Bottom: Corresponding XRPD patterns focusing on how the intensity of the reflection corresponding to porosity varies with hydrogen peroxide. H₂O₂ 30 v/v%, XS, RT, 24 h.

5.2.8.2. Phthalic anhydride

Phthalic anhydride was chosen as a candidate for template removal. Phthalic anhydride reacts and binds strongly to amines and is often used as a protecting group during organic synthesis.³⁹ In theory, the phthalic anhydride would bind to the amine template and be washed out from the material (figure 5.2.8.2.1).

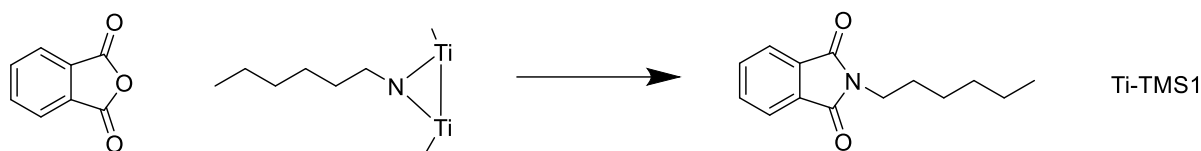


Figure 5.2.8.2.1: Proposed template removal with phthalic anhydride. The phthalic anhydride binds strongly to hexylamine and this was proposed to occur within the pores and thus detach the amine template from the porous structure.

From the FTIR-ATR (figure 5.2.8.2.2), the template *is* completely removed when using phthalic anhydride. However, the porosity is also completely lost. Although this is not desired, this result proved that template removal, whether acids or non-acids are used, porosity does not remain in mesoporous titanium oxide samples produced in this way.

With the conclusion that the template cannot be removed and thus the porous template-free material cannot be achieved through methods described so far, an alternative synthesis was needed. Furthermore, although the as synthesised samples still contain a template, they could still have some sites free for catalysis and thus were applied to alkane oxidation.

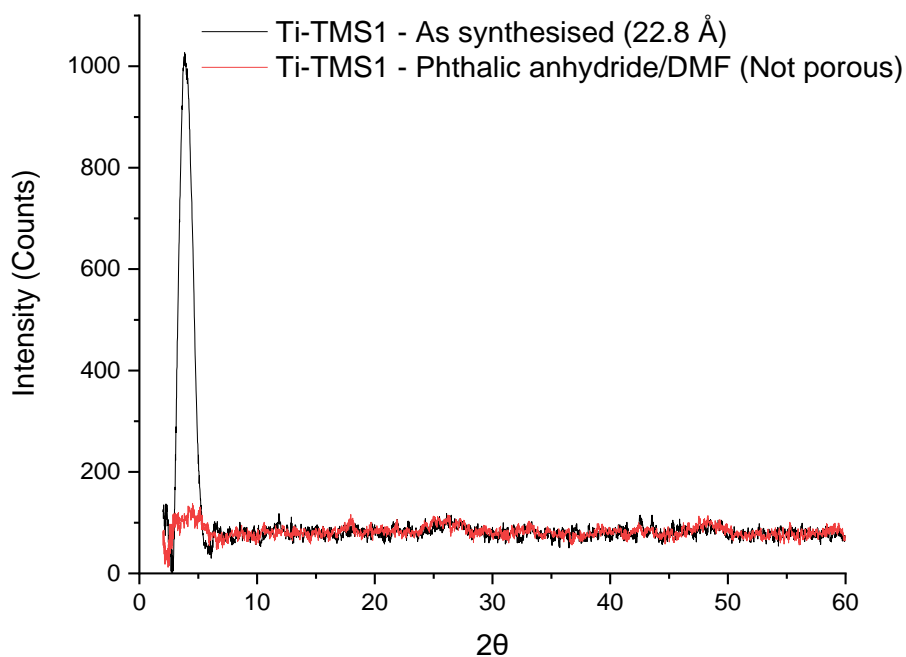
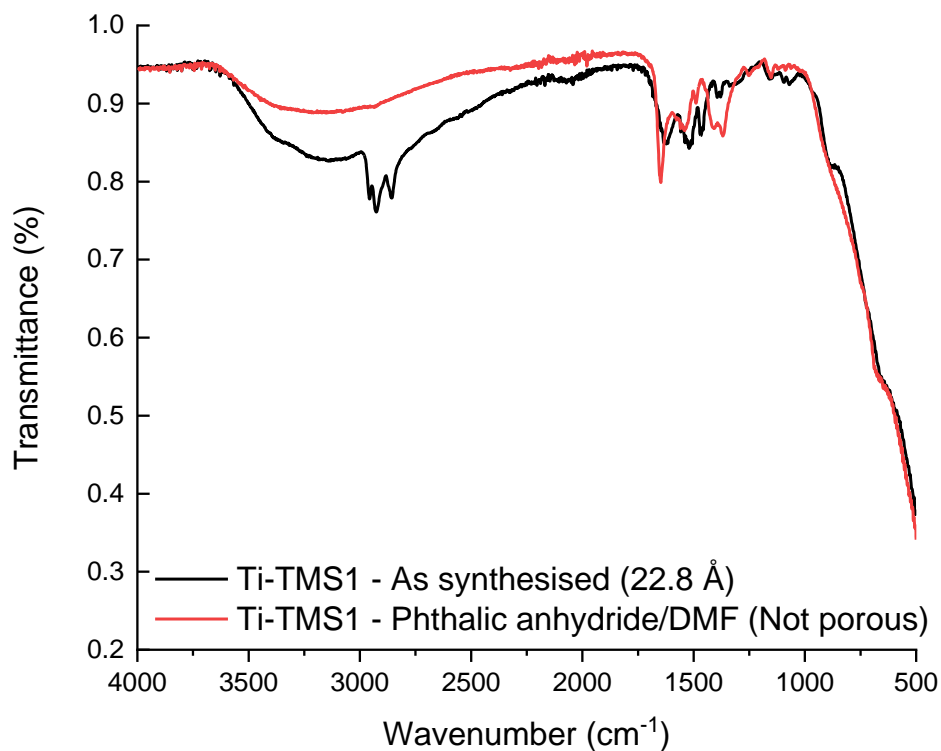


Figure 5.2.8.2.2 Top: ATR-FTIR spectra to show template removal from mesoporous titanium oxide after treatment with phthalic anhydride/DMF, complete loss of the C-H stretch (2500 – 3000 cm⁻¹) is observed, indicating the complete removal of the template. Bottom: Corresponding XRPD patterns showing the complete loss of the reflection corresponding to porosity after treatment with phthalic anhydride. Phthalic anhydride: Hexylamine = 1:1, RT, 24 h.

5.2.9. Reaction resistance and catalytic tests

A catalyst is required to be thermally, mechanically and chemically robust. The porous structure of mesoporous titanium oxide has been found to be not as thermally resistant as desired nor could it withstand strong acidic conditions. As a consequence, if these materials were used for catalysis the conditions would have to have a temperature below their thermal decomposition temperature and not be in the presence of acid. Tests were conducted to determine if the porous framework could withstand the conditions during a catalytic test.

The XRPD patterns of before and after catalytic tests (figure 5.2.9.1) clearly show a significant drop in intensity in the reflection corresponding to porosity. This result shows the potential for catalyst deactivation after multiple uses. Furthermore, a control test where mesoporous titanium oxide was stirred under the same conditions, but without heating and under atmospheric conditions, showed a similar drop in intensity of the porous peak in the XRPD. This concludes that the material has inappropriate mechanical properties for the nature of catalyst testing.

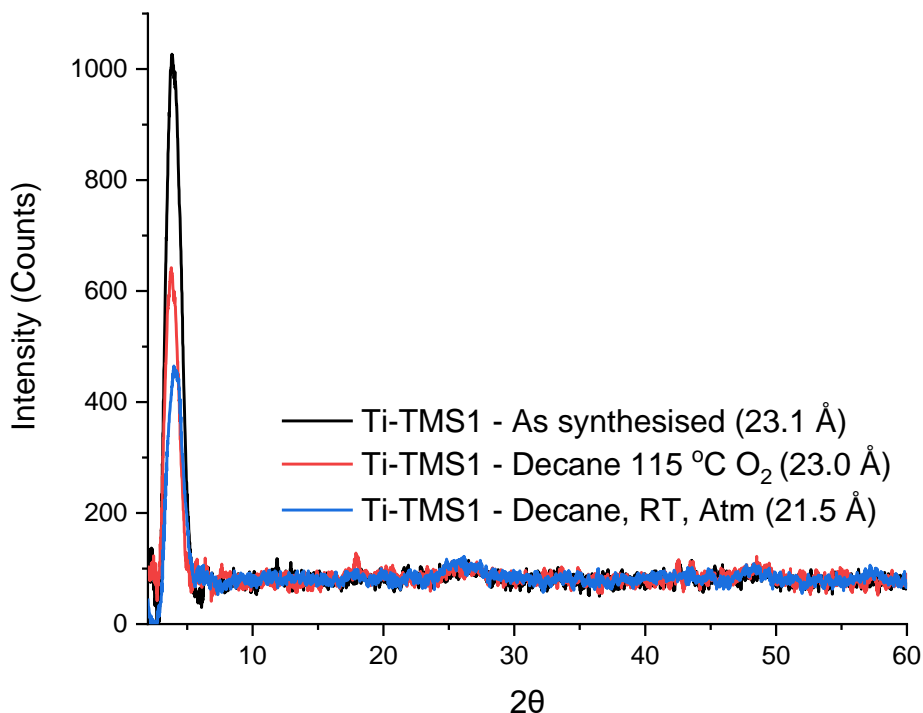


Figure 5.2.9.1: XRPD patterns for mesoporous titanium oxide subjected to ‘typical’ catalyst test conditions for the oxidation of *n*-decane, showing the variation in intensity of the peak corresponding to porosity after catalytic tests. *n*-decane (3 mL), mesoporous titanium oxide (200 mg), T = 115 °C, PO_2 = 2 bar, t = 24 h. Identical conditions for the control tests where T = room temperature under atmospheric pressure.

Despite the loss of porosity upon stirring, the iron doped mesoporous titanium oxide was applied to *n*-decane oxidation. GC-MS (gas chromatography – mass spectrometry) analysis of the reaction mixture showed only *n*-decane, with no products or leached template, was observed. The results demonstrate that the template does indeed need to be removed prior to reaction for *n*-decane oxidation.

It followed that Antonelli and co-workers’ protocol for the synthesis of microporous titanium oxide was no longer pursued. Because of the drawbacks of the material, such as not being as mechanically robust as desired and the challenge of template removal yielding only amorphous material, alternative syntheses were conducted.

5.3. Dai and Zhang synthesis of microporous titanium oxide

Two authors other than Antonelli have demonstrated the synthesis of microporous titanium oxide and its subsequent template removal (summarised in table 5.3.1). Although the differences tend to be minor, a small change in one of the many parameters could lead to a material with completely different properties.

Table 5.3.1 A comparison of different conditions used in the synthesis of meso/microporous titanium oxide amongst authors claiming successful template removal.

Conditions in original syntheses					
Author	Titanium precursor	Amine template	Solvent	Autoclave	Template removal
Antonelli ⁶	Isopropoxide	Hexylamine	Water	40, 60, 80 (2, 2 and 4 days)	Solvent washes
Dai ²⁴	Isopropoxide	Dodecylamine	Ethanol/Water	80, 100, 180 °C (1, 1 and 7 days)	HNO ₃ , pH 2, reflux 24 h
Zhang ⁴⁰	Ethoxide	Hexadecylamine	Ethanol/Water	None	HCl, pH 2, 24 h

From the data collected in Antonelli's samples with varying conditions, the above syntheses were also modified to optimise conditions for crystalline porosity.

5.3.1. Alternative synthesis of microporous titanium oxide with amine templates

The optimised conditions of the synthesis for Antonelli, Dai and Zhang yielded porous materials. With regards to the XRPD pattern, only minor changes were observed (figure 5.3.1.1). Both Dai's and Zhang's synthesis^{24,40} utilise a co-solvent (ethanol) during the initial introduction of titanium alkoxide and template, this is thought to influence the micelle formation before the autoclave step. However, comparing materials obtained from the protocols of Antonelli's and Dai's, it appears their XRPD patterns have little difference as both mesoporous peaks have similar broadness, intensity, and pore size (statistically identical).

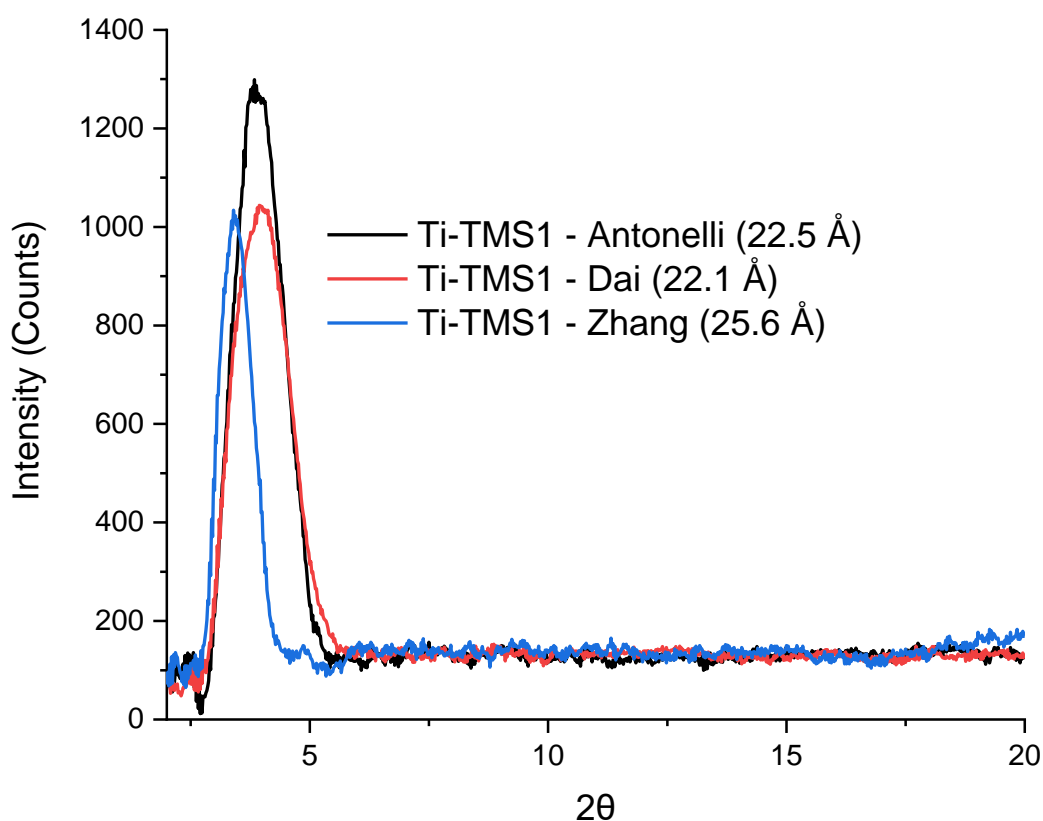


Figure 5.3.1.1: XRPD patterns for mesoporous titanium oxide with varying synthetic parameters according to individual authors, with optimized conditions. Antonelli: Titanium isopropoxide, Hexylamine, Water, Autoclave step: T = 80 °C, t = 96 h. Dai: Titanium ethoxide, Hexylamine, Water/Ethanol, Autoclave 80 °C, 96 h. Zhang: Titanium isopropoxide, Dodecylamine, Water/Ethanol, no autoclave step.

Perhaps most surprising is the presence of porosity in materials obtained using Zhang's protocol. In fact, in this procedure, there is no hydrothermal step, whereas the 'dogma' in

microporous synthesis is precisely the hydrothermal step which is believed to provide the driving force for crystallisation of meso/micropores. As expected, the pore size has increased as a longer template was used. Furthermore, the reflection is around half as broad of that in sample using Dai's protocol of almost equal intensity, suggesting a smaller pore size distribution. This could be due to the longer template leading to more uniform micelles.

Despite XRPD patterns showing similar crystallinity amongst pores, this does not necessarily imply the chemical resistance of these materials, and thus they were tested for template removal.

The material obtained using Dai's protocol led to complete pore collapse when the template removal stated within the literature was conducted, and subsequent optimisation reflected materials from Antonelli's protocol. However, materials obtained from Zhang's protocol seemed more resistant.

5.3.2. Template removal - Zhang

As mentioned previously, mesoporous titanium oxide obtained from Zhang's protocol is interesting due to the presence of pores despite no hydrothermal step. The literature claimed the material could withstand pH 2 acidic washing, however, when this was conducted it was found that only a trace reflection remained in the porous region of the XRPD (figure 5.3.2.1). Although this material is still technically more resilient than that from Antonelli's method as a mesoporous reflection at $4^\circ 2\theta$ is still observed, uniform porosity is almost completely removed. Optimisation of template removal was conducted by varying the pH of solution. However, it was found that pH 2 – 3 was required for complete template removal, but by this point the micro/meso porous peak in the XRPD pattern is almost completely lost.

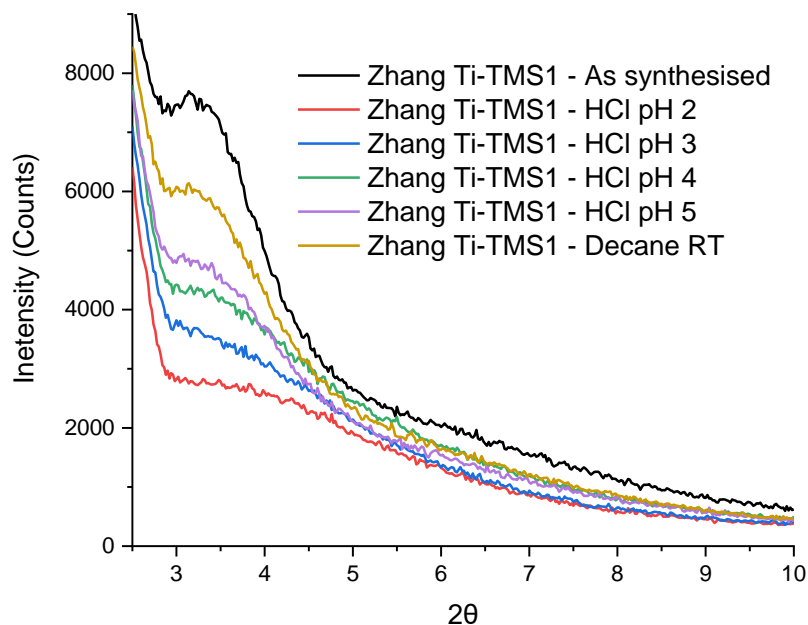


Figure 5.3.2.1: XRPD samples of mesoporous titanium oxide as synthesised following Zhang’s patent with dodecylamine as the template, with template removal treatment with HCl of varying pH and a mechanical resistance test with Decane. Mesoporous titanium oxide (200 mg), Decane (3 mL), RT, atmospheric pressure, 24 h.

The mechanical properties of the material were also tested. The as synthesised material was stirred at room temperature with *n*-decane to determine its mechanical resistance. It was found, as in the sample obtained from Antonelli’s protocol, even at room temperature the intensity drops by almost a half.

Because of the unsuccessful attempts of template removal despite varying the many parameters of both the synthesis and removal, an alternative method to prepare porous titanium oxide where no template is used during the synthesis was sought.

5.4. Non-template synthesis method: Peptization

An alternative and recent synthesis which avoids amine templates was sought. *Yin et al.* showed that under very strong basic and hydrothermal conditions, anatase was capable of forming microporous channels.⁴¹ In this context, peptization refers to treating titanium oxide under hydrothermal conditions with a peptizing agent (in our case NaOH), this allows different morphologies to be achieved. This has been studied with varying peptizing agents.⁴²

5.4.1. Synthesis and subsequent metal loading

It was found that peptization of bulk anatase leads to microporous titanium oxide, as reflections are seen in the XRPD (figure 5.4.1.1). Furthermore, unlike the other methods, the material is resilient to calcination (400 °C was chosen as reported in the literature). The material was capable of remaining porous and although calcination does have some effect on pore size, even after wetness impregnation a peak in the XRPD remained - thus yielding microporous Fe/Ti-TMS1.

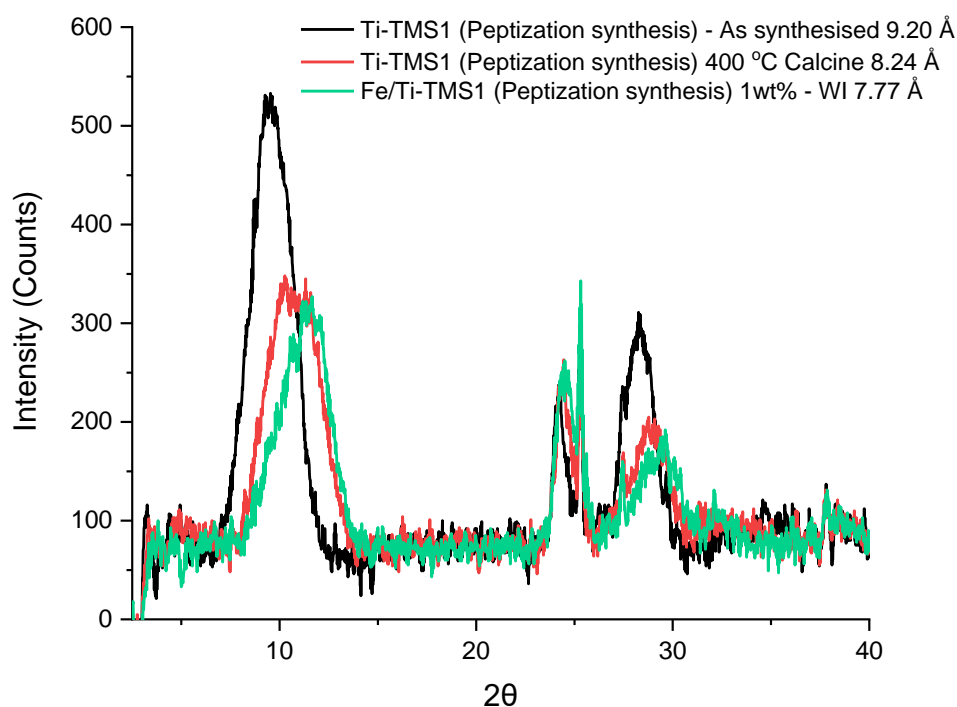


Figure 5.4.1.1: XRPD of microporous titanium oxide samples as synthesised through the peptization of bulk anatase. Anatase (2 g), NaOH (10M, 20 mL), T = 120 °C and t = 3 days (-). Corresponding calcination (400 °C, 4 h, 10 °C min⁻¹) (-) and wetness impregnation (Fe(NO₃)₃·9H₂O, 1 wt%, 400 °C) (-).

The material is significantly more thermally resistant than alternative syntheses listed so far. Mesoporous titanium oxide synthesised via a template method had its pores completely removed post 190 °C, whereas the peptization synthesis is capable of calcination to 400 °C. Although a loss of intensity is observed initially, the material maintains XRD peak intensity and in turn porosity after being loaded with iron oxide. This material was then used for alkane oxidation.

The final product's pore size is also more appropriate for shape selectivity than the template-synthesised materials as less of the *n*-decane molecule can fit into the pore. However, this may influence the diffusion.

5.4.2. Catalytic testing

5.4.2.1. *n*-decane

When the materials obtained by using the *Yin* et al. (peptization) protocol were applied to *n*-decane oxidation, no conversion was observed. It was expected that some conversion would occur as wetness impregnation would lead to iron being present both within and outside the pores. Therefore, some oxidation from iron loaded on the outside of the material was expected to occur, and thus lead to conversion.

The reason for the lack of activity could be either or a combination of:

- 1) A significant amount of iron oxide is within the porous framework and, if in the presence of diffusion limitations, the *n*-decane is unable to reach the active site.
- 2) Although some iron oxide is present on the outside of the titanium oxide, the amount is too small to provide conversions detectable from GC-MS.
- 3) As the crystallinity of the material is different to bulk titanium oxide, this may have led to different surface-metal interactions and therefore generated the inactive species.

From this data, it was concluded that the materials synthesised via peptization protocol applied to the 'ideal' conditions for *n*-decane oxidation were not able to perform as shape selective catalysts for linear alkanes as harsher conditions would lead to autoxidation.

5.4.2.2. Cyclooctane

As linear alkanes are harder to activate than cyclic analogues (C-H bond dissociation energies varies from ca. 420 to 390 kJ mol^{-1} from linear to cyclic species),^{43–45} peptization synthesis-based catalysts were tested on cyclooctane to determine if the presence of pores has any effect on oxidation.

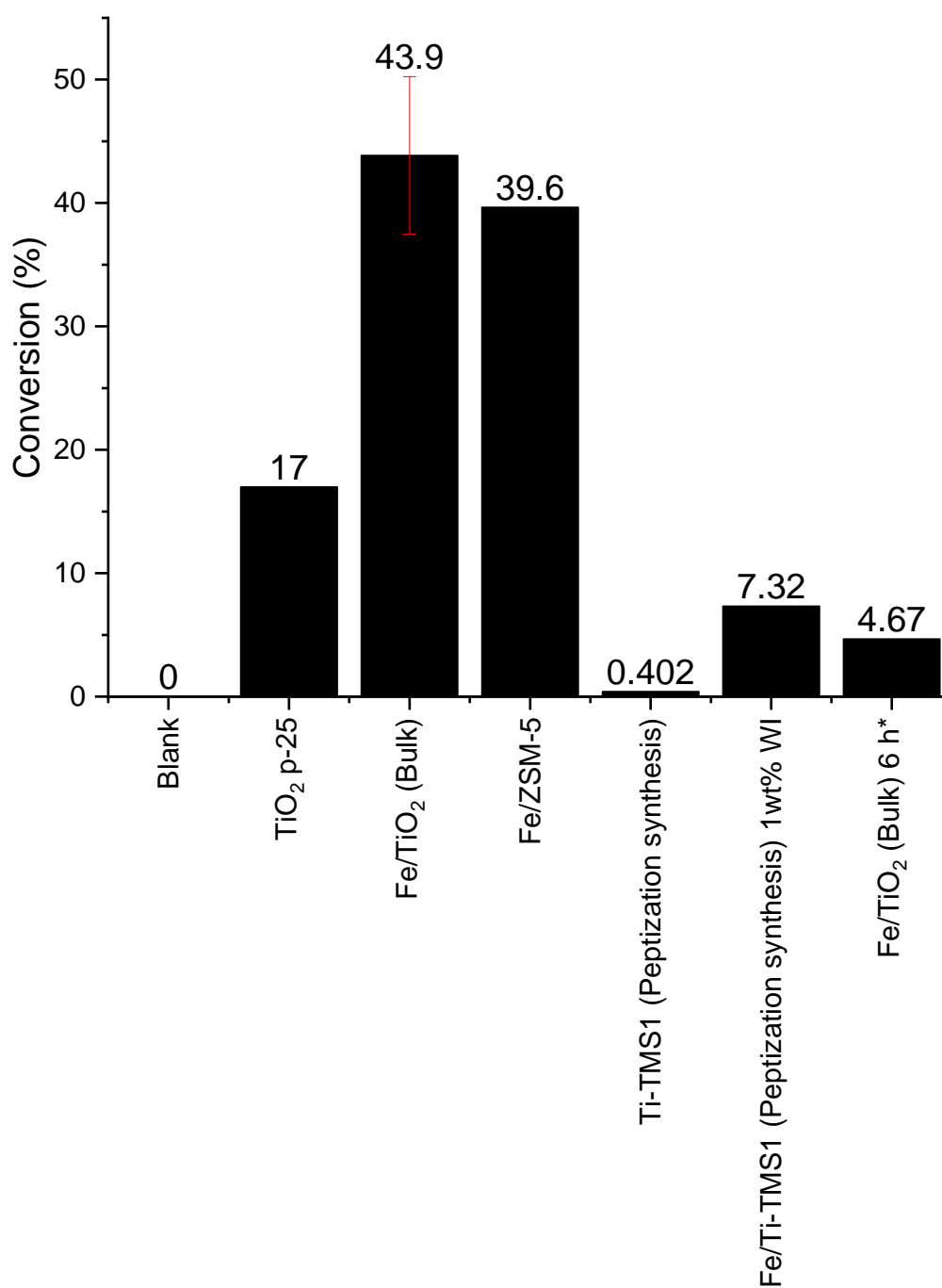


Figure 5.4.2.2.1: Conversion data for cyclooctane oxidation with iron on titania and porous frameworks. Cyclooctane (3 mL), M:S 1:1000, T = 110 °C, $PO_2 = 2$ bar, t = 24 h, *t = 6 h.

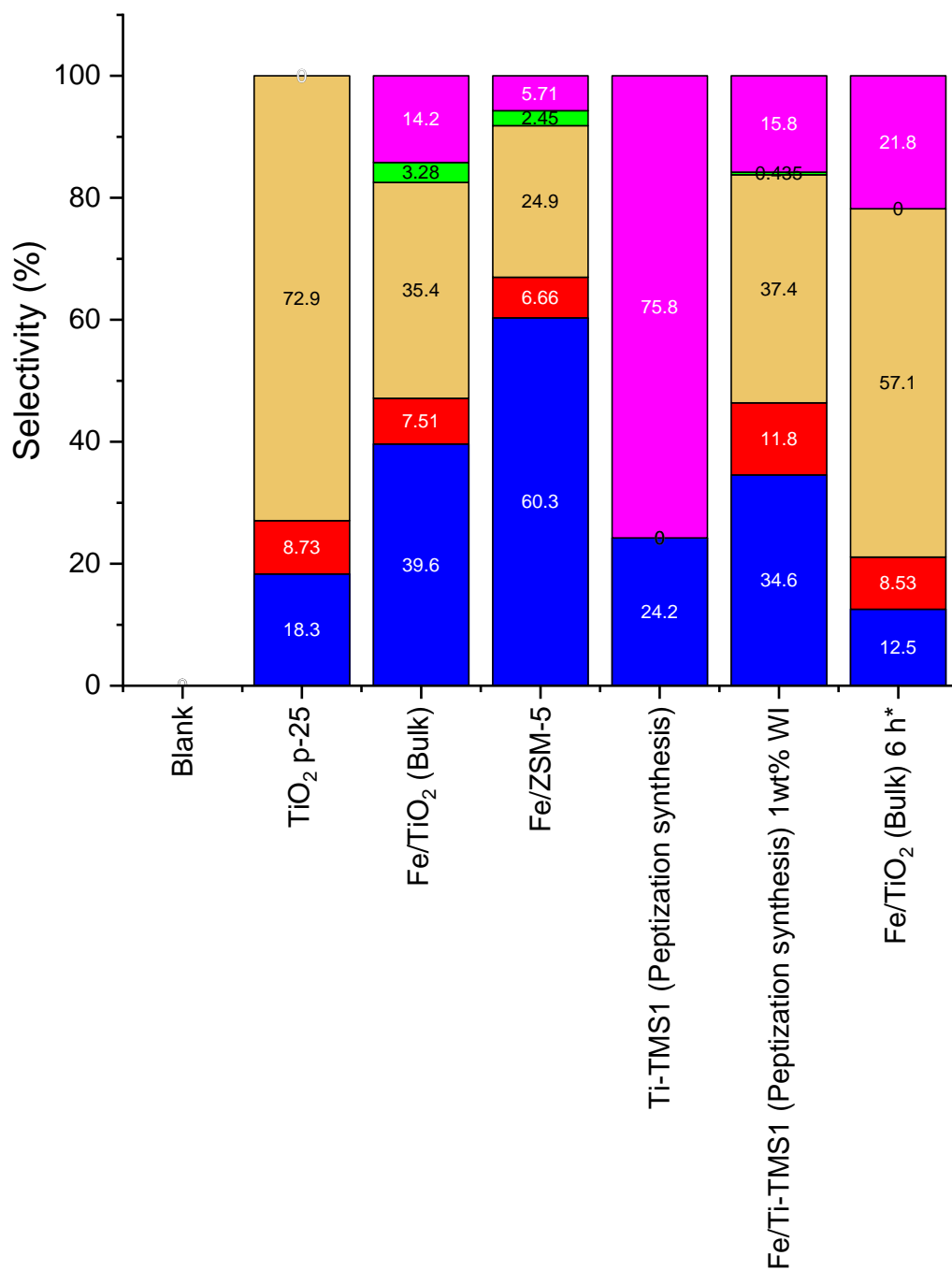


Figure 5.4.2.2.2: Selectivity data for cyclooctane oxidation with iron on titania and porous frameworks. Cyclooctane (3 mL), M:S 1:1000, T = 110 °C, PO_2 = 2 bar, t = 24 h, *t = 6 h. (■) Cyclooctanone, (■) Cyclooctanol, (■) Cyclooctyl hydroperoxide, (■) other products, (■) unknown products. Note: Other products refer to other oxidation products (e.g. epoxides), whereas unknown products are suspected condensation and dehydration products.

Figure 5.4.2.2.1 shows that bulk Fe/TiO₂ has a significantly higher catalytic activity than the corresponding microporous Fe/Ti-TMS1 under identical conditions. As Fe/ZSM-5 also shows a conversion that is statistically identical to that of bulk Fe/TiO₂ but a different distribution of products (figure 5.4.2.2.2), this shows that a different mechanism is occurring (this is discussed further in section 4.3.1).

On the other hand, ZSM-5 has a pore size in the range of ca. 5.6 Å, which is even smaller than our materials. Either there is no diffusion limitation (and in turn not for our materials) or the reaction takes place outside the pores. However, as all iron loaded catalysts here were prepared identically, this suggests that the lower conversion of microporous Fe/Ti-TMS1 is likely to be due to differing (and thus inhibiting) metal-surface interactions.

As bulk TiO₂ (p-25) shows a significant conversion also, this is evidence that indeed the metal-support interactions are responsible for the lack of activity in Fe/Ti-TMS1.

A catalytic test where bulk Fe/TiO₂ has similar conversion to that of the microporous Fe/Ti-TMS1 was conducted. A 6 h run with bulk Fe/TiO₂ yielded the closest possible conversion when varying the time of reaction, this is because strictly speaking comparisons of selectivity from different catalysts makes sense only if the conversion is similar due to the presence of secondary reaction pathways or by-products. Microporous Fe/Ti-TMS1 does indeed have a different selectivity to its bulk counterpart. Favourably, a lower amount of unknown and peroxide products and higher amounts of alcohol are formed with the microporous sample, however, the major product in the porous sample is cyclooctanone. From an industrial viewpoint, this is favourable as cyclooctanone is the desired product within current industrial demand. However, a trade-off from activity to selectivity must be considered owing to the low activity of the porous sample. Ultimately, Fe/Ti-TMS1 does not show any significant advantage to that of the bulk Fe/TiO₂ (furthermore, the latter is significantly easier to synthesise) and thus further optimization of its synthesis is required. It does, however, show that selectivity control is possible due to its porous structure with respect to an open surface in a bulk metal oxide support.

5.5. Conclusions and future work

In summary, microporous titanium oxide synthesised via a hydrothermal template technique was sought. This was successfully repeated from the literature and the parameters governing porosity were varied to optimise synthesis conditions, including the novel use of titanium (IV) (triethanolaminate)isopropoxide as a precursor. Furthermore, the novelty of adding dopant metals to the porous framework was also successfully accomplished showing porosity is only affected slightly, and even increased when using some iron precursors. However, the final desired template-free product was not able to be achieved yet. This could be due to other parameters not explored here (type of autoclave used, head space, etc.), or fundamentally microporous titanium oxide is unable to exist without an organic scaffold to keep the pores in place. Other synthetic routes using a template were explored, and although some were promising, none led to the robust material desired for catalytic oxidation.

Finally, an alternative method to template synthesis, where peptization was used instead, yielded porous titanium oxide. However, when an active metal was loaded onto this, it did not achieve any *n*-decane oxidation. From our data this could be due to diffusion limitations but is more likely from inhibiting metal-surface interactions. The material did, however, show conversion when applied to cyclooctane and even gave a higher selectivity to alcohols and ketones.

Further optimisation of the microporous synthesis could be conducted in future work, for both template synthesis and peptization synthesis. This would include studying mesoporous samples (e.g. synthesised with dodecylamine) as these showed greater resistance to template removal, but this could be a trade-off for primary oxidation selectivity. Alternatively, synthesis with templates such as cetyltrimethylammonium bromide (CTAB) used to produce MCM-41 could be modified to utilise titanium only precursors.

5.6. References

- 1 D. M. Antonelli and J. Y. Ying, *Angew. Chemie Int. Ed. English*, 1996, **35**, 426–430.
- 2 G. Yudoyono, N. Ichzan, V. Zharvan, R. Daniyati, H. Santoso, B. Indarto, Y. H. Pramono, M. Zainuri and Darminto, in *AIP Conference Proceedings*, 2016, vol. 1725.
- 3 Z. Kónya, V. F. Puentes, I. Kiricsi, J. Zhu, J. W. Ager, M. K. Ko, H. Frei, P. Alivisatos and G. A. Somorjai, *Chem. Mater.*, 2003, **15**, 1242–1248.
- 4 V. F. Stone and R. J. Davis, *Chem. Mater.*, 1998, **10**, 1468–1474.
- 5 T. D. Nguyen-Phan, H. D. Pham, S. Kim, E. S. Oh, E. J. Kim and E. W. Shin, *J. Ind. Eng. Chem.*, 2010, **16**, 823–828.
- 6 X. Hu, M. Trudeau and D. M. Antonelli, *Chem. Mater.*, 2007, **19**, 1388–1395.
- 7 D. M. Antonelli, *Adv. Mater.*, 1999, **11**, 487–492.
- 8 A. Lezau, M. Trudeau, G. M. Tsoi, L. E. Wenger and D. Antonelli, *J. Phys. Chem. B*, 2004, **108**, 5211–5216.
- 9 X. Hu, B. O. Skadtchenko, M. Trudeau and D. M. Antonelli, *J. Am. Chem. Soc.*, 2006, **128**, 11740–11741.
- 10 X. An, H. Liu, J. Qu, S. J. A. Moniz and J. Tang, *New J. Chem.*, 2015, **39**, 314–320.
- 11 X. Jiang, M. Manawan, T. Feng, R. Qian, T. Zhao, G. Zhou, F. Kong, Q. Wang, S. Dai and J. H. Pan, *Catal. Today*, 2018, **300**, 12–17.
- 12 D. Chen, F. Huang, Y. B. Cheng and R. A. Caruso, *Adv. Mater.*, 2009, **21**, 2206–2210.
- 13 T. Sun and J. Y. Ying, *Nature*, 1997, **389**, 704.
- 14 D. M. Antonelli, A. Nakahira and J. Y. Ying, *Inorg. Chem.*, 1996, **35**, 3126–3136.
- 15 R. Raja, J. M. Thomas, M. Greenhill-Hooper and V. Doukova, *Chem. Commun.*, 2007,

- 1924–1926.
- 16 L. Matachowski, K. Pamin, J. Połtowicz, E. M. Serwicka, W. Jones and R. Mokaya, *Appl. Catal. A Gen.*, 2006, **313**, 106–111.
 - 17 J. M. Thomas, R. Raja, G. Sankar and R. G. Bell, *Acc. Chem. Res.*, 2001, **34**, 191–200.
 - 18 D. M. Antonelli and J. Y. Ying, *Chem. Mater.*, 1996, **8**, 874–881.
 - 19 S. M. Park and D. S. Kim, *Polym. Eng. Sci.*, 2019, **59**, 752–756.
 - 20 P.-P. Knops-Gerrits, A. Verberckmoes, R. Schoonheydt, M. Ichikawa and P. A. Jacobs, *Microporous Mesoporous Mater.*, 1998, **21**, 475–486.
 - 21 M. D. Alba, Z. Luan and J. Klinowski, *J. Phys. Chem.*, 1996, **100**, 2178–2182.
 - 22 J. Y. Ying, C. P. Mehnert and M. S. Wong, *Angew. Chemie Int. Ed.*, 1999, **38**, 56–77.
 - 23 S. R. Gajjela, K. Ananthanarayanan, C. Yap, M. Grätzel and P. Balaya, *Energy Environ. Sci.*, 2010, **3**, 838.
 - 24 Q. Dai, Z. Zhang, N. He, P. Li and C. Yuan, *Mater. Sci. Eng. C*, 1999, **8–9**, 417–423.
 - 25 R. Joyner and M. Stockenhuber, *J. Phys. Chem. B*, 1999, **103**, 5963–5976.
 - 26 W. M. H. Sachtler, *Acc. Chem. Res.*, 1993, **26**, 383–387.
 - 27 P. Serna and B. C. Gates, *Acc. Chem. Res.*, 2014, **47**, 2612–2620.
 - 28 G. I. N. Waterhouse, G. A. Bowmaker and J. B. Metson, *Phys. Chem. Chem. Phys.*, 2001, **3**, 3838–3845.
 - 29 G. Ovejero, J. L. Sotelo, F. Martínez, J. A. Melero and L. Gordo, *Ind. Eng. Chem. Res.*, 2001, **40**, 3921–3928.
 - 30 M. Stöcker, *Microporous Mater.*, 1996, **6**, 235–257.
 - 31 A. H. Lu, J. J. Nitz, M. Comotti, C. Weidenthaler, K. Schlichte, C. W. Lehmann, O.

- Terasaki and F. Schüth, *J. Am. Chem. Soc.*, 2010, **132**, 14152–14162.
- 32 M. Thommes, K. Kaneko, A. V. Neimark, J. P. Olivier, F. Rodriguez-Reinoso, J. Rouquerol and K. S. W. Sing, *Pure Appl. Chem.*, 2015, **87**, 1051–1069.
- 33 J. D. Marty, M. Tizra, M. Mauzac, I. Rico-Lattes and A. Lattes, *Macromolecules*, 1999, **32**, 8674.
- 34 M. Conte, K. Wilson and V. Chechik, *Org. Biomol. Chem.*, 2009, **7**, 1361–1367.
- 35 J. C. Gee and R. C. Williamson, *J. Am. Oil Chem. Soc.*, 1997, **74**, 65–67.
- 36 M. Kidwai and S. Bhardwaj, *Synth. Commun.*, 2011, **41**, 2655–2662.
- 37 B. Jain, A. K. Singh, H. Kim, E. Lichtfouse and V. K. Sharma, *Environ. Chem. Lett.*, 2018, **16**, 947–967.
- 38 E. Brillas, I. Sirés and M. A. Oturan, *Chem. Rev.*, 2009, **109**, 6570–6631.
- 39 S. K. Upadhyay, S. R. K. Pingali and B. S. Jursic, *Tetrahedron Lett.*, 2010, **51**, 2215–2217.
- 40 USOO5718878A, *US Pat. Appl. Publ.*, 1996.
- 41 S. G. Lee, H. J. Lee, I. Song, S. Youn, D. H. Kim and S. J. Cho, *Sci. Rep.*, 2015, **5**, 12702.
- 42 W. Chen, X. Sun and D. Weng, *Mater. Lett.*, 2006, **60**, 3477–3480.
- 43 J. Zheng, T. Yu and D. G. Truhlar, *Phys. Chem. Chem. Phys.*, 2011, **13**, 19318–19324.
- 44 R. D. Bach and O. Dmitrenko, *J. Am. Chem. Soc.*, 2004, **126**, 4444–4452.
- 45 Z. Tian, A. Fattahi, L. Lis and S. R. Kass, *J. Am. Chem. Soc.*, 2006, **128**, 17087–17092.

CHAPTER 6: The synthesis of microporous niobium oxide

Contents

CHAPTER 6: The synthesis of microporous niobium oxide	275
Abbreviations	276
6.1. Introduction	277
6.2. The synthesis of microporous niobium oxide.....	278
6.2.1. Sun Tao's protocol for the synthesis of microporous niobium oxide	278
6.2.2. Antonelli's protocol for the synthesis of porous niobium oxide.....	283
6.3. Introduction of dopant metals during synthesis	285
6.4. Microporous Nb ₂ O ₅ thermal resistance and calcination for template removal.....	287
6.5. Template removal: Acidification	289
6.6. Template removal: Alternatives to acid	295
6.7. Catalyst testing and metal oxide framework reaction resistance	298
6.7.1. As synthesised materials	298
6.7.2. Template free materials	300
6.8. Conclusions and future work.....	305
6.9. References	306

Abbreviations

FTIR-ATR – Fourier Transform Infra-Red – Attenuated Total Reflectance

ICP-OES – Inductively Coupled Plasma – Optical Emission Spectrometry

M:S – Metal to substrate ratio

PO_2 – Pressure Gauge O_2

p-TSA – *para* Toluene Sulphonic Acid

TGA – Thermogravimetric Analysis

TMS-1 – Transition Metal Oxide Molecular Sieve #1

XRPD – X-Ray Powder Diffraction

6.1. Introduction

As previously described the focus of this project was to create a porous framework, based on a metal oxide to provide alternative materials to zeolites for the oxidation of alkanes. Conclusions drawn from section 5.2 – 5.3 revealed an alternative was needed to mesoporous titanium oxide. Although the synthesis of microporous TiO_2 and subsequent synthesis featuring dopant metals were successful, template removal ultimately led to complete pore collapse. Furthermore, synthesis via peptization led to catalytically inactive materials or materials not sufficiently active for our scope. Examples of the synthesis of other meso/microporous metal oxides including frameworks based on: Nb, Ta, Zr, Mn and Fe are present in the literature (see section 1.5.1).¹⁻⁵ In this context, microporous niobium oxide (of expected stoichiometry Nb_2O_5) was chosen for the focus of this project due to its theoretical inert chemistry towards alkane oxidation (and as such to be conveniently used as a framework to exploit the activity of a dopant metal), and a literature presence where the template removal is documented.⁶⁻⁸ Similarly to mesoporous titanium oxide, a niobium alkoxide precursor can be bound to an amine to form micelles, which ultimately becomes a porous network via hydrothermal conditions. Again, the template is removed with acidification amongst literature sources.^{6,7}

6.2. The synthesis of microporous niobium oxide

6.2.1. Sun Tao's protocol for the synthesis of microporous niobium oxide

The synthesis of microporous niobium oxide was documented by Tao *et al.*⁶ The synthesis reported is analogous to that of mesoporous titanium oxide's described in section 5.2. However, significantly higher temperatures and longer autoclave conditions are used, summarised in table 6.2.1.1.

Table 6.2.1.1: A comparison of autoclave conditions between mesoporous titanium oxide and microporous niobium oxide.

Material	Autoclave temperature (°C)	Autoclave duration (days)	Ref
Mesoporous titanium oxide	80	4	[9]
Microporous niobium oxide	180	10	[6]

Microporous niobium oxide synthesis was successfully reproduced from the literature using a hexylamine template (this will be referred to as Nb-TMS1, as it was in the original literature). The as synthesised sample's XRPD (x-ray powder diffraction) patterns (figure 6.2.1.1) shows a significant reflection in the microporous region ($1 - 15^\circ 2\theta$) corresponding to a pore diameter of $19.7 (\pm 0.1 \text{ \AA})$, and thus qualifies as a microporous material ($< 20 \text{ \AA}$). In the current work, the synthesis was repeated several times and pore size was always within experimental error, unlike mesoporous titanium oxide which showed small deviation from batch to batch. Furthermore, the intensity of the reflection associated to the interplanar distance of the pores is significantly higher in microporous niobium oxide (ca. a factor of 4), when compared to mesoporous titanium oxide prepared in an analogous way. Interestingly, there is only two additional peaks in the microporous sample's XRPD at ca. 9 and $28^\circ 2\theta$.

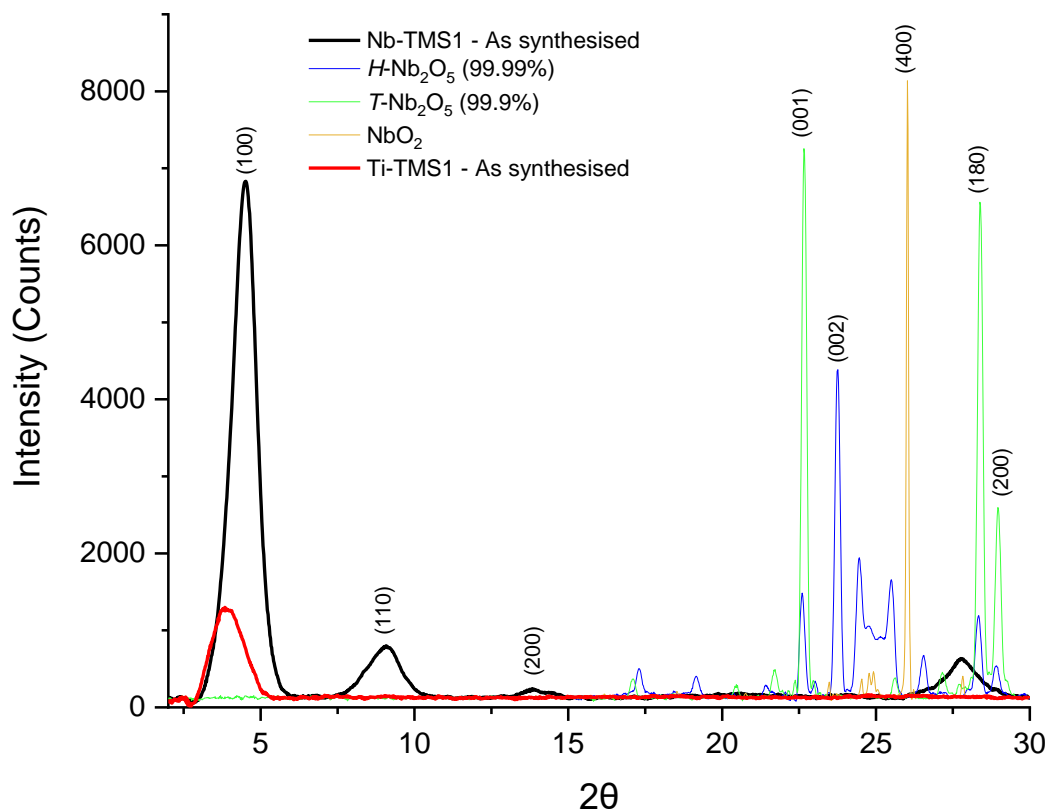


Figure 6.1.2.1: XRPD patterns of as synthesised microporous niobium oxide and corresponding bulk Nb_2O_5 and NbO_2 (scaled down y-axis) shown here as comparisons. Mesoporous TiO_2 obtained by using Antonelli's protocol is shown here for additional comparison. (-) Microporous niobium oxide: $\text{Nb}(\text{OEt})_5$ and hexylamine (1:1), Autoclave 180 °C, 10 days, washed with H_2O (3×50 mL), MeOH (3×50 mL) and Et_2O (3×50 mL). (-) Mesoporous titanium oxide obtained from: $\text{Ti}(\text{O}^i\text{Pr})_4$ and hexylamine (2:1), Autoclave 80 °C, 4 days, washed with H_2O (3×50 mL), MeOH (3×50 mL) and Et_2O (3×50 mL). The most intense peaks of the commercial niobium oxide patterns are assigned from literature,¹⁰⁻¹² along with the microporous niobium oxide.^{6,8}

The peak at 9.04° 2θ (corresponding to a d -spacing of 9.78 \AA) could be due to a hierarchal structure where a second set of crystalline pores exist. The peak's identity at 27.8° 2θ is unknown. This, however, is not quartz (a common contaminant in many XRPD patterns,¹³ as it would be expected at 26.7° 2θ).¹⁴ On the other hand, it does not correspond to any common crystal phase from commercial Nb_2O_5 , nor NbO_2 , this could be due to the microporous niobium oxide not being a stoichiometric material (this is further discussed below). The intensity difference between microporous niobium oxide and mesoporous titanium oxide could be due to numerous factors. Specifically, the higher temperature and longer duration in the autoclave

is likely promoting the crystallisation of this sample, whereas any temperature greater than 110 °C, and duration more than 4 days leads to decomposition of the pores in mesoporous titanium oxide. This suggests that the crystallisation of microporous niobium oxide could be more robust than that of the mesoporous titanium oxide (for comparison, longer times and higher temperatures of autoclave steps were found to increase crystallinity within samples of zeolites).^{15,16} As the microporous niobium oxide synthesis already yielded very crystalline porous material, and considered appropriate for our aims, no further optimisation of the synthesis parameters was conducted.

It should be noted, however, that details of the composition of microporous niobium oxide from literature^{2,6,8} are often vague and therefore further study using other analytical techniques were conducted, here in this work FTIR-ATR (Fourier transform infrared – attenuated total reflectance) and TGA (thermogravimetric analysis) were carried out (figures 6.2.1.2 and 6.2.1.3 and table 6.2.1.2).

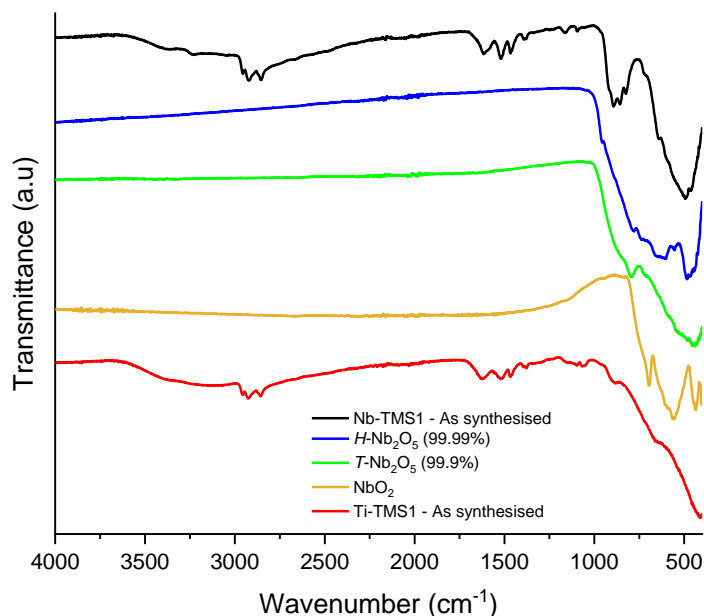


Figure 6.2.1.2: FTIR-ATR of as synthesised microporous niobium oxide and corresponding bulk Nb_2O_5 and NbO_2 as comparisons. Bulk Nb_2O_5 samples have been denoted *H*- or *T*- determined from their crystal structure.¹⁷ Mesoporous titanium oxide synthesised via Antonelli's protocol is shown here for additional comparison. The C-H stretch ($2700 - 3100 \text{ cm}^{-1}$), O-H stretch ($\sim 2750 - 3500 \text{ cm}^{-1}$) and potentially additional hexylamine N-H/lattice vibration peaks ($1250 - 1700 \text{ cm}^{-1}$) can be seen.

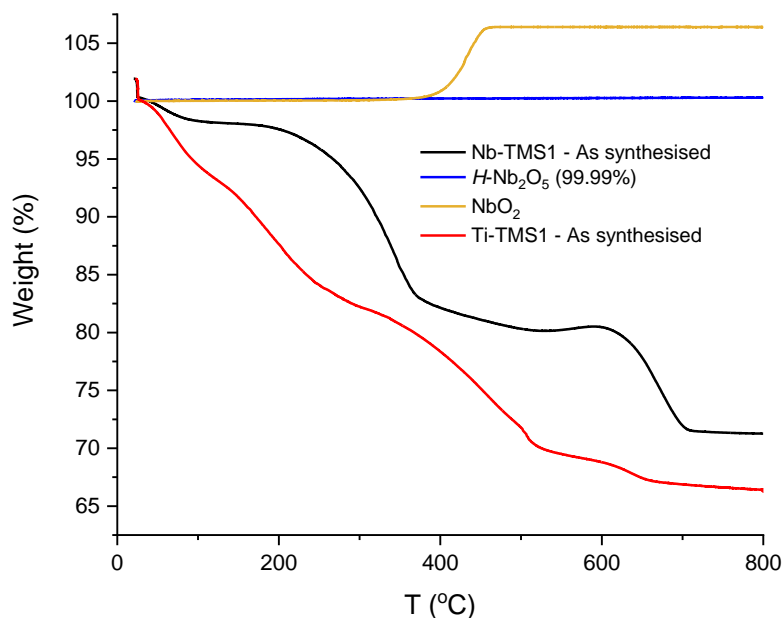


Figure 6.2.1.3: TGA of as synthesised microporous niobium oxide and corresponding bulk Nb_2O_5 and NbO_2 as comparisons. Mesoporous titanium oxide synthesised via Antonelli's protocol is shown here for additional comparison.

As with the mesoporous titanium oxide, the template is still present in the as-synthesised microporous niobium oxide. This is shown by the bands associated to the C-H stretching between 2800 – 3000 cm^{-1} in the FTIR-ATR.³ Furthermore, this is corroborated by the mass loss up to 500 °C from TGA determination in air, which is typical of organic matter being combusted.^{3,18} As the protocol used for the synthesis of these materials has numerous solvent washes, the chemically bound amine template remains in place and requires further treatment for removal (section 6.4 – 6.6). Peaks around 1500-1750 cm^{-1} are again observed, likely to be due to other organic frequencies³ (e.g. N-H)¹⁹ and potential lattice vibrations seen in zeolites.^{20,21} However, IR data hint to changes in the framework structure. Interestingly, when comparing the FTIR-ATR of the Nb-TMS1, bulk Nb_2O_5 and NbO_2 a different sequence of peaks is observed $< 1000 \text{ cm}^{-1}$. Specifically, there is an absence of absorbance at 750 cm^{-1} . This is indicative of a different crystal structure as observed amongst the polymorphs of Nb_2O_5 .²² This is expected as the microporous Nb_2O_5 has a proposed regular hexagonal structure versus the bulk.⁸

Table 6.2.1.2: TGA data summary of mass loss with corresponding descriptions of mass loss.

Material	T (°C)	Δ Weight (%)	Description
Nb-TMS1	~50 – 100	< -2	Surface H_2O
Nb-TMS1	180 – 400	~ -20	Organic template combustion
Nb-TMS1	550 – 700	~ -10	Potential changes in Nb:O stoichiometry
NbO_2	370 – 470	~ +7	$2\text{NbO}_2 + \frac{1}{2}\text{O}_2 \rightarrow \text{Nb}_2\text{O}_5$

Also, the TGA trace shows interesting features (figure 6.2.1.3 and table 6.2.1.2). Up to 500 °C there is a significant drop in wt%, (ca. 20%) this is expected and can be attributed to the combustion of the organic template. The molar ratio of Nb:hexylamine from the TGA is 1:1.3. As the initial ratio was 1:1, this could suggest that not all the niobium from the original niobium ethoxide is present in the sample, and thus was not bound to the hexylamine precursor and

washed away during the synthesis. On the other hand, this loss of precursor may in principle occur in hydrothermal synthesis with the metal forming soluble oligomer species.^{23,24} To test this hypothesis, the mother liquor decanted from the autoclave was characterized by ICP-OES (inductively coupled plasma – optical emission spectroscopy). No niobium was detected thus meaning the introduction of water during the synthesis completely hydrolysed all the niobium alkoxide/niobium amine compounds to insoluble material. Therefore, the additional mass loss could be from organic precursor material which did not completely hydrolyse (i.e. the ethoxy ligands).

However, a shoulder is observed beginning at 600 °C. This is unlike Nb₂O₅ which shows no change in the TGA (as expected), or NbO₂ which shows a weight gain at 400 °C (which is $2\text{NbO}_2 + \frac{1}{2}\text{O}_2 \rightarrow \text{Nb}_2\text{O}_5$). It is still uncertain what this change could be due to. One possible explanation is the presence of oxygen bridges and not having a stoichiometric niobium oxide (as observed in defective TiO₂, for example).²⁵ Therefore, at higher temperatures, the oxygen is released due to lattice mobility, like for example MoO₃ and thus leading to the mass loss observed in the TGA.²⁶

6.2.2. Antonelli's protocol for the synthesis of porous niobium oxide

Antonelli has also reported a synthesis for porous niobium oxide.⁷ As a term of comparison Antonelli's protocol was conducted to determine if it may offer a material with beneficial properties.

Antonelli's reported synthesis differs from Tao's as it utilises ethanol as a solvent during the initial introduction of niobium ethoxide to the amine template. Also, the amine template used is tetradecylamine. The amine is much larger than hexylamine and therefore was expected to give a larger pore size in the final product. Although micropores were desired, this was still attempted to ensure this was not a limiting factor for successful template removal.

It was found that Antonelli's protocol does indeed lead to larger pore sizes (figure 6.2.2.1). Using a C₁₄ template, the pore size increases to 41.2 Å – 32.1 Å. The additional peaks

observed in the microporous region could be due to a hierarchal structure existing within the framework. The pore size increase is not linearly correlative to the size of template as the diameter with a C₆ template at 19.7 Å would predict a pore size of ~46 Å with a C₁₄ template. However, this is likely to be due to the restricted flexible nature of the alkyl chain instead of being permanently taught.²⁷ As for the intensity of the peaks there is little difference, with Antonelli's being only slightly higher in intensity.

When the template removal was attempted as stated in the literature, by washing with nitric acid at pH 2,⁷ the pores completely collapsed. As the pore size is already further out of range from the desired microporous framework, and template removal would need significant optimization, Tao's protocol⁶ was chosen to be pursued instead.

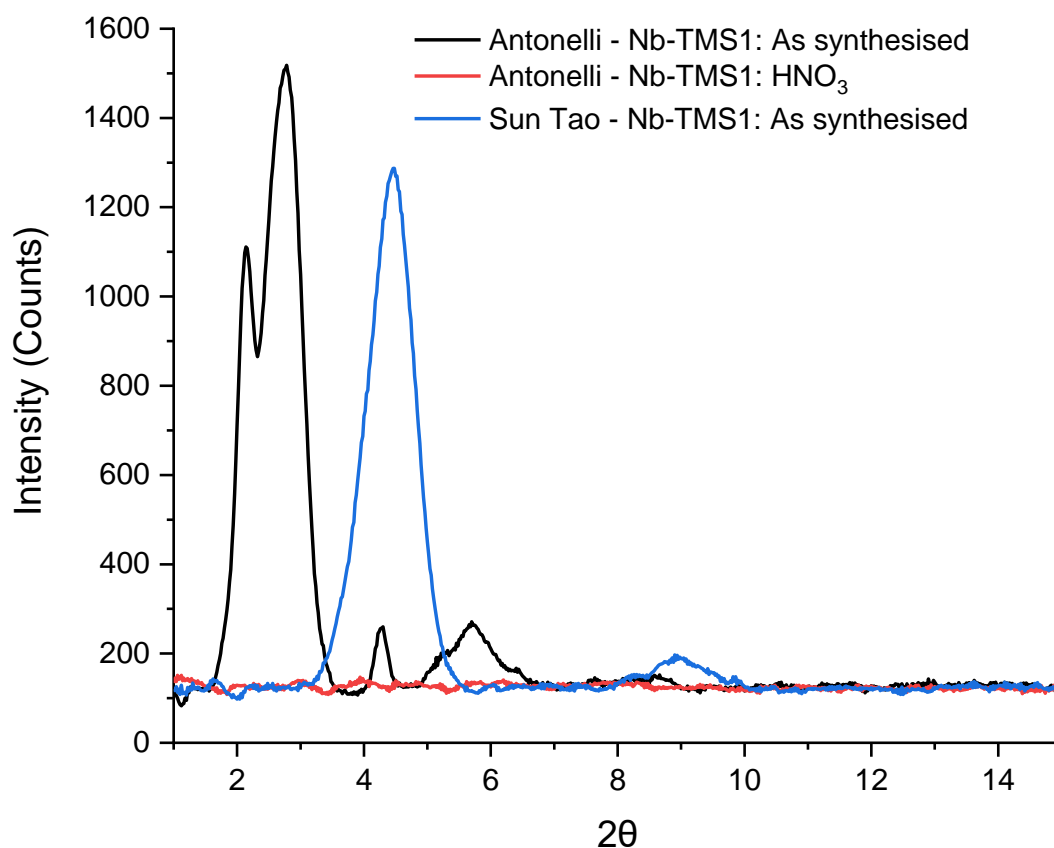


Figure 6.2.2.1: XRPD patterns of mesoporous niobium oxide samples obtained from Antonelli's protocol and the corresponding template removed sample as described within the literature (via HNO₃). A sample from Sun Tao's protocol is shown here for comparison.

6.3. Introduction of dopant metals during synthesis

The next challenge of the project was to include intra-framework dopant metals to the niobium oxide. As in the same case of mesoporous TiO_2 , no literature to our knowledge exists where a dopant metal alkoxide is used during the synthesis of microporous Nb_2O_5 . Due to the data showing iron as the most active metal towards oxidation for both *n*-decane and cyclooctane (see section 4.2 – 4.3), it was prioritised for the incorporation into the framework. This was successfully achieved with iron ethoxide, as shown in figures 6.3.1a and 6.3.1b.

The incorporation of the iron seemed to not cause any significant changes in porosity, which is highly desirable for our applications. Both the XRPD and FTIR-ATR almost completely overlap. The intensity for the porous reflection ($4.5\ 2\Theta$) is slightly lower in the iron doped sample, or if intensity is normalized the peak is broader, which suggests a material with a lower degree of crystallinity. However, the intensity is still significantly higher than any samples of mesoporous Fe/Ti-TMS1 (by a factor of ~ 3). The XRPD shows no additional peaks between the samples, however, as described previously (section 4.2.1.6) iron oxide at such low loading is unlikely to be detected.

No other metals have presently been trialled for doping in microporous Nb_2O_5 synthesis, however, to our knowledge this is the first example where iron has been incorporated into the structure of microporous niobium oxide via a templating method.

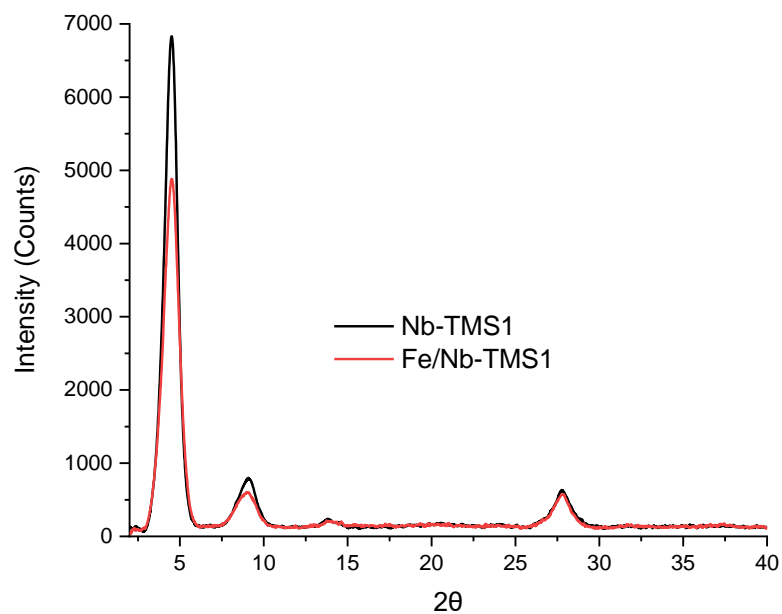


Figure 6.3.1a: XRPD patterns of as synthesised microporous niobium oxide and Fe/Nb-TMS1 2 mol%.

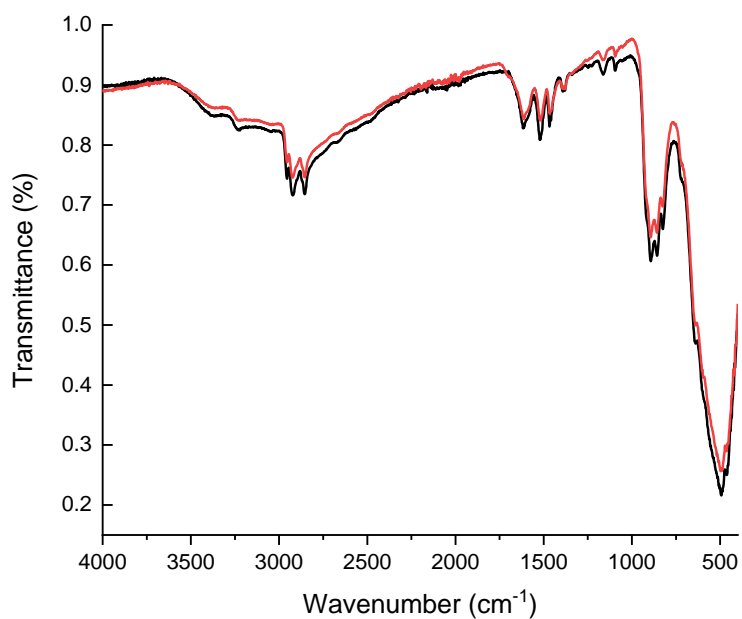


Figure 6.3.1b: FTIR-ATR data of as synthesised microporous niobium oxide and Fe/Nb-TMS1 2 mol%. The C-H stretch (2700 – 3100 cm⁻¹), O-H stretch (~2750 – 3500 cm⁻¹) and potentially additional hexylamine N-H/lattice vibration peaks (1250 – 1700 cm⁻¹) can be seen.

6.4. Microporous Nb₂O₅ thermal resistance and calcination for template removal

Due to the convenience of a calcination process to remove a template²⁸ this method was also tested with microporous Nb₂O₅. However, attempts of calcination led to complete pore collapse and crystallisation in the bulk phase. Therefore, in order to investigate the thermal resistance of microporous Nb₂O₅ systematically, the material was subjected to *in-situ* X-ray diffraction at different temperatures.

The thermal stability of as synthesised iron doped microporous niobium oxide is demonstrated in figures 6.4.1 and 6.4.2. As temperature increases, the pores remain stable until 200 °C, where then collapse begins and by 240 °C porosity is completely lost. Furthermore, the peak at 4.8° 2 θ associated to the pore structure starts to shift to higher 2 θ values, signifying a decrease in interplanar distance and in turn shrinking of the pores as the intensity drops. The correlation between intensity of reflection, with its corresponding *d*-spacing value (estimated pore size) is shown in figure 6.4.1 to illustrate this phenomenon.

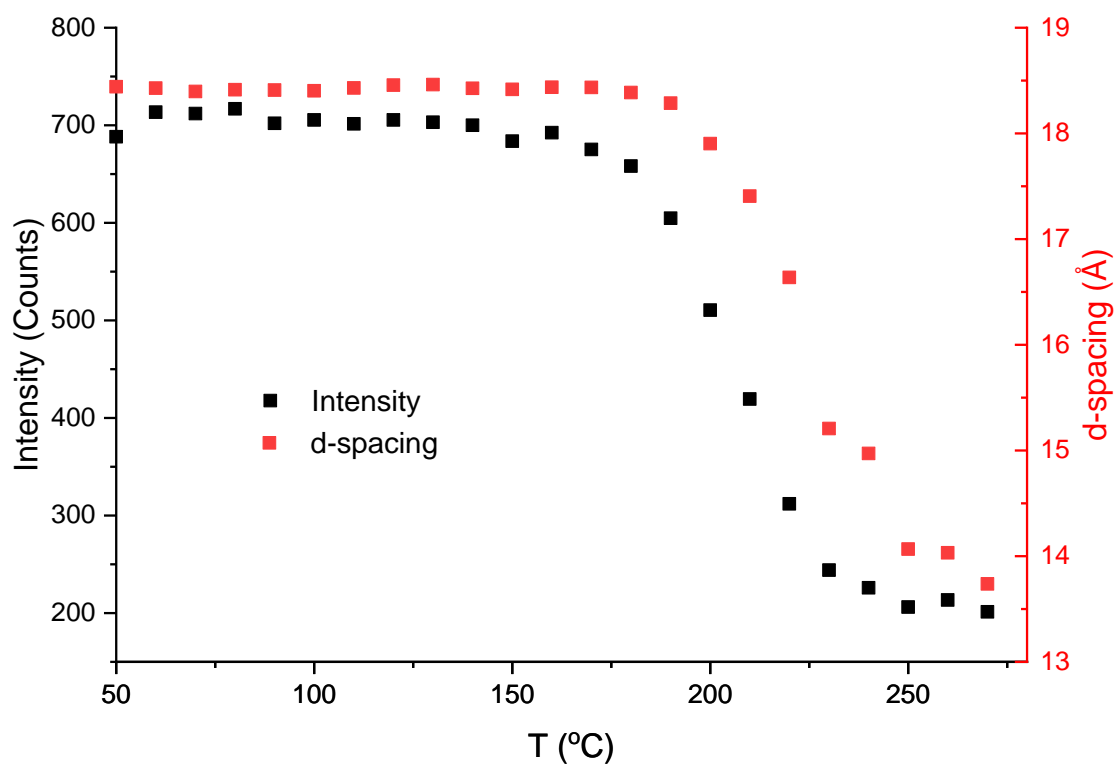


Figure 6.4.1: A plot to show how temperature affects the intensity of the reflection from porosity in the XRPD pattern of microporous iron doped niobium oxide and the corresponding *d*-spacing.

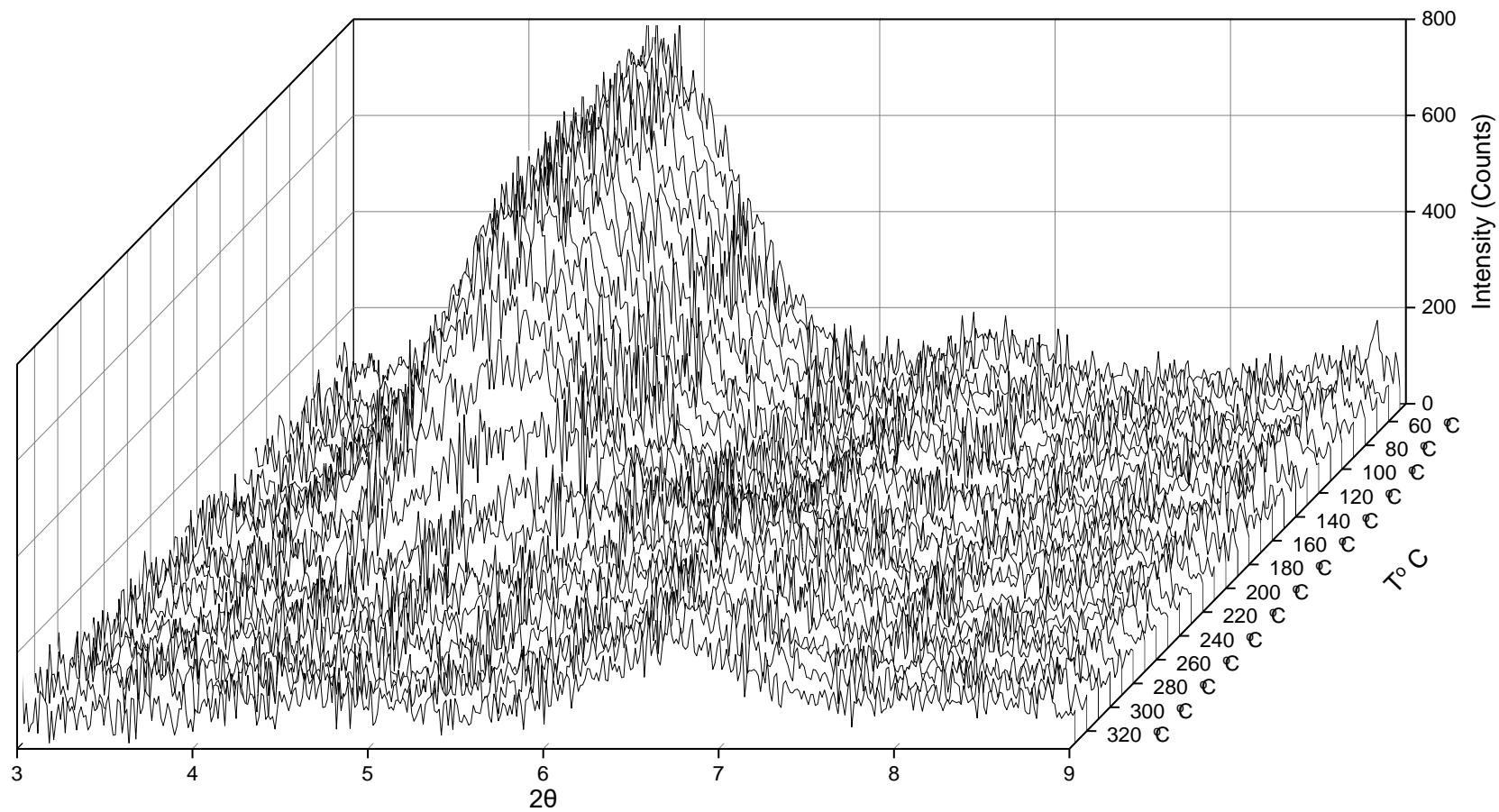


Figure 6.4.2: In-situ XRPD patterns of microporous iron doped (2 mol%) Nb₂O₅ collected using an Anton-Paar cell in air, scanning the microporous region and how it changes with temperature. Pore collapse as indicated from the loss of intensity starts to occur around 200 °C until 240 °C where all porosity is lost. Air flow = 10 ml min⁻¹, 3 bar T = 10 °C min⁻¹.

6.5. Template removal: Acidification

Washing in nitric acid/ethanol solution is stated to be an efficient method to remove the amine template,^{3,5,8} as protonation of the amine group is required due to the strong interaction that it can have with a metal-oxide framework.⁷ Accordingly, template removal by acidification was conducted for microporous Nb₂O₅. Literature data^{6,7} claim these materials are acid resistant, and template removal should or can be carried out at pH 2. Below this value a loss of porosity may occur. However, repeated tests carried out in our lab showed that washing at pH 2 leads to complete loss of porosity. Furthermore, even template removal with HNO₃ at pH 4 it was found to completely remove the template in mesoporous TiO₂ (which was then chosen as optimal pH, section 5.2.6). However, for mesoporous TiO₂ this did lead to complete pore collapse, but thus far niobium oxide has shown to be more thermally and mechanically robust. The results of microporous niobium oxide template removal with nitric acid are summarised in figure 6.5.1a and 6.5.1b. Interestingly, the template has not been completely removed (quantified via TGA), and the porous framework remains. The as-synthesised material contains 18 wt% corresponding to the amine template in comparison to the 12 wt% remaining post HNO₃ pH 4 wash. A small pore shrinkage was observed from 19.7 Å to 19.2 Å.

This means that although the microporous Nb₂O₅ is more robust than its TiO₂ counterpart, it is also more difficult to remove the template via acidification. It can also be seen that the other minor porous reflection at 9.04° 2 θ is damaged by the acidic conditions.

In view of this, and given some of the results reported in chapter 5, no further optimisation of template removal via HNO₃ was conducted due to conflicting reports in the literature²⁹ alongside data from the titanium oxide template removal attempts.

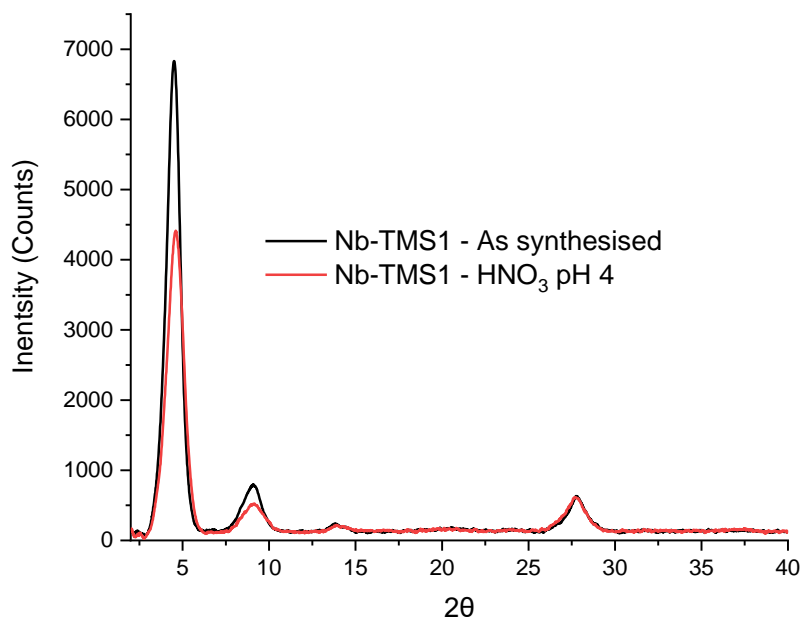


Figure 6.5.1a: XRPD patterns of as synthesised microporous niobium oxide and a sample treated with HNO₃ pH 4.

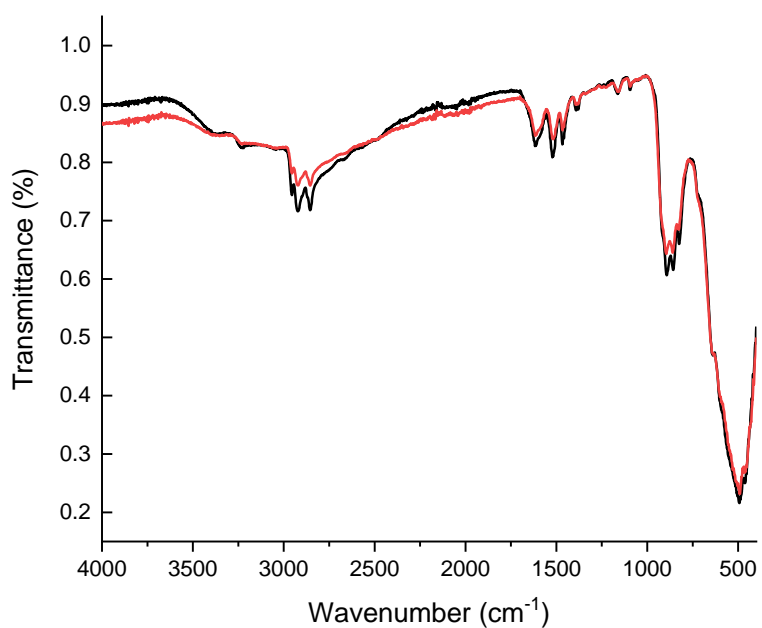


Figure 6.3.1b: FTIR-ATR data of as synthesised microporous niobium oxide and Fe/Nb-TMS1 2 mol%. The C-H stretch (2700 – 3100 cm⁻¹), O-H stretch (~2750 – 3500 cm⁻¹) and potentially additional hexylamine N-H/lattice vibration peaks (1250 – 1700 cm⁻¹) can be seen.

From data reported in section 5.2.6.2 indicating *p*-TSA is a slightly better candidate for acidic template removal,³⁰ as it efficiently removed the template at higher pH solutions, this route was pursued instead. Quite promisingly, template removal with a 1:1 molar ratio of *p*-TSA to hexylamine showed complete template removal from the FTIR-ATR and TGA (figure 6.5.2 and table 6.5.1) and pores remaining from the XRPD figure 6.5.3.

However, it was found that the characteristic reflection associated to the microporosity at $4.5^\circ 2\theta$ in the XRD patterns (figure 6.5.3) had its intensity drastically affected by the template removal and significant pore shrinkage had occurred. Although the pore size is still considered suitable for *n*-decane and cyclooctane oxidation (i.e. they can still fit within the pores),^{31,32} most of the resulting material is amorphous. In view of this, washes reducing the molar ratio of acid to template was attempted. As demonstrated in the mesoporous titanium oxide, nearly complete template removal can occur with a fractional amount of acid compared to that expected. Therefore, a series of tests were conducted where the *p*-TSA to hexylamine ratio was reduced.

Table 6.5.1: A summary of how d-spacing and hexylamine:Nb ratio changes as increasing amount of *p*-TSA in MeOH is used for template removal with microporous niobium oxide.

Test	d-spacing (Å)	Nb:Hexylamine	Hexylamine wt%
As synthesised - expected	-	1:1	44
As synthesised - actual	19.6	1:1.3	19
10 mol%	19.1	1:1.03	16.5
20 mol%	18.8	1:0.69	12
50 mol% (10 then 40 mol%)	11.7	1:0.26	4.7
100 mol%	11.6	1:0	0

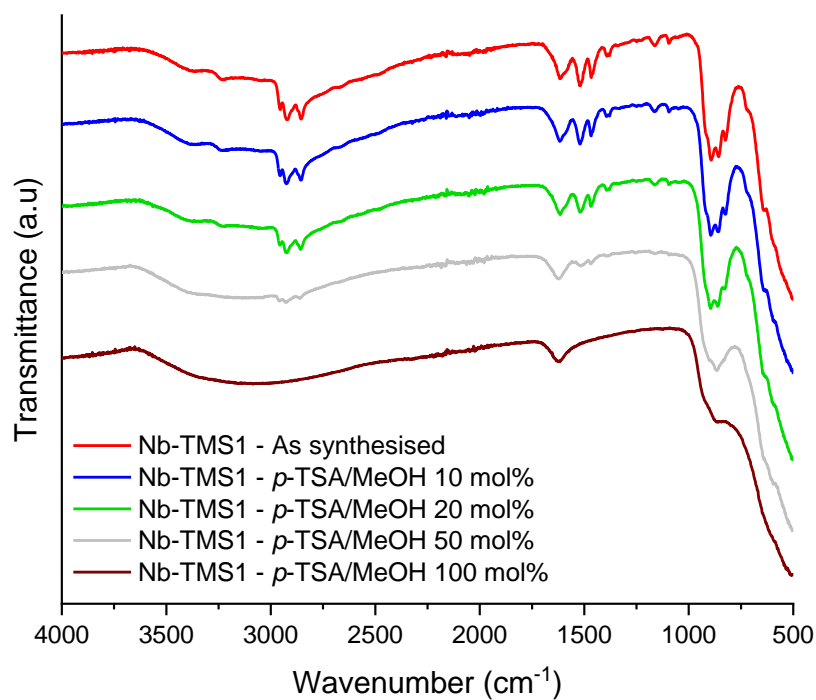


Figure 6.5.2: ATR-FTIR data for the microporous niobium oxide as synthesised and increasing mol% *p*-TSA/MeOH washes.

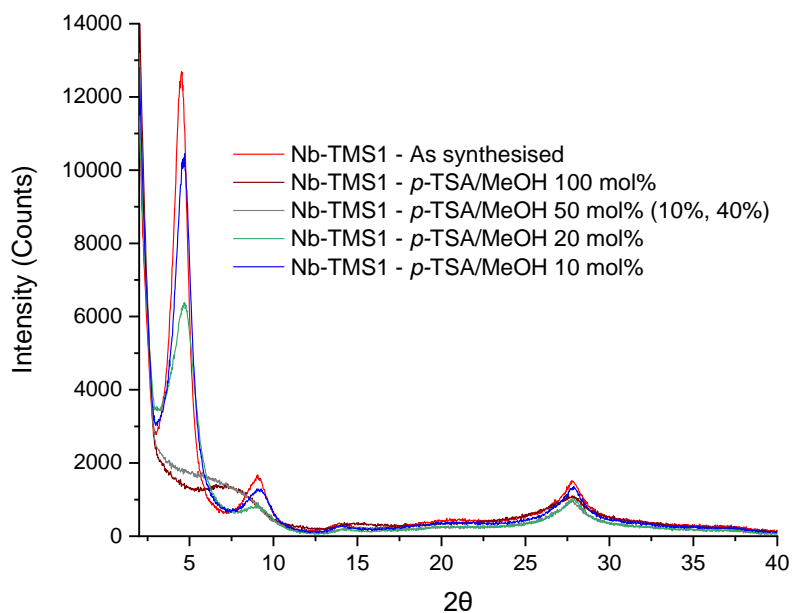


Figure 6.5.3: XRPD patterns for the microporous niobium oxide as synthesised and increasing mol% of *p*-TSA/MeOH washes (based on amount of hexylamine). The reflection from the porosity (4.5° 2θ) can be seen to decrease in intensity and get broader, meaning a larger pore size distribution, with increasing mol% of *p*-TSA added.

Although a significant amount of amine is removed at lower mol% of *p*-TSA, a 1:1 molar ratio of acid to template seems the most viable option for template removal. At 50 mol% of *p*-TSA, the porous peak ($7.2^\circ 2\theta$) reaches a minimum intensity in the XRPD, however, not all the template was removed. This led to the conclusion that even the more robust niobium oxide suffers significant attack from acids, regardless if they are organic or not. It should be noted that all metal oxides are, by definition, basic in their bulk.³³ This means eventually an acid attack will occur; however, our pH values at which these microporous materials are affected by acidic conditions contrast those reported in literature,^{6,7} despite accurate calibration of our experimental devices. Therefore, alternatives to acid washes that proved promising with mesoporous titanium oxide were tested.

6.6. Template removal: Alternatives to acid

The most promising alternative to acid seemed to be phthalic anhydride, as this was capable of complete template removal when used as an alternative to acid for mesoporous titanium oxide (section 5.2.8). Although this led to complete pore collapse in mesoporous titanium oxide, it is (at least in principle) the mildest way to remove the hexylamine as no acid is involved and the only interactions should be between the amine and the phthalic anhydride. It can be seen from FTIR-ATR measurements (figure 6.6.1) that phthalic anhydride is capable of completely removing all the organic template from microporous niobium oxide. As in the same way with mesoporous titanium oxide, no longer are the C-H peaks observed, and only a single peak at around 1500-1600 cm^{-1} , which is present due to suspected lattice vibrations.^{20,21} This is also backed up from the TGA which shows < 2 wt% organic material.

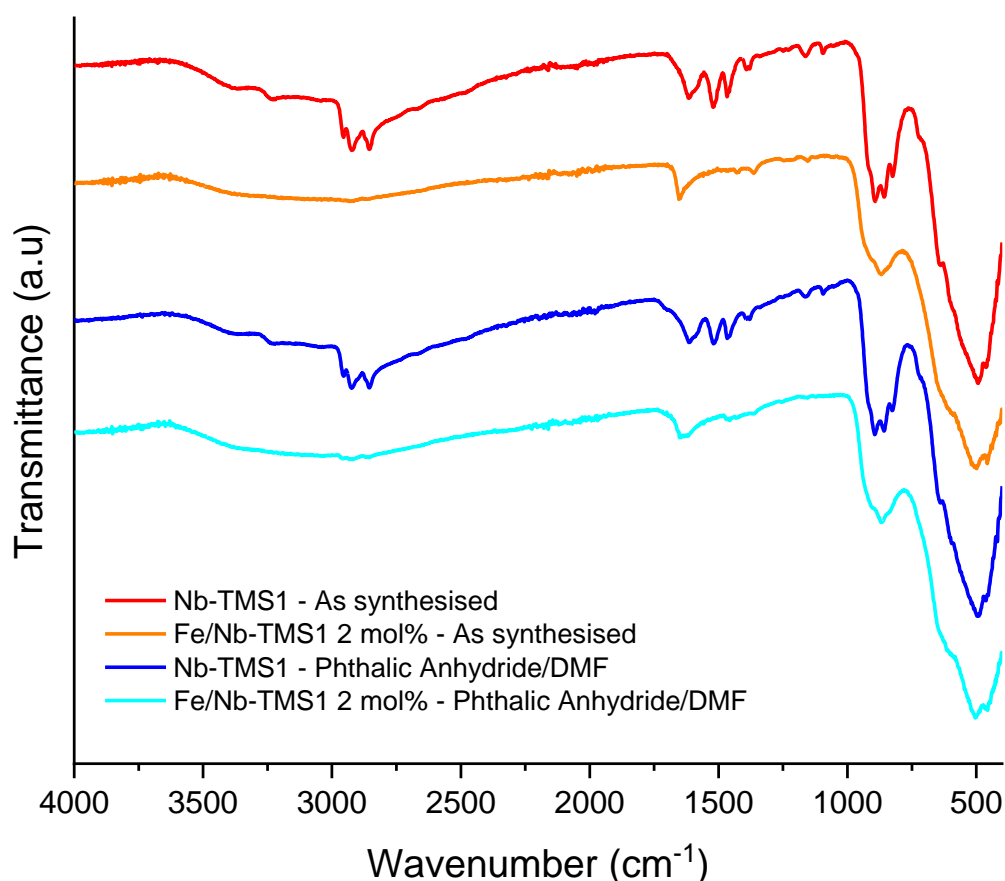


Figure 6.6.1: An overlay of FTIR-ATR spectra from as synthesised and phthalic anhydride treated microporous niobium oxide (200 mg scale) and Fe/Nb-TMS1 (500 mg scale).

Most importantly, from the XRPD pattern of phthalic anhydride treated microporous Nb₂O₅ (figure 6.6.2), a small peak at 8.0° 2 θ can still be seen. This suggests that a porous framework is still present after template removal, albeit the reflection is very low in intensity, pores are still present. A pore shrinkage has also been observed from 19.7 Å to 11.5 Å. The pore shrinkage is in the same range from data obtained with *p*-TSA template removal, this suggests that whichever template removal method is used for Nb-TMS1 pore shrinkage occurs in a similar manner. Although this is a significant reduction in pore diameter, it is still theoretically suitable for *n*-decane and cyclooctane oxidation.^{31,32}

In comparison to template-removal via *p*-TSA, the XRPD peaks are slightly less defined than in samples treated with phthalic anhydride. Therefore, a phthalic anhydride wash was chosen for the most ideal method for template removal as the risk of over acidification is not possible. This was applied to microporous Fe/Nb-TMS1 and was able to be conducted on a 500 mg scale. To our knowledge, this is the first example of porous iron doped niobium oxide where the template is removed, and where template removal is achieved with phthalic anhydride in microporous niobium oxide.

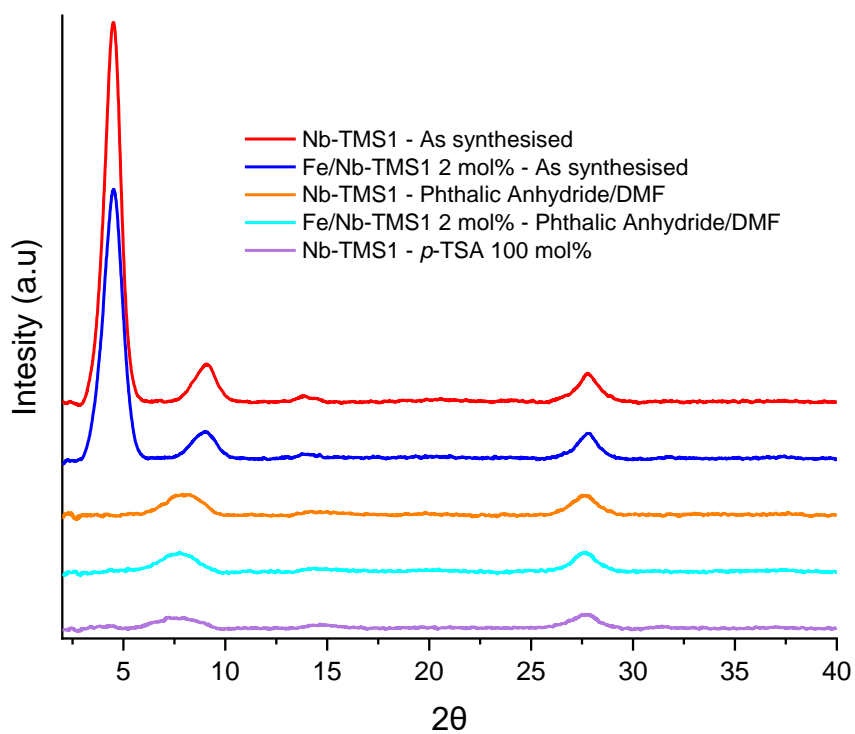


Figure 6.6.2: An overlay of XRPD patterns from as synthesised and phthalic anhydride treated microporous niobium oxide (200 mg scale) and Fe/Nb-TMS1 (500 mg scale). The *p*-TSA washed sample is included as comparison.

6.7. Catalyst testing and metal oxide framework reaction resistance

6.7.1. As synthesised materials

Thus far, microporous niobium oxide has proved to be more resilient than the corresponding mesoporous titanium oxide. Therefore, it was used for the hydrocarbon oxidation reactions at the centre of this project. Both the as synthesised and template removed materials were tested.

From figure 6.7.1.1 it can be seen that little change has occurred in the XRPD pattern of the as synthesised materials after catalytic tests. For the non-doped microporous niobium oxide, *n*-decane oxidation conditions seem to have not affected the structure at all, whereas cyclooctane oxidation led to a slight decrease in the intensity of the material's pore reflection.

As for the iron doped sample, both *n*-decane and cyclooctane oxidation conditions show a reduction in intensity in the XRPD pattern. This could be due to the presence of the iron within the framework, and possible leaching of Fe. However, the decrease in intensity is relatively minor (< ~20%) when compared to the loss of intensity observed in the mesoporous titanium oxide samples (~50%).

The as synthesised materials, however, showed no conversion for either *n*-decane nor cyclooctane oxidation. This is, to some extent, to be expected as all the active sites for oxidation catalysis would be blocked by the amine template. However, these tests were carried out anyway for the following reasons: (i) partial oxidation reactions of hydrocarbons can generate acids, and these could remove the template *in situ*, and (ii) given the results reported for TiO₂ (see section 5.2.9) these tests are crucial in determining mechanical resistance under harsh conditions.

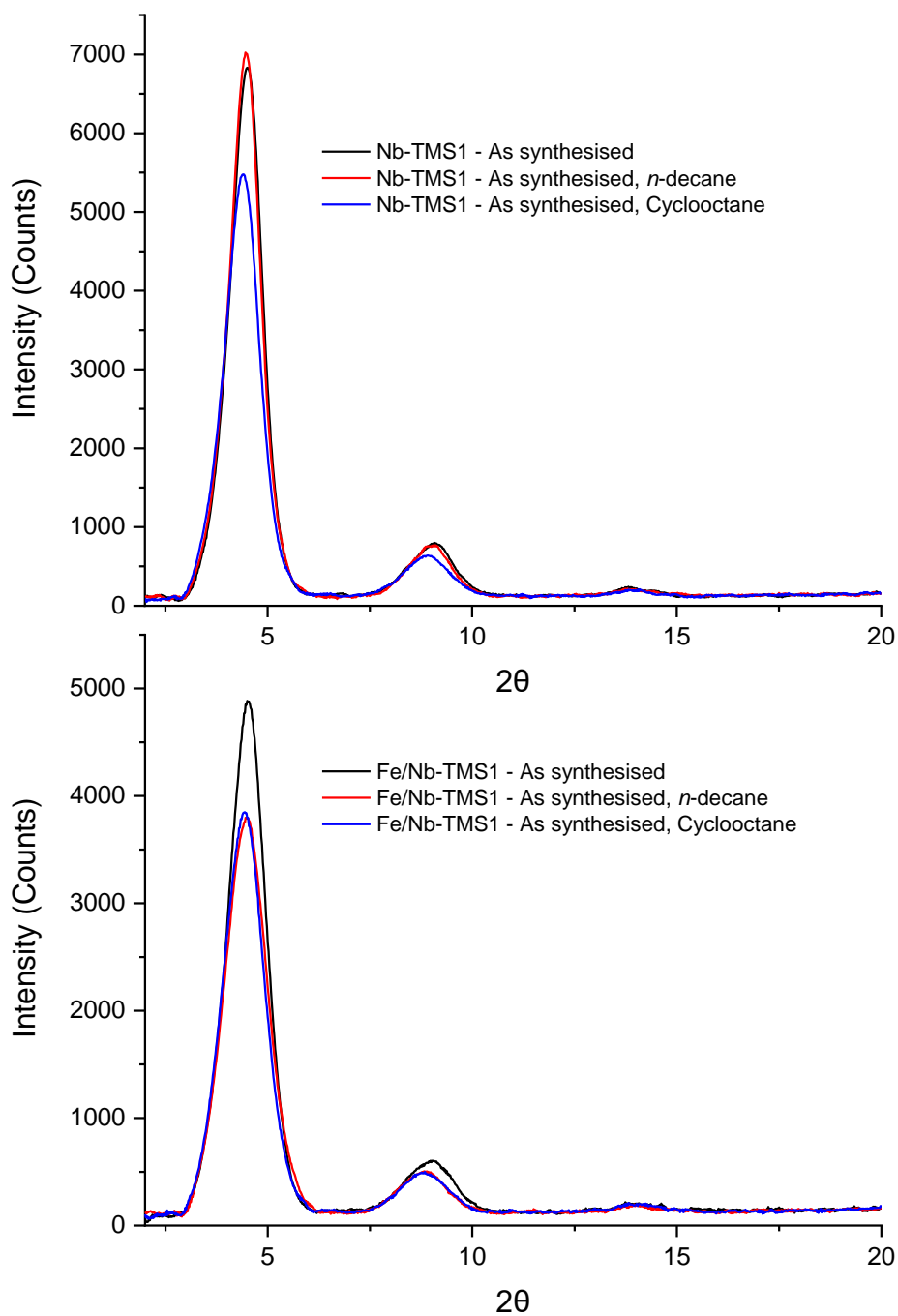


Figure 6.7.1.1: XRPD patterns of as synthesised microporous niobium oxide (top) and the corresponding iron doped material (bottom) subjected to catalytic conditions for alkane oxidation. *n*-decane (3 mL), M:S = 1:1000; 115 °C; $PO_2 = 1$ bar; 24 h. Cyclooctane (3 mL), M:S = 1:1000; 110 °C; $PO_2 = 2$ bar; 24 h.

6.7.2. Template free materials

Figure 6.7.2.1 shows how the XRPD pattern changed for the template removed samples after oxidation reactions. There is seemingly very little difference before and after oxidation catalysis for the iron doped template free microporous niobium oxide. Both samples subjected to conditions required for both *n*-decane and cyclooctane oxidation remain unchanged after reaction. This is highly desirable as it means that the pores are resilient to the catalytic conditions. However, it was found no conversion was observed for *n*-decane oxidation. But, for cyclooctane, minor oxidation was observed. We ascribe this effect as the oxidation of cyclic hydrocarbons has been reported to be less energy demanding than that of linear.^{34–36} The results of which are summarised in table 6.7.2.1. All template containing samples showed no conversion. And although these could be, in principle, removed *in situ* under reaction conditions, this result fits with the theory that template removal is essential so diffusion of the substrate can occur and access the active site, complimenting data in section 5.2.9.

Interestingly, however, is the lack of conversion observed in template free microporous niobium oxide. As the template has been removed, the cyclooctane should have access to any active sites present. However, as the Nb-TMS1 may have a different oxidation state to bulk Nb₂O₅ and a different crystal structure, this has caused the material to be catalytically inactive. This is thought to be the case as differences in conversion were observed amongst different crystal structures in section 4.2.2 and this is documented within the literature of other materials.^{37,38}

Conversely, Fe/Nb-TMS1 shows that template free microporous niobium oxide doped with iron is catalytically active. Although the conversion is significantly lower than the bulk counterpart under identical conditions, it can still oxidise cyclooctane. When compared to results obtained from bulk Fe/Nb₂O₅ over a 6 h timescale (a time deliberately chosen in order to allow comparison of the selectivity at the same conversion) the selectivity between bulk and microporous Fe/Nb₂O₅ is indeed different. Microporous Fe/Nb₂O₅ shows a significantly higher selectivity to cyclooctanone and cyclooctanol (44.2% and 12.9% respectively) compared to

the cyclooctyl peroxide (26.9%), whereas the bulk Fe/Nb₂O₅ yields no alcohol and predominately cyclooctyl peroxide (62.7%). This difference is likely from the iron present within the porous structure having a different environment to that of the bulk, and thus can provide an alternative active site.

Table 6.7.2.1: A compilation of conversion and selectivity data obtained with varying microporous niobium oxide catalysts, as synthesised and with the template removed via phthalic anhydride. Bulk analogues are included as a means of comparison. Cyclooctane (3 mL), Catalyst mass based on M:S = 1:1000, 110 °C, PO₂ 2 bar, 24 h. Note a 6 h run with bulk Fe/Nb₂O₅ was conducted for means of comparison.

	Conversion	Ketone	Alcohol	Peroxide	Others and Unknown	K/A
	(%)	(%)	(%)	(%)	(%)	
Blank	0.00	0.00	0.00	0.00	0.00	0.0
Nb-TMS1:	0.00	0.00	0.00	0.00	0.00	0.0
As synthesised						
Nb-TMS1:	0.00	0.00	0.00	0.00	0.00	0.0
Template removed						
Fe/Nb-TMS1:	0.00	0.00	0.00	0.00	0.00	0.0
As synthesised						
Fe/Nb-TMS1:	3.97	44.2	12.9	26.9	15.9	3.4
Template removed						
Commercial Nb₂O₅	51.5	39.6	12.3	30.3	17.9	3.2
Bulk Fe/Nb₂O₅	67.8	42.2	11.3	8.09	38.4	3.8
Bulk Fe/Nb₂O₅ 6 h	2.00	11.5	0.00	62.7	25.9	No Alcohol

Finally, it was found that the structure of the template free microporous niobium oxide changed significantly after cyclooctane and *n*-decane oxidation conditions. It can be seen in the XRPD patterns (figure 6.7.2.1) two peaks are present for the post-reaction samples at $4.4^\circ 2\Theta$ and $8.6^\circ 2\Theta$. It is undetermined whether the original peak at $8.0^\circ 2\Theta$ shifted to $8.6^\circ 2\Theta$ and the peak at $4.4^\circ 2\Theta$ formed, or even if the original peak has shifted to smaller $4.4^\circ 2\Theta$ values and another peak has arisen in its place. Either result is not desired as ideally the structure would be unaffected from the reaction conditions. This could be due to a low amount of porosity remaining after template removal and the pores being left weak to chemical attack or the material even exists as a metastable crystalline phase, which is observed in bulk niobium oxides.¹⁷ Therefore, under the higher temperature and pressure this changes the form of the pores.

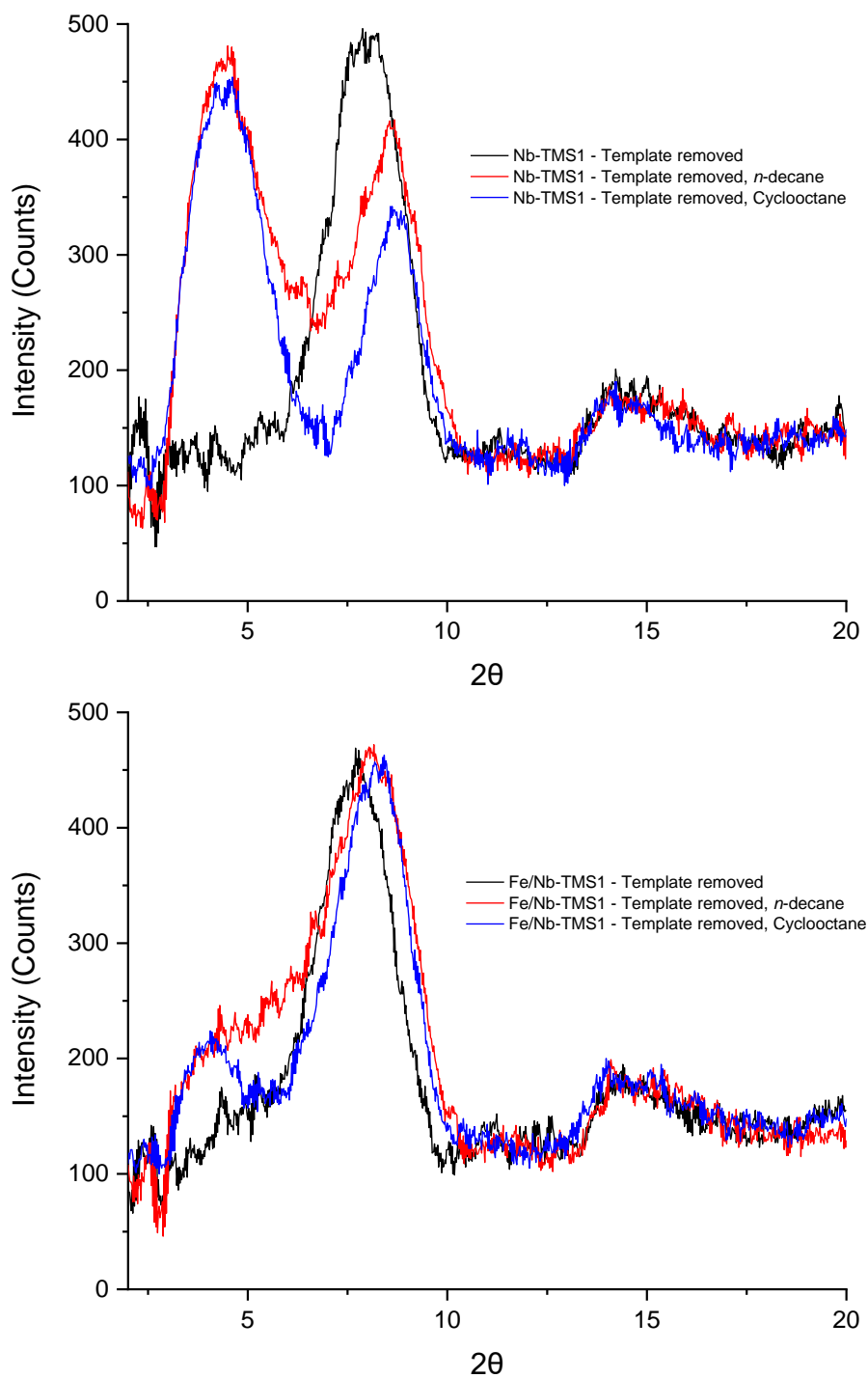


Figure 6.7.2.1: XRPD patterns of template removed microporous niobium oxide (top) and the corresponding iron doped material (bottom) subjected to catalytic conditions for alkane oxidation. *n*-decane (3 mL), M:S = 1:1000; 115 °C; PO_2 = 1 bar; 24 h. Cyclooctane (3 mL), M:S = 1:1000; 110 °C; PO_2 2 bar; 24 h.

6.8. Conclusions and future work

To summarise, the synthesis of microporous niobium oxide and samples doped with iron has been successfully achieved. To our knowledge, this is the first example of iron being incorporated during a hydrothermal synthesis of niobium oxide. Mirroring the results in chapter 5, template removal from these materials proved difficult. Although the microporous niobium oxide was found to be much more resilient when compared to mesoporous titanium oxide synthesised in a similar way, template removal was not able to be performed as described in the literature without causing complete pore collapse. However, the template was successfully removed with pores remaining when treated with dilute *p*-TSA and with phthalic anhydride. Despite significant pore collapse, catalytic tests were conducted and found that cyclooctane oxidation catalysis can occur on microporous Fe/Nb-TMS1 when the template has been removed, and the porous structure is unchanged. Although desired products were produced selectively, conversion is very low when using this material. However, it shows that not only can these materials exist without the template but are also capable of some catalysis. Future work would develop synthesis of microporous niobium oxide further and its subsequent template removal steps by changing the parameters during the autoclave step. Materials synthesised in this chapter could be applied to other selective oxidation reactions (e.g. *p*-xylene to terephthalic acid)³⁹ due to the potential confined sites of the iron within the porous framework.

6.9. References

- 1 S. L. Brock, N. Duan, Z. R. Tian, O. Giraldo, H. Zhou and S. L. Suib, *Chem. Mater.*, 1998, **10**, 2619–2628.
- 2 T. Sun and J. Y. Ying, *Angew. Chemie Int. Ed.*, 1998, **37**, 664–667.
- 3 D. M. Antonelli and J. Y. Ying, *Chem. Mater.*, 1996, **8**, 874–881.
- 4 D. M. Antonelli, *Adv. Mater.*, 1999, **11**, 487–492.
- 5 A. Lezau, M. Trudeau, G. M. Tsoi, L. E. Wenger and D. Antonelli, *J. Phys. Chem. B*, 2004, **108**, 5211–5216.
- 6 T. Sun and J. Y. Ying, *Nature*, 1997, **389**, 704.
- 7 D. M. Antonelli and J. Y. Ying, *Angew. Chemie Int. Ed. English*, 1996, **35**, 426–430.
- 8 D. M. Antonelli, A. Nakahira and J. Y. Ying, *Inorg. Chem.*, 1996, **35**, 3126–3136.
- 9 X. Hu, M. Trudeau and D. M. Antonelli, *Chem. Mater.*, 2007, **19**, 1388–1395.
- 10 S. Li, Q. Xu, E. Uchaker, X. Cao and G. Cao, *CrystEngComm*, 2016, **18**, 2532–2540.
- 11 A. Le Viet, M. V. Reddy, R. Jose, B. V. R. Chowdari and S. Ramakrishna, *J. Phys. Chem. C*, 2010, **114**, 664–671.
- 12 Y. Zhao, Z. Zhang and Y. Lin, *J. Phys. D. Appl. Phys.*, 2004, **37**, 3392–3395.
- 13 S. J. Chipera, *Clays Clay Miner.*, 2001, **49**, 398–409.
- 14 C. A. Wilde, Y. Ryabenkova, I. M. Firth, L. Pratt, J. Railton, M. Bravo-Sanchez, N. Sano, P. J. Cumpson, P. D. Coates, X. Liu and M. Conte, *Appl. Catal. A Gen.*, 2019, **570**, 271–282.
- 15 S. F. Mousavi, M. Jafari, M. Kazemimoghadam and T. Mohammadi, *Ceram. Int.*, 2013, **39**, 7149–7158.
- 16 Q. H. Xia and Z. Gao, *Mater. Chem. Phys.*, 1997, **47**, 225–230.

- 17 I. Nowak and M. Ziolk, *Chem. Rev.*, 1999, **99**, 3603–3624.
- 18 M. M. Mohamed, W. A. Bayoumy, M. Khairy and M. A. Mousa, *Microporous Mesoporous Mater.*, 2007, **103**, 174–183.
- 19 S. M. Park and D. S. Kim, *Polym. Eng. Sci.*, 2019, **59**, 752–756.
- 20 P.-P. Knops-Gerrits, A. Verberckmoes, R. Schoonheydt, M. Ichikawa and P. A. Jacobs, *Microporous Mesoporous Mater.*, 1998, **21**, 475–486.
- 21 M. D. Alba, Z. Luan and J. Klinowski, *J. Phys. Chem.*, 1996, **100**, 2178–2182.
- 22 M. P. F. Graça, A. Meireles, C. Nico and M. A. Valente, *J. Alloys Compd.*, 2013, **553**, 177–182.
- 23 T. Masuda, T. Takahashi and T. Higashimura, *J. Chem. Soc. Chem. Commun.*, 1982, 1297–1298.
- 24 A. Aronne, E. Marenga, V. Califano, E. Fanelli, P. Pernice, M. Trifuoggi and A. Vergara, *J. Sol-Gel Sci. Technol.*, 2007, **43**, 193–204.
- 25 M. Menetrey, A. Markovits and C. Minot, *Surf. Sci.*, 2003, **524**, 49–62.
- 26 M. Conte and V. Chechik, *Chem. Commun.*, 2010, **46**, 3991–3993.
- 27 I. J. Lin and P. Somasundaran, *J. Colloid Interface Sci.*, 1971, **37**, 731–743.
- 28 P. T. Tanev and T. J. Pinnavaia, *Chem. Mater.*, 1996, **8**, 2068–2079.
- 29 V. F. Stone and R. J. Davis, *Chem. Mater.*, 1998, **10**, 1468–1474.
- 30 J. D. Marty, M. Tizra, M. Mauzac, I. Rico-Lattes and A. Lattes, *Macromolecules*, 1999, **32**, 8674.
- 31 J. M. Thomas, R. Raja, G. Sankar and R. G. Bell, *Acc. Chem. Res.*, 2001, **34**, 191–200.
- 32 R. P. John, J. Park, D. Moon, K. Lee and M. S. Lah, *Chem. Commun.*, 2006, 3699–

- 3701.
- 33 J. C. Lavalley, *Catal. Today*, 1996, **27**, 377–401.
- 34 J. Zheng, T. Yu and D. G. Truhlar, *Phys. Chem. Chem. Phys.*, 2011, **13**, 19318–19324.
- 35 R. D. Bach and O. Dmitrenko, *J. Am. Chem. Soc.*, 2004, **126**, 4444–4452.
- 36 Z. Tian, A. Fattahi, L. Lis and S. R. Kass, *J. Am. Chem. Soc.*, 2006, **128**, 17087–17092.
- 37 Z. Paál, X. L. Xu, J. Paál-Lukács, W. Vogel, M. Muhler and R. Schlögl, *J. Catal.*, 1995, **152**, 252–263.
- 38 J. M. Grau, J. C. Yori, C. R. Vera, F. C. Lovey, A. M. Condó and J. M. Parera, *Appl. Catal. A Gen.*, 2004, **265**, 141–152.
- 39 R. K. Grasselli, *Catal. Today*, 1999, **49**, 141–153.

CHAPTER 7: Conclusion and future work

This research work has developed three different aspects; i) the study of the autoxidation of *n*-decane, ii) synthesis of bulk materials and their applications to alkane oxidation and iii) the synthesis of microporous/mesoporous metal oxides and their application to alkane oxidation.

To summarise, the main achievements from this work are:

- Development of conversion and selectivity calculators, for both *n*-octane and *n*-decane utilising ¹H-NMR and GC-MS.
- Determination of conditions when autoxidation occurs for *n*-decane (≥ 125 °C under atmospheric conditions, ≥ 120 °C at PO_2 2 bar) and subsequent quantification of conversion and selectivity.
- The application of Fe/TiO₂ to the optimisation of *n*-decane oxidation by varying reaction parameters, catalyst screening across a range of metals and supports (along with; comparisons of activity, selectivity towards *n*-decane and cyclooctane oxidation and characterization between catalysts) and developing catalysts capable of significant cyclooctane oxidation with selectivity towards cyclooctanone for use in KA oil manufacture.
- Having a deeper understanding on the soft-template synthesis of microporous titanium oxide and microporous niobium oxide, conflicting that reported within the literature. This work provides further analysis of materials reported within the literature, showing FTIR-ATR, XRPD and BET before and after template removal with novel *in situ* XRPD analysis of how crystal structure of these materials changes as a function of temperature. Additionally, to our knowledge, the work reports analysis of novel microporous titanium oxide and microporous niobium oxide where a dopant metal has been included during the synthesis. The work has also demonstrated a range of commonly reported template removal techniques that are not suitable for template removal with our materials due to loss of porosity and/or insufficient template removal. Subsequently, the work also developed novel template removal techniques with

hydrogen peroxide and phthalic anhydride, the latter of which was capable of removing the template within microporous niobium oxide, whilst retaining its crystalline porous structure.

Selective alkane oxidation was the focus of this research. Through studies with autoxidation, which were also used as a benchmark for our materials in terms of selectivity control, it was determined where appropriate reaction conditions could be used to test catalysts. Autoxidation becomes a dominating feature beyond 120 °C, where the product distribution of ketone to alcohol is roughly 2:1. This fits with results from literature on other linear alkane oxidation.¹ No catalyst tested at temperatures where autoxidation was occurring changed the conversion or selectivity. This shows how dominating the autoxidation mechanisms are (also agreeing with literature),² and why it is essential to develop a catalyst capable to operate where autoxidation is not occurring. Furthermore, over oxidation of the alcohol to unwanted by-products occurred under autoxidation control, more reason to avoid these conditions. All these observations were capable through analytical methods also developed here. Although ¹H-NMR is an attractive candidate for the study of reaction mixtures from alkane oxidation, as the samples are analysed at room temperature without any pre-treatment, our study showed that due to the complex nature of reaction mixtures it was not possible to accurately quantify products with this method. Furthermore, its advantages over GC-MS³ (see section 3.1 for further details) made it a hard decision to move onto another tool. For our purposes another analytical tool was required to be developed. A GC-MS conversion calculator, with relatively low error (~15% standard error) was achieved. This allowed quantification of every reaction product, something not possible with ¹H-NMR, but at a cost of a much longer analysis time and lengthy calibrations of the analytical apparatus. This tool could be further developed and applied to an array of linear alkanes, with small changes required (for example, different internal standards depending on chain length). Moreover, this could be improved further through pre-preparation of hydroperoxides and carboxylic acids (section 3.1).³⁻⁶ However, owing to the low conversion and low amount of acids formed in our tests, this was not deemed essential. Future work for

autoxidation reaction analysis would be heavily focused on time online type experiments and including radical scavengers into the reaction mixture. This would allow development on the understanding of kinetics of certain steps and how the products are evolved *in situ*, and ultimately the mechanisms occurring within the reaction.

Applying supported metals and metal oxides to alkane oxidation gave a clear indication that iron is the most active metal in the series we have tested. Using Fe/TiO₂ the optimal conditions for *n*-decane oxidation were developed. By varying parameters such as temperature, oxygen pressure, metal to substrate ratio, etc., the conversion of *n*-decane oxidation was optimised, to where then other catalysts would be tested then compared. On the main supports tested (TiO₂, MCM-41), but not niobium oxide, iron gave significant conversion of *n*-decane (>5%). In most cases, chosen supports were not active towards *n*-decane oxidation, thus proving iron's involvement in catalysis. Moreover, even when supports were active towards cyclooctane oxidation, doping with iron provided a significant increase in conversion (~2 – 3 times). This led to iron being the main contender for doping into porous frameworks (sections 5.2.4 and 6.3). Further still, iron's presence significantly increased the yield of cyclooctanone (up to ~65% of the reaction mixture with iron doped zeolite catalysts). Although the primary focus of this project was on linear alcohols, cyclooctanone is interesting due to its potential industrial applications for fibre synthesis (and is analogous to cyclohexanone). It is expected that a further development of iron doped zeolites could lead to efficient catalysts to produce KA oil. By changing the Si/Al ratio and pore size, an optimized catalyst for ketone synthesis could be developed. On the other hand, iron seemed to not affect the conversion of niobium oxide when applied to cyclooctane oxidation. Non-doped Nb₂O₅ was found to give relatively high conversions of alkane oxidation (2 – 7% with *n*-decane), especially when compared to common oxidation catalysts. This unusual property was initially investigated by considering different suppliers and determining if the presence of additional metals (as impurities) changed its activity. While in most cases the presence of a dopant metal led to deactivation (deactivation was also observed when the non-doped material was reduced), non-doped

Nb_2O_5 was capable of alkane oxidation. It is still uncertain what exactly caused this result, but future work would certainly explore this further, for example by considering the presence of impurities in the hydrocarbon substrate(s). XPS, UV-VIS, Raman and other analytical techniques could give more information on why non-doped niobium oxide is active and doped/reduced niobium oxide is inactive, for example to determine if the presence of different niobia surface species occurs between samples.⁷ Furthermore, the presence of trace impurities which are the source of activity could be detected by additional analysis, as observed in ZSM-5 which was found to have iron impurities detected by x-ray absorption spectroscopy.⁸

Perhaps the most significant result from the bulk material tests was determining catalytic activity's strong dependence on metal/support interactions, specifically inhibiting reactions. Noble metals and manganese were initially put as priority for catalytic tests due to their presence in the literature,⁹⁻¹³ especially manganese due to its selectivity towards alcohols.^{14,15} However, in most cases metal oxides (manganese, palladium, gold, silver) were not active towards *n*-decane oxidation. Although metal salts were often active, this was not desired for our research due to the potential requirement of calcining a catalyst, and ease of separation of a reaction mixture when deposited onto a support. This gave rise to potential problems and considerations for chapters 5 and 6 where these metals were to be part of a porous framework. Ideally, XRPD would have given some insight into potential active phases, however, due to the low metal loading this was not possible. Future work would focus on determining a trend why some supports allow activity while others lead to inactivity – specifically determining oxidation state, particle sizes and surface species of dopant metals would be the next conceptual points to follow. This would be done with extensive analysis, again XPS, UV-VIS, Raman, X-ray adsorption techniques and others would allow further insight into the surface of these materials.¹⁶ For example, with manganese oxide it is likely that amongst the several oxidation states of manganese some are more active than others¹⁷ and calcination may affect how the metal oxide is bound to the support.¹⁸ These would then be investigated in turn to see

if at all they affect conversion in our systems. Another aspect which must be developed, as mentioned previously, are time on stream type experiments. As with the autoxidation reactions, determining the kinetics and mechanisms within these reactions when a catalyst is present would not only improve our understanding, but combined with surface analysis would allow specific steps to be promoted with iterative development of the catalysts tested.^{19,20} Finally, with respect to catalytic testing, reactor design must be considered – especially when considering using flammable substrates under oxygen pressure. For example, aerobic liquid phase oxidations have been developed and scaled up when used with microreactor technology to overcome the implications of hazardous materials and low oxygen transfer.²¹

In addition, microporous metal oxides were developed. Template removal from microporous materials is not as straightforward as stated within the literature. For microporous TiO₂, a crystalline porous template-free material from a template-assisted synthesis was not possible. An array of synthesis optimisation techniques (differing metal alkoxide to surfactant ratio, type of metal alkoxide, temperature and duration of autoclave step), and template removal tests (differing the concentration, ratio and types of acid; varying the nature of species which interacts with the template and calcination tests) were conducted, and even a novel analysis of how calcination changes pores *in situ* (this gave effective quantification of a temperature range of when pore collapse occurred - for microporous TiO₂ this started at 160 °C and no sign of pores remained by 190 °C according to the XRD). Whilst these results are not what we desired; they certainly gave insight on the fragility of microporous titanium oxide – a characteristic which is not reported in literature, and could explain the need of the addition of Si to form stable titanium silicates. Nevertheless, dopant metals were capable of being incorporated into the synthesis of microporous titanium oxide, and thus we synthesised novel doped microporous metal oxides. Although they were found to be inactive to the applications we desired, future work would be searching for their application in other fields of catalysis.²² Additional parameters would be adjusted for microporous titanium oxide synthesis in the future work. For example, focusing on longer-chain templates with more ionic character may provide

stronger micelle formation, a key part of the synthesis.²³ Or alternatives to amines would be used, for example polyethylene glycol (PEG)²⁴ or porous polymers²⁵ that can also be removed through calcination. While these may lead to larger pore sizes, having an intact porous framework may still provide a degree of conversion and selectivity as opposed to our observed inactivity in completely destroyed pores. On the other hand, microporous niobium oxide was slightly more resilient. Although again the template removal was not as easy as stated (acidic template removal with nitric acid was not possible and calcination with *in situ* XRD shows pore collapse between 200 – 240 °C), treatment with phthalic anhydride was able to yield template free material. To our knowledge this is the first-time phthalic anhydride has been used to remove a template from a porous framework. This method of removal may open access to other template-free porous materials synthesised via an amine template which are otherwise too fragile for calcination/acid washes. However, the template-free material was unable to catalyse the oxidation of *n*-decane. This is thought to be due to the challenging nature of linear alkane oxidation with bulk materials, additional diffusion limitations and potential inhibiting metal/support interactions. At present we speculate that oxygen vacancies in these materials could trap alkyl peroxides involved in the oxidation process. However, if these materials were to be improved by exploring the systematic parameter changes made with TiO₂, then perhaps more pores could be accessed by *n*-decane and thus more active sites. On the other hand, cyclooctane was oxidised by template-free microporous Fe/Nb₂O₅. Although the conversion was significantly lower than that of the bulk material (~4% versus ~68%), a preference for ketones was observed (44% in a 24 h test with microporous Fe/Nb₂O₅ in comparison to 11.5% in a 6 h test with bulk material of statistically similar conversions). Again, if the material was more porous, perhaps a catalyst with high conversion and selectivity to the ketone could be developed.

Finally, microporous materials without a template were also developed. Microporous titanium oxide was synthesised via the peptization of anatase. Although not as porous as the template-containing microporous titanium oxide, the peptized material was template-free and porous.

To our knowledge, this is the first time this material has been doped with iron via wetness impregnation and applied to alkane oxidation. Whilst the material was able to oxidise cyclooctane, it was incapable of any significant changes in selectivity. This suggested that all the active sites involved in the reaction were on the external surface of the porous framework. However, this synthesis could be further optimised (i.e. longer times in autoclave, varying temperature – parameters which may affect crucial nanotube formation) and potentially lead to a more porous framework.

To summarise, alkane oxidation is a challenging process in chemistry, here we have demonstrated how porous catalysts can be developed and applied to alkane oxidation to yield different conversions and selectivity to that of the bulk materials.

References

- 1 F. Garcia-Ochoa, J. Querol and A. Romero, *Ind. Eng. Chem. Res.*, 1990, **29**, 1989–1994.
- 2 B. Z. Zhan, B. Modén, J. Dakka, J. G. Santiesteban and E. Iglesia, *J. Catal.*, 2007, **245**, 316–325.
- 3 B. P. C. Hereijgers and B. M. Weckhuysen, *J. Catal.*, 2010, **270**, 16–25.
- 4 M. A. Farajzadeh, N. Nouri and P. Khorram, *TrAC Trends Anal. Chem.*, 2014, **55**, 14–23.
- 5 J. D. Chen and R. A. Sheldon, *J. Catal.*, 1995, **153**, 1–8.
- 6 P. T. Wierzchowski and L. Wiesław Zatorski, *Chromatographia*, 2000, **51**, 83–86.
- 7 I. E. Wachs, J.-M. Jehng, G. Deo, H. Hu and N. Arora, *Catal. Today*, 1996, **28**, 199–205.
- 8 C. Hammond, N. Dimitratos, R. L. Jenkins, J. A. Lopez-Sanchez, S. A. Kondrat, M. Hasbi ab Rahim, M. M. Forde, A. Thetford, S. H. Taylor, H. Hagen, E. E. Stangland, J. H. Kang, J. M. Moulijn, D. J. Willock and G. J. Hutchings, *ACS Catal.*, 2013, **3**, 689–699.
- 9 M. Aryafar and F. Zaera, *Catal. Letters*, 1997, **48**, 173–183.
- 10 P. Gallezot, *Catal. Today*, 1997, **37**, 405–418.
- 11 W.-X. Li, C. Stampfl and M. Scheffler, *Phys. Rev. Lett.*, 2003, **90**, 256102.
- 12 H. Zhao, J. Zhou, H. Luo, C. Zeng, D. Li and Y. Liu, *Catal. Letters*, 2006, **108**, 49–54.
- 13 R. Lloyd, R. L. Jenkins, M. Piccinini, Q. He, C. J. Kiely, A. F. Carley, S. E. Golunski, D. Bethell, J. K. Bartley and G. J. Hutchings, *J. Catal.*, 2011, **283**, 161–167.
- 14 L. M. Slaughter, J. P. Collman, T. A. Eberspacher and J. I. Brauman, *Inorg. Chem.*,

- 2004, **43**, 5198–5204.
- 15 B. R. Cook, T. J. Reinert and K. S. Suslick, *J. Am. Chem. Soc.*, 1986, **108**, 7281–7286.
- 16 C. Nozaki, C. G. Lugmair, A. T. Bell and T. D. Tilley, *J. Am. Chem. Soc.*, 2002, **124**, 13194–13203.
- 17 C. Reed, Y. K. Lee and S. Ted Oyama, *J. Phys. Chem. B*, 2006, **110**, 4207–4216.
- 18 X. Lou, P. Liu, J. Li, Z. Li and K. He, *Appl. Surf. Sci.*, 2014, **307**, 382–387.
- 19 M. M. Forde, R. D. Armstrong, R. McVicker, P. P. Wells, N. Dimitratos, Q. He, L. Lu, R. L. Jenkins, C. Hammond, J. A. Lopez-Sanchez, C. J. Kiely and G. J. Hutchings, *Chem. Sci.*, 2014, **5**, 3603–3616.
- 20 L. Kesavan, R. Tiruvalam, M. H. A. Rahim, M. I. Bin Saiman, D. I. Enache, R. L. Jenkins, N. Dimitratos, J. A. Lopez-Sanchez, S. H. Taylor, D. W. Knight, C. J. Kiely and G. J. Hutchings, *Science*, 2011, **331**, 195–199.
- 21 H. P. L. Gemoets, V. Hessel and T. Noël, in *Liquid Phase Aerobic Oxidation Catalysis: Industrial Applications and Academic Perspectives*, Wiley-VCH Verlag GmbH & Co. KGaA, Weinheim, Germany, 2016, pp. 397–419.
- 22 T. Sun and J. Y. Ying, *Nature*, 1997, **389**, 704.
- 23 D. M. Antonelli, A. Nakahira and J. Y. Ying, *Inorg. Chem.*, 1996, **35**, 3126–3136.
- 24 S. J. Bu, Z. G. Jin, X. X. Liu, L. R. Yang and Z. J. Cheng, *J. Eur. Ceram. Soc.*, 2005, **25**, 673–679.
- 25 G. J. de A. A. Soler-Illia, C. Sanchez, B. Lebeau and J. Patarin, *Chem. Rev.*, 2002, **102**, 4093–4138.

Appendix

Contents

Appendix.....	318
A.1 ¹ H NMR spectra of <i>n</i> -octane and corresponding oxidation products.....	319
A.2 ¹ H NMR spectra of <i>n</i> -decane and corresponding oxidation products.....	329

A.1 ^1H NMR spectra of *n*-octane and corresponding oxidation products

n-octane

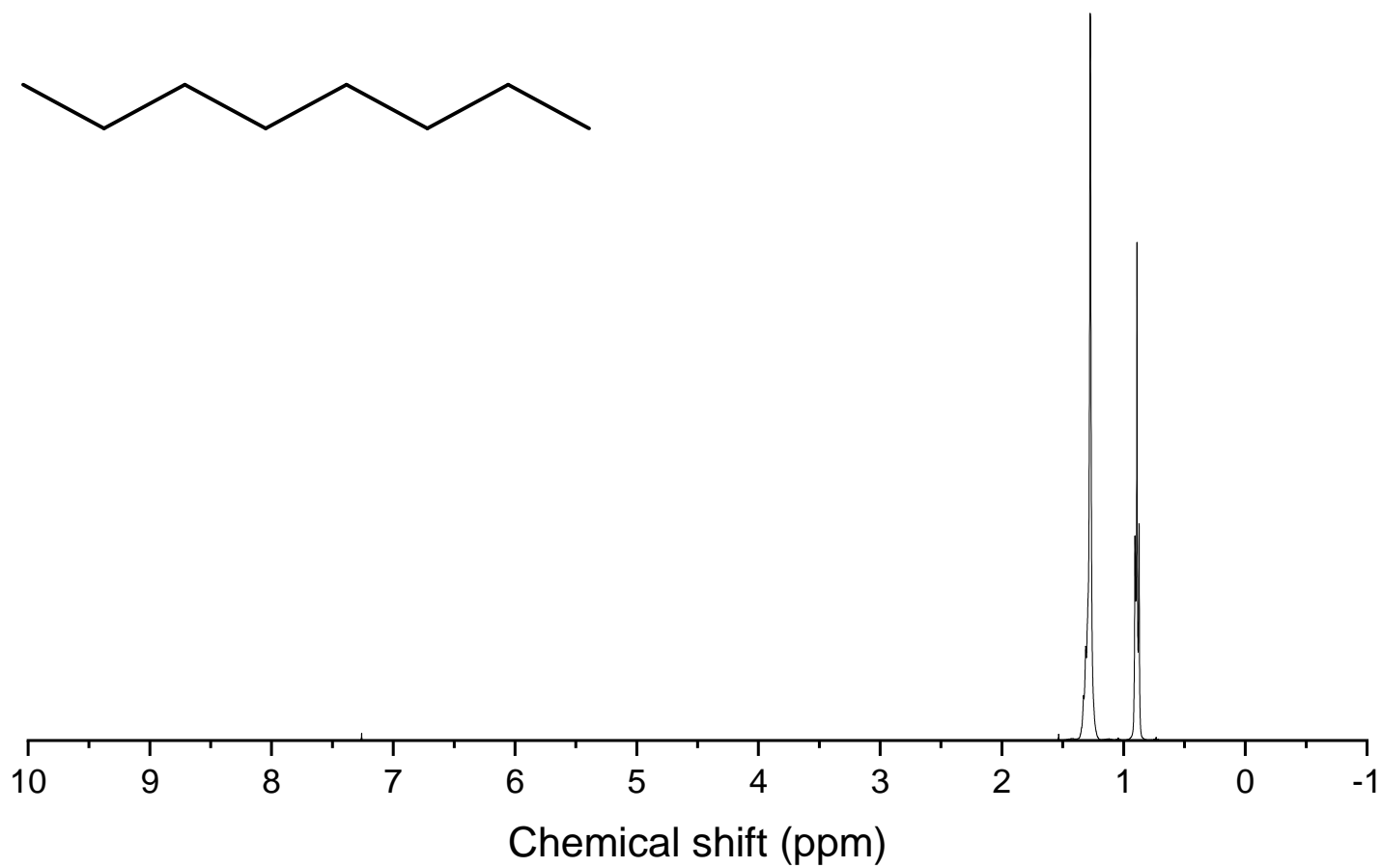


Figure A.1.1: ¹H NMR of *n*-octane used for both standard tests and oxidation reactions. ¹H NMR (CDCl₃ 400 MHz), *n*-octane, δ (ppm): 1.29 (CH₂, m, 12H), 0.89 (CH₂, t, 6H)

1-Octanol

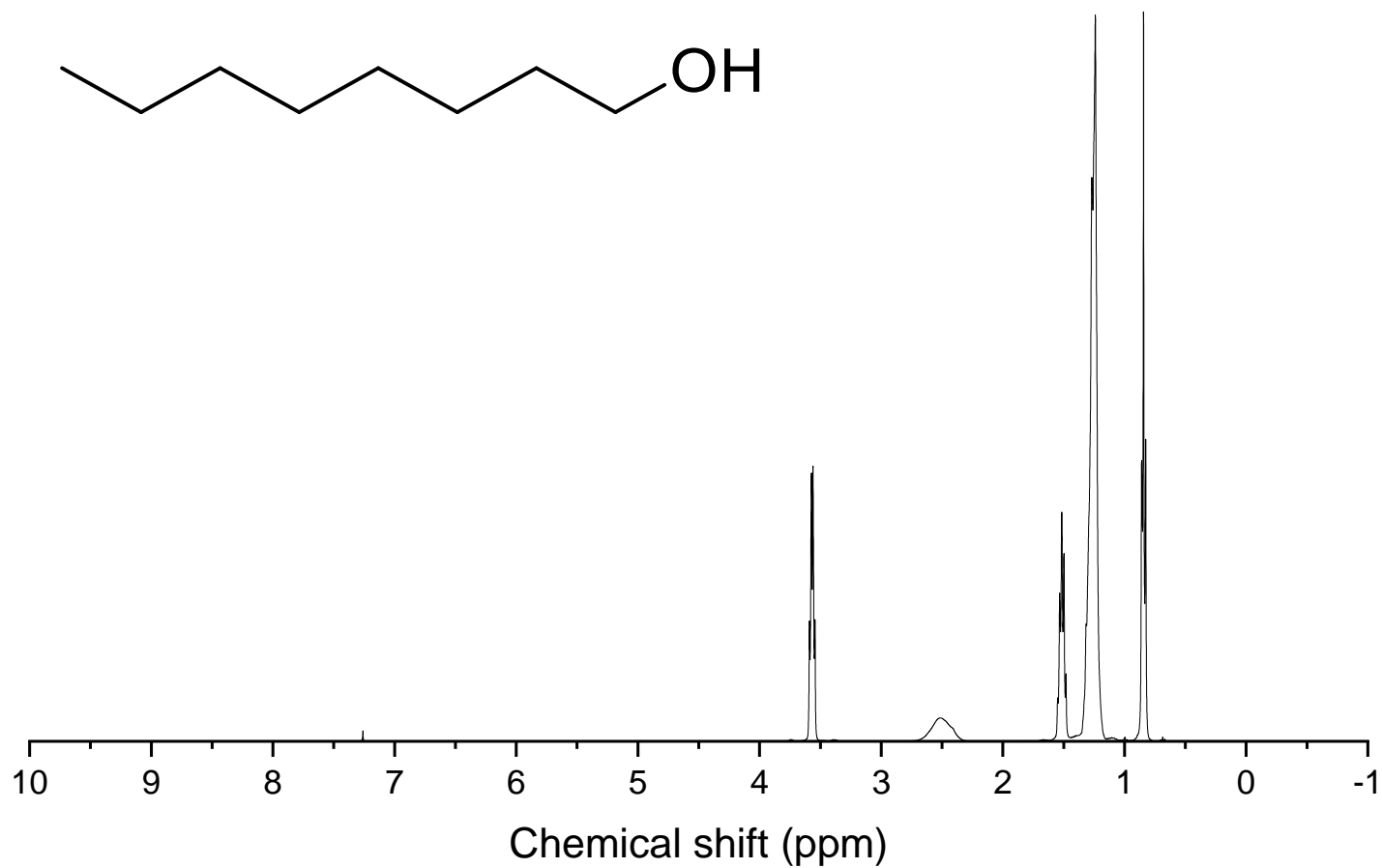


Figure A.1.2: ¹H NMR of 1-Octanol used for standard tests. ¹H NMR (CDCl₃ 400 MHz), 1-Octanol, δ (ppm): 3.56 (CH₂, m, 2H), 2.52 (OH, s broad, 1H), 1.52-1.25 (CH₂, m, 12H), 0.83 (CH₃, t, 3H). The peak at 3.56 ppm was used as the characteristic peak in reaction mixtures.

2-Octanol

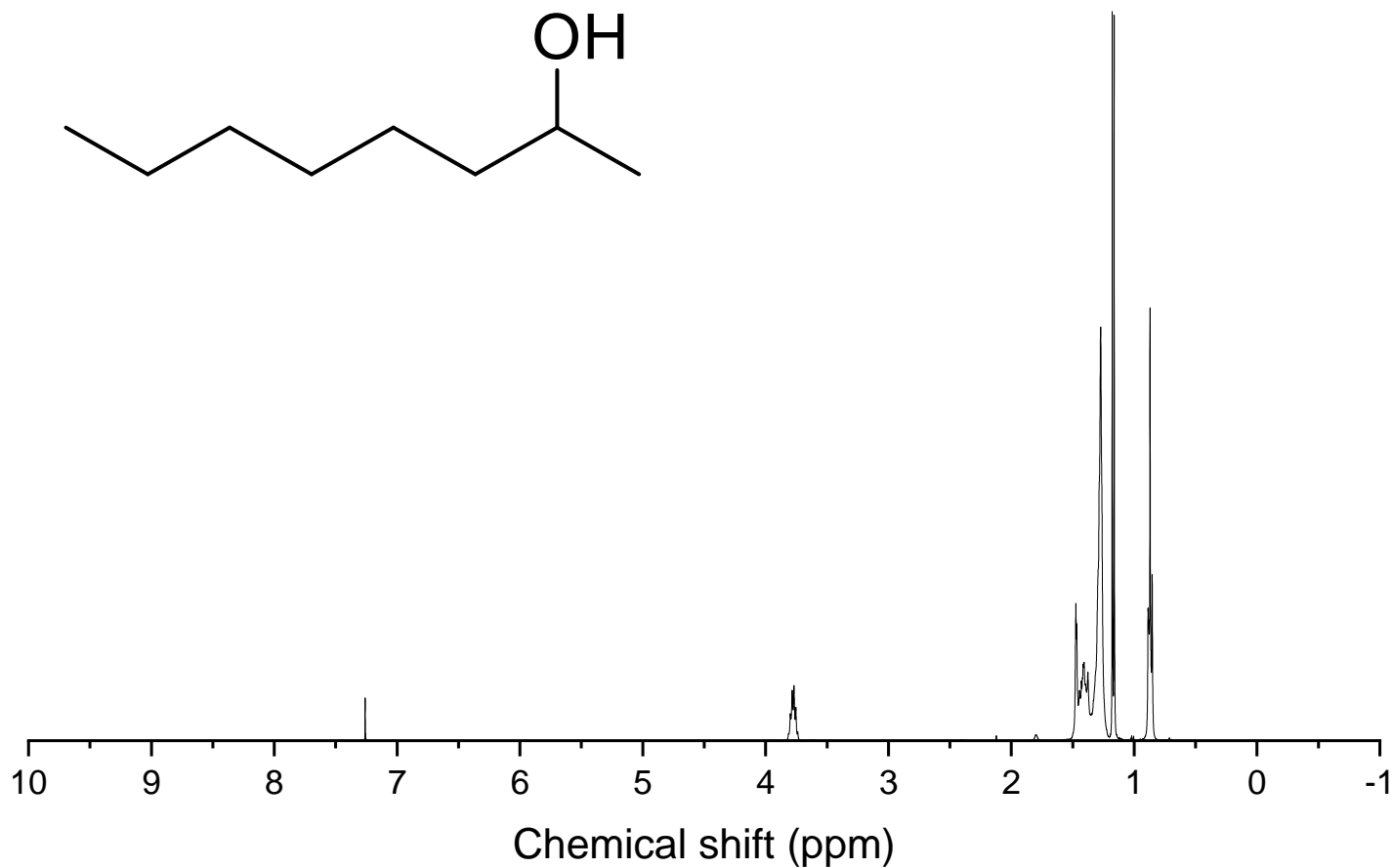


Figure A.1.3: ¹H NMR of 2-Octanol used for standard tests. ¹H NMR (CDCl₃ 400 MHz), 2-Octanol, δ (ppm): 3.78 (CH, m, 1H), 1.48-1.27 (CH₂ incl. OH, m, 11H), 1.17 (CH₃, d, 3H), 0.87 (CH₃, t, 3H). The peak at 3.78 ppm was used as the characteristic peak in reaction mixtures.

3-Octanol

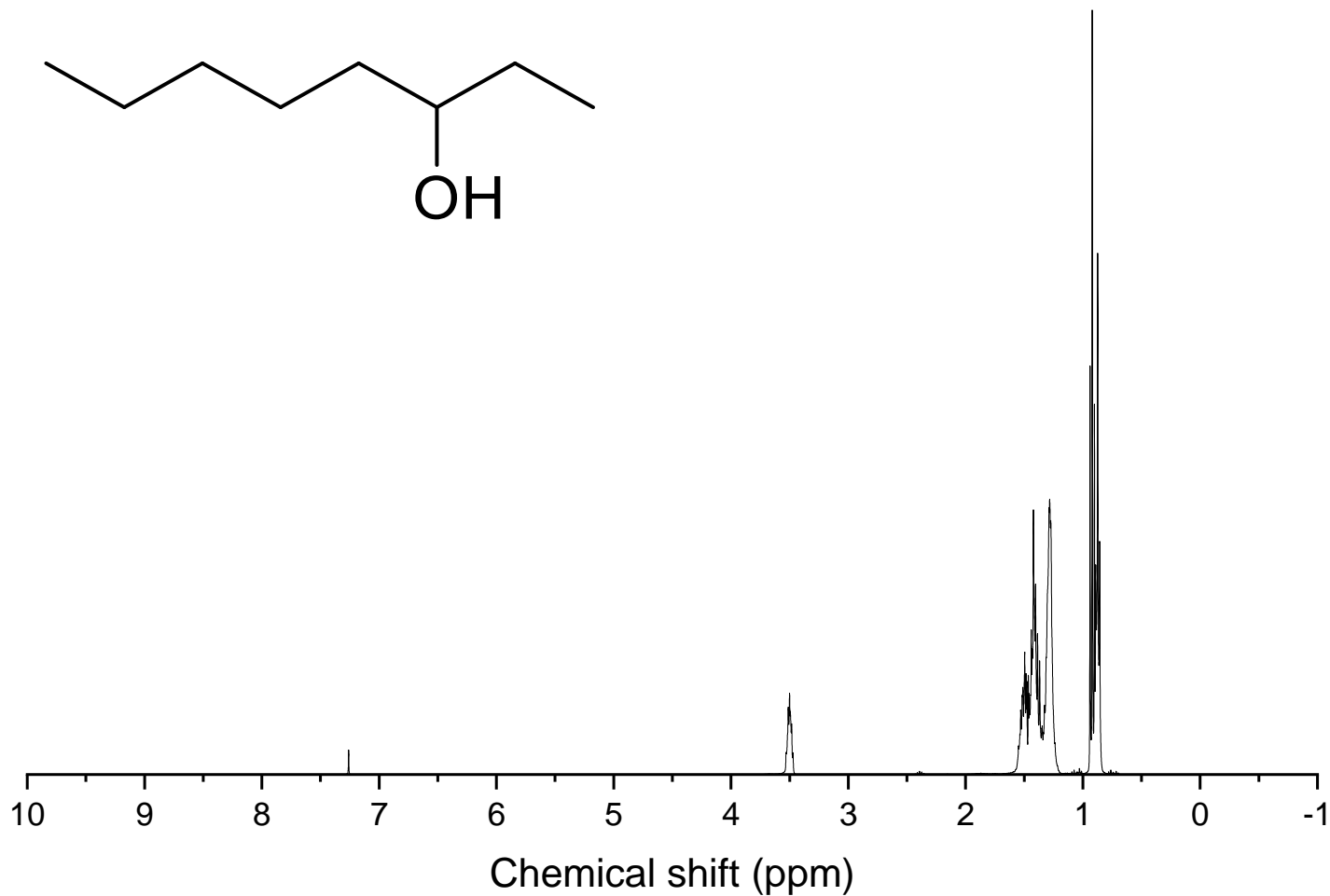


Figure A.1.4: ¹H NMR of 3-Octanol used for standard tests. ¹H NMR (CDCl₃ 400 MHz), 3-Octanol, δ (ppm): 3.50 (CH, m, 1H), 1.50-1.29 (CH₂ incl. OH, m, 11H), 0.87 (CH₃, t, 6H). The peak at 3.50 ppm was used as the characteristic peak in reaction mixtures.

Octanal

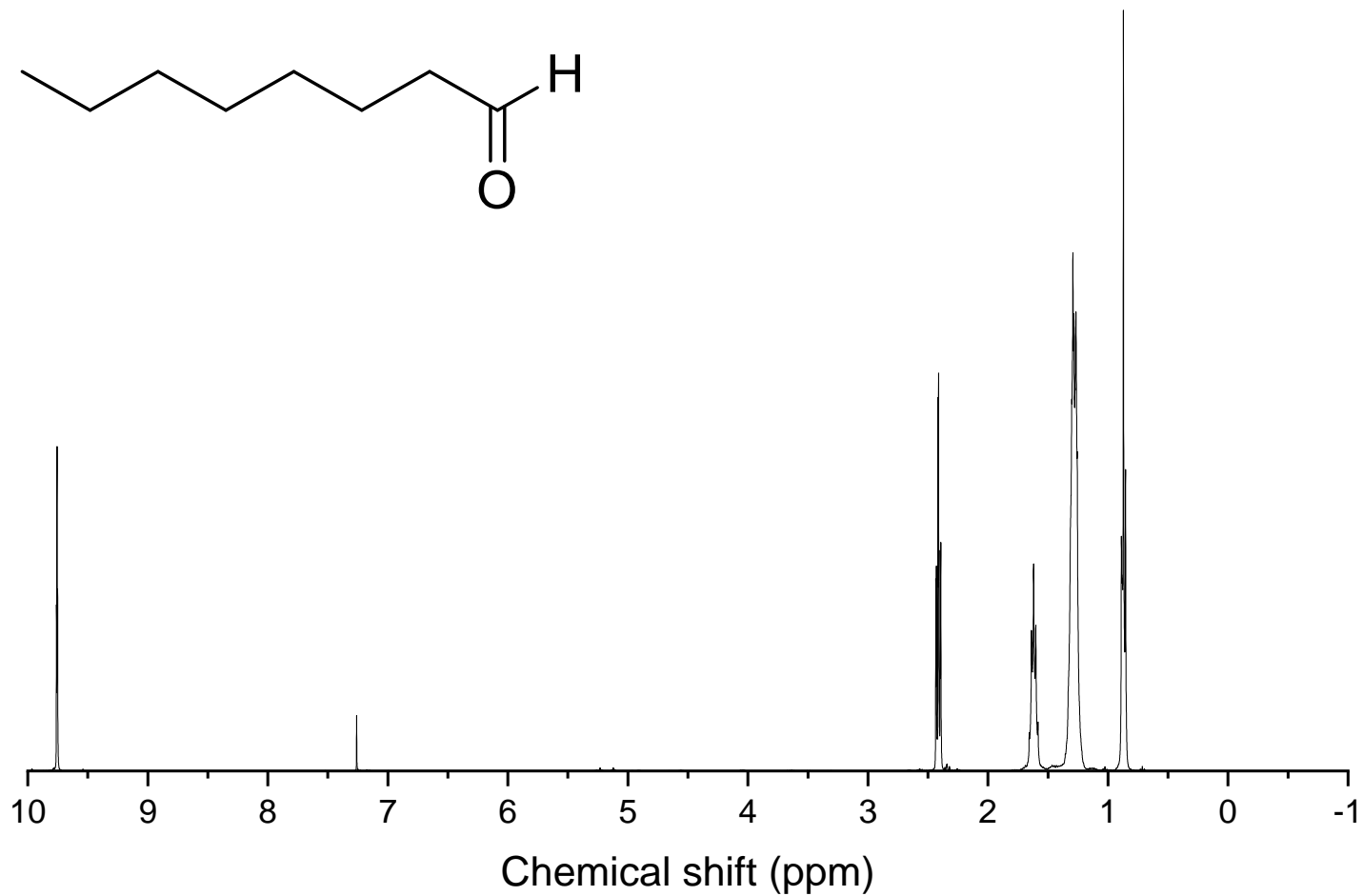


Figure A.1.5: ^1H NMR of Octanal used for standard tests. ^1H NMR (CDCl_3 400 MHz), Octanal, δ (ppm): 9.74 (CH, s, 1H), 2.43 (CH_2 , t, 2H) 1.61-1.27 (CH_2 , m, 10H), 0.86 (CH_3 , t, 3H). The peak at 9.74 ppm was used as the characteristic peak in reaction mixtures.

2-Octanone

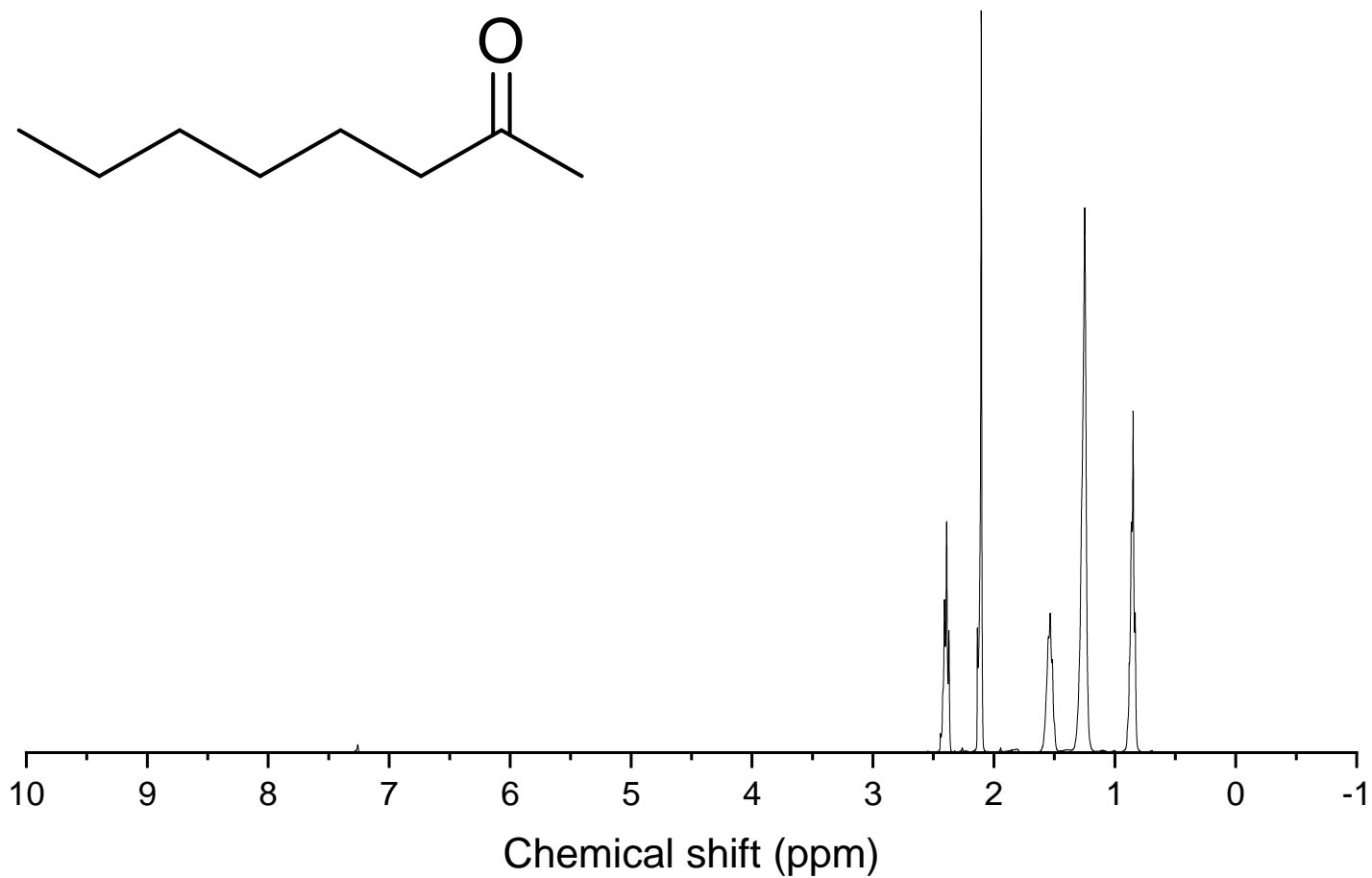


Figure A.1.6: ¹H NMR of 2-Octanone used for standard tests. ¹H NMR (CDCl₃ 400 MHz), 2-Octanone, δ (ppm): 2.47 (CH₂, m, 2H). 2.18 (CH₃, s, 3H), 1.61-1.27 (CH₂, m, 8H), 0.86 (CH₃, t, 3H). The peak at 2.18 ppm was used as the characteristic peak in reaction mixtures.

3-Octanone

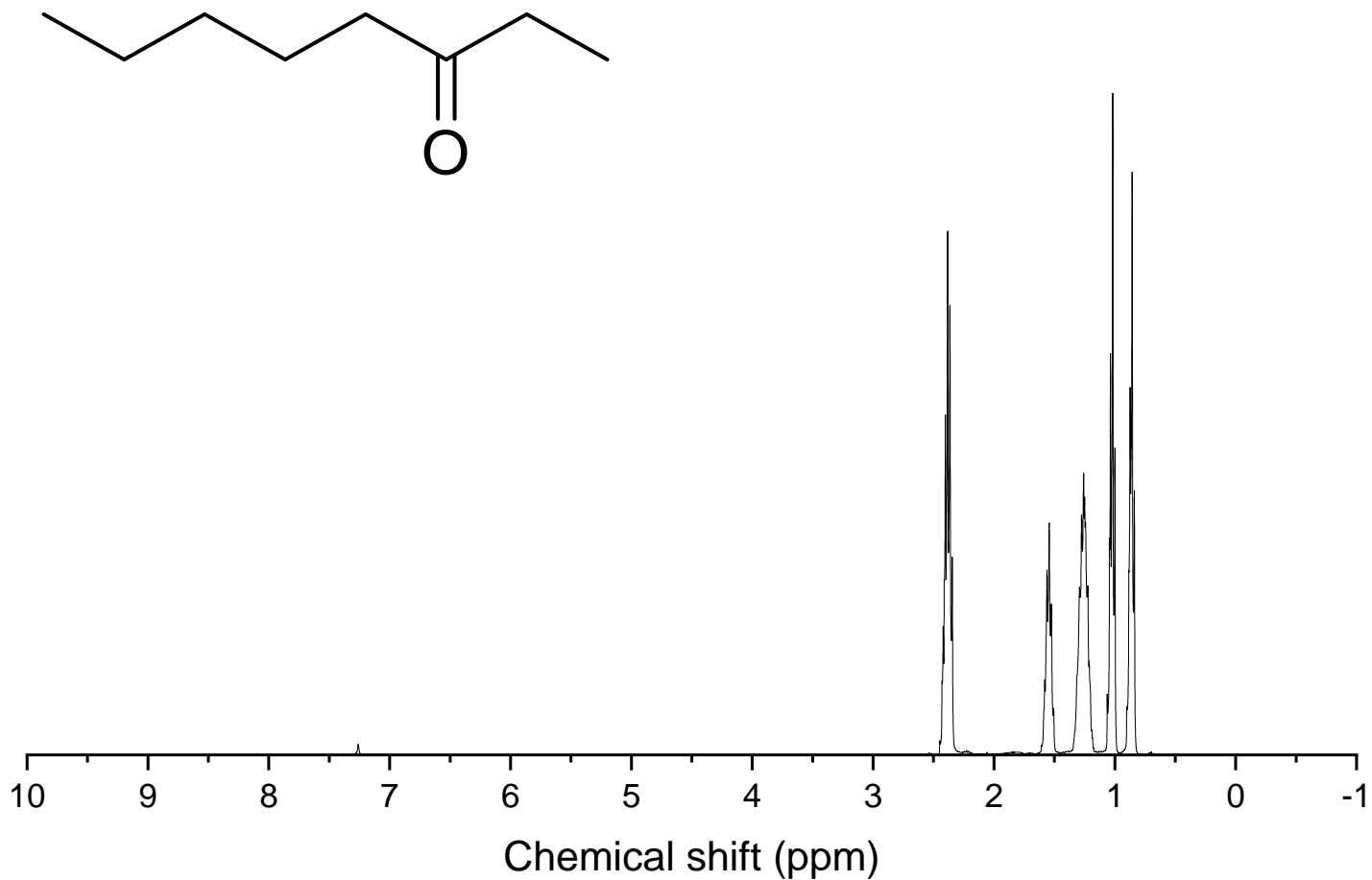


Figure A.1.7: ¹H NMR of 3-Octanone used for standard tests. ¹H NMR (CDCl₃ 400 MHz), 3-Octanone, δ (ppm): 2.39 (CH₂, m, 4H), 1.54-1.26 (CH₂, m, 6H), 1.02-0.86 (CH₃, t, 6H). The peak at 2.39 ppm was used as the characteristic peak in reaction mixtures.

1-Octene

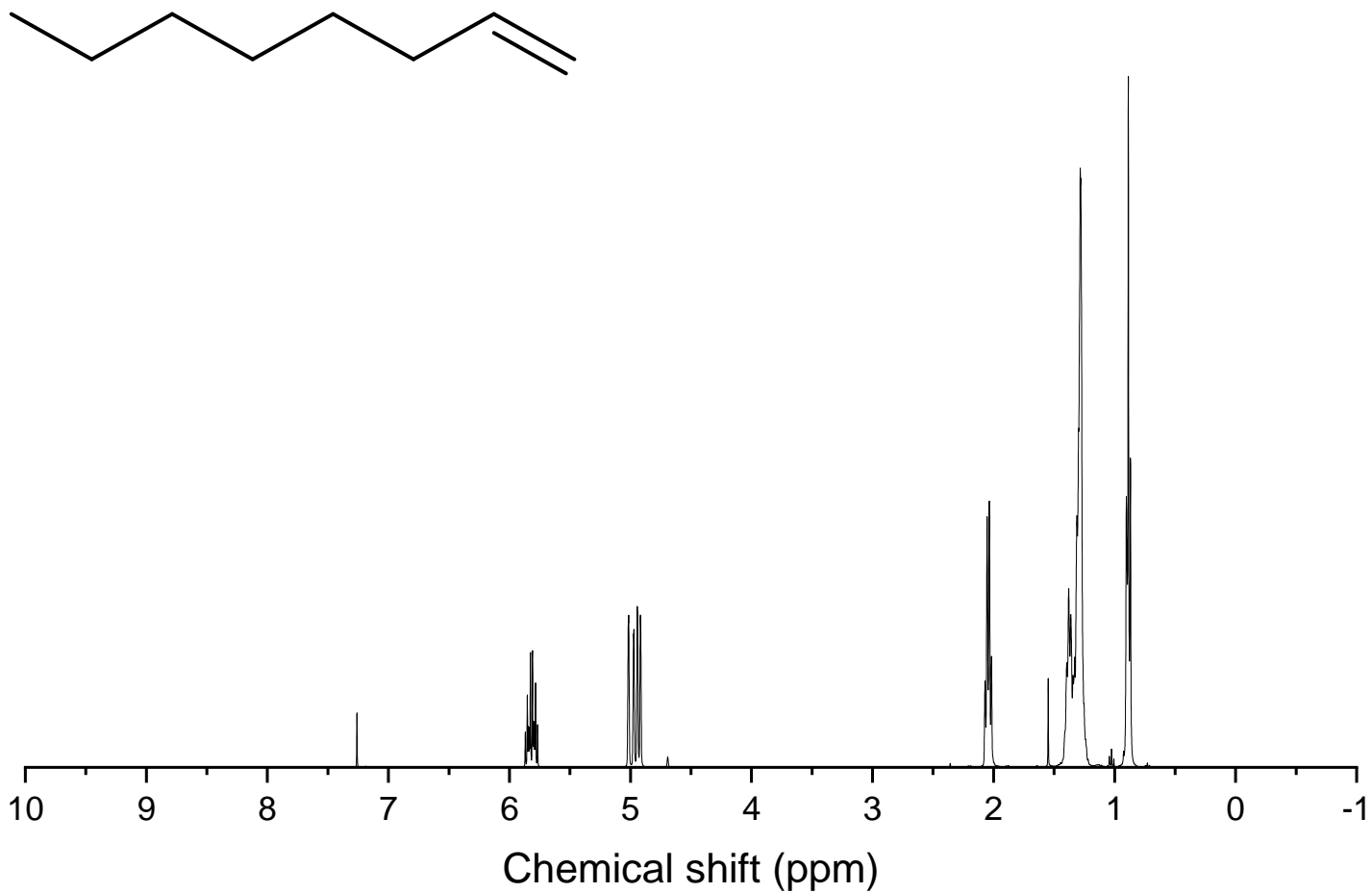


Figure A.1.8: ¹H NMR of 1-Octene used for standard tests. ¹H NMR (CDCl₃ 400 MHz), 1-Octene, δ (ppm): 5.82-4.96 (CH and CH₂, m, 3H), 2.07 (CH₂, m, 2H), 1.37-1.28 (CH₂, m, 8H), 0.90 (CH₃, t, 3H). The peak at 5.82-4.96 ppm was used as the characteristic peak in reaction mixtures.

2-Octene

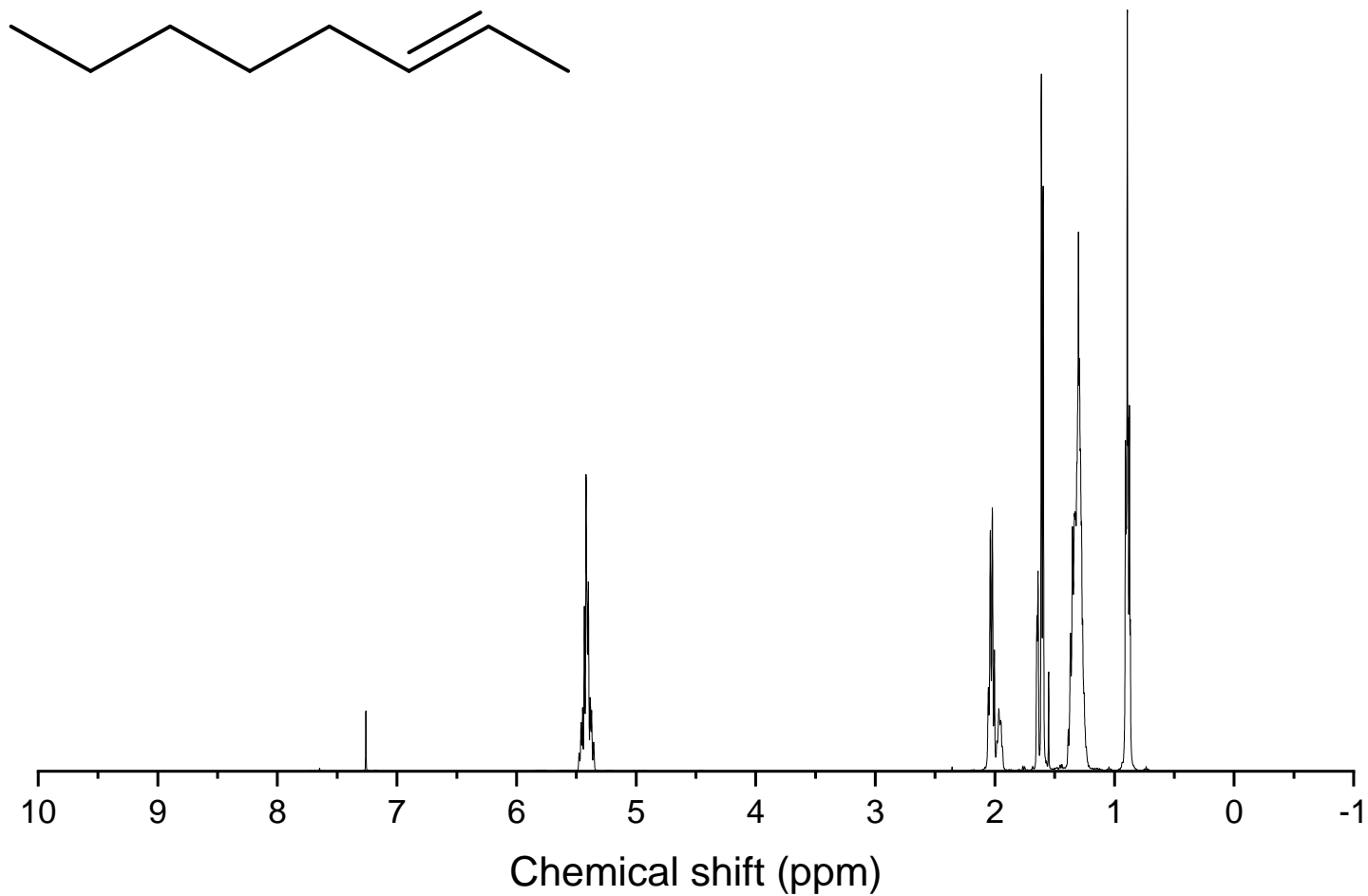


Figure A.1.9: ¹H NMR of 2-Octene used for standard tests. ¹H NMR (CDCl₃ 400 MHz), 2-Octene, δ (ppm): 5.45 (CH-CH, m, 2H), 2.03-1.61 (CH₂, m, 5H), 1.32 (CH₂, m, 6H), 0.91 (CH₃, t, 3H). The peak at 5.45 ppm was used as the characteristic peak in reaction mixtures.

A.2 ^1H NMR spectra of *n*-decane and corresponding oxidation products

n-decane

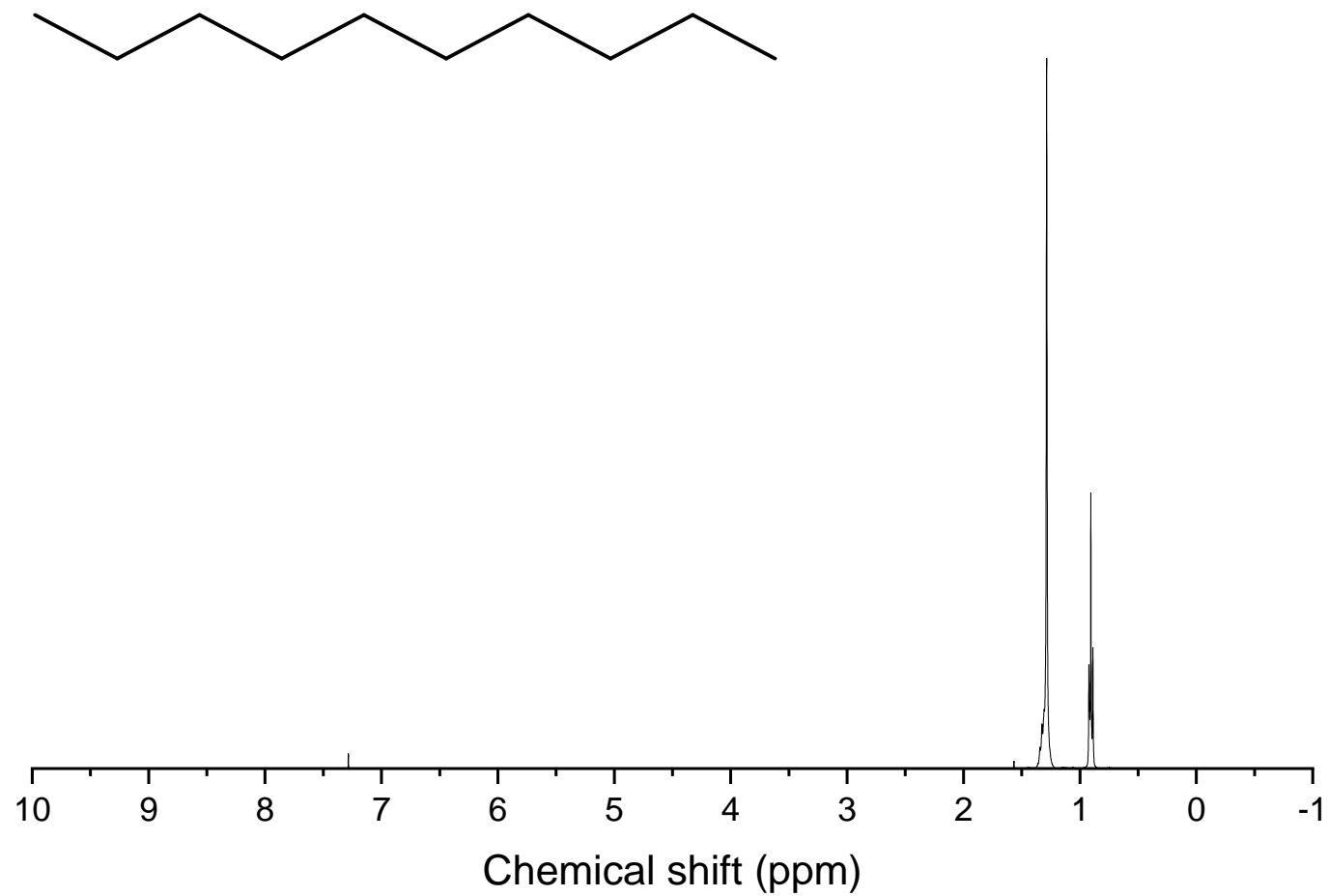


Figure A.2.1: ¹H NMR of *n*-decane used for both standard tests and oxidation reactions. ¹H NMR (CDCl₃ 400 MHz), *n*-decane, δ (ppm): 1.31 (CH₂, m, 16H), 0.91 (CH₂, t, 6H)

1-Decanol

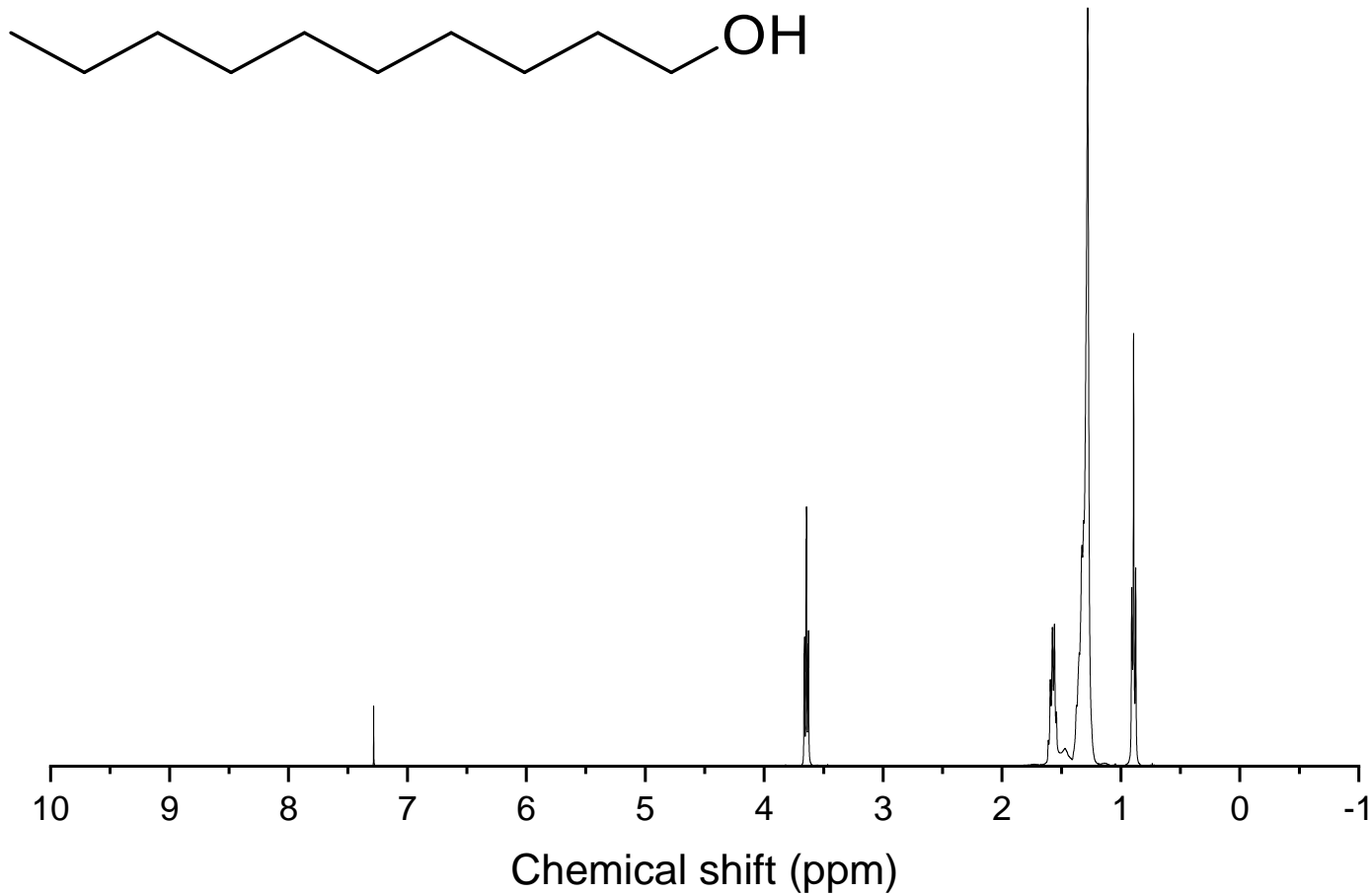


Figure A.2.2: ¹H NMR of 1-Decanol used for standard tests. ¹H NMR (CDCl₃ 400 MHz), 1-Decanol, δ (ppm): 3.62 (CH₂, m, 2H), 1.54-1.25 (CH₂ incl. OH, m, 17H), 0.86 (CH₃, t, 3H). The peak at 3.62 ppm was used as the characteristic peak in reaction mixtures.

2-Decanol

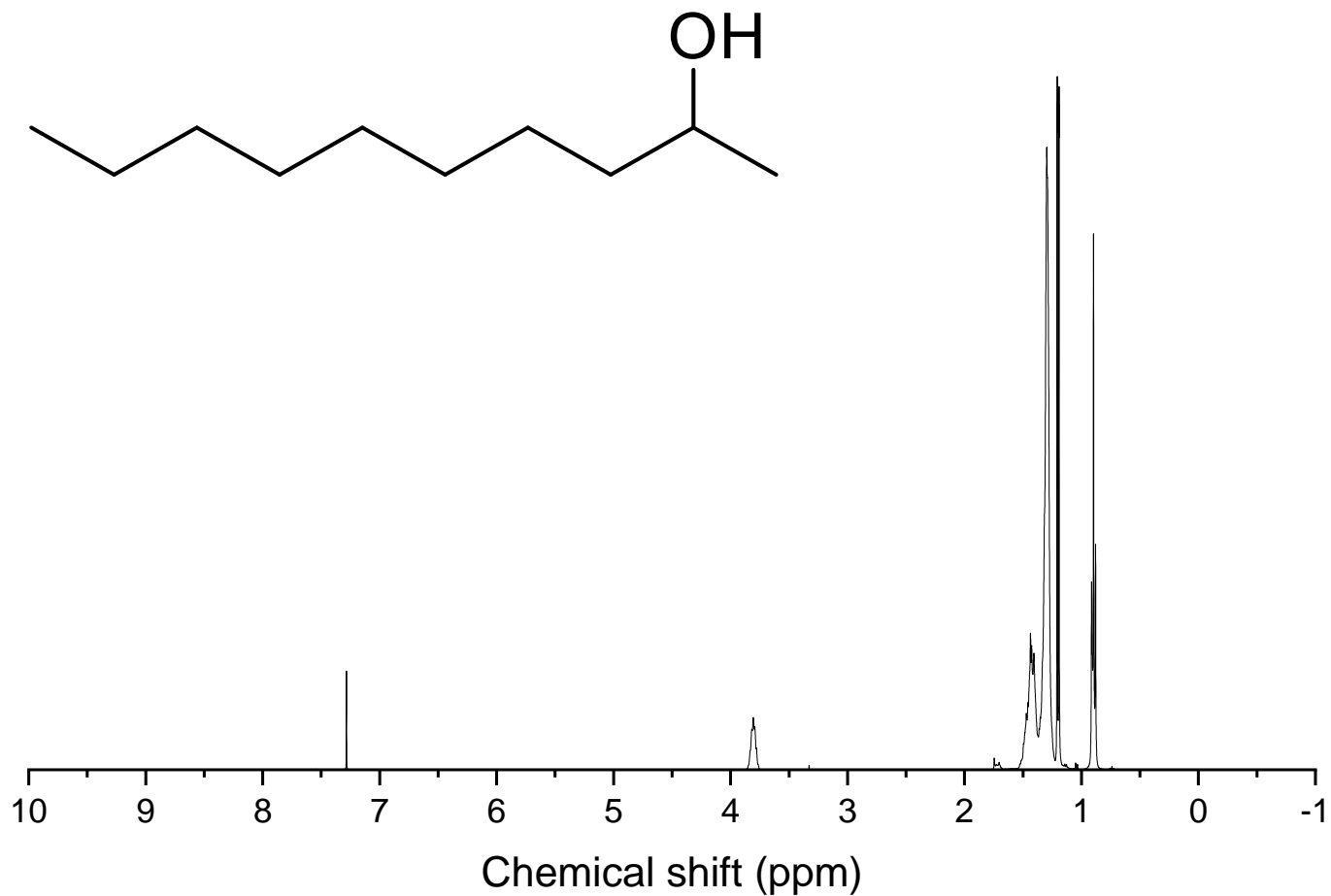


Figure A.2.3: ¹H NMR of 2-Decanol used for standard tests. ¹H NMR (CDCl₃ 400 MHz), 2-Decanol, δ (ppm): 3.78 (CH, m, 1H), 1.70-1.27 (CH₂ incl. OH, m, 15H), 1.17 (CH₃, d, 3H), 0.87 (CH₃, t, 3H). The peak at 3.78 ppm was used as the characteristic peak in reaction mixtures.

3-Decanol

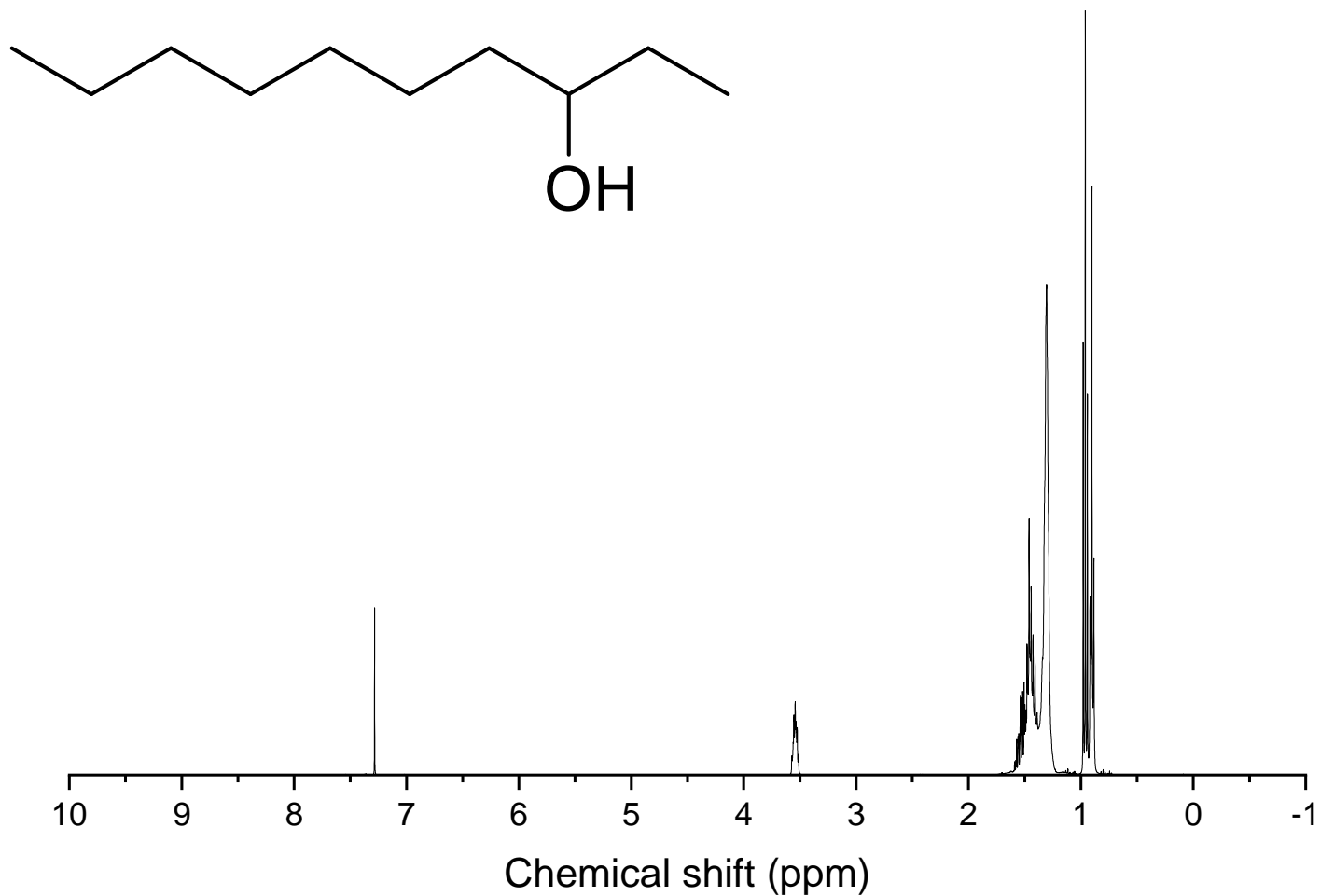


Figure A.2.4: ¹H NMR of 3-Decanol used for standard tests. ¹H NMR (CDCl₃ 400 MHz), 3-Decanol, δ (ppm): 3.52 (CH, m, 1H), 1.50-1.29 (CH₂ incl. OH, m, 15H), 0.87 (CH₃, t, 6H). The peak at 3.52 ppm was used as the characteristic peak in reaction mixtures.

4-Decanol

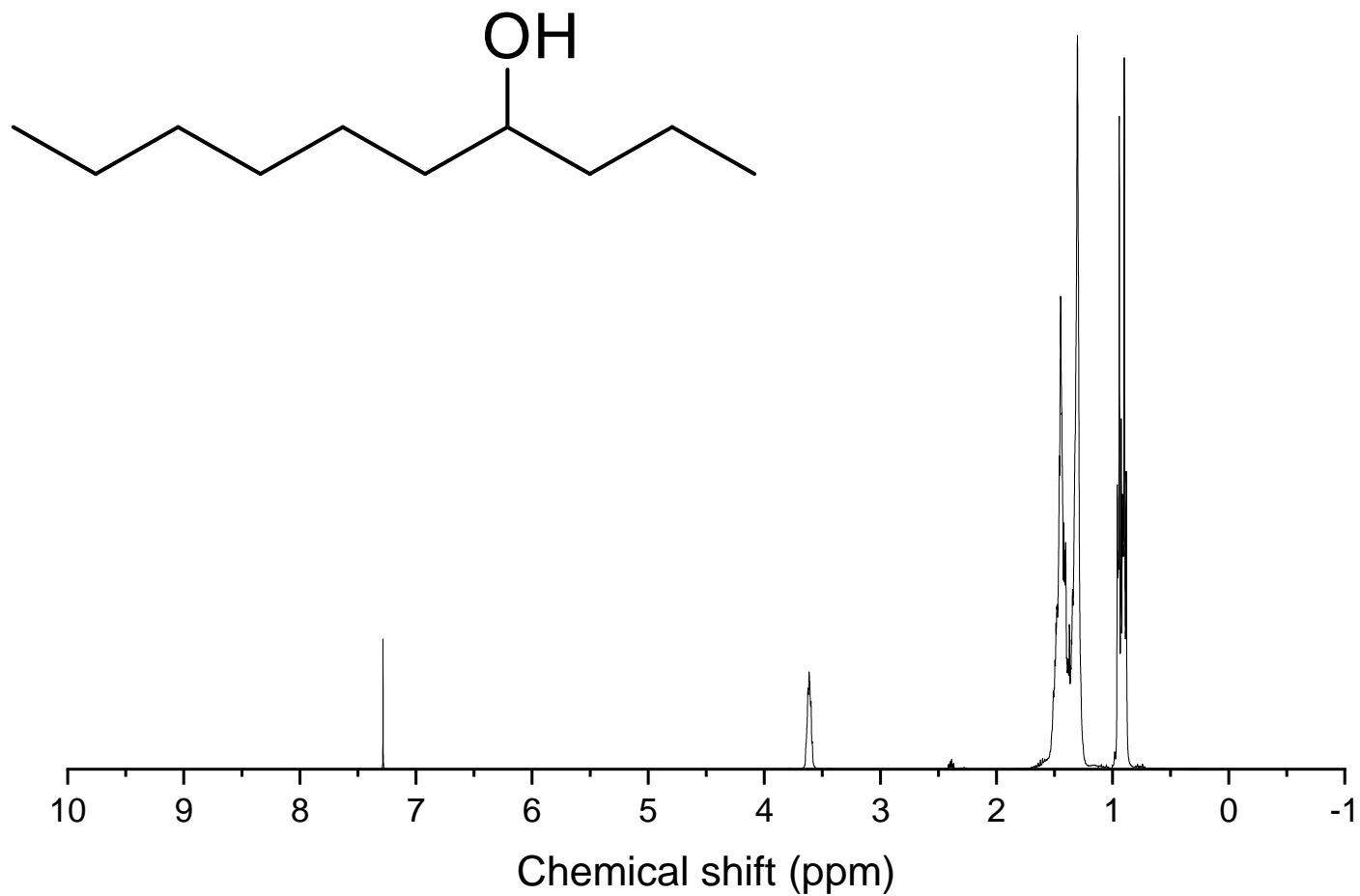


Figure A.2.5: ¹H NMR of 4-Decanol used for standard tests. ¹H NMR (CDCl₃ 400 MHz), 4-Decanol, δ (ppm): 3.59 (CH, m, 1H), 1.42-1.28 (CH₂ incl. OH, m, 15H), 0.87 (CH₃, t, 6H). The peak at 3.59 ppm was used as the characteristic peak in reaction mixtures.

Decanal

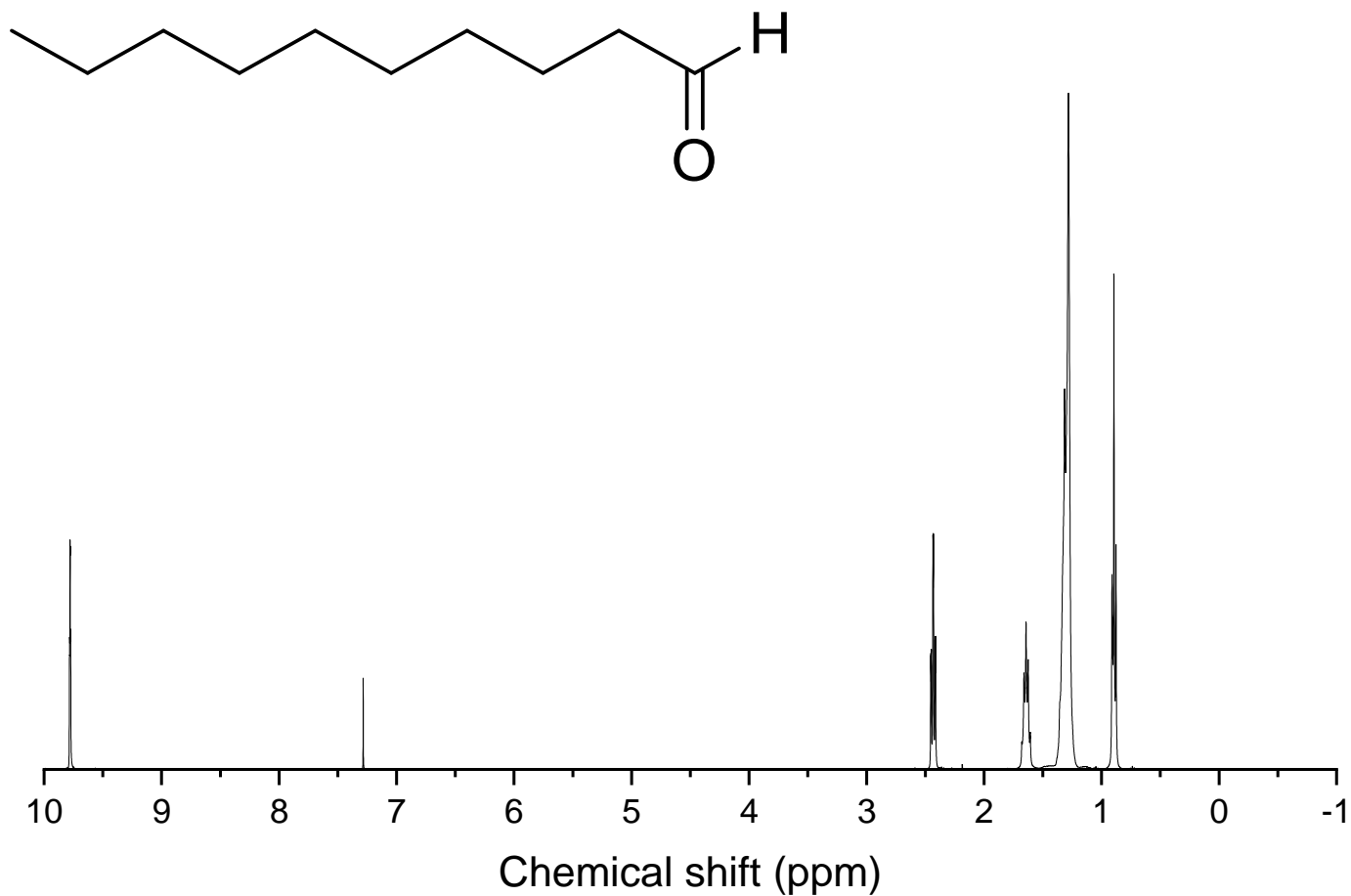


Figure A.2.6: ¹H NMR of Decanal used for standard tests. ¹H NMR (CDCl₃ 400 MHz), Decanal, δ (ppm): 9.75 (CH, s, 1H), 2.41 (CH₂, m, 2H) 1.62-1.26 (CH₂, m, 14H), 0.86 (CH₃, t, 3H). The peak at 9.75 ppm was used as the characteristic peak in reaction mixtures.

2-Decanone

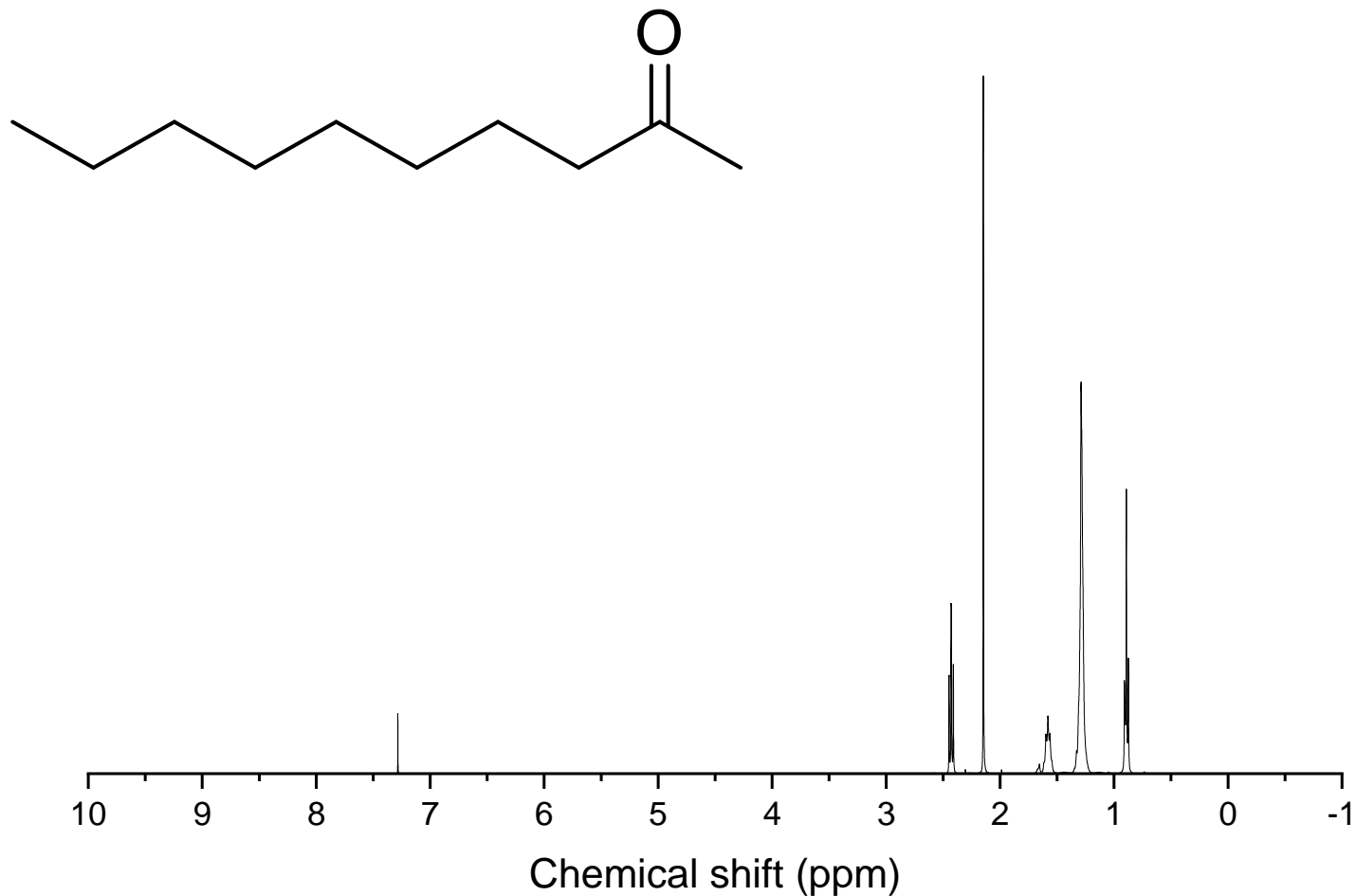


Figure A.2.7: ¹H NMR of 2-Decanone used for standard tests. ¹H NMR (CDCl₃ 400 MHz), 2-Decanone, δ (ppm): 2.45 (CH₂, m, 2H). 2.12 (CH₃, s, 3H), 1.56-1.27 (CH₂, m, 12H), 0.86 (CH₃, t, 3H). The peak at 2.12 ppm was used as the characteristic peak in reaction mixtures.

3-Decanone

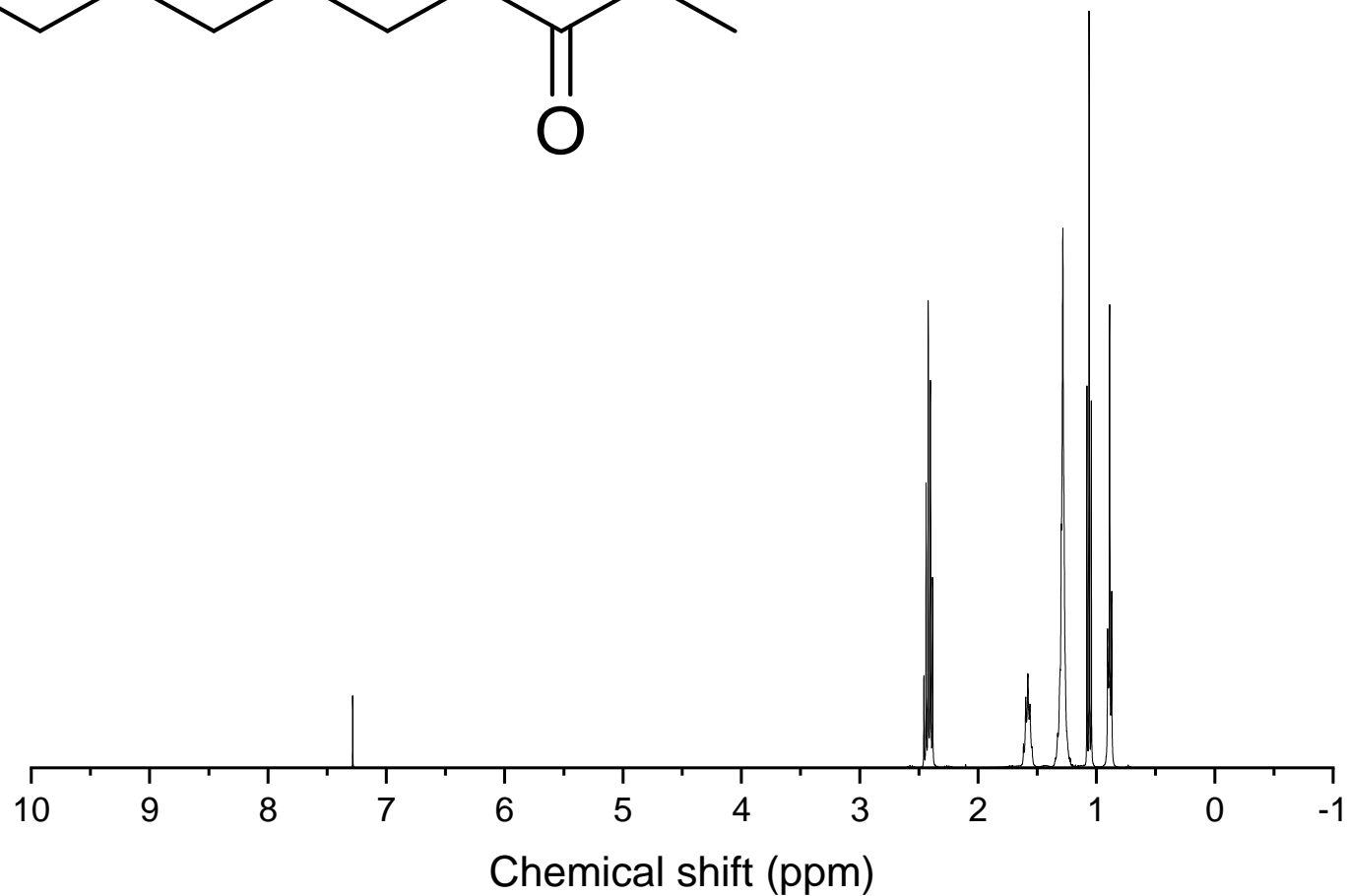
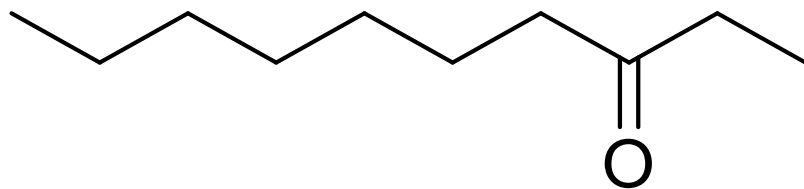


Figure A.2.8: ¹H NMR of 3-Decanone used for standard tests. ¹H NMR (CDCl₃ 400 MHz), 3-Decanone, δ (ppm): 2.39 (CH₂, m, 4H), 1.56-1.26 (CH₂, m, 10H), 1.04-0.87 (CH₃, t, 6H). The peak at 2.39 ppm was used as the characteristic peak in reaction mixtures.

